공학박사 학위논문

Weighted-Perpendicular-Tangent-Based Path-Following Control for Aerial Vehicles in Time-Varying Ambient Wind

대기바람을 고려한 비행체의 수직-접선벡터 가중치 기반 경로추종 제어

2023 년 2 월

서울대학교 대학원

기계항공공학부

서 용 준

Weighted-Perpendicular-Tangent-Based Path-Following Control for Aerial Vehicles in Time-Varying Ambient Wind

대기바람을 고려한 비행체의 수직-접선벡터 가중치 기반 경로추종 제어

지도교수 김 유 단

이 논문을 공학박사 학위논문으로 제출함

2022 년 11 월

서울대학교 대학원

기계항공공학부

서 용 준

서용준의 공학박사 학위논문을 인준함

2022 년 12 월

위 원 장	김 현 진	(인)
부위원장	김 유 단	(인)
위 원	박 찬 국	(인)
위 원	심 형 보	(인)
위 원	박 종 호	(인)

Weighted-Perpendicular-Tangent-Based Path-Following Control for Aerial Vehicles in Time-Varying Ambient Wind

Yongjun Seo

Department of Mechanical and Aerospace Engineering

Seoul National University

APPROVED:

H. Jin Kim, Chair, Ph.D.

Youdan Kim, Vice-Chair, Ph.D.

Chan Gook Park, Ph.D.

Hyungbo Shim, Ph.D.

Jongho Park, Ph.D.

Weighted-Perpendicular-Tangent-Based Path-Following Control for Aerial Vehicles in Time-Varying Ambient Wind

A Dissertation

by

Yongjun Seo

Presented to the Faculty of the Graduate School of

Seoul National University

in Partial Fulfillment

of the Requirements

for the Degree of

DOCTOR OF PHILOSOPHY

Department of Mechanical and Aerospace Engineering

Seoul National University

Supervisor : Professor Youdan Kim

February 2023

Abstract

In this dissertation, a versatile path-following control method for aerial vehicles that can effectively deal with an ambient wind shear is proposed. Novel equations of motion for aerial vehicles considering the effect of continuously differentiable time-varying ambient winds are derived, and a path-following control law in a three-dimensional Euclidean space, called the Weighted-Perpendicular-Tangent-based Path-Following Control (WPTPFC), that makes the vehicle asymptotically follow a given sufficiently smooth desired path is developed.

The proposed equations of motion consist of the aerodynamic angles and the inertial flight path angles as state variables. The equations cover a large range of ambient wind speeds without any approximation or linearization. Two unique angles of sequential rotations called the path-relative wind angles are proposed to parametrize the difference between the air-relative velocity and the inertial velocity caused by ambient wind terms. The conventional aerodynamic roll angle is not defined in a wind condition; thus, a compatible modified version is also proposed. The resulting state equations are structured to form a cascade system, which helps designers interpret the physical and geometrical meaning of individual subsystems and efficiently design a corresponding feedback control law. The model particularly fits motion control problems such as trajectory tracking or path-following control of fixed-wing-type aerial vehicles in the presence of time-varying ambient wind. The properties and potential of the proposed formulation are discussed in depth by focusing on the meaning and use of each proposed angle and the wind estimation techniques.

In the design of WPTPFC, a reference point called the perpendicular foot

is proposed for path-following control as an alternative to the closest point. Though the notion of perpendicular foot suffers from a similar singularity issue that the closest point has, it guarantees the continuity of solution with respect to the motion of the vehicle provided that the point does not reach some geometrical region, and it is shown that the region can be effectively avoided by the proposed singularity avoidance strategies. A Velocity Direction Input (VDI) and Steering Input (SI), which are common input configurations for mobile robots with nonzero moving speed, are considered the inputs of the control system. In particular, a special barrier function-based method called the Barrier Weighting Method (BWM) is developed to fully utilize the characteristics of the backstepping control for a certain class of constrained systems. Using the proposed technique, it is demonstrated that the velocity direction control law can be efficiently reused for the steering input control design preserving the singularity avoidance capability.

Finally, the flight control system and WPTPFC are unified based on the time-scale decomposition technique. The compatibility between the methods is investigated, and appropriate coordinate transformations and control allocation methods are developed. Numerical simulations are performed to demonstrate the effectiveness of the proposed control scheme.

Keywords: Flight Dynamics, Ambient Wind, Path-Following Control, Backstepping, Barrier Weighting

Student Number: 2013-23070

Contents

List of Tables

List of Figures

Chapter 1

Introduction

1.1 Motivation and Objective

1.1.1 Effects of Wind Shear on Aerial Vehicles

A few fatal accidents in aviation history later turned out to be attributed to a low-level wind shear such as microburst [1]. The influence of strong wind shear on aircraft is particularly hazardous in take-off and landing phases due to low airspeed and thrust [2]. An abrupt change in wind speed and direction can cause a severe decrease in the airspeed of an aircraft, which often leads to aircraft upset. In particular, the detrimental effect is greater on small-sized unmanned aerial vehicles (UAVs) whose airspeed is relatively less than that of manned aircraft, where the wind speed can reach 50 percent or more of the airspeed of the UAV during operation [3]. On the contrary, wind can be exploited to make an efficient flight. Several flight techniques make use of a steady wind shear formed by meteorological phenomena such as terrain-induced flow or atmospheric convection, where dynamic soaring and thermalling are

representative examples. By intentionally flying through the wind shear layers, an aerial vehicle can gain additional energy which consequently extends the overall flight time or raises the altitude using less thrust [4].

With regard to controller design, especially for fixed-wing aircraft, both the two foregoing opposite points of view on wind shear suggest that the flight control system should deliberately take the effects of wind into account. The stability and performance of a model-based control law are primarily determined by the fidelity of the equations of motion. In other words, the model should reflect the actual system as close as possible. However, a zero-wind or constant wind condition is often assumed for the flight dynamics in the literature [5, 6], which is not usually the case in the general aviation environment. The linearization technique is used under the assumption that the angle deviations due to wind are sufficiently small [7]. The performance of the flight control laws resorting to such an ideal situation can be largely degraded during a flight across a wind field and, consequently, the flight envelope must be limited to an extent. The issues particularly apply to fixed-wing-type aerial vehicles in which changes in the angle of attack due to turbulence critically affect the performance and stability, whereas multi-rotor-type vehicles are relatively easier to deal with the wind disturbance [8, 9].

Various robust control and adaptive control laws have been developed to handle the issue and they show a satisfactory performance allowing moderately bounded uncertainty or disturbance. However, the bounds were often determined based on the empirical data or subjective evaluation of the designers, and the wind was simply modeled and treated as an unstructured disturbance [10, 11]. In this case, large estimated bounds are inevitable in general. The approach essentially entails a problem that the controller gains or adaptation rate chosen based on the large disturbance bounds may result in somewhat

degraded transient response [12]. In contrast, as control system with an exact disturbance model does not suffer from large estimated bounds, the trade-off between the performance and the robustness of the closed-loop system can be mitigated. This stresses the need for a precise flight dynamics considering the wind effect.

1.1.2 Path-Following Control for Aerial Vehicles

The mobility of a mobile robot such as aerial, marine, automotive vehicle, and missile is often realized by making it accurately follow a predefined spatial trajectory or path, where a trajectory is a parametric curve whose parameter is a time variable. The motion control of robots is usually formalized as a trajectory tracking problem due to its relatively affordable difficulty in controller design whose primary goal is to drive a robot to track a trajectory [13]. Consequently, the temporal parametrization of the desired trajectory directly affects the performance of the tracking control. However, for some underactuated robots, designing a physically feasible timing law is not a trivial task [14–16]. Unpowered vehicles or powered vehicles without active speed controllers such as a glider or solid-propellant rocket are equipped only with steering actuators. For such vehicles, trajectory tracking can generate a command that a specific vehicle cannot comply with. In this case, path-following control (PFC) is a good alternative because the behavior of the reference point, a point that a vehicle is supposed to follow, is determined online by the motion of the vehicle [13, 17].

There exist numerous well-designed PFC schemes aimed at the effective utilization of fixed-wing aerial vehicles. However, fundamental shortcomings of existing works that motivated this study stem from the use of local reference frames and inverse trigonometric functions. Local reference frames built on the differential geometric properties of a path are not free from an inherent

singularity. The Frenet-Serret (FS) frame has been the most widely used for the parametric PFC [18–22], whose bases are determined by the derivatives of a regular path. As the definition implies, the frame has singular points where the curvature vanishes though many of the related works utilize it without justification. A few approaches resort to the FS frame constructed by sequential rotations from the world frame using inverse trigonometric functions [18,20,22, 23]. From a mathematical point of view, such a formulation cannot attain a global stability property.

The most important motivation for this study is the reference point for PFC. The closest point [18, 24–26] is a common reference favored in a vast amount of research because of its simple form and geometric advantages; it provides the fastest route that the maneuverable point can take to reach the desired path. However, it has an apparent limitation (usually not explicitly referred to in the literature) that it is mathematically allowed only for a straight-line path because, for general differentiable curves, the closest point is not unique, not even continuous respect to the motion of the maneuverable point, and finding the point involves numerical optimization that does not guarantee a global solution. Furthermore, there is a singularity where the closest point is indeterminate; the speed of the point diverges as the maneuverable point approaches the center of curvature of the path.

1.1.3 Unification of Flight Controller and PFC

Flight control generally refers to the tracking control of the vehicle's direction, and flight guidance is a higher-level control that determines the direction the vehicle should track to follow the designated path. They are referred to as dynamics-level and kinematics-level control, respectively. In this aspect, PFC can be classified as a guidance. A typical approach to this flight control and

guidance problem is to separate the design process treating each dynamics level as a subsystem of a cascaded system and to consolidate the individual control law under the time-scale decomposition principle [27, 28]. If the inner-loop dynamics is not sufficiently "faster" than the outer loop, the control problem is usually addressed by a more rigorous control scheme such as backstepping or sliding mode control [5, 6]. The advantages of these approaches include the inherent robustness and the ease in unifying the controllers for each subsystem. However, a few of the existing control approaches overlook some details of the problem by blurring the importance of the domain of interest. Some classical methods make use of the linearized or feedback-linearized model of the entire system and apply a robust and adaptive linear feedback controller. However, though the linear control system is well-understood, it sometimes ignores the characteristics of each subsystem and thus make it harder to interpret the performance in handling nonlinearity [7].

1.1.4 Study Objective

The objective of this study can be summarized as follows: First, the study carefully inspects the flight dynamics and path-following geometry. Then, corresponding high-performance control laws are designed and unified. Motivated by the aforementioned limitation of existing methods, the author aims not only for developing a practical solution for the PFC problem considering ambient wind shear but also for mathematically rigorous reasoning.

1.2 Literature Survey

1.2.1 Flight in Ambient Wind Shear

There have been several achievements regarding the development of equations of motion describing the three-dimensional relative motion of an aerial vehicle with respect to an unsteadily moving atmosphere (air mass). One of the most famous formulations was proposed by Frost and Bowles [29]. They introduced a total of three air-relative angles to describe the sequential rotations from the inertial frame to the wind frame: the air-relative roll angle, the air-relative flight path angle, and the air-relative course angle, where the latter two are together called the air-relative flight path angles. These angles concisely formulate the motion of the aircraft relative to the air mass, but none of them can be directly measured by existing sensors. Moreover, the inefficient angle transformation must be accompanied to apply the model to design a spatial trajectory tracking because the angles do not represent the motion relative to the inertial frame.

The inertial flight path angles, simply called the flight path angles, are defined to parametrize the direction of the inertial velocity. By using the flight path angles, the conventional aerodynamic roll angle in [30] is also defined to parametrize the rotation from the inertial velocity frame to the wind frame about the inertial velocity direction in the no-wind condition. The notion of the aerodynamic roll angle is quite useful for designing a trajectory tracking control law in that it provides an intuitive geometrical interpretation of the relation between aerodynamic forces and the spatial motion of the aircraft with respect to the inertial frame [5, 6]. However, the definition is valid only in the no-wind condition because the coordinate transformation can no longer be represented by a single rotation about the inertial velocity direction in wind conditions as the air-mass-relative velocity deviates away from the inertial velocity by the

ambient wind terms; therefore, it cannot be directly used under wind conditions without modification.

1.2.2 PFC for Aerial Vehicles

PFC methods can be classified into two major categories depending on whether the desired path (geometric curve) is parametric. A PFC law based on a parametric curve utilizes the curve parameter to determine a reference point to follow, whereas one based on a nonparametric curve describes the path as a set of spatial points. A vector-field-based PFC is a representative nonparametric PFC, whose desired path is described as a 1-manifold defined by a system of implicit equations consisting of differentiable path functions [16]. By using the gradient of the path functions, a vector field is designed to make the desired path (set) attractive. However, the performance of the method heavily depends on the design of the path functions, whose difficulty is practically manageable only for simple paths such as circles or straight lines. Therefore, the method is usually applied to simple planar paths [28]. Though some algorithms guarantee their effectiveness for general multidimensional smooth paths, the estimation of the region of attraction involves a tricky analysis of the critical points where the vector field degenerates [16,31,32]. Another drawback of the nonparametric PFC is that it does not allow self-intersecting paths [33].

Parametric PFC is usually preferred because it easily overcomes the foregoing drawbacks. The method is further divided into two subcategories by the way the reference point is defined: static and dynamic. A static reference refers to a point defined solely by the position of the maneuverable point (robot as a point mass) [18, 24–26, 34]. A few research took the closest point [18, 24–26] as a static reference due to its simplistic definition and ease of handling. On the other hand, a dynamic reference has the state and dynamics augmented to

the system that determines the behavior of the reference point, which can be utilized to eliminate the limitations [13, 20, 35, 36].

For many underactuated or nonholonomic mobile robots, insufficient control authority over traversing speed due to slow thrust dynamics or absence of pertaining actuators makes it more efficient for PFC laws to treat the speed as a measured exogenous signal rather than a state variable of the system. In this case, the speed is augmented as a constraint on the control system, and the steering force is applied in the normal direction to the velocity as usual in missile guidance [20,25,36,37]. Otherwise, the robot should be equipped with a thruster to actively control the speed, and a PFC law is then designed to make the speed of the maneuverable point approach the desired speed [13,15,21,22,26,33,38,39].

One of the most effective parametric PFC laws for mobile robots is the lookahead-based line-of-sight guidance method, extensively refined by Breivik and Fossen [20], which is pure pursuit of the lookahead point of a reference point [22–25]. The lookahead distance, not necessarily a constant, is the key design parameter of the method as it determines the trend of the transient response; thus, several variations of the method have been proposed regarding the design of the lookahead distance [25, 40]. There exist both static and dynamic reference versions of lookahead-based PFC. Particularly, the former, based on the closest point reference, shows a better smooth transient response admitting some singularity issue [24, 25].

1.3 Research Contribution

The main contributions of the dissertation are twofold: The derivation of a novel equations of motion for aerial vehicles and the development of a versatile PFC called WPTPFC.

1.3.1 Flight Dynamics

This dissertation proposes a novel nonlinear equations of motion for the three-dimensional flight dynamics, which models the effects of continuously differentiable time-varying ambient winds without approximation or linearization. The difference between the air-relative velocity and the inertial velocity caused by the wind component is parametrized by two angles of sequential rotation called the path-relative wind angles. Moreover, a generalized version of the aerodynamic roll angle is proposed to describe the rolling motion of the aerial vehicle in the presence of wind, which is identical to the definition of the conventional aerodynamic roll angle in the no-wind condition.

The formulation is particularly beneficial for trajectory tracking or path-following problems since it explicitly shows the geometrical relation between the forces exerted on the vehicle and the motion in the inertial frame. Another advantage of using the proposed equations of motion is that existing high-performance flight controllers initially developed by assuming no-wind condition can be easily reused for wind-conditioned environment while keeping their overall form. Therefore, the equations of motion help expand the fields of application of the conventional flight controllers by enabling them to deal with ambient winds. The equations of motion are applicable to any flight controllers that exploit the flight path angles and aerodynamic roll angle convention, which include [5, 6, 30, 41–43].

1.3.2 Weighted-Perpendicular-Tangent-based PFC

A parametric PFC law, called the weighted-perpendicular-tangent-based path-following control (WPTPFC), is proposed for three-dimensional regular paths. It is assumed that the speed profile of the maneuverable point is predetermined. Being continuously differentiable and having bounded locally Lipschitz derivatives are the only conditions required for the paths. A point called the perpendicular foot is selected as a dynamic reference point. A control law for the kinematics-level system that takes the velocity direction as input is designed first; the tangent vector of the path at the perpendicular foot, the perpendicular, and appropriate weighting functions are utilized to form the desired velocity direction. The design of a dynamics-level control law with steering input follows afterwards, where a backstepping-based approach is developed to reuse the kinematics-level control law. The proposed design consists of only vector operations that reject any use of local reference frames or angle-based geometry; thus, it can be applied to planar dynamical systems including ground or surface vehicles without modification. Moreover, the region of operation where the method guarantees the effectiveness of the PFC law, which is analogous to the region of attraction, is estimated through rigorous analysis.

The perpendicular foot concept leverages the idea of the closest point while addressing discontinuity by incorporating the path parameter into the system dynamics as a state; the formulation renders the system classified as the semi-explicit differential-algebraic equation of index 1 [44]. Because the definition of the point also entails the same singularity issue that the closest point has, corresponding reasonable singularity avoidance methods are presented; special attention has been paid to developing the set-invariance-based avoidance strategy [45, 46] handling the kinematics-level (geometric) singularity that occurs

when the maneuverable point reaches the line passing through the center of curvature of the path. In particular, the dynamics-level controller design is featured by a unique method called the Lyapunov barrier weighting for backstepping control developed to efficiently inherit the singularity avoidance designed for kinematics-level systems.

1.3.3 Summary

- The difference between the air-relative velocity and the inertial velocity caused by the wind component is parametrized by two angles of sequential rotation called the longitudinal and lateral *path-relative wind angles*.

- A generalized version of the *aerodynamic roll angle* is proposed to describe the rolling motion of the aerial vehicle in the presence of wind, which coincides with the definition of the conventional aerodynamic roll angle in the no-wind condition.

- Existing high-performance flight controllers initially developed by assuming no-wind condition can be easily reused for wind-conditioned environment while keeping their overall form by using the proposed equations of motion.

- A reference point called the perpendicular foot is proposed for PFC as an alternative to the closest point. Though the notion of perpendicular foot suffers from a similar singularity issue that the closest point has, it guarantees the continuity of solution with respect to the motion of the vehicle provided that the point does not reach some geometrical region, and it is shown that the region can be effectively avoided.

- A special barrier function based method called the Barrier Weighting

Method (BWM) is developed to fully utilize the characteristic of the back-stepping control for a certain class of constrained systems. It is shown that the velocity direction control law can be efficiently reused for the steering input control design preserving the singularity avoidance capability.

- After a flight control system based on the proposed equations of motion is designed, it is integrated with WPTPFC to form a unified control system. A subsystem of the flight control system is carefully selected to have a compatibility with the WPTPFC method in each input configuration, Velocity Direction Input (VDI) and Steering Input (SI), by using the nonlinear control allocation method.

1.4 Dissertation Organization

The dissertation is organized as follows:

Chapter 2 focuses on the flight dynamics in the presence of continuously differentiable ambient winds. In Section 2.1, the equations of motion are derived. In Section 2.2, the properties of the equations of motion and their possible applications as well as the ambient wind estimation techniques are discussed.

Chapter 3 deals with the design of flight control system. Sections 3.1 and 3.2 introduce preliminaries. A flight control system is developed by designing separate controllers for each subsystem of the flight dynamics by viewing it as a cascade system from Section 3.3 to 3.5. Section 3.6 demonstrates the performance of the flight controller and the usefulness of the proposed equations of motion.

Chapter 4 provides the essential theoretic bases for the development of WPTPFC. Section 4.1 summarizes the notation used in Chapter 4, and Section 4.2 presents the mathematical preliminary. Fundamental propositions about barrier-based methods for constrained systems are introduced in Section 4.3. Section 4.4 introduces the Lyapunov barrier weighting method for constrained systems.

Chapter 5 develops WPTPFC. Section 5.1 summarizes the notation, and the definition of the path-following problem is stated in Section 5.2. Sections 5.3 and 5.4 propose design strategies for PFC laws. In Section 5.5, the simulation results are given.

Chapter 6 deals with the unification of the flight control system and WPTPFC.

Finally, a summary of the dissertation is presented in Chapter 7.

Chapter 2

Flight Dynamics Considering Time-Varying Ambient Wind

This chapter derives the equations of motion of aerial vehicles in the differentiable time-varying wind shear. The equations of motion model the dynamics of angular velocity $\boldsymbol{\omega}$, aerodynamic roll angle μ, aerodynamic angles (angle of attack α and sideslip angle β), and flight-path angles (lateral flight-path angle χ and longitudinal γ). The main contribution of this chapter is the introduction of two angles called the path-relative wind angles χ_w and γ_w to incorporate the effect of ambient winds to the equations of motion. The equations of motion are structured by considering which states each dynamics is dominantly dependent on from a control design perspective. The practical aspects of the proposed equations of motion are discussed in depth later in this chapter.

2.1 Derivation of Equations of Motion

Let us introduce some notations for compact representation of the equations. $|\cdot|$ denotes the absolute value for scalars and the Euclidean norm for vectors. For an angle θ, the coordinate transformations pertaining to the right-handed rotation about each axis of the three-dimensional Cartesian coordinate system are represented by

$$\begin{aligned}
\mathbf{C}_x(\theta) &= \begin{bmatrix} 1 & 0 & 0 \\ 0 & \cos\theta & \sin\theta \\ 0 & -\sin\theta & \cos\theta \end{bmatrix}, \\
\mathbf{C}_y(\theta) &= \begin{bmatrix} \cos\theta & 0 & -\sin\theta \\ 0 & 1 & 0 \\ \sin\theta & 0 & \cos\theta \end{bmatrix}, \\
\mathbf{C}_z(\theta) &= \begin{bmatrix} \cos\theta & \sin\theta & 0 \\ -\sin\theta & \cos\theta & 0 \\ 0 & 0 & 1 \end{bmatrix}.
\end{aligned} \tag{2.1}$$

For $\mathbf{u} = [u_1\ u_2\ u_3]^\top \in \mathbb{R}^3$, the operator $[\cdot]_\times$ that maps a vector to a cross product matrix is represented by

$$[\mathbf{u}]_\times = \begin{bmatrix} 0 & -u_3 & u_2 \\ u_3 & 0 & -u_1 \\ -u_2 & u_1 & 0 \end{bmatrix}. \tag{2.2}$$

The function atan2 : $\left\{(y,x) \in \mathbb{R}^2 \;\middle|\; x \neq 0 \text{ or } y \neq 0\right\} \to \mathbb{R}$ is defined by

$$\operatorname{atan2}(y,x) = \begin{cases} \arctan(y/x), & x > 0 \\ \arctan(y/x) + \pi, & x < 0 \text{ and } y \geq 0 \\ \arctan(y/x) - \pi, & x < 0 \text{ and } y < 0 \\ \pi/2, & x = 0 \text{ and } y > 0 \\ -\pi/2, & x = 0 \text{ and } y < 0. \end{cases} \tag{2.3}$$

The physical vector and matrix notations are summarized in Table 2.1. In particular, $\mathbf{C}_{c/a} = \mathbf{C}_{c/b}\mathbf{C}_{b/a}$ and $\mathbf{C}_{b/a}^{-1} = \mathbf{C}_{b/a}^{\top} = \mathbf{C}_{a/b}$ for arbitrary coordinate system a, b, and c. The coordinate transformation matrices are used to change the coordinate system in which a physical vector is represented, i.e., $\mathbf{v}^b = \mathbf{C}_{b/a}\mathbf{v}^a$. On the other hand, $\boldsymbol{\omega}_{c/a} = \boldsymbol{\omega}_{c/b} + \boldsymbol{\omega}_{b/a}$ and $\boldsymbol{\omega}_{b/a} = -\boldsymbol{\omega}_{a/b}$ for arbitrary frames $\mathcal{F}_a$, $\mathcal{F}_b$, and $\mathcal{F}_c$. See [47, Chapter 1] for more detail of the properties of the vectors and transformation matrices.

Table 2.1: Vector and matrix notations

$\mathbf{p}_{A/B}$	=	position vector of point A with respect to point B
$\mathbf{v}_{A/i}$	=	velocity vector of point A in frame $\mathcal{F}_i$
${}^b\dot{\mathbf{v}}_{A/i}$	=	derivative of $\mathbf{v}_{A/i}$ taken in frame $\mathcal{F}_b$
$\mathbf{v}^c$	=	vector represented in coordinate system c
$\boldsymbol{\omega}_{b/a}$	=	angular velocity of $\mathcal{F}_b$ with respect to $\mathcal{F}_a$
$\mathbf{C}_{b/a}$	=	coordinate transformation matrix: from system a to system b

$\mathbf{i}_a$, $\mathbf{j}_a$, and $\mathbf{k}_a$ are right-handed orthonormal bases of the frame of reference $\mathcal{F}_a$. Without any subscript, they indicate the column vectors: $\mathbf{i} = [1\ 0\ 0]^{\top}$, $\mathbf{j} = [0\ 1\ 0]^{\top}$, and $\mathbf{k} = [0\ 0\ 1]^{\top}$; thus, $\mathbf{i}_a^a = \mathbf{i}$, $\mathbf{j}_a^a = \mathbf{j}$, and $\mathbf{k}_a^a = \mathbf{k}$ for any coordinate system a. The frames and the coordinate systems used in this study are summarized in Table. 2.2. Coordinate transformation matrices that represent

the rotations between some important coordinate systems are given as follows:

$$\begin{aligned} \mathbf{C}_{w/s} &= \mathbf{C}_z(\beta) \\ \mathbf{C}_{s/b} &= \mathbf{C}_y(-\alpha) \\ \mathbf{C}_{\sigma/i} &= \mathbf{C}_y(\gamma)\,\mathbf{C}_z(\chi), \end{aligned} \tag{2.4}$$

where β is the sideslip angle, α is the angle of attack, γ is the flight path angle (elevation), and χ is the course angle (azimuth). The coordinate transformations, for instance, can be use to derive the stability frame $\mathcal{F}_s$ by rotating the body frame $\mathcal{F}_b$ by $-\alpha$ about the y-axis of the body-fixed coordinate system $(\mathbf{j}_b)$ as shown in Fig. 2.1; thus, the angular velocity of $\mathcal{F}_s$ relative to $\mathcal{F}_b$ is $\boldsymbol{\omega}_{s/b} = -\dot{\alpha}\mathbf{j}_b$.[1] Note that $\mathbf{C}_{\sigma/i}$ is defined to indicate the direction of the inertial velocity, that is, $\mathbf{C}_{i/\sigma}\mathbf{i}_\sigma^\sigma = \mathbf{C}_{\sigma/i}^\top \mathbf{i}$ is the direction of flight represented in the coordinate system i. The rest of the relations are developed in the later part of this section. Function arguments will be often omitted throughout the dissertation for simplicity.

The state vector of the system is given by

$$\mathbf{x} = [P\ Q\ R\ \mu\ \beta\ \alpha\ \chi\ \gamma\ V_T\ p_N\ p_E\ p_D]^\top, \tag{2.5}$$

where P, Q, R are the roll, pitch, yaw rate in the body-fixed coordinate system b, μ is the aerodynamic roll angle, V_T is the airspeed, and p_N, p_E, p_D denote the position in the flat-earth-fixed coordinate system i. Formulation of the flight dynamics is carried out under the following assumptions:

Assumption 2.1.1: The aerodynamic force coefficient vector $\mathbf{C}_F = [-C_D\ C_Y\ -C_L]^\top$ and the moment coefficient vector $\mathbf{C}_M = [C_l\ C_m C_n]^\top$ of

[1] Because the coordinate systems s and b share the same y-axis, it follows that $\boldsymbol{\omega}_{s/b} = -\dot{\alpha}\mathbf{j}_b = -\dot{\alpha}\mathbf{j}_s$.

Table 2.2: Frames and Coordinate Systems

Frame of Reference	Coordinate System	Origin of Coordinate System
$\mathcal{F}_i$, inertial frame	i, flat-earth-fixed coordinate system North-East-Down configuration	point fixed to space, O
$\mathcal{F}_a$, air mass frame	a, air coordinate system	point fixed to air mass, W
$\mathcal{F}_b$, body frame	b, body-fixed coordinate system Forward-Starboard-Down configuration	center of mass, G
$\mathcal{F}_s$, stability frame	s, stability coordinate system	G
$\mathcal{F}_w$, wind frame	w, wind coordinate system	G
$\mathcal{F}_\sigma$, inertial velocity frame	σ, inertial velocity coordinate system	G

the vehicle are functions of the time t, the state $\mathbf{x}$, and the control surface deflection $\boldsymbol{\delta}$, i.e., $\mathbf{C}_F = \mathbf{C}_F(t, \mathbf{x}, \boldsymbol{\delta})$ and $\mathbf{C}_M = \mathbf{C}_M(t, \mathbf{x}, \boldsymbol{\delta})$, where C_D, C_Y, and C_L are the drag, sideforce (lateral force), and lift coefficient in wind coordinate system w, and C_l, C_m, and C_n are moment coefficients in the system b, respectively. This assumption can be easily relaxed by simple modification depending on the application; one can assume that the coefficients are general time-varying parameters such that $\mathbf{C}_F = \mathbf{C}_F(t)$ and $\mathbf{C}_M = \mathbf{C}_M(t)$.

Assumption 2.1.2: The center of mass of the vehicle is fixed to the origin of the body-fixed coordinate system. The whole airframe is assumed to be a rigid body; the mass m is constant.

Assumption 2.1.3: The flat-earth assumption is applied; the inertial velocity indicates the velocity of an aerial vehicle with respect to the ground.

Assumption 2.1.4: The ambient wind velocity $\mathbf{v}^i_{W/i} : [t_0,\ \infty) \to \mathbb{R}^3$ is continuously differentiable, and its derivative ${}^i\dot{\mathbf{v}}^i_{W/i}$ is denoted by $\mathbf{a}^i_{W/i}$. The air mass frame $\mathcal{F}_a$ is an imaginary frame defined by viewing the atmosphere as a rigid body as opposed to the real world property: The frame moves at the same velocity as the ambient wind measured at the center of mass of the vehicle, and the airframe does not influence the air flow [29]. Moreover, the frame does not rotate with respect to the inertial frame.

Assumption 2.1.5: The ambient wind speed is smaller than the airspeed of the aerial vehicle, that is,

$$\forall t \geq t_0 : \left|\mathbf{v}^i_{W/i}(t)\right| < V_T(t). \tag{2.6}$$

According to Assumption 2.1.5, the domain of the system is chosen as

$$\mathcal{D}_t = \left\{ \mathbf{x} \in \mathbb{R}^{12} \;\middle|\; |\beta| < 90^\circ,\ |\gamma| < 90^\circ,\ V_T > \left|\mathbf{v}^i_{W/i}(t)\right| \right\} \tag{2.7}$$

which is dependent on time t. For bounded ambient wind speeds, a static domain can be chosen instead; $V_T > \bar{w}$, where $\left|\mathbf{v}^i_{W/i}(t)\right| \leq \bar{w}$ for all $t \geq t_0$.

Remark 2.1.1: It is apparent from Assumption 2.1.5 that the airspeed V_T should be nonzero for the other state variables to be well-defined, and this requirement makes the proposed equation suitable for aerial vehicles with fixed lifting apparatus such as wings or fins including conventional fixed-wing aircraft or missiles that do not hover consistently. This constraint is inherently entailed by every equation of motion involving aerodynamic angles and should not be perceived as a limitation of the proposed model.

The key identity used in this study is the equation that represents the derivative of a vector observed in the other frame. For an arbitrary physical vector $\mathbf{u}$, and frames $\mathcal{F}_a$ and $\mathcal{F}_b$ moving in the relative angular velocity $\boldsymbol{\omega}_{b/a}$, it follows that

$${}^a\dot{\mathbf{u}} = {}^b\dot{\mathbf{u}} + \boldsymbol{\omega}_{b/a} \times \mathbf{u}. \tag{2.8}$$

If the coordinate system of a vector is attached to the frame where the derivative of the vector is taken, the vector derivative is composed of the very time-derivative of each component, that is, for any frame of reference $\mathcal{F}_a$ and the corresponding system a, $\mathbf{u}^a = [u_1\ u_2\ u_3]^\top$ implies ${}^a\dot{\mathbf{u}}^a = [\dot{u}_1\ \dot{u}_2\ \dot{u}_3]^\top$.

2.1.1 External Force and Moment

The force $\mathbf{F}$ exerted on the aircraft is composed of the aerodynamic force $\mathbf{F}_A$, the thrust $\mathbf{T}$, and the weight $m\mathbf{g}$, where m is the mass of the aircraft and $\mathbf{g}$

is the gravitational acceleration. The aerodynamics force is usually modeled as $\mathbf{F}_A^w = qS\mathbf{C}_F$, where $q = \rho V_T^2/2$ is the dynamic pressure, ρ is the air density, S is the wing area. The total force in the wind coordinate system w is then represented as

$$\mathbf{F}^w = \mathbf{F}_A^w + \mathbf{T}^w + m\mathbf{g}^w = qS\mathbf{C}_F + T\boldsymbol{\lambda} + m\mathbf{C}_{w/\sigma}\mathbf{C}_{\sigma/i}\mathbf{g}^i, \tag{2.9}$$

where T is the magnitude of thrust,

$$\begin{aligned}\boldsymbol{\lambda} &= \mathbf{C}_{w/b}\mathbf{C}_y\left(-\alpha_T\right)\mathbf{i} = \mathbf{C}_{w/s}\mathbf{C}_{s/b}\mathbf{C}_y\left(-\alpha_T\right)\mathbf{i} \\ &= \mathbf{C}_z\left(\beta\right)\mathbf{C}_y\left(-(\alpha+\alpha_T)\right)\mathbf{i} \\ &= \left[\cos\bar{\alpha}\cos\beta \;\; -\cos\bar{\alpha}\sin\beta \;\; -\sin\bar{\alpha}\right]^\top\end{aligned}$$

is the direction of thrust represented in the wind coordinate system, $\bar{\alpha} = \alpha + \alpha_T$, and α_T is the longitudinal angle between thrust and the reference line (x-axis) of the vehicle. $\mathbf{C}_{w/\sigma}$ is the most important matrix that motivated this study, which accounts for the relation between the vehicle's inertial motion and relative motion with respect to the air mass. $\mathbf{C}_{w/\sigma}$ and its transpose are used throughout the dissertation and their components will be developed in Section 2.1.7.

The moment $\mathbf{M}$ exerted on the aircraft is composed of the aerodynamic moment $\mathbf{M}_A$ and the moment due to the thrust $\mathbf{M}_T$ as a function of T. The aerodynamic moment is modeled as $\mathbf{M}_A^b = qS\mathbf{B}\mathbf{C}_M$, where $\mathbf{B} = \mathrm{diag}\left(b_s, \bar{c}, b_s\right)$, b_s is the wing span, and $\bar{c}$ is the mean aerodynamic chord. The total moment in the body-fixed coordinate system b can be represented as

$$\mathbf{M}^b = \mathbf{M}_A^b + \mathbf{M}_T^b = qS\mathbf{B}\mathbf{C}_M + \mathbf{M}_T^b, \tag{2.10}$$

2.1.2 Angular Velocity Dynamics

The dynamics of the angular velocity $\boldsymbol{\omega}$ is directly obtained from the Newton-Euler equation as [47, Ch. 1]

$$\dot{\boldsymbol{\omega}} = \mathbf{J}^{-1}\left\{\mathbf{M}^b - \boldsymbol{\omega} \times (\mathbf{J}\boldsymbol{\omega})\right\}, \tag{2.11}$$

where $\boldsymbol{\omega} = \boldsymbol{\omega}^b_{b/i} = [P\ Q\ R]^\top$ is the angular velocity and $\mathbf{J}$ is the moment of inertia of the aircraft. Equation (2.11) can be structured as follows:

$$\dot{\boldsymbol{\omega}} = \mathbf{f}_\omega(\boldsymbol{\omega}, T) + \mathbf{g}_\omega(t, \mathbf{x}, \boldsymbol{\delta}), \tag{2.12}$$

where

$$\mathbf{f}_\omega(\boldsymbol{\omega}, T) = \mathbf{J}^{-1}\left\{\mathbf{M}^b_T - \boldsymbol{\omega} \times (\mathbf{J}\boldsymbol{\omega})\right\} \tag{2.13a}$$

$$\mathbf{g}_\omega(t, \mathbf{x}, \boldsymbol{\delta}) = qS\mathbf{J}^{-1}\mathbf{B}\mathbf{C}_M. \tag{2.13b}$$

2.1.3 Aerodynamic Angle Dynamics

The air-relative velocity $\mathbf{v}_r := \mathbf{v}_{G/a}$, the inertial velocity $\mathbf{v} := \mathbf{v}_{G/i}$, and the wind velocity $\mathbf{v}_{W/i}$ have the following relation, called the *wind triangle*:

$$\mathbf{v}_r = \mathbf{v} - \mathbf{v}_{W/i}. \tag{2.14}$$

Note that $\mathbf{v}_r = V_T\mathbf{i}_w$ and $\mathbf{v} = \overline{V}_T\mathbf{i}_\sigma$; thus, $V_T = |\mathbf{v}_r|$ and $\overline{V}_T = |\mathbf{v}|$, where $\overline{V}_T$ is the ground speed. The air-relative velocity is the velocity of the center of mass with respect to the air mass, and the inertial velocity is with respect to the ground. The aerodynamic angles are defined by

$$\beta = \arcsin\frac{V_r}{V_T},\ \ \alpha = \operatorname{atan2}(W_r, U_r), \tag{2.15}$$

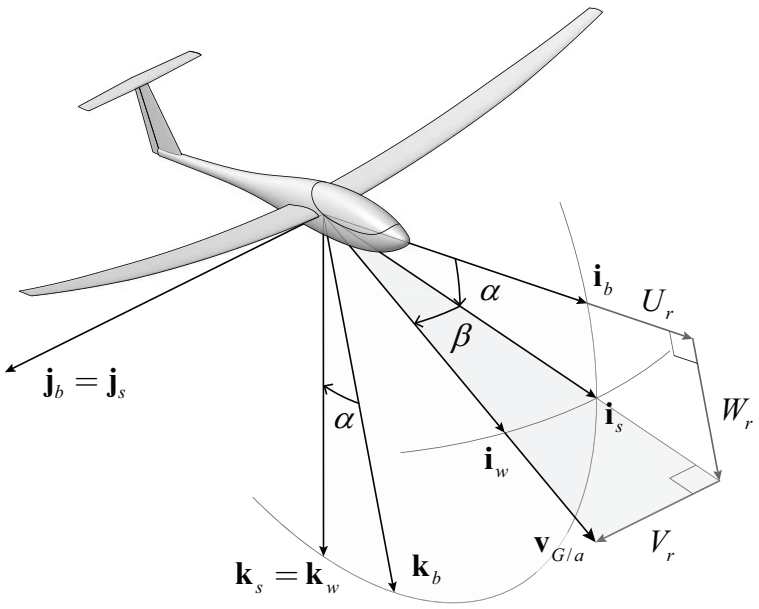

Figure 2.1: Geometry of wind axes

where $\mathbf{v}_r^b = [U_r \; V_r \; W_r]^\top$. Figure 2.1 shows the geometry of the aerodynamic angles and the components of the air-relative velocity in the body-fixed coordinate system.

The aerodynamic angle dynamics can be derived from Newton's second law of motion $m^i\dot{\mathbf{v}} = \mathbf{F}$ [47, Ch. 2]:

$$^i\dot{\mathbf{v}} = {}^i\dot{\mathbf{v}}_r + {}^i\dot{\mathbf{v}}_{W/i} = {}^w\dot{\mathbf{v}}_r + \boldsymbol{\omega}_{w/i} \times \mathbf{v}_r + \mathbf{a}_{W/i} = \frac{\mathbf{F}}{m}, \tag{2.16}$$

where $\mathbf{a}_{W/i} = {}^i\dot{\mathbf{v}}_{W/i}$ is the acceleration of the air mass. By using the relation $\boldsymbol{\omega}_{w/i} = \boldsymbol{\omega}_{w/b} + \boldsymbol{\omega}_{b/i}$, Eq. (2.16) can be rearranged as

$$^w\dot{\mathbf{v}}_r + \boldsymbol{\omega}_{w/b} \times \mathbf{v}_r = \frac{\mathbf{F}}{m} - \boldsymbol{\omega}_{b/i} \times \mathbf{v}_r - \mathbf{a}_{W/i}. \tag{2.17}$$

In the wind coordinate system, the vector components of the left-hand side of

Eq. (2.17) are

$$ {}^{w}\dot{\mathbf{v}}_r^w + \boldsymbol{\omega}_{w/b}^w \times \mathbf{v}_r^w = \begin{bmatrix} \dot{V}_T \\ 0 \\ 0 \end{bmatrix} + \begin{bmatrix} -\dot{\alpha}\sin\beta \\ -\dot{\alpha}\cos\beta \\ \dot{\beta} \end{bmatrix} \times \begin{bmatrix} V_T \\ 0 \\ 0 \end{bmatrix} = \boldsymbol{\Lambda}_a \begin{bmatrix} \dot{V}_T \\ \dot{\beta} \\ \dot{\alpha} \end{bmatrix}, \tag{2.18} $$

where $\boldsymbol{\Lambda}_a = \mathrm{diag}\,(1, V_T, V_T\cos\beta)$, $\mathbf{v}_r^w = V_T\mathbf{i}_w^w = V_T\mathbf{i}$, and

$$ \begin{aligned} \boldsymbol{\omega}_{w/b}^w &= \boldsymbol{\omega}_{w/s}^w + \boldsymbol{\omega}_{s/b}^w = \boldsymbol{\omega}_{w/s}^w + \mathbf{C}_{w/s}\boldsymbol{\omega}_{s/b}^s \\ &= \dot{\beta}\mathbf{k} + \mathbf{C}_z\,(\beta)\,(-\dot{\alpha}\mathbf{j}) \\ &= \begin{bmatrix} 0 \\ 0 \\ \dot{\beta} \end{bmatrix} + \begin{bmatrix} \cos\beta & \sin\beta & 0 \\ -\sin\beta & \cos\beta & 0 \\ 0 & 0 & 1 \end{bmatrix} \begin{bmatrix} 0 \\ -\dot{\alpha} \\ 0 \end{bmatrix} = \begin{bmatrix} -\dot{\alpha}\sin\beta \\ -\dot{\alpha}\cos\beta \\ \dot{\beta} \end{bmatrix}. \end{aligned} \tag{2.19} $$

Then, it follows that

$$ \begin{aligned} \begin{bmatrix} \dot{V}_T & \dot{\beta} & \dot{\alpha} \end{bmatrix}^\top &= \boldsymbol{\Lambda}_a^{-1}\left(\frac{\mathbf{F}^w}{m} - \boldsymbol{\omega}_{b/i}^w \times \mathbf{v}_r^w - \mathbf{a}_{W/i}^w\right) \\ &= \boldsymbol{\Lambda}_a^{-1}\boldsymbol{\tau}_w + \boldsymbol{\Lambda}_a^{-1}\left[\mathbf{v}_r^w\right]_\times \mathbf{C}_{w/b}\boldsymbol{\omega}, \end{aligned} \tag{2.20} $$

where $\boldsymbol{\omega}_{b/i}^w \times \mathbf{v}_r^w = -\left[\mathbf{v}_r^w\right]_\times \mathbf{C}_{w/b}\boldsymbol{\omega}$, $\mathbf{C}_{w/b} = \mathbf{C}_{w/s}\mathbf{C}_{s/b}$, and

$$ \boldsymbol{\tau}_w = \frac{\mathbf{F}^w}{m} - \mathbf{C}_{w/i}\mathbf{a}_{W/i}^i. \tag{2.21} $$

[2]

The dynamics of the aerodynamics angles $\boldsymbol{\xi}_a = [\beta\ \alpha]^\top$ can be extracted from Eq. (2.20) as

$$ \dot{\boldsymbol{\xi}}_a = [\mathbf{j}\ \mathbf{k}]^\top \begin{bmatrix} \dot{V}_T & \dot{\beta} & \dot{\alpha} \end{bmatrix}^\top = \mathbf{f}_a\,(t, \mathbf{x}, \boldsymbol{\delta}, T) + \mathbf{G}_a\,(\boldsymbol{\xi}_a)\,\boldsymbol{\omega}, \tag{2.22} $$

[2]The measurement of the ambient wind $\mathbf{v}_{W/i}$ or its derivative $\mathbf{a}_{W/i}$ is usually given in the flat-earth-fixed coordinate system i. Therefore, the ambient wind will always be transformed from the system i; for instance, $\mathbf{C}_{\sigma/i}\mathbf{v}_{W/i}^i$ represents the ambient wind in the inertial velocity coordinate system $\mathbf{v}_{W/i}^\sigma$.

where

$$\mathbf{f}_a\left(t,\mathbf{x},\boldsymbol{\delta},T\right)=\left[\mathbf{j}\ \mathbf{k}\right]^\top\boldsymbol{\Lambda}_a^{-1}\boldsymbol{\tau}_w=\frac{1}{V_T}\begin{bmatrix}0&1&0\\0&0&1/\cos\beta\end{bmatrix}\boldsymbol{\tau}_w \tag{2.23a}$$

$$\begin{aligned}\mathbf{G}_a\left(\boldsymbol{\xi}_a\right)&=\left[\mathbf{j}\ \mathbf{k}\right]^\top\boldsymbol{\Lambda}_a^{-1}\left[\mathbf{v}_r^w\right]_\times\mathbf{C}_{w/b}\\&=\begin{bmatrix}\sin\alpha&0&-\cos\alpha\\-\cos\alpha\tan\beta&1&-\sin\alpha\tan\beta\end{bmatrix}.\end{aligned} \tag{2.23b}$$

2.1.4 Flight Path Angle Dynamics

The flight path angles are defined by

$$\chi=\operatorname{atan2}\left(V_E,V_N\right),\ \gamma=-\arcsin\frac{V_D}{\overline{V}_T} \tag{2.24}$$

where $\mathbf{v}^i=\left[V_N\ V_E\ V_D\right]^\top$. Applying Newton's second law of motion yields

$${}^i\dot{\mathbf{v}}={}^\sigma\dot{\mathbf{v}}+\boldsymbol{\omega}_{\sigma/i}\times\mathbf{v}=\frac{\mathbf{F}}{m} \tag{2.25}$$

The left-hand side of Eq. (2.25) in the inertial velocity coordinate system σ can be written as follows:

$${}^\sigma\dot{\mathbf{v}}^\sigma+\boldsymbol{\omega}_{\sigma/i}^\sigma\times\mathbf{v}^\sigma=\begin{bmatrix}\dot{\overline{V}}_T\\0\\0\end{bmatrix}+\begin{bmatrix}-\dot{\chi}\sin\gamma\\\dot{\gamma}\\\dot{\chi}\cos\gamma\end{bmatrix}\times\begin{bmatrix}\overline{V}_T\\0\\0\end{bmatrix}=\boldsymbol{\Lambda}_f\begin{bmatrix}\dot{\overline{V}}_T\\\dot{\chi}\\\dot{\gamma}\end{bmatrix} \tag{2.26}$$

where $\boldsymbol{\Lambda}_f=\operatorname{diag}\left(1,\overline{V}_T\cos\gamma,-\overline{V}_T\right)$, $\mathbf{v}^\sigma=\overline{V}_T\mathbf{i}$, and

$$\begin{aligned}\boldsymbol{\omega}_{\sigma/i}^\sigma&=\dot{\gamma}\mathbf{j}+\mathbf{C}_y\left(\gamma\right)\left(\dot{\chi}\mathbf{k}\right)\\&=\begin{bmatrix}0\\\dot{\gamma}\\0\end{bmatrix}+\begin{bmatrix}\cos\gamma&0&-\sin\gamma\\0&1&0\\\sin\gamma&0&\cos\gamma\end{bmatrix}\begin{bmatrix}0\\0\\\dot{\chi}\end{bmatrix}=\begin{bmatrix}-\dot{\chi}\sin\gamma\\\dot{\gamma}\\\dot{\chi}\cos\gamma\end{bmatrix}\end{aligned} \tag{2.27}$$

Therefore, we have

$$\begin{aligned}\left[\dot{\overline{V}}_T \ \dot{\chi} \ \dot{\gamma}\right]^\top &= \frac{1}{m}\mathbf{\Lambda}_f^{-1}\mathbf{C}_{\sigma/w}\mathbf{F}^w \\ &= \mathbf{\Lambda}_f^{-1}\mathbf{C}_{\sigma/i}\mathbf{g}^i + \frac{1}{m}\mathbf{\Lambda}_f^{-1}\mathbf{C}_{\sigma/w}\left(T\boldsymbol{\lambda} + qS\mathbf{C}_F\right)\end{aligned} \tag{2.28}$$

The dynamics of the flight path angle $\boldsymbol{\xi}_f = [\chi \ \gamma]^\top$ can be extracted from Eq. (2.28) as

$$\begin{aligned}\dot{\boldsymbol{\xi}}_f &= [\mathbf{j} \ \mathbf{k}]^\top \left[\dot{\overline{V}}_T \ \dot{\chi} \ \dot{\gamma}\right]^\top \\ &= \mathbf{f}_f\left(t, V_T, \boldsymbol{\xi}_f\right) + \mathbf{G}_f\left(t, \mathbf{x}\right)\boldsymbol{\eta}_f\left(t, \mathbf{x}, \boldsymbol{\delta}\right)\end{aligned} \tag{2.29}$$

where

$$\mathbf{f}_f\left(t, V_T, \boldsymbol{\xi}_f\right) = [\mathbf{j} \ \mathbf{k}]^\top \mathbf{\Lambda}_f^{-1}\mathbf{C}_{\sigma/i}\mathbf{g}^i = -\frac{g}{\overline{V}_T}\begin{bmatrix} 0 \\ \cos\gamma \end{bmatrix} \tag{2.30a}$$

$$\mathbf{G}_f\left(t, V_T, \boldsymbol{\xi}_f\right) = \frac{1}{m}[\mathbf{j} \ \mathbf{k}]^\top \mathbf{\Lambda}_f^{-1}[\mathbf{j} \ \mathbf{k}] = \frac{1}{m\overline{V}_T}\begin{bmatrix} 1/\cos\gamma & 0 \\ 0 & -1 \end{bmatrix} \tag{2.30b}$$

$$\boldsymbol{\eta}_f\left(t, \mathbf{x}, \boldsymbol{\delta}, T\right) = [\mathbf{j} \ \mathbf{k}]^\top \mathbf{C}_{\sigma/w}\left(T\boldsymbol{\lambda} + qS\mathbf{C}_F\right), \tag{2.30c}$$

where $\mathbf{g}^i = [0 \ 0 \ g]^\top$.

2.1.5 Airspeed Dynamics

The dynamics of the airspeed V_T can be extracted from Eq. (2.20) as

$$\begin{aligned}\dot{V}_T &= \mathbf{i}^\top\left[\dot{V}_T \ \dot{\beta} \ \dot{\alpha}\right]^\top \\ &= \mathbf{i}^\top\mathbf{\Lambda}_a^{-1}\boldsymbol{\tau}_w + \mathbf{i}^\top\mathbf{\Lambda}_a^{-1}\left[\mathbf{v}_r^w\right]_\times \mathbf{C}_{w/b}\boldsymbol{\omega} = \mathbf{i}^\top\boldsymbol{\tau}_w,\end{aligned} \tag{2.31}$$

where the identity $\mathbf{i}^\top\mathbf{\Lambda}_a^{-1}\left[\mathbf{v}_r^w\right]_\times = V_T\mathbf{i}^\top[\mathbf{i}]_\times = \mathbf{0}$ is applied. As a result, Eq. (2.31) can be structured as follows:

$$\dot{V}_T = f_V\left(t, \mathbf{x}, \boldsymbol{\delta}\right) + g_V\left(\boldsymbol{\xi}_a\right)T, \tag{2.32}$$

where

$$f_V(t, \mathbf{x}, \boldsymbol{\delta}) = \frac{qS}{m}\mathbf{i}^\top \mathbf{C}_F - \mathbf{i}^\top \mathbf{C}_{w/i}\mathbf{a}^i_{W/i} + g\mathbf{i}^\top \mathbf{C}_{w/\sigma}\mathbf{C}_{\sigma/i}\mathbf{k} \tag{2.33a}$$

$$g_V(\boldsymbol{\xi}_a) = \frac{1}{m}\mathbf{i}^\top \boldsymbol{\lambda} = \frac{1}{m}\cos\bar{\alpha}\cos\beta. \tag{2.33b}$$

2.1.6 Ground Speed Dynamics

Though the ground speed is not a state variable of the system, that is, $\overline{V}_T = \overline{V}_T\left(t, V_T, \boldsymbol{\xi}_f\right)$ by Eq. (2.14), its equation of motion is presented because it is useful for motion control problems such as path-following. The dynamics of the ground speed $\overline{V}_T$ can be extracted from Eq. (2.28) as follows:

$$\begin{aligned}\dot{\overline{V}}_T &= \mathbf{i}^\top \left[\dot{\overline{V}}_T \;\; \dot{\chi} \;\; \dot{\gamma}\right]^\top = \frac{1}{m}\mathbf{i}^\top \boldsymbol{\Lambda}_f^{-1}\mathbf{C}_{\sigma/w}\mathbf{F}^w \\ &= \frac{1}{m}\mathbf{i}^\top \mathbf{C}_{\sigma/w}\left(qS\mathbf{C}_F + T\boldsymbol{\lambda}\right) + \mathbf{i}^\top \mathbf{g}^\sigma \\ &= f_{\overline{V}}(t, \mathbf{x}, \boldsymbol{\delta}) + g_{\overline{V}}(t, \mathbf{x})\, T,\end{aligned} \tag{2.34}$$

where

$$f_{\overline{V}}(t, \mathbf{x}, \boldsymbol{\delta}) = \frac{qS}{m}\mathbf{i}^\top \mathbf{C}_{\sigma/w}\mathbf{C}_F + \mathbf{i}^\top \mathbf{C}_{\sigma/i}\mathbf{g}^i \tag{2.35a}$$

$$g_{\overline{V}}(t, \mathbf{x}) = \frac{1}{m}\mathbf{i}^\top \mathbf{C}_{\sigma/w}\boldsymbol{\lambda}. \tag{2.35b}$$

Remark 2.1.2: For zero ambient wind speeds, i.e., $\mathbf{v}_{W/i}(t) \equiv \mathbf{0}$, $f_{\overline{V}}$ and $g_{\overline{V}}$ should coincide with f_V and g_V in Eq. (2.32), respectively. This property can be easily derived from the structure of $\mathbf{C}_{w/\sigma}$ defined in Section 2.1.7, by which $\mathbf{i}^\top \mathbf{C}_{w/\sigma} = \mathbf{i}^\top \mathbf{C}_{\sigma/w} = \mathbf{i}$ given that $\mathbf{v}_{W/i} \equiv 0$.

On the other hand, the position can be obtained by the following kinematical

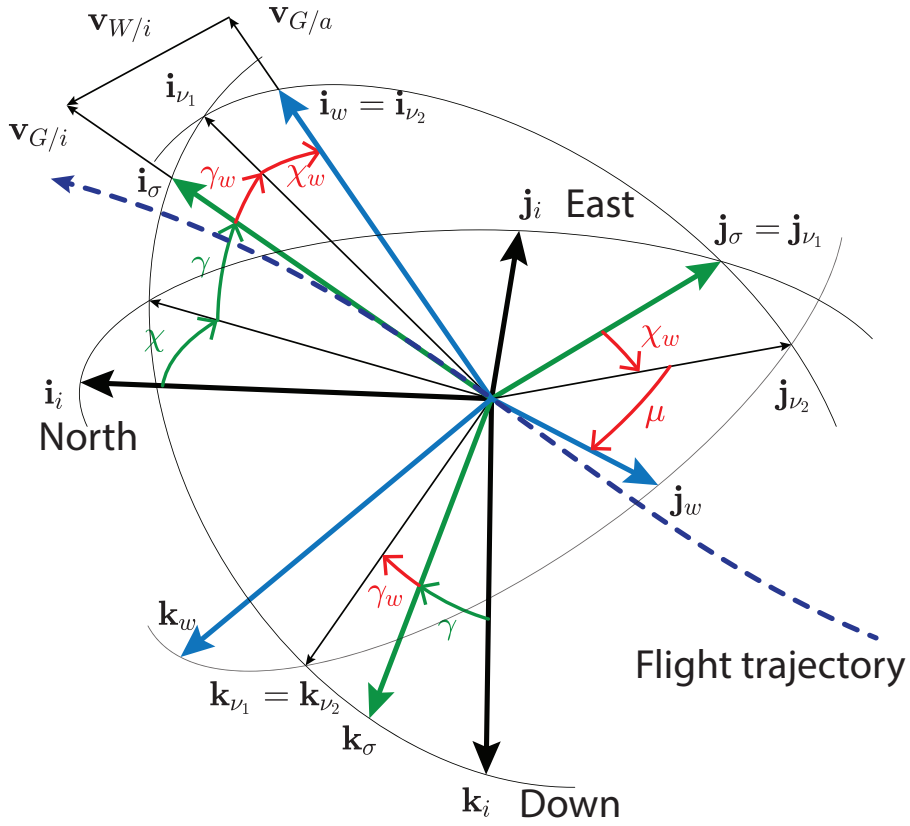

Figure 2.2: Geometry of path-relative wind angles

equation:

$$\dot{\mathbf{p}} = \mathbf{v}^i = \mathbf{C}_{i/\sigma}\mathbf{v}^\sigma = \mathbf{C}_{\sigma/i}^\top\left(\overline{V}_T\mathbf{i}\right) = \overline{V}_T\begin{bmatrix}\cos\chi\cos\gamma\\ \sin\chi\cos\gamma\\ -\sin\gamma\end{bmatrix}, \tag{2.36}$$

where $\mathbf{p} = [p_N\ p_E\ p_D]^\top$.

2.1.7 Aerodynamic Roll Angle Dynamics

To formulate the relation between the wind frame $\mathcal{F}_w$ and the inertial velocity frame $\mathcal{F}_\sigma$, several angles and frames are introduced: the path-relative wind

angles χ_w and γ_w, the aerodynamic roll angle μ, and the intermediate frames $\mathcal{F}_{\nu_1}$ and $\mathcal{F}_{\nu_2}$. They are defined to describe the sequential rotations from $\mathcal{F}_\sigma$ to $\mathcal{F}_w$ as shown in Fig. 2.2. Note that $\mathbf{i}_\sigma$, $\mathbf{i}_{\nu_1}$, $\mathbf{k}_i$, $\mathbf{k}_\sigma$, $\mathbf{k}_{\nu_1}$, and $\mathbf{k}_{\nu_2}$ lie on the same plane. The path-relative wind angles are restricted to have the following range:

$$|\chi_w| < 90^\circ, \ |\gamma_w| < 90^\circ. \tag{2.37}$$

Definition of longitudinal path-relative wind angle γ_w

Let $\mathcal{F}_{\nu_1}$ be the frame defined by the right-handed rotation of the frame $\mathcal{F}_\sigma$ about the vector $\mathbf{j}_\sigma$ so that $\mathbf{k}_{\nu_1}$ is perpendicular to $\mathbf{i}_w$:

$$\mathbf{k}_{\nu_1} = \frac{\mathbf{i}_w \times \mathbf{j}_\sigma}{|\mathbf{i}_w \times \mathbf{j}_\sigma|}. \tag{2.38}$$

The rotation angle γ_w, called the *longitudinal path-relative wind angle*, is represented by $\mathbf{k}_\sigma \times \mathbf{k}_{\nu_1} = \sin\gamma_w \mathbf{j}_\sigma$; therefore,

$$\begin{aligned} \sin\gamma_w &= \mathbf{j}_\sigma \cdot (\mathbf{k}_\sigma \times \mathbf{k}_{\nu_1}) = \mathbf{k}_{\nu_1} \cdot (\mathbf{j}_\sigma \times \mathbf{k}_\sigma) = \mathbf{k}_{\nu_1} \cdot \mathbf{i}_\sigma \\ &= \frac{1}{|\mathbf{i}_w \times \mathbf{j}_\sigma|} (\mathbf{i}_w \times \mathbf{j}_\sigma) \cdot \mathbf{i}_\sigma = -\frac{\mathbf{i}_w \cdot \mathbf{k}_\sigma}{|\mathbf{i}_w \times \mathbf{j}_\sigma|} \\ &= -\frac{\mathbf{i}_w \cdot \mathbf{k}_\sigma}{\sqrt{1 - (\mathbf{i}_w \cdot \mathbf{j}_\sigma)^2}}. \end{aligned} \tag{2.39}$$

Definition of lateral path-relative wind angle χ_w

Since both $\mathbf{i}_{\nu_1}$ and $\mathbf{i}_w$ are perpendicular to $\mathbf{k}_{\nu_1}$, $\mathbf{i}_{\nu_1}$ can be made identical to $\mathbf{i}_w$ by a single right-handed rotation about the vector $\mathbf{k}_{\nu_1}$; let $\mathcal{F}_{\nu_2}$ be the frame defined by the foregoing rotation of the frame $\mathcal{F}_{\nu_1}$. The rotation angle χ_w, called the *lateral path-relative wind angle*, is represented by $\mathbf{i}_{\nu_1} \times \mathbf{i}_w = \sin\chi_w \mathbf{k}_{\nu_1}$. Thus,

$$\begin{aligned} \sin\chi_w &= \mathbf{k}_{\nu_1} \cdot (\mathbf{i}_{\nu_1} \times \mathbf{i}_w) = \mathbf{i}_w \cdot (\mathbf{k}_{\nu_1} \times \mathbf{i}_{\nu_1}) \\ &= \mathbf{i}_w \cdot \mathbf{j}_{\nu_1} = \mathbf{i}_w \cdot \mathbf{j}_\sigma. \end{aligned} \tag{2.40}$$

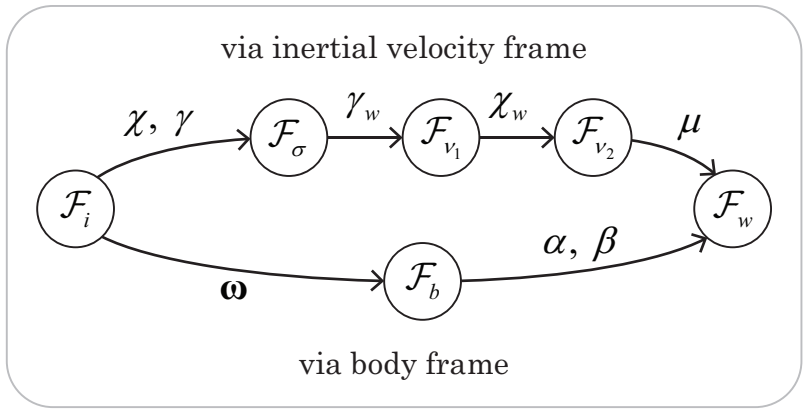

Figure 2.3: Rotations from $\mathcal{F}_i$ to $\mathcal{F}_w$

Substituting Eq. (2.40) into Eq. (2.39) yields

$$\sin\gamma_w = -\frac{\mathbf{i}_w \cdot \mathbf{k}_\sigma}{\cos\chi_w}. \tag{2.41}$$

Finally, $\chi_w = \arcsin(\mathbf{i}_w \cdot \mathbf{j}_\sigma)$ and $\gamma_w = -\arcsin(\mathbf{i}_w \cdot \mathbf{k}_\sigma / \cos\chi_w)$ are obtained.

Definition of aerodynamic roll angle μ

By the above two sequential rotations, $\mathbf{i}_{\nu_2} = \mathbf{i}_w$ is obtained; thus, the frames $\mathcal{F}_{\nu_2}$ and $\mathcal{F}_w$ differ by only a single right-handed rotation about $\mathbf{i}_w$. This raises the definition of the *aerodynamic roll angle* μ, which can be represented by $\mathbf{j}_{\nu_2} \times \mathbf{j}_w = \sin\mu\mathbf{i}_w$ and $\cos\mu = \mathbf{j}_w \cdot \mathbf{j}_{\nu_2}$. The value of $\sin\mu$ can be obtained by

$$\sin\mu = \mathbf{i}_w \cdot (\mathbf{j}_{\nu_2} \times \mathbf{j}_w) = -(\mathbf{i}_w \times \mathbf{j}_w) \cdot \mathbf{j}_{\nu_2} = -\mathbf{k}_w \cdot \mathbf{j}_{\nu_2}, \tag{2.42}$$

which gives $\mu = \text{atan2}(-\mathbf{k}_w \cdot \mathbf{j}_{\nu_2},\ \mathbf{j}_w \cdot \mathbf{j}_{\nu_2})$.

Time-derivative of Aerodynamic Roll Angle

There are two distinct ways to describe the sequential rotations from the inertial frame to the wind frame as shown in Fig. 2.3, where the rotation angles are written above the arrows, while the angular velocities are written below them. In

particular, the rotation from the inertial frame to the body frame is represented by the angular velocity, which is integrated to be orientation parameters such as quaternion or Euler angles.

The two representations provide an expedient way to derive the dynamics of the aerodynamic roll angle μ. The angular velocity of $\mathcal{F}_w$ with respect to $\mathcal{F}_i$ can be obtained either by $\boldsymbol{\omega}_{w/i} = \dot{\mu}\mathbf{i}_w + \dot{\chi}_w\mathbf{k}_{\nu_2} + \dot{\gamma}_w\mathbf{j}_{\nu_1} + \dot{\gamma}\mathbf{j}_\sigma + \dot{\chi}\mathbf{k}_i$ or by $\boldsymbol{\omega}_{w/i} = \boldsymbol{\omega}_{w/b} + \boldsymbol{\omega}_{b/i}$. Equating the two representations of the angular velocity in the wind coordinate system yields

$$\begin{aligned}\boldsymbol{\omega}_{w/i}^{w} &= \dot{\mu}\mathbf{i} + \dot{\chi}_w\mathbf{C}_{w/\nu_2}\mathbf{k} + (\dot{\gamma}_w + \dot{\gamma})\,\mathbf{C}_{w/\sigma}\mathbf{j} + \dot{\chi}\mathbf{C}_{w/i}\mathbf{k} \\ &= \mathbf{C}_{w/b}\boldsymbol{\omega} + \boldsymbol{\omega}_{w/b}^{w},\end{aligned} \tag{2.43}$$

where the coordinate transformation matrices defined by the path-relative wind angles and aerodynamic roll angle have the following relation:

$$\mathbf{C}_{w/\sigma} = \mathbf{C}_\mu\mathbf{C}_{\chi_w}\mathbf{C}_{\gamma_w}, \tag{2.44}$$

where

$$\begin{aligned}\mathbf{C}_\mu &:= \mathbf{C}_{w/\nu_2} = \mathbf{C}_x\left(\mu\right) \\ \mathbf{C}_{\chi_w} &:= \mathbf{C}_{\nu_2/\nu_1} = \mathbf{C}_z\left(\chi_w\right) \\ \mathbf{C}_{\gamma_w} &:= \mathbf{C}_{\nu_1/\sigma} = \mathbf{C}_y\left(\gamma_w\right)\end{aligned}$$

To expand $\boldsymbol{\omega}_{w/b}^{w}$ in Eq. (2.43), recall Eqs. (2.19) and (2.22) to get

$$\begin{aligned}\boldsymbol{\omega}_{w/b}^{w} &= \begin{bmatrix} 0 & -\sin\beta \\ 0 & -\cos\beta \\ 1 & 0 \end{bmatrix}\dot{\boldsymbol{\xi}}_a = \begin{bmatrix} 0 & -\sin\beta \\ 0 & -\cos\beta \\ 1 & 0 \end{bmatrix}\left(\mathbf{f}_a\left(t, \mathbf{x}, \boldsymbol{\delta}, T\right) + \mathbf{G}_a\left(\boldsymbol{\xi}_a\right)\boldsymbol{\omega}\right) \\ &= \mathbf{F}_1\boldsymbol{\tau}_w + \mathbf{G}_1\boldsymbol{\omega},\end{aligned} \tag{2.45}$$

where

$$\mathbf{F}_1 = \frac{1}{V_T}\begin{bmatrix} 0 & 0 & -\tan\beta \\ 0 & 0 & -1 \\ 0 & 1 & 0 \end{bmatrix}$$

$$\mathbf{G}_1 = \begin{bmatrix} \cos\alpha\sin\beta\tan\beta & -\sin\beta & \sin\alpha\sin\beta\tan\beta \\ \cos\alpha\sin\beta & -\cos\beta & \sin\alpha\sin\beta \\ \sin\alpha & 0 & -\cos\alpha \end{bmatrix}.$$

Applying Eq. (2.45) to Eq. (2.43) yields

$$\begin{aligned} &\mathbf{C}_{w/\nu_2}\mathbf{k}\dot{\chi}_w + \mathbf{C}_{w/\sigma}\mathbf{j}\dot{\gamma}_w + \begin{bmatrix}\mathbf{i} & \mathbf{C}_{w/\sigma}\mathbf{j} & \mathbf{C}_{w/i}\mathbf{k}\end{bmatrix}\left[\dot{\mu}\ \dot{\gamma}\ \dot{\chi}\right]^\top \\ &\quad = \mathbf{F}_1\boldsymbol{\tau}_w + \left(\mathbf{C}_{w/b} + \mathbf{G}_1\right)\boldsymbol{\omega}. \end{aligned} \tag{2.46}$$

The next step is to derive the relation between $\dot{\chi}_w$, $\dot{\gamma}_w$ and $[\dot{\mu}\ \dot{\gamma}\ \dot{\chi}]^\top$. From the definitions $\mathbf{v}_r = V_T\mathbf{i}_w$ and $\mathbf{v} = \overline{V}_T\mathbf{i}_\sigma$, together with Eq. (2.14), it follows that

$$\mathbf{i}_w = \frac{\overline{V}_T}{V_T}\mathbf{i}_\sigma - \frac{1}{V_T}\mathbf{v}_{W/i}. \tag{2.47}$$

Applying Eq. (2.47) to Eqs. (2.40) and (2.41) yields the salient equations:

$$\sin\chi_w = -\frac{\mathbf{j}_\sigma\cdot\mathbf{v}_{W/i}}{V_T} \tag{2.48a}$$

$$\sin\gamma_w = \frac{\mathbf{k}_\sigma\cdot\mathbf{v}_{W/i}}{V_T\cos\chi_w}. \tag{2.48b}$$

The value of the path-relative wind angles can be computed from the wind and states by selecting coordinate systems as follows:

$$\begin{aligned} \mathbf{j}_\sigma\cdot\mathbf{v}_{W/i} &= \mathbf{j}^\top\mathbf{C}_{\sigma/i}\mathbf{v}^i_{W/i} \\ \mathbf{k}_\sigma\cdot\mathbf{v}_{W/i} &= \mathbf{k}^\top\mathbf{C}_{\sigma/i}\mathbf{v}^i_{W/i}. \end{aligned} \tag{2.49}$$

Hence, χ_w and γ_w are functions of t, V_T, χ, and γ because $\mathbf{v}_{W/i}$ is a function of time t, and $\mathbf{C}_{\sigma/i}$ is a function of χ and γ. On the other hand, since μ is independent of any other states or time-varying components, it is assigned as a

state of the system; having the other state variables fixed still leaves the degree of freedom by 1.

Taking time derivatives of Eq. (2.48) yields

$$\dot{\chi}_w \cos\chi_w = \frac{\mathbf{j}_\sigma \cdot \mathbf{v}_{W/i}}{V_T^2}\dot{V}_T - \frac{1}{V_T}\mathbf{j}_\sigma \cdot {}^\sigma\dot{\mathbf{v}}_{W/i} = -\frac{\sin\chi_w}{V_T}\dot{V}_T - \frac{1}{V_T}\mathbf{j}^\top {}^\sigma\dot{\mathbf{v}}^\sigma_{W/i} \tag{2.50a}$$

$$\begin{aligned}\dot{\gamma}_w \cos\gamma_w &= -\frac{\mathbf{k}_\sigma \cdot \mathbf{v}_{W/i}}{V_T^2 \cos\chi_w}\dot{V}_T + \frac{\mathbf{k}_\sigma \cdot \mathbf{v}_{W/i}}{V_T \cos^2\chi_w}\sin\chi_w\dot{\chi}_w + \frac{1}{V_T\cos\chi_w}\mathbf{k}_\sigma \cdot {}^\sigma\dot{\mathbf{v}}_{W/i} \\ &= -\frac{\sin\gamma_w}{V_T}\dot{V}_T + \tan\chi_w \sin\gamma_w\dot{\chi}_w + \frac{1}{V_T\cos\chi_w}\mathbf{k}^\top {}^\sigma\dot{\mathbf{v}}^\sigma_{W/i}.\end{aligned} \tag{2.50b}$$

As a result, the derivatives of the path-relative wind angles are obtained as follows:

$$\dot{\chi}_w = -\frac{\tan\chi_w}{V_T}\dot{V}_T - \frac{\sec\chi_w}{V_T}\mathbf{j}^\top {}^\sigma\dot{\mathbf{v}}^\sigma_{W/i} \tag{2.51a}$$

$$\begin{aligned}\dot{\gamma}_w = &-\frac{\sec^2\chi_w\tan\gamma_w}{V_T}\dot{V}_T \\ &+ \frac{1}{V_T}\left(-\tan\chi_w\sec\chi_w\tan\gamma_w\mathbf{j}^\top + \sec\chi_w\sec\gamma_w\mathbf{k}^\top\right){}^\sigma\dot{\mathbf{v}}^\sigma_{W/i}\end{aligned} \tag{2.51b}$$

where Eq. (2.51a) is applied to Eq. (2.50b) to obtain Eq. (2.51b), and $1 + \tan^2\chi_w = \sec^2\chi_w$ is used.

To find the path-relative wind angle derivatives in relation to $[\dot{\mu}\ \dot{\gamma}\ \dot{\chi}]^\top$, let us factorize Eq. (2.27) as follows:

$$\boldsymbol{\omega}^\sigma_{\sigma/i} = \mathbf{H}_\gamma \left[\dot{\mu}\ \dot{\gamma}\ \dot{\chi}\right]^\top, \tag{2.52}$$

where

$$\mathbf{H}_\gamma = \begin{bmatrix} 0 & 0 & -\sin\gamma \\ 0 & 1 & 0 \\ 0 & 0 & \cos\gamma \end{bmatrix}.$$

The identity ${}^\sigma\dot{\mathbf{v}}_{W/i} = {}^i\dot{\mathbf{v}}_{W/i} + \boldsymbol{\omega}_{i/\sigma} \times \mathbf{v}_{W/i}$ in the inertial velocity coordinate

system is

$$ {}^{\sigma}\dot{\mathbf{v}}^{\sigma}_{W/i} = \mathbf{a}^{\sigma}_{W/i} + \mathbf{v}^{\sigma}_{W/i} \times \boldsymbol{\omega}^{\sigma}_{\sigma/i} = \mathbf{a}_{\sigma} + \mathbf{B}_{\sigma} \left[\dot{\mu}\ \dot{\gamma}\ \dot{\chi}\right]^{\top}, \tag{2.53} $$

where $\mathbf{a}_{\sigma} = \mathbf{C}_{\sigma/i}\mathbf{a}^{i}_{W/i}$ and $\mathbf{B}_{\sigma} = \left[\mathbf{C}_{\sigma/i}\mathbf{v}^{i}_{W/i}\right]_{\times}\mathbf{H}_{\gamma}$. Applying Eqs. (2.31) and (2.53) to Eq. (2.51) gives

$$ \dot{\chi}_w = \mathbf{b}_{\chi_w}\boldsymbol{\tau}_w + \mathbf{c}_{\chi_w}\mathbf{a}_{\sigma} + \mathbf{c}_{\chi_w}\mathbf{B}_{\sigma}\left[\dot{\mu}\ \dot{\gamma}\ \dot{\chi}\right]^{\top} \tag{2.54a} $$

$$ \dot{\gamma}_w = \mathbf{b}_{\gamma_w}\boldsymbol{\tau}_w + \mathbf{c}_{\gamma_w}\mathbf{a}_{\sigma} + \mathbf{c}_{\gamma_w}\mathbf{B}_{\sigma}\left[\dot{\mu}\ \dot{\gamma}\ \dot{\chi}\right]^{\top}, \tag{2.54b} $$

where

$$ \begin{aligned} \mathbf{b}_{\chi_w} &= -\left(\tan\chi_w/V_T\right)\mathbf{i}^{\top} \\ \mathbf{b}_{\gamma_w} &= -\left(\sec^2\chi_w\tan\gamma_w/V_T\right)\mathbf{i}^{\top} \\ \mathbf{c}_{\chi_w} &= -\left(\sec\chi_w/V_T\right)\mathbf{j}^{\top} \\ \mathbf{c}_{\gamma_w} &= \left(-\tan\chi_w\sec\chi_w\tan\gamma_w\mathbf{j}^{\top} + \sec\chi_w\sec\gamma_w\mathbf{k}^{\top}\right)/V_T\,. \end{aligned} $$

Applying Eq. (2.54) to Eq. (2.46) yields

$$ \begin{aligned} &\mathbf{C}_{w/\nu_2}\mathbf{k}\left(\mathbf{b}_{\chi_w}\boldsymbol{\tau}_w + \mathbf{c}_{\chi_w}\mathbf{a}_{\sigma}\right) + \mathbf{C}_{w/\sigma}\mathbf{j}\left(\mathbf{b}_{\gamma_w}\boldsymbol{\tau}_w + \mathbf{c}_{\gamma_w}\mathbf{a}_{\sigma}\right) + \mathbf{N}\left[\dot{\mu}\ \dot{\gamma}\ \dot{\chi}\right]^{\top} \\ &\quad = \mathbf{F}_1\boldsymbol{\tau}_w + \left(\mathbf{C}_{w/b} + \mathbf{G}_1\right)\boldsymbol{\omega}, \end{aligned} \tag{2.55} $$

where

$$ \mathbf{N} = \left(\mathbf{C}_{w/\nu_2}\mathbf{k}\mathbf{c}_{\chi_w} + \mathbf{C}_{w/\sigma}\mathbf{j}\mathbf{c}_{\gamma_w}\right)\mathbf{B}_{\sigma} + \begin{bmatrix}\mathbf{i} & \mathbf{C}_{w/\sigma}\mathbf{j} & \mathbf{C}_{w/i}\mathbf{k}\end{bmatrix}. $$

Finally, the dynamics of the aerodynamic roll angle is represented as

$$ \dot{\mu} = f_{\mu}\left(t, \mathbf{x}, \boldsymbol{\delta}, T\right) + \mathbf{g}_{\mu}\left(\boldsymbol{\xi}_a\right)\boldsymbol{\omega}, \tag{2.56} $$

where

$$ f_{\mu}\left(t, \mathbf{x}, \boldsymbol{\delta}, T\right) = \mathbf{i}^{\top}\mathbf{N}^{-1}[\left(\mathbf{F}_1 - \mathbf{C}_{w/\nu_2}\mathbf{k}\mathbf{b}_{\chi_w} - \mathbf{C}_{w/\sigma}\mathbf{j}\mathbf{b}_{\gamma_w}\right)\boldsymbol{\tau}_w \tag{2.57a} $$

$$ - \left(\mathbf{C}_{w/\nu_2}\mathbf{k}\mathbf{c}_{\chi_w} + \mathbf{C}_{w/\sigma}\mathbf{j}\mathbf{c}_{\gamma_w}\right)\mathbf{a}_{\sigma}] \tag{2.57b} $$

$$ \mathbf{g}_{\mu}\left(\boldsymbol{\xi}_a\right) = \mathbf{i}^{\top}\mathbf{N}^{-1}\left(\mathbf{C}_{w/b} + \mathbf{G}_1\right). \tag{2.57c} $$

Remark 2.1.3 (range of path-relative wind angles): From the definition, Eq. (2.6) implies Eq. (2.37) whenever the angles, χ_w and γ_w, are in the domain of arcsin function: $[-90°,\ 90°]$. Suppose that $\left|\mathbf{v}_{W/i}\right| < V_T$ and let $\mathbf{v}_{W/i}^{\sigma} = [w_1\ w_2\ w_3]^\top$; thus, $w_1^2 + w_2^2 + w_3^2 < V_T^2$. Then, from Eq. (2.48a), we obtain

$$|\sin\chi_w| = \frac{|w_2|}{V_T} < 1 \tag{2.58}$$

On the other hand, from Eq. (2.48b),

$$|\sin\gamma_w| = \frac{|w_3|}{V_T\cos\gamma_w} = \frac{|w_3|}{V_T\sqrt{1-\dfrac{w_2^2}{V_T^2}}} = \frac{|w_3|}{\sqrt{V_T^2 - w_2^2}}. \tag{2.59}$$

If $w_3 = 0$, $\sin\gamma_w = 0$. In the case of $w_3 \neq 0$, the following holds:

$$\frac{|w_3|}{\sqrt{V_T^2 - w_2^2}} < \frac{|w_3|}{\sqrt{w_1^2 + w_3^2}} \leq 1. \tag{2.60}$$

Therefore, it follows that $|\sin\gamma_w| < 1$. From the analysis, it is shown that Assumption 2.1.5 guarantees the path-relative wind angles to be well-defined.

Remark 2.1.4 (no ambient wind): The no-ambient-wind condition $\mathbf{v}_{W/i} = 0$ implies that $\mathbf{i}_w = \mathbf{i}_\sigma$ from Eq. (2.47); hence, $\mathbf{i}_w \cdot \mathbf{j}_\sigma = 0$ and $\mathbf{i}_w \cdot \mathbf{k}_\sigma = 0$, i.e., $\chi_w = \gamma_w = 0$ from Eqs. (2.39) and (2.40). Then, $\mathbf{C}_{w/\sigma} = \mathbf{C}_\mu$ because $\mathbf{C}_{\chi_w} = \mathbf{C}_{\gamma_w} = \mathbf{I}$. This property was used in Remark 2.1.2, which is equivalent to the identity $\mathbf{i}^\top\mathbf{C}_\mu = \mathbf{i}^\top\mathbf{C}_\mu^\top = \mathbf{i}$ derived from the structure of $\mathbf{C}_\mu = \mathbf{C}_x(\mu)$. Note that, as a more general case, the path-relative wind angles are both zero whenever the direction of the inertial velocity $\mathbf{v} = \overline{V}_T\mathbf{i}_\sigma$ is parallel to the

ambient wind $\mathbf{v}_{W/i}$ because $\mathbf{j}_\sigma \cdot \mathbf{v}_{W/i}$ and $\mathbf{k}_\sigma \cdot \mathbf{v}_{W/i}$ in Eq. (2.48) are all zero in that case.

Remark 2.1.5 (computation of aerodynamic roll angle): In practice, it is hard to directly measure the aerodynamic roll angle. Therefore, it is circuitously computed by measuring $\mathbf{C}_{b/i}$ which is often parametrized by a quaternion or Euler angles:

$$\mathbf{C}_\mu \mathbf{C}_{\chi_w} \mathbf{C}_{\gamma_w} \mathbf{C}_{\sigma/i} = \mathbf{C}_{w/b} \mathbf{C}_{b/i} \tag{2.61a}$$

$$\mathbf{C}_\mu = \mathbf{C}_{w/b} \mathbf{C}_{b/i} \mathbf{C}_{\sigma/i}^\top \mathbf{C}_{\gamma_w}^\top \mathbf{C}_{\chi_w}^\top. \tag{2.61b}$$

As a result,

$$\mu = \operatorname{atan2}\left(c_{23}, c_{22}\right), \tag{2.62}$$

where c_{ij} represents the (i, j)-th component of the right-hand side of Eq. (2.61b).

2.1.8 Overall Dynamics

The flight dynamics under continuously differentiable wind on the domain $\mathcal{D}_t$ is summarized in Table 2.3. The state equations are structured based on the dominance of each state or control input over the state functions. The angular velocity $\boldsymbol{\omega}$ is dominantly affected by the control surface deflection $\boldsymbol{\delta}$ such as the elevator, aileron, and rudder. The aerodynamic moment coefficient $\mathbf{C}_M$ is often formulated in input-affine form with respect to control surface deflection, which can be readily handled by the control allocation technique [48, 49]. The aerodynamic roll angle μ and the aerodynamic angles $\boldsymbol{\xi}_a$ can be efficiently controlled by taking $\boldsymbol{\omega}$ as input, which is a typical approach exploited by a cascade control scheme such as backstepping or a time-scale decomposition technique [5, 6]. Note that the coefficients of $\boldsymbol{\omega}$, i.e., $\mathbf{G}_a$ and $\mathbf{g}_\mu$, are all functions

of only $\boldsymbol{\xi}_a$. On the other hand, $\boldsymbol{\xi}_a$ has a large effect on the motion of flight path angles $\boldsymbol{\xi}_f$, whereby it can be viewed as input for the flight path angle dynamics. However, the relation is basically nonlinear, which is represented by the function $\boldsymbol{\eta}_f$. Therefore, for some control schemes, an appropriate nonlinear pseudo-inverse mapping of $\boldsymbol{\eta}_f$ on a confined domain with the rest of the state variables fixed must be found [43]. The airspeed V_T and the ground speed $\overline{V}_T$ are typically controlled by the thrust T.

Although the proposed state functions are structured based on several assumptions on the aerodynamics, one may utilize the intermediate result found during the derivation. Then, some state functions would not be structured as proposed. However, the whole derivation procedure given in this dissertation sufficiently shows how to obtain the state functions corresponding to such modified assumptions.

Table 2.3: Overall equations of motion

Variables	Equations of motion	Equation No.
Angular velocity	$\dot{\boldsymbol{\omega}} = \mathbf{f}_{\omega}\left(\boldsymbol{\omega}, T\right) + \mathbf{g}_{\omega}\left(t, \mathbf{x}, \boldsymbol{\delta}\right)$	Eq. (2.12)
Aerodynamic roll angle	$\dot{\mu} = f_{\mu}\left(t, \mathbf{x}, \boldsymbol{\delta}, T\right) + \mathbf{g}_{\mu}\left(\boldsymbol{\xi}_a\right)\boldsymbol{\omega}$	Eq. (2.56)
Aerodynamic angles	$\dot{\boldsymbol{\xi}}_a = \mathbf{f}_a\left(t, \mathbf{x}, \boldsymbol{\delta}, T\right) + \mathbf{G}_a\left(\boldsymbol{\xi}_a\right)\boldsymbol{\omega}$	Eq. (2.22)
Flight path angles	$\dot{\boldsymbol{\xi}}_f = \mathbf{f}_f\left(t, V_T, \boldsymbol{\xi}_f\right) + \mathbf{G}_f\left(t, V_T, \boldsymbol{\xi}_f\right)\boldsymbol{\eta}_f\left(t, \mathbf{x}, \boldsymbol{\delta}, T\right)$	Eq. (2.29)
Airspeed	$\dot{V}_T = f_V\left(t, \mathbf{x}, \boldsymbol{\delta}\right) + g_V\left(\boldsymbol{\xi}_a\right)T$	Eq. (2.32)
Ground speed	$\dot{\overline{V}}_T = f_{\overline{V}}\left(t, \mathbf{x}, \boldsymbol{\delta}\right) + g_{\overline{V}}\left(t, \mathbf{x}\right)T$	Eq. (2.34)
Position	$\dot{\mathbf{p}} = \overline{V}_T \mathbf{C}_{\sigma/i}^{\top}\mathbf{i}$	Eq. (2.36)

2.2 Discussions

The flight dynamics developed in this study has many advantageous features. Some of them are introduced in this section considering potential applications. Issues that arise regarding hardware implementation are also discussed.

2.2.1 Aerodynamic Roll Angle

The essence of the notion of the aerodynamic roll angle defined in wind conditions is that it provides a convenient way for designing a control law capable of coordinated-turn (bank-to-turn) by which the aircraft can keep the sideforce being zero while changing its flight direction even in the presence of varying wind. Since $\mathbf{i}_w = \mathbf{i}_{\nu_2}$, the aerodynamic force $\mathbf{F}_A$ can be made lie on the $z-x$ plane of the wind coordinate system w through a rolling motion about $\mathbf{i}_{\nu_2}$, i.e., by controlling the aerodynamic roll angle using Eq. (2.56), as shown in Fig. 2.4, where the desired wind frame, in which the sideforce is zero, is denoted by $\mathcal{F}_{w'}$. In other words, the frame $\mathcal{F}_{w'}$ should satisfy $\mathbf{F}_A \cdot \mathbf{j}_{w'} = 0$ because $\mathbf{F}_A^w = [-D \;\; Y \;\; -L]^\top$, where D, Y, and L are the drag, sideforce, and lift, respectively. The projection of the aerodynamic force $\mathbf{F}_A$ on the $y-z$ plane of the coordinate system ν_2 is $(\mathbf{F}_A \cdot \mathbf{j}_{\nu_2})\,\mathbf{j}_{\nu_2} + (\mathbf{F}_A \cdot \mathbf{k}_{\nu_2})\,\mathbf{k}_{\nu_2}$. Therefore, by using the following aerodynamic angle command

$$\mu_c = \operatorname{atan2}\left(\mathbf{F}_A \cdot \mathbf{j}_{\nu_2}, -\mathbf{F}_A \cdot \mathbf{k}_{\nu_2}\right), \tag{2.63}$$

the sideforce $\mathbf{F}_A \cdot \mathbf{j}_w$ tends to zero as μ approaches μ_c, which means that the roll angle command is determined such that the sideforce Y converges to zero.

In addition, in the no-wind condition, the aerodynamic roll angle defined in this study is exactly the same as the conventional aerodynamic roll angle [5, Appendix B]. If $\mathbf{v}_{W/i} = \mathbf{0}$, the path-relative wind angles χ_w and γ_w in Eq. (2.49)

are zero; thus, $\mathbf{C}_{w/\sigma} = \mathbf{C}_{\mu}$ is obtained as derived in Remark 2.1.4, which is desirable in that it maintains consistency with the conventional description of flight dynamics for flight path angle control.

2.2.2 Path-Relative Wind Angles

The path-relative wind angles χ_w and γ_w that appear in the coordinate transformation from σ to w, represented by $\mathbf{C}_{w/\sigma}$, are used throughout the derivation of the equations of motion. As discussed earlier, they are functions of time (due to ambient winds), airspeed, flight path angles, and aerodynamic roll angle. Therefore, the derivation of the coordinate transformation matrix $\mathbf{C}_{w/\sigma}$ explicitly shows that they do not depend on the aerodynamic angles β and α. More specifically, the pseudo-inverse mapping of the function $\boldsymbol{\eta}_f$ in Eq. (2.30c) can be easily obtained by taking $\boldsymbol{\xi}_a$ as the only variable. Owing to this property, a control design approach for cascade systems can be applied effectively.

2.2.3 Compensation of Unsteady Winds

The equations of motion derived in this study comprise the analytic formulation of the effect of varying wind on the motion of an aerial vehicle. Therefore, once the wind profile is known *a priori* or measured on-line, the wind effect can be efficiently compensated by applying an adequate flight controller based on the proposed model. Model-based robust or adaptive controllers with an accurate model exhibit more satisfactory performance since the estimated bounds of the uncertainty or disturbance are much smaller than those of a controller based on a roughly evaluated model. In particular, as the bounds of disturbance increase, the robust controllers are necessarily forced to have a higher control gain due to the desired ultimate boundedness of states, which may result in excitation of an un-modeled high-frequency dynamics or even imperil the stability of the

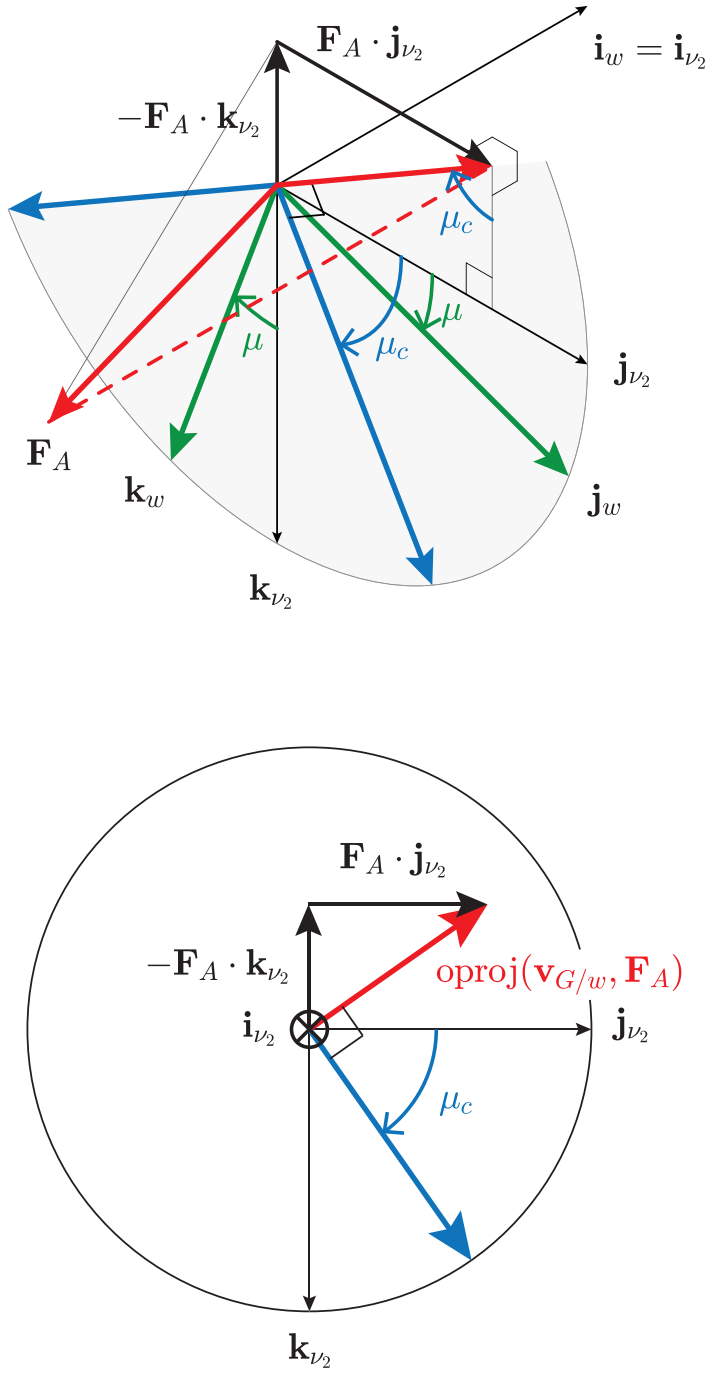

Figure 2.4: Geometry of the aerodynamic roll angle in coordinated turn

system due to physical constraints on the actuators.

2.2.4 Local Wind Field

If a local wind field is provided for some position domain $\mathcal{D}_p \subseteq \mathbb{R}^3$, then the wind can be treated as a part of the plant rather than an exogenous time-varying signal as previously assumed. Consider a continuously differentiable wind field

$$\mathbf{v}_{W/i}^{i} = \mathbf{w}\left(t, \mathbf{p}\right). \tag{2.64}$$

The ambient wind dynamics is derived from the following equation [29]:

$$\dot{\mathbf{w}} = \frac{\partial \mathbf{w}}{\partial t} + \frac{\partial \mathbf{w}}{\partial \mathbf{p}}\dot{\mathbf{p}} = \frac{\partial \mathbf{w}}{\partial t} + \overline{V}_T \frac{\partial \mathbf{w}}{\partial \mathbf{p}} \mathbf{C}_{\sigma/i}^{\top}\mathbf{i}. \tag{2.65}$$

The wind velocity can be estimated by a model-based nonlinear estimator such as the extended Kalman filter. Furthermore, if the dependence of the wind on the time t is negligible, i.e., $\partial \mathbf{w}/\partial t \approx \mathbf{0}$, then the overall equations of motion are approximated to a time-invariant system by substituting $\overline{V}_T \left(\partial \mathbf{w}/\partial \mathbf{p}\right) \mathbf{C}_{\sigma/i}^{\top}\mathbf{i}$ for $\mathbf{a}_{W/i}^{i}$; thereby all the state equations are functions of only state and input.

The approach based on the local wind field is effective particularly in the crosswind take-off and landing situations. With a well-developed ambient wind shear profile around the runway that is measured in real-time or formulated beforehand, the crosswind take-off and landing can be more safely performed with wind compensation. Representative examples are the projects North Illinois Meteorological Research on Downbursts (NIMROD) and Joint Airport Weather Studies (JAWS) that were conducted as a part of an effort to alleviate the hazardous influence of microbursts [50]. Control theoretic approaches concerning the takeoff or landing of an aircraft in wind shear using a parametrized wind shear model are proposed in [2, 51, 52]

Another recommended application is found in the flight control for dynamic

soaring and thermalling of a sailplane. Dynamic soaring is one of the flight techniques by which an aircraft flies across the boundary between layers of significantly different wind velocities to gain energy. Such a wind shear is typically formed by the terrain, e.g., mountains or cliffs, where the wind field is almost steady. Thermalling is a flight technique that makes use of the thermal lift induced by columns of rising air formed by solar energy, which also has a steady wind field. In summary, the flight dynamics considering varying ambient winds can be utilized for the design of the controller for effective coordinated flight across the steady wind shear.

2.2.5 Wind Estimation

The equations of motion developed in this study require the differentiability of ambient wind velocity to get the wind acceleration $\mathbf{a}_{W/i}$. Considering hardware implementations, however, the requirement confronts numerical issues. While wind velocities can be observed through on-board air data sensors such as pitot tube [53] or ground-fixed wind shear detecting devices including Doppler radar [50], there is no physical sensor that directly measures the wind acceleration, and therefore it must be numerically estimated from the velocity measurements. However, wind measurements are usually corrupted by noises significantly heavier than typical IMU measurement noises. Thus, an adequate estimation method needs to be deliberately chosen to obtain a reliable wind acceleration estimate; it is required that the estimate should be smooth enough to prevent any instability in feedback control with the estimation delay being minimized [53]. In this dissertation, two representative simple real-time numerical differentiation methods are introduced and compared.

The first one is a linear second-order low-pass filter (LPF). Let x_1 and x_2 be the filtered wind velocity and acceleration, respectively, and let w be one of

the measured wind components w_N, w_E, and w_D. Then, the LPF has the form

$$\dot{\mathbf{x}} = \begin{bmatrix} 0 & 1 \\ -\omega_n^2 & -2\zeta\omega_n \end{bmatrix} \mathbf{x} + \begin{bmatrix} 0 \\ \omega_n^2 \end{bmatrix} w \tag{2.66}$$

where ζ is the damping ratio, ω_n is the natural angular rate, and $\mathbf{x} = [x_1 \; x_2]^\top$. Because the measurements are discrete-time data, the filter should be discretized accordingly for the sampling time T_s [54] to get $\mathbf{x}_{k+1} = \mathbf{F}_{\text{lpf}}\mathbf{x}_k + \mathbf{G}_{\text{lpf}}w_k$, where $\mathbf{x}_k$ and w_k are the k-th estimate and measurement, respectively, and the coefficient matrices are constant.

Another method called the Kalman filter differentiator (KFD) uses the Kalman filtering technique to estimate the derivative of noisy discrete signal [55]. The target system is represented by the following stochastic differential equation and measurement equation:

$$\dot{\mathbf{x}} = \begin{bmatrix} 0 & 1 \\ 0 & 0 \end{bmatrix} \mathbf{x} + \begin{bmatrix} 0 \\ 1 \end{bmatrix} u(t) \tag{2.67a}$$

$$w_k = \begin{bmatrix} 1 & 0 \end{bmatrix} \mathbf{x} + v_k \tag{2.67b}$$

where u is a continuous-time white noise with the power spectral density (PSD) A_d, and v_k is a discrete-time white noise with the standard deviation σ_m. A_d and σ_m are the design parameters of KFD. As shown in the system equation, KFD models the wind acceleration as a random walk whose integration is the wind velocity that is measured as w_k. Similar to the LPF case, the process can be discretized as well [56]. Due to the time-invariance of the process, there exists a steady-state Kalman filter $\mathbf{x}_{k+1} = \mathbf{F}_{\text{kfd}}\mathbf{x}_k + \mathbf{G}_{\text{kfd}}w_k$, where the (constant) coefficient matrices are obtained by solving an algebraic Riccati equation.

To compare the methods, the filter parameters are set as $\zeta = 0.7$, $\omega_n = 2$, $A_d = 0.36$, and $\sigma_m = 0.25$ with the sampling time $T_s = 0.1$ s, which yield the

coefficient matrices

$$\mathbf{F}_{\text{lpf}} = \begin{bmatrix} 0.982 & 0.087 \\ -0.346 & 0.737 \end{bmatrix}, \ \mathbf{G}_{\text{lpf}} = \begin{bmatrix} 0.018 \\ 0.346 \end{bmatrix}$$

$$\mathbf{F}_{\text{kfd}} = \begin{bmatrix} 0.759 & 0.076 \\ -0.331 & 0.967 \end{bmatrix}, \ \mathbf{G}_{\text{kfd}} = \begin{bmatrix} 0.241 \\ 0.331 \end{bmatrix}$$

They are applied to a generated noisy wind profile obtained in the following chapter, whose simulation result is shown in Fig. 2.5. Note that in the wind velocity estimate plot, the output of a Savitzky-Golay filter (SGF) of a polynomial order 3 [3] is presented as a reference, and in the wind acceleration estimate plot, the output of a direct finite difference-based differentiation (FD) of wind velocity measurement and the output of a finite difference applied to the SGF output (SGF + FD) are presented as well for comparison.

First of all, it is obvious that the acceleration estimates obtained by LPF and KFD are almost identical in contrast to the velocity estimates where a severe time lag is observed from the former compared to the latter. Besides this property, however, because the integration of the acceleration estimate x_2 is precisely the x_1 estimate from LPF by definition, it is apparent that the x_1 and x_2 estimates by KFD do not form an exact integration-differentiation relationship. Nonetheless, the result of KFD is more desirable in practice due to its low time lag capability in x_1 estimation. Furthermore, KFD even shows a better acceleration estimate profile than SGF + FD, not to mention FD that is severely corrupted by amplified noises, in that it exhibits far less fluctuation. In the estimation error plot, SGF shows the smallest estimation error leaving KFD and LPF to follow in order, whose RMS errors read 0.370, 0.535, and

[3] SGF is a discrete signal data smoother that cannot be applied in real-time. However, due to its high-quality denoising capability, it is used to assess the performance of real-time filters that inherently cannot be free from a certain amount of estimation time lags.

0.947 m/s, respectively. KFD gives an estimation error bound since KFD is an estimator, which is particularly useful for controller design and is constant for steady-state Kalman filters.

Figure 2.6 shows the PSD estimations of each signal and the cross-correlations between each estimate and the measurement, which are quantitative indicators of the smoothness and time lags of the filtered signals, respectively. As discussed previously, the LPF output mostly gives the lowest PSD estimate values, which means that it is smoother than the others, but suffers from a large estimation lag (0.7 s) as it can be found from the peak of the cross-correlation graph. The KFD output has slightly higher PSD estimate values than SGF at larger frequencies, but the overall trends of the amplitudes agree. The KFD method is superior to LPF in time lag property where the estimation lag of KFD is 0.2 s. This analysis suggests that differentiator parameters can be systematically chosen by designating safety envelopes on the PSD spectrum and time lag values that are mainly dependent on the controller design and aircraft dynamics.

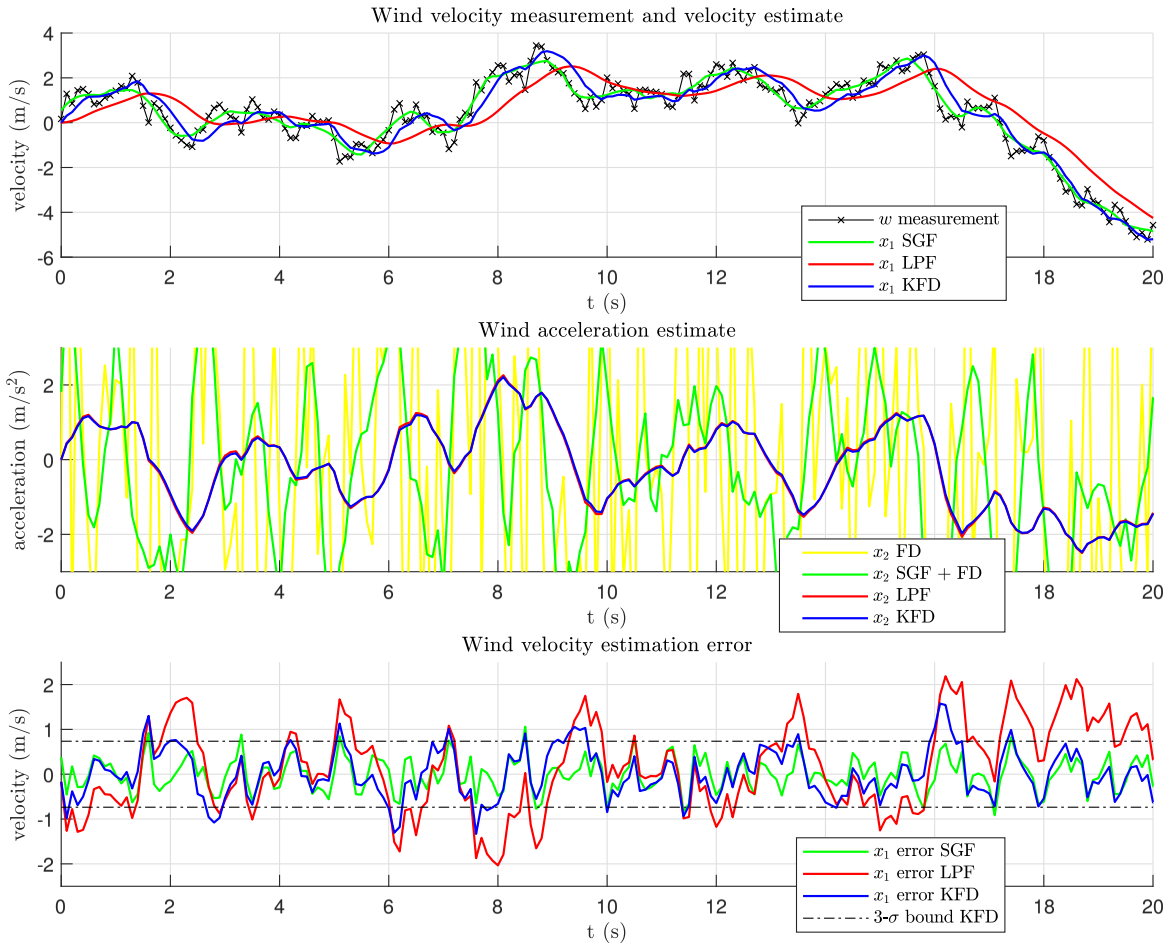

Figure 2.5: Wind velocity and acceleration estimate profiles

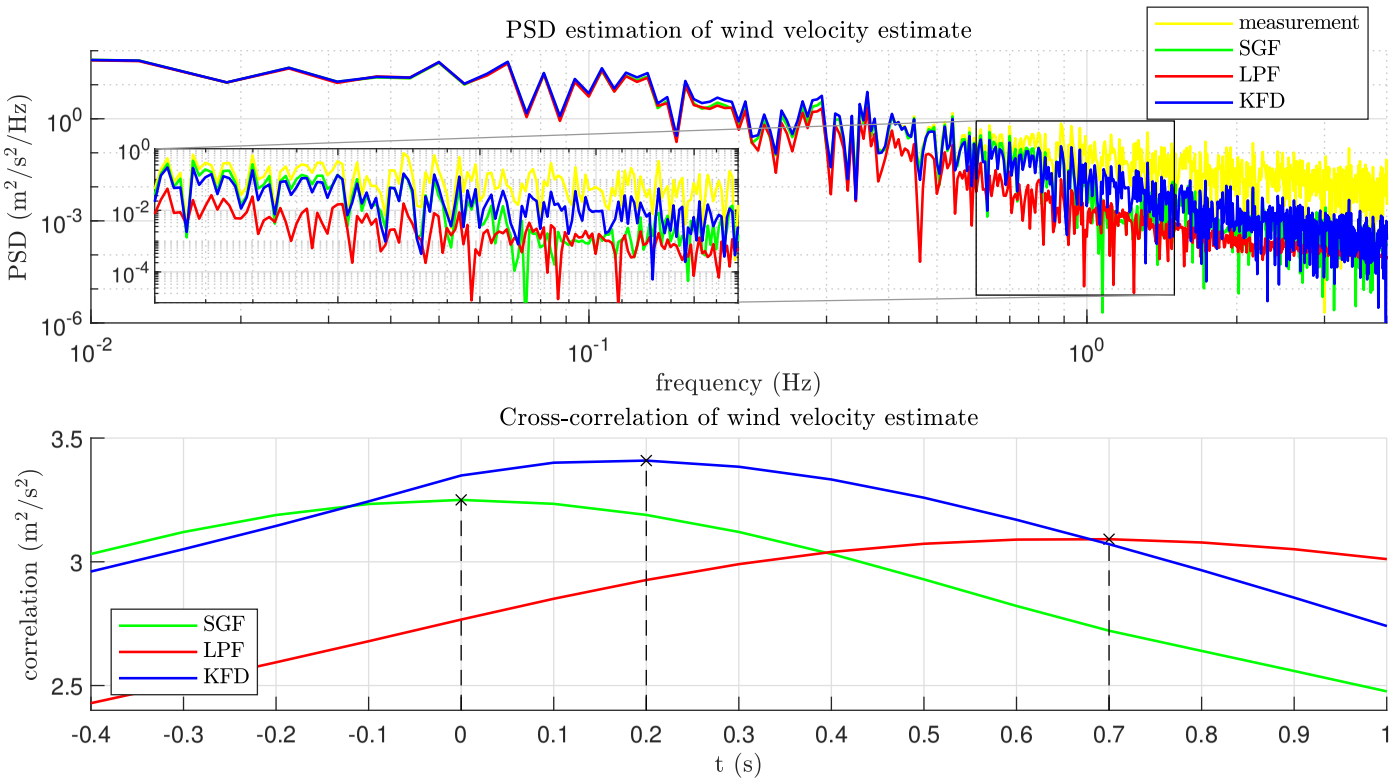

Figure 2.6: Signal analysis of the filtered wind velocities

Chapter 3

Design of Flight Control System

This chapter develops tracking controllers for the flight dynamics summarized in Table 2.3. The flight control laws are efficiently designed by treating the flight dynamics as a cascade system. For the systems whose error state equations are not affine in their inputs, an nonlinear control allocation based on optimization method is employed. The performance of the flight control laws is verified through numerical simulations.

3.1 State Representation

The state vector $\mathbf{x}$ of the overall control system consists of the vehicle state vector $\mathbf{x}_v$ and the foot parameter α of WPTPFC. The vehicle state is defined by

$$\mathbf{x}_v = \begin{bmatrix} \mathbf{v} \\ \boldsymbol{\omega} \\ \mathbf{q} \\ \mathbf{p} \end{bmatrix} \tag{3.1}$$

where $\mathbf{v} = \mathbf{v}^i_{G/i}$ is the vehicle velocity, $\boldsymbol{\omega} = \boldsymbol{\omega}^b_{b/i}$ is the angular velocity, $\mathbf{q} = \mathbf{q}_{b/i}$ is the attitude quaternion, and $\mathbf{p} = \mathbf{p}^i_{G/O}$ is the position. The other states will be gradually augmented as the control laws are developed for each given control problem. Note that the state variables are chosen in order to avoid any internal singularity in the plant dynamics. For example, the state variables defined for the development of the flight dynamics in Chapter 2 has a singularity at $|\gamma| = \pi/2$. If the state representation is used in the control design, it will cause a unwanted problem even if the controller does not make use of the definition of γ. Therefore, each state variable in Chapter 2 will be obtained by the transformation from $\mathbf{x}_v$ only when it is mandatory, while they are also called state variables.

3.2 Cascade System Approximation

The dynamics of aerial vehicle dynamics is not a cascade system as shown in Table 2.3. In spite of this fact, a crucial design strategy in this dissertation is treating the vehicle dynamics as if it were a cascade system. For example, the angular velocity dynamics Eq. (2.12) has a dependency on the angle of attack α because the aerodynamic moment coefficient $\mathbf{C}_M$ varies with α; thus, the $\boldsymbol{\omega}$-dynamics cannot be an inner loop of the α-dynamics. In this dissertation, α in the $\boldsymbol{\omega}$-dynamics is treated as an exogenous time-varying parameters rather than a state and simply canceled out through an equivalent control. Based on this strategy, tracking controllers are designed separately for each subsystem and integrated by using the time-scale decomposition technique.

In particular, the flight control design in this dissertation treats the thrust $T(t)$ of the vehicle as a time-varying parameters for entire subsystems as the development of the equations of motion does for the ambient wind velocity $\mathbf{v}_{W/i}(t)$. It is assumed that the derivative of the thrust is available on-line by thrust sensors or numerical differentiation.

3.3 Angular Velocity Tracking Control

Let the aerodynamic moment coefficient multiplied by $\mathbf{B} = \mathrm{diag}(b_s, \bar{c}, b_s)$, be denoted by $\mathbf{E} = \mathbf{B}\mathbf{C}_M$. Due to Assumption 2.1.1, $\mathbf{E}$ is a function of t, $\mathbf{x}_v$, and $\boldsymbol{\delta}$. Since the coefficient varies effectively with the control surface $\boldsymbol{\delta}$ in an ordinary flight condition, $\boldsymbol{\delta}$ is chosen as input to this subsystem.

The control design takes $\mathbf{E}$ as a virtual input to the angular velocity system Eq. (2.12), and then the control surface deflection command $\boldsymbol{\delta}_\mathrm{c}$ will be sought by a control allocation method that makes the virtual control effective. Let $\mathbf{r}_\omega(t)$ be a differentiable reference for the angular velocity. The tracking error is then

$$\mathbf{e}_\omega = \boldsymbol{\omega} - \mathbf{r}_\omega(t) \tag{3.2}$$

whose derivative is

$$\begin{aligned} \dot{\mathbf{e}}_\omega &= \mathbf{f}_\omega(\boldsymbol{\omega}, T(t)) + \mathbf{g}_\omega(t, \mathbf{x}_v, \boldsymbol{\delta}) - \dot{\mathbf{r}}_\omega(t) \\ &= \mathbf{f}_\omega(\boldsymbol{\omega}, T(t)) + qS\mathbf{J}^{-1}\mathbf{E}(t, \mathbf{x}_v, \boldsymbol{\delta}) - \dot{\mathbf{r}}_\omega(t) \end{aligned} \tag{3.3}$$

The desired error dynamics of the closed-loop system is designed as

$$\dot{\mathbf{e}}_\omega = -\mathbf{K}_\omega \mathbf{e}_\omega \tag{3.4}$$

with the positive definite control gain $\mathbf{K}_\omega$. The dynamic inversion method is then applied to get the desired $\mathbf{E}$ that is denoted by $\mathbf{E}_\mathrm{d}$:

$$\mathbf{E}_\mathrm{d} = \frac{1}{qS}\mathbf{J}(\dot{\mathbf{r}}_\omega - \mathbf{f}_\omega - \mathbf{K}_\omega \mathbf{e}_\omega) \tag{3.5}$$

The next step is to find a control surface deflection command $\boldsymbol{\delta}_\mathrm{c}$ that makes the error between $\mathbf{E}(t, \mathbf{x}_v, \boldsymbol{\delta}_\mathrm{c})$ and $\mathbf{E}_\mathrm{d}$ minimized while fixing all the variables other than $\boldsymbol{\delta}$. This is a control allocation problem that can be formalized as the

following optimization problem:

$$\begin{aligned} &\text{minimize} && \|\mathbf{E}(t, \mathbf{x}_v, \boldsymbol{\delta}) - \mathbf{E}_\mathrm{d}\|^2 + w_\delta \|\boldsymbol{\delta}\|^2 \\ &\text{subject to} && \mathbf{c}_\delta(\boldsymbol{\delta}) \leq \mathbf{0} \end{aligned} \tag{3.6}$$

where t and $\mathbf{x}_v$ are fixed, $w_\delta > 0$ is the regularization weighting, and $\mathbf{c}_\delta$ is a vector-valued function that represents the control surface deflection limits.[1] A minimizer of the problem is then chosen as $\boldsymbol{\delta}_\mathrm{c}$. A strong assumption is introduced in this dissertation for the sake of simplicity that a unique solution exists for the optimization problem Eq. (3.6), and the solution is continuous in t and $\mathbf{x}_v$. This property is strongly dependent on the form of the aerodynamic moment coefficient.

[1] Control surface constraints are usually given by simple angle limits; $\boldsymbol{\delta}_\mathrm{min} \leq \boldsymbol{\delta} \leq \boldsymbol{\delta}_\mathrm{max}$.

3.4 Aerodynamic Angle Tracking Control

From this point on, the state vector $\boldsymbol{\xi}_b = [\mu\ \beta\ \alpha]^\top$ for the aerodynamic roll angle μ and the aerodynamic angles β, α will be called the aerodynamic angle (vector), and the corresponding state function is formed by concatenating Eqs. (2.56) and (2.22) accordingly as follows:

$$\dot{\boldsymbol{\xi}}_b = \mathbf{f}_b(t, \mathbf{x}, \boldsymbol{\delta}, T(t)) + \mathbf{G}_b(\boldsymbol{\xi}_b)\boldsymbol{\omega} \tag{3.7}$$

where

$$\mathbf{f}_b(t, \mathbf{x}, \boldsymbol{\delta}, T) = \begin{bmatrix} \mathbf{f}_\mu(t, \mathbf{x}, \boldsymbol{\delta}, T) \\ \mathbf{f}_a(t, \mathbf{x}, \boldsymbol{\delta}, T) \end{bmatrix}$$

$$\mathbf{G}_b(\boldsymbol{\xi}_a) = \begin{bmatrix} \mathbf{G}_\mu(\boldsymbol{\xi}_a) \\ \mathbf{G}_a(\boldsymbol{\xi}_a) \end{bmatrix} = \begin{bmatrix} \dfrac{\cos\alpha}{\cos\beta} & 0 & \dfrac{\sin\alpha}{\cos\beta} \\ \sin\alpha & 0 & -\cos\alpha \\ -\cos\alpha\tan\beta & 1 & -\sin\alpha\tan\beta \end{bmatrix}$$

Let $\mathbf{r}_b = \mathbf{r}_b(t) = [\mu_\mathrm{r}(t)\ \beta_\mathrm{r}(t)\ \alpha_\mathrm{r}(t)]^\top$ be a differentiable tracking reference and define the tracking error:

$$\mathbf{e}_b = \boldsymbol{\xi}_b - \mathbf{r}_b \tag{3.8}$$

whose time-derivative is

$$\dot{\mathbf{e}}_b = \mathbf{f}_b(t, \mathbf{x}, \boldsymbol{\delta}, T(t)) + \mathbf{G}_b(\boldsymbol{\xi}_a)\boldsymbol{\omega} - \dot{\mathbf{r}}_b(t) \tag{3.9}$$

The desired error dynamics of the closed-loop system is designed as

$$\dot{\mathbf{e}}_b = -\mathbf{K}_b\mathbf{e}_b \tag{3.10}$$

with the positive definite control gain $\mathbf{K}_b$.

The determinant and the condition number of the matrix-valued function

$\mathbf{G}_b(\boldsymbol{\xi}_a)$ are

$$\det \mathbf{G}_b = \frac{1}{\cos\beta} \tag{3.11}$$

and

$$\kappa(\mathbf{G}_b) = \frac{|\sin\beta| + 1}{\sqrt{1 - \sin^2\beta}} \tag{3.12}$$

respectively. It is easy to see that the values are close to unity for a small sideslip angle β. Therefore, it can be said that $\mathbf{G}_b$ is well-conditioned in an ordinary flight condition. Therefore, $\boldsymbol{\omega}$ is chosen as input to this subsystem from the fact that $\mathbf{G}_b$ serves as a coefficient of $\boldsymbol{\omega}$ in the error dynamics Eq. (3.9). Because the error state function in Eq. (3.9) is affine in $\boldsymbol{\omega}$, it is straightforward to find the angular velocity command $\boldsymbol{\omega}_\mathrm{c}$:

$$\boldsymbol{\omega}_\mathrm{c} = \mathbf{G}_b^{-1}(\dot{\mathbf{r}}_b - \mathbf{f}_b - \mathbf{K}_b\mathbf{e}_b) \tag{3.13}$$

3.5 Flight-path Angle Tracking Control

Let $\mathbf{r}_f(t)$ be a differentiable reference for the flight-path angle $\boldsymbol{\xi}_f = [\chi\ \gamma]^\top$. The tracking error is

$$\mathbf{e}_f = \boldsymbol{\xi}_f - \mathbf{r}_f(t) \tag{3.14}$$

whose derivative is

$$\dot{\mathbf{e}}_f = \mathbf{f}_f(t, \mathbf{x}_v) + \mathbf{G}_f(t, \mathbf{x}_v)\boldsymbol{\eta}_f(t, \mathbf{x}_v, \boldsymbol{\delta}, T(t)) - \dot{\mathbf{r}}_f(t) \tag{3.15}$$

The desired error dynamics of the closed-loop system is designed as

$$\dot{\mathbf{e}}_f = -\mathbf{K}_f\mathbf{e}_f \tag{3.16}$$

with the positive definite control gain $\mathbf{K}_f$. The dynamic inversion method is then applied to get the desired $\boldsymbol{\eta}_f$ that is denoted by $\boldsymbol{\eta}_{fd}$:

$$\boldsymbol{\eta}_{fd} = \mathbf{G}_f^{-1}(\dot{\mathbf{r}}_f - \mathbf{f}_f - \mathbf{K}_f\mathbf{e}_f) \tag{3.17}$$

From the structure of $\boldsymbol{\eta}_f$ in Eq. (2.30c)

$$\boldsymbol{\eta}_f(t, \mathbf{x}_v, \boldsymbol{\delta}, T) = [\mathbf{j}\ \mathbf{k}]^\top \mathbf{C}_{\sigma/w}(T\boldsymbol{\lambda} + qS\mathbf{C}_F)$$

it follows that $\boldsymbol{\eta}_f$ is dependent on the aerodynamic force coefficient $\mathbf{C}_F$. Since $\mathbf{C}_F$ effectively varies with $\boldsymbol{\xi}_a$ in an ordinary flight condition, $\boldsymbol{\xi}_a$ is taken as an input to the Flight-path Angle (FPA) tracking control system.

A control allocation method is used to find the aerodynamic angle command $\boldsymbol{\xi}_{ac} = [\beta_c\ \alpha_c]^\top$ that minimizes the error between $\boldsymbol{\eta}_f(t, \mathbf{x}_v, \boldsymbol{\delta}, T(t))$ and $\boldsymbol{\eta}_{fd}$:

$$\begin{aligned} &\text{minimize} && \left\|\boldsymbol{\eta}_f(t, \mathbf{x}_v, \boldsymbol{\delta}, T(t)) - \boldsymbol{\eta}_{fd}\right\|^2 + w_a\|\boldsymbol{\xi}_a\|^2 \\ &\text{subject to} && c_a(\boldsymbol{\xi}_a) \le 0 \end{aligned} \tag{3.18}$$

where t and $\mathbf{x}_v^{(a)}$ are fixed, $w_a > 0$ is the regularization weighting, $\mathbf{x}_v^{(a)}$ denotes

the state vector with $\boldsymbol{\xi}_a$ removed, and c_a is a function that represents the flight envelope of β and α. A minimizer of Eq. (3.18) is chosen as $\boldsymbol{\xi}_{a\mathrm{c}}$. Similar to Section 3.3, it is assumed that a unique solution exists for the optimization problem Eq. (3.18), and the solution is continuous in t and $\mathbf{x}_v^{(a)}$. This property is strongly dependent on the form of the aerodynamic force coefficient.

3.6 Numerical Examples

In this section, the FPA controller developed in Section 3.5 is applied to the high-fidelity F/A-18 High Angle of Attack Research Vehicle (HARV) aircraft model [57]. The aim of the flight control is to make the aircraft track the time-varying flight path angle references χ_r and γ_r while minimizing the excursion of sideslip angle; the aerodynamic roll angle reference μ_r is geometrically determined by the condition discussed in Section 2.2.1. The controller is applied without any adaptation or integral terms to exclusively assess the advantages of using the model alone. In all scenarios, the aircraft is commanded to make a level flight, i.e., $\gamma_r(t) \equiv 0$. In Example 3.1, a straight level flight is followed by a zig-zag maneuver starting at $t = 30$ s. The aircraft in Example 3.2 makes simple coordinated turns with a large range of course angle changes, and make a straight line trajectory in Example 3.3. In Example 3.1 and 3.2, numerical simulations are performed each for no-wind and wind condition and the results are compared, where the conventional equations of motion are used in the case of no-wind condition. In particular, the second example takes a closer look at the performance of the wind estimators in an intense wind condition. In Example 3.3, both the conventional and proposed equations of motion are used in the wind condition to see how the tracking performance is degraded by the inaccuracy in the model.

The initial conditions and nominal ambient wind profiles are summarized in Table 3.1 and 3.2, respectively. Note that the initial aerodynamic roll angle is non-zero because of the presence of the ambient wind. The average magnitude of nominal ambient wind in Example 3.1 and 3.2 is about 32 m/s that is nearly a quarter of the airspeeds throughout the simulation. In particular, Example 3.2 exploits a more challenging ambient wind profile that varies with time along

sinusoidal waves, and the direction of flight is constantly changed; thus, the relative direction and magnitude of wind with respect to the aircraft vary widely at a high frequency. In addition, the nominal wind profiles are corrupted by Dryden wind turbulence model represented in the Military Specification MIL-F-8785C with wind speed 15 m/s at a height of 6 m, which determines the intensity of the turbulence and is relatively intense for general fighter aircraft at a low airspeed. The KFD designed in Section 2.2.5 is used for the wind estimation.

Table 3.1: Initial conditions

States	Units	Example 3.1	Example 3.2	Example 3.3
$P,\ Q,\ R$	deg/s	0.0, 0.0, 0.0	0.0, 0.0, 0.0	0.0, 0.0, 0.0
μ	deg	-0.6	-1.2	0.0
β	deg	0.0	0.0	3.2
α	deg	5.2	4.7	6.5
χ	deg	0.0	180.0	0.0
γ	deg	0.0	0.0	0.0
V_T	m/s	125.5	135.0	180.0
$p_N,\ p_E,\ p_D$	m	$0,\ 0,\ -1000$	$0,\ 0,\ -1000$	$0,\ 0,\ -4000$

Table 3.2: Nominal ambient wind profiles

Components	Units	Example 3.1	Example 3.2	Example 3.3
w_N	m/s	0	$10\sin(\pi t/5) - 10 + t/4$	0
w_E	m/s	30	$30 + 5\cos(\pi t/5)$	-10
w_D	m/s	-10	$-10 + 2\cos(\pi t/5)$	0

3.6.1 Example 3.1

The result of Example 3.1 is shown in Figs. 3.1 and 3.2, where ψ, θ, and ϕ are the 3-2-1 attitude Euler angles, δ_{el}, δ_{er}, δ_a, and δ_r are the left and right

horizontal stabilizer, aileron, and rudder deflections, respectively, and nw stands for the no-wind case. The most remarkable result of this example is the attitude correction feature achieved by replacing only the model. Because the direction of the ambient wind is almost perpendicular to the flight path, the aircraft should slightly turn its heading toward the opposite direction to the wind velocity to reduce the sideforce, which can be explicitly confirmed by the ψ history compared to no-wind case. This kind of attitude correction against the external wind disturbance is essentially attributed to the equations of motion because there are no adaptive terms applied. Figure 3.3 shows the wind, filtered wind, and the filtered path-relative wind angle profiles.

In Fig. 3.4, the tracking errors remain less than 1 deg for both flight path angles. Another notable important aspect of this example is that the tracking error profiles in the wind and no-wind cases are the same in shape and magnitude except for filter noises in the presence of ambient wind. It implies that in spite of large ambient wind disturbances, the performance degradation of the controller can be effectively prevented by simply replacing the equations of motion. It can be expected that the burden on the controller which would be problematic when conventional equations of motion were used is greatly mitigated accordingly by reducing the magnitude of disturbances to be compensated by the controller.

3.6.2 Example 3.2

The actual influence of the ambient wind on an aircraft can be better estimated from the path-relative wind angles rather than the wind terms themselves represented in the flat-earth-fixed coordinate system. This claim can be confirmed from the definition of the path-relative wind angles Eq. (2.48). For example, even if the magnitude of the wind is relatively large, when the airspeed of the

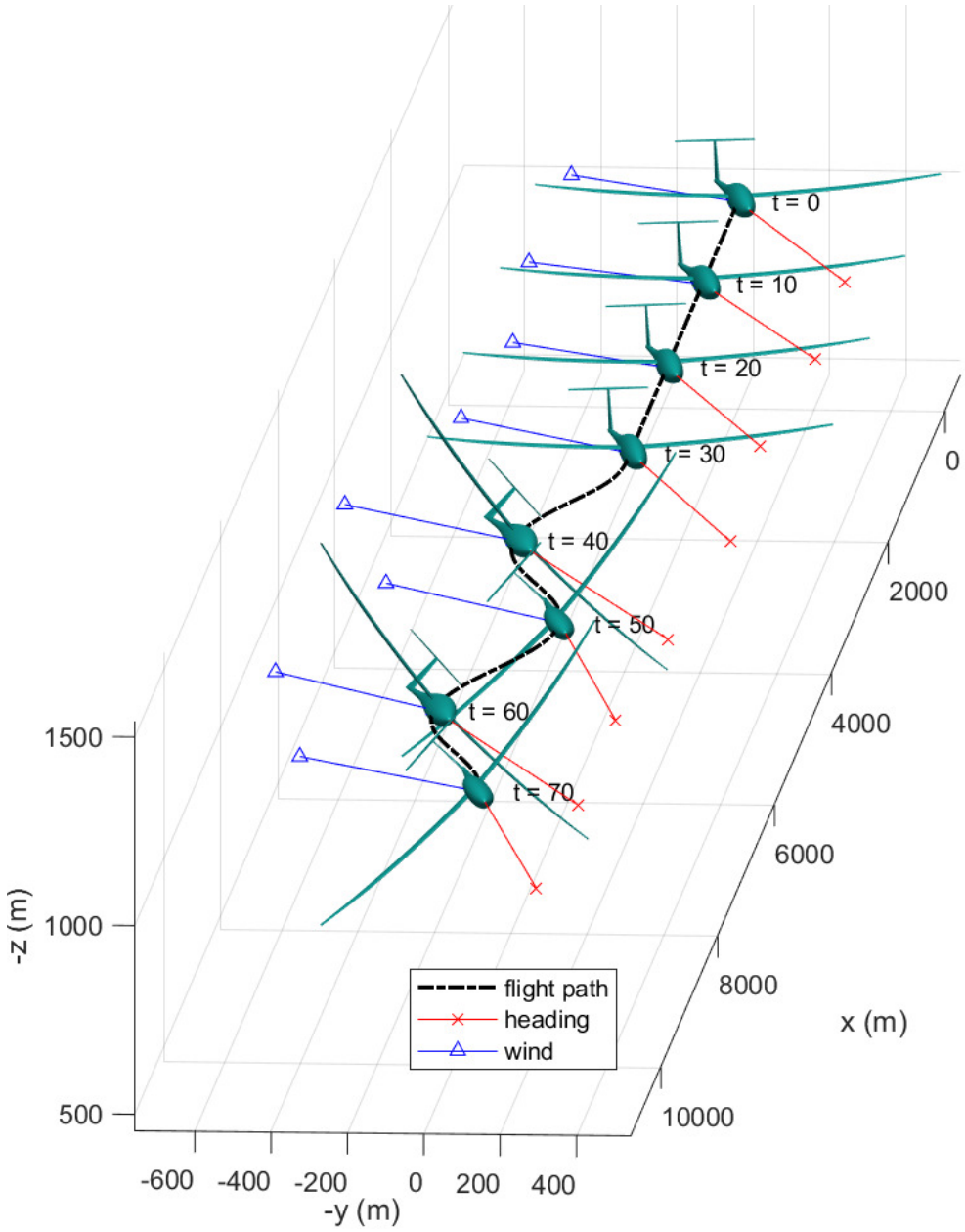

Figure 3.1: Flight trajectory under wind condition: Example 3.1

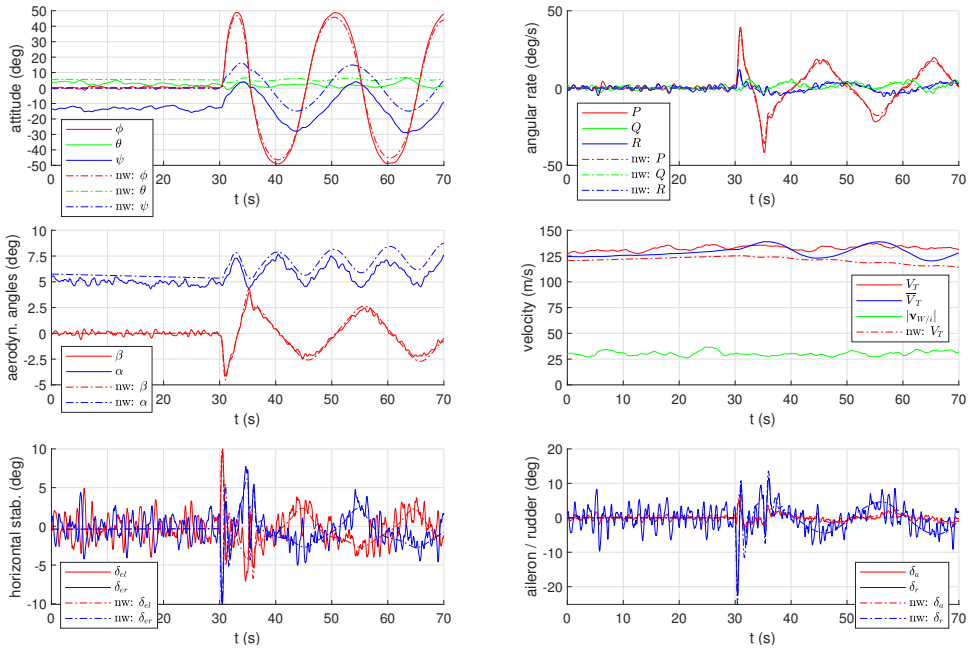

Figure 3.2: State and input history: Example 3.1

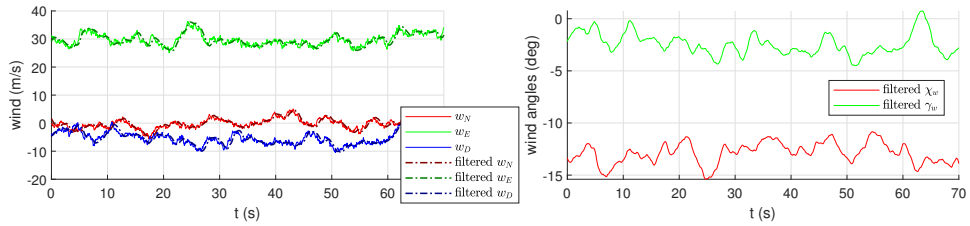

Figure 3.3: Wind profile: Example 3.1

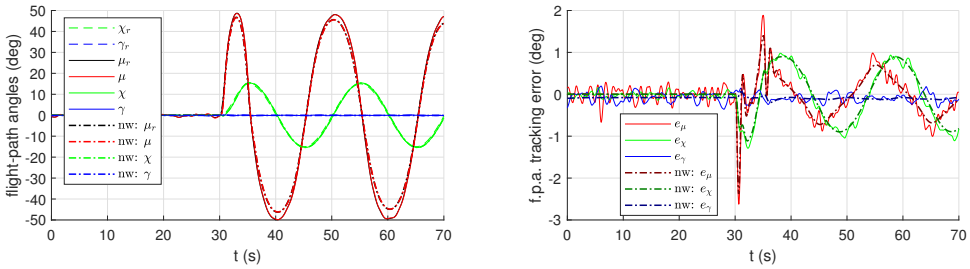

Figure 3.4: Flight path angles and tracking error: Example 3.1

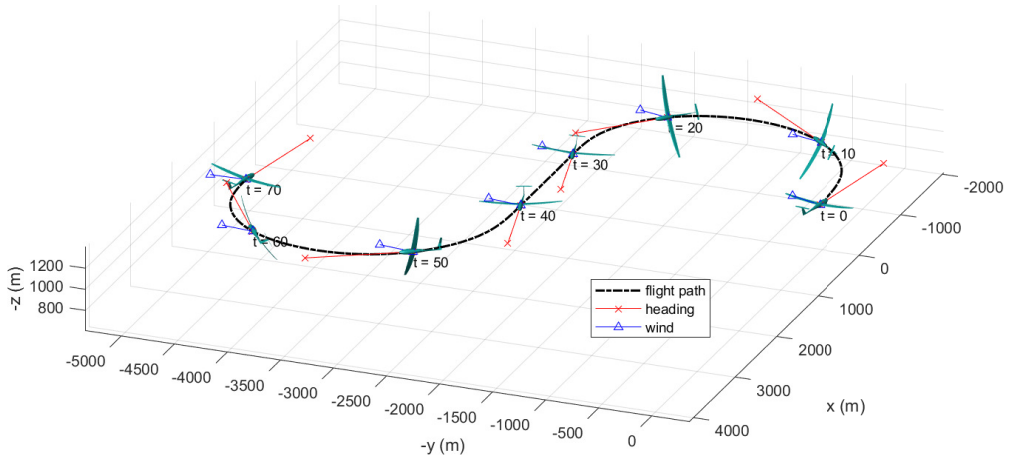

Figure 3.5: Flight trajectory under wind condition: Example 3.2

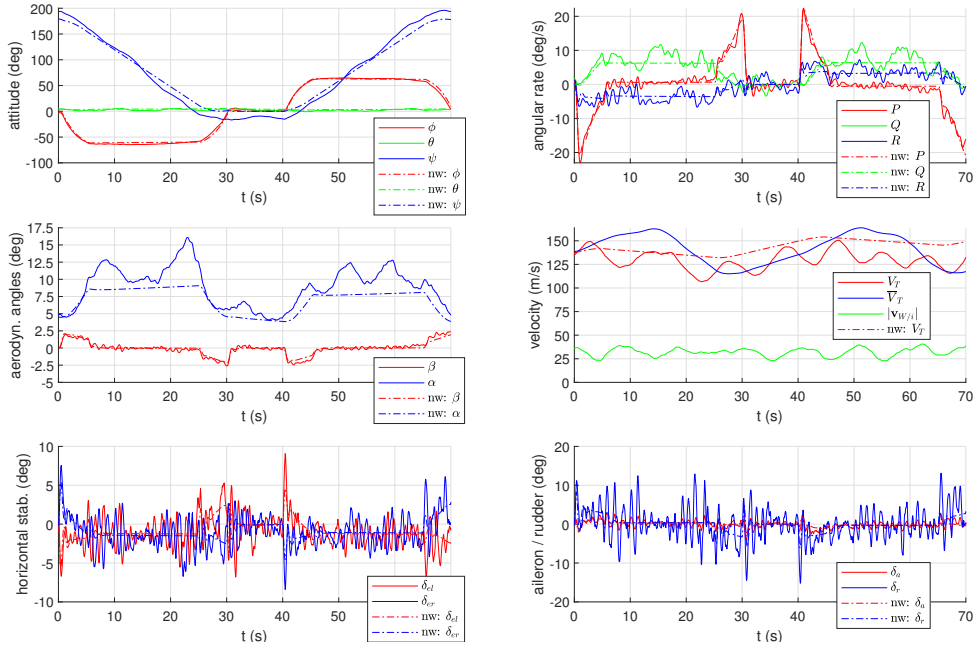

Figure 3.6: State and input history: Example 3.2

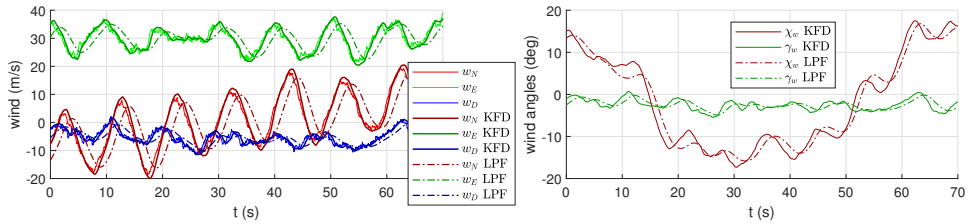

Figure 3.7: Wind profile: Example 3.2

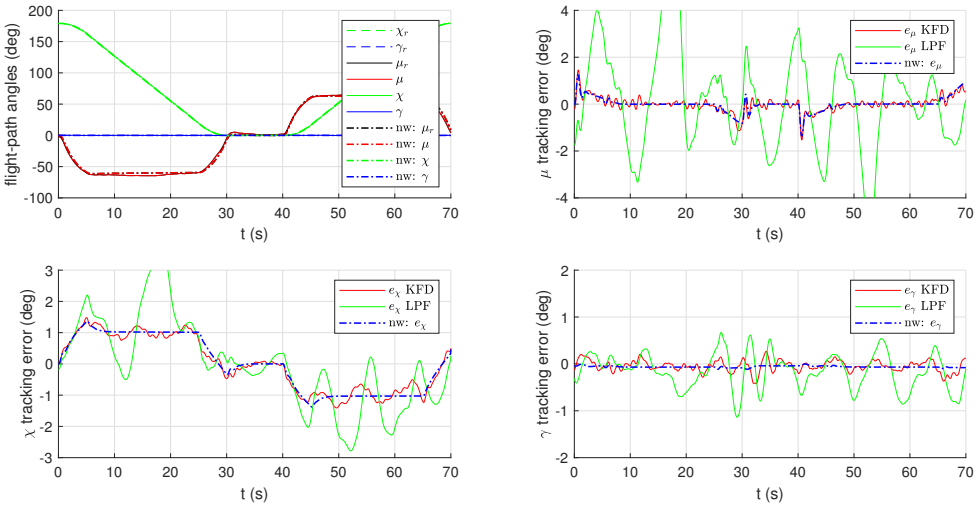

Figure 3.8: Flight path angles and tracking error: Example 3.2

aircraft is much higher, the resulting impact will not be significant, and vice versa. From this aspect, it can be said that the aircraft in Example 3.2 is undergoing an ambient wind that severely varies with time both in magnitude and direction as shown in Fig. 3.7; see Fig. 3.3 for comparison. In Fig. 3.5 and 3.6, it is shown from the attitude history that the heading of the aircraft is actively controlled to track the commanded flight path angles by compensating for the consistently varying ambient wind compared to the no-wind case. In particular, the angle of attack aggressively fluctuates to adjust the aerodynamic lift to compensate for the sinusoidal noisy wind profile. This compensation capability is also achieved by the proposed model.

Additionally, in this example, each result obtained by using wind estimators based on LPF and KFD is also presented. In Fig. 3.7, the most apparent difference between wind estimates comes from the time lags as expected. It turns out that the lag severely affects the performance of the feedback controller as shown in Fig. 3.8, where the tracking error profile generated by applying the KFD wind estimator is almost identical to the no-wind case, similar to the result in Example 3.1, even under severe wind conditions. In contrast, the tracking errors compensated by the LPF wind estimator oscillate largely around the no-wind case profile with the same frequency as the wind fluctuates though it does not at least cause an instability. The results demonstrate the advantage of the KFD wind estimator.

3.6.3 Example 3.3

As shown in Fig. 3.9, the proposed model exactly compensates for the wind term by the wind estimate, while the conventional no-wind model exhibits large deviation of FPA from the zero commands. The result shows the effectiveness of the proposed model. On the other hand, the deviation grows as time passes;

this is because the aircraft gains airspeeds losing altitude due to the inaccurate tracking, and high airspeeds yield more intense deviation.

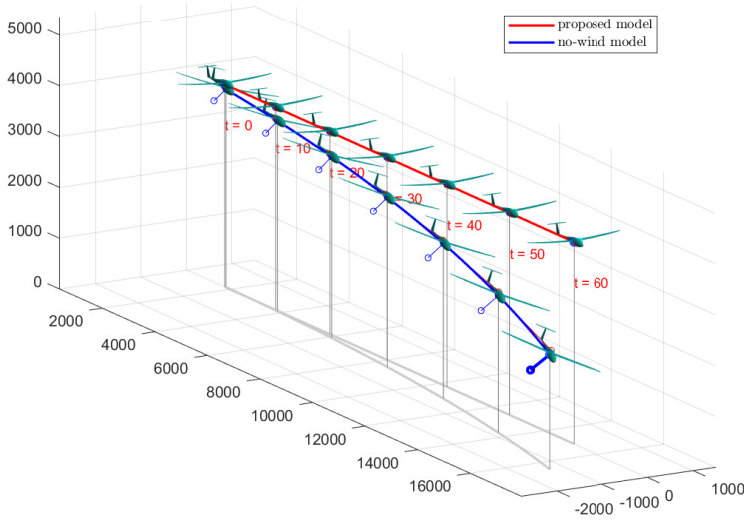

Figure 3.9: Comparison between the proposed model and no-wind model: trajectory

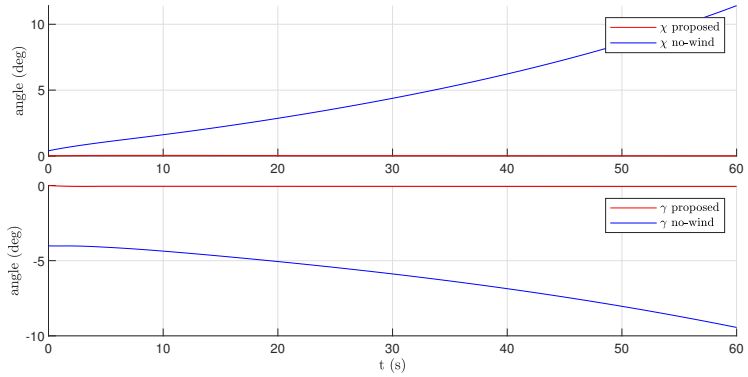

Figure 3.10: Comparison between the proposed model and no-wind model: FPA

Chapter 4

Lyapunov Barrier Weighting Method

A function is usually said to have a singularity if its domain is a proper subset of the space. That is, the function is not defined on some region.[1] Similarly, for a dynamical system, a singularity matters when the solution trajectory approaches the boundary of the domain of the state function or has a finite escape property. Therefore, the singularity avoidance of a dynamical system is closely related to the notion of set invariance. Given that a solution of the system is guaranteed to stay inside a closed set whose boundary does not intersect that of the domain,[2] the singularity will not occur. Furthermore, the solution is expected to be continued indefinitely if the derivative of the states is bounded. This chapter develops several useful claims on this problem.

Barrier methods are the most easy and effective approaches that guarantee

[1] The general definition of singularity of a function in analysis includes several more cases, but this study will not extend to such cases.

[2] The domain of a dynamical system is a nonempty open connected subset of the Euclidean space.

the set invariance of a dynamical system. In this section, several well-known studies on this topic are introduced. The first study to note is summarized in [58], where Ngo et al. designed a backstepping-based controller for feedback linearizable system to have the boundedness of each state and to perform a tracking control of the most-lower-indexed state. The study is especially famous for introducing a logarithmic barrier function to form a barrier Lyapunov function. The approach was further refined by Tee et al. In [59], a strict feedback system is controlled to have a bounded states and output. They specialized the study by considering uncertainties that are linear in the parameters, which is handled by adding adaptive terms, and at the same time, the augmented closed-loop system still avoids a constraint violation. Liu et al. [60] also inherited the main idea of [58]. They applied an approximation-based adaptive control made of a neural network of radial basis functions to a strict feedback system to achieve a bounded control signals and the uniform ultimate boundedness of the tracking error. On the other hand, Ames et al. dealt with general autonomous nonlinear systems using control Lyapunov function (CLF) and control barrier function method. In contrast to the foregoing studies, the constraints are given by a superlevel set of a continuous function of states; thus, it can handle a much larger class of constraints compared to the methods imposing bounds to individual states only. However, finding a control law that makes the control Lyapunov function have a desired property is not an easy task. Their study manages to find one using optimization-based approach resorting to quadratic programming.

The Lyapunov Barrier Weighting Method (BWM) proposed in this dissertation specializes itself by extracting the advantage of the aforementioned studies. BWM can handle constraints given by a closed superlevel set of a continuous function using singular barrier weighting but avoids the use of numerical op-

timization algorithm by exploiting the backstepping control scheme. Furthermore, it applies to nonautonomous (time-varying) system, and it can be used when only the part of the states need to be regulated (set stability). A summary of the studies are given in Table 4.1

Table 4.1: Comparison of barrier methods

	Time-dep.	System	Constraint	Barrier	Adaptation	Set stability	CLF
[58]	✗	FL[a]	state bound	log	✗	✗	✗
[59]	✗	SF[b]	state / output bound	log	✓	✗	✗
[60]	✗	SF	state bound	log	✓	✗	✗
[46]	✗	general	superlevel set	general non-singular / log	✗	✗	✓
BWM	✓	SF	superlevel set	general singular	✗	✓	✗

[a] feedback linearizable system
[b] strict feedback form

4.1 Notation

- The prime $'$ denotes the derivative of a function with respect to its argument. t and the upper dot denote the time and the time-derivative of a function, respectively.
- C^r refers to the differentiability class of order r.
- $\mathbb{R}_+$ denotes the set of nonnegative real numbers.
- For $a \in (0, \infty]$, a continuous function $f : [0, a) \to \mathbb{R}_+$ is said to belong to class $\mathcal{K}$ if it is strictly increasing and $f(0) = 0$; class $\mathcal{K}_\infty$ denotes class $\mathcal{K}$ functions with $a = \infty$ and $f(r) \to \infty$ as $r \to \infty$.
- A continuous function $f : [0, a) \times \mathbb{R}_+ \to \mathbb{R}_+$ is of class $\mathcal{KL}$ if, for each fixed s, $f(r, s)$ is a class $\mathcal{K}$ function with respect to r and, for each fixed r, $f(r, s)$ decreases with respect to s and $f(r, s) \to 0$ as $s \to \infty$.
- $B_r(\mathbf{x})$ and $\overline{B}_r(\mathbf{x})$ are balls of radius r centered at $\mathbf{x}$ open and closed, respectively.
- The value of a function f along the solution of a dynamical system at a time t is occasionally denoted by $f|_t$.

4.2 Mathematical Preliminary

As is well-known, a positive definite Lyapunov function is a useful tool for finding a positively invariant set because a sublevel set is a positively invariant subset of the region of attraction if the set is compact. However, the idea stops to work for a semidefinite Lyapunov function, because a sublevel set cannot be compact. In other words, the negative semidefinite derivative of the Lyapunov function alone does not guarantee the forward completeness[3] of the solution. The following discussion focuses on this issue.

Let the function $\mathbf{f}(t, \mathbf{x})$ be continuous in t and locally Lipschitz in $\mathbf{x}$ on $\mathbb{R}_+ \times \mathcal{D}$ where $\mathcal{D}$ is an open subset of $\mathbb{R}^n$. Consider the differential equation

$$\dot{\mathbf{x}} = \mathbf{f}(t, \mathbf{x}), \ \mathbf{x}(t_0) = \mathbf{x}_0, \tag{4.1}$$

where $t_0 \geq 0$ and $\mathbf{x}_0 \in \mathcal{D}$. Let $I = [t_0, T)$ for some $T > 0$ be the maximal interval of existence.

The following proposition, Lemma 4.2.1, is a crucial basis for the majority of the propositions in this chapter. The design of the lemma was inspired by Theorem 3.3 in [61]. The theorem requires the solution to stay inside a compact subset of $\mathcal{D}$, whereas the lemma concerns for a closed set and the boundedness of the state function in the set. This is a slight modification of the Theorem 3.3. However, the lemma is useful when it is needed to test the forward completeness of the solution of a dynamical system associated with a positive-semidefinite Lyapunov function that has a unbounded sublevel set. The author was hinted by the proof of the first theorem in p. 173 of [62], and the same result can be obtained by applying Theorem 3.1[4] of [63].

[3] The solution is defined for all future time.

[4] The hypothesis of this theorem is slightly stronger than Lemma 4.2.1 in the dissertation, for $\mathbf{f}$ should be bounded on the entire domain D.

Lemma 4.2.1 Let $A \subseteq \mathcal{D}$ be closed, $\mathbf{x}_0 \in A$, and $\mathbf{f}$ be bounded on $\mathbb{R}_+ \times A$. Suppose that the solutions of Eq. (4.1) lie entirely in A. Then, there is a unique solution defined for all $t \geq 0$. $\diamond$

Proof: Note that the proof uses Theorem 3.1 in [61], known as Picard's (existence) theorem. The maximal interval of existence has the form $[0, T)$, where $T \in (0, \infty]$ [63, Section 2.3]. Let $I = [0, T)$ and $\mathbf{x} : I \to \mathbb{R}^n$ be a solution. For all $t_1, t_2 \in I$, the solution satisfies the integral equation $\mathbf{x}(t_2) = \mathbf{x}(t_1) + \int_{t_1}^{t_2} \mathbf{f}(\tau, \mathbf{x}(\tau))\mathrm{d}\tau$. Let $M > 0$ be the bound of $\mathbf{f}$. Since $\mathbf{x}(t) \in A$ for all $t \in I$,

$$\begin{aligned} \|\mathbf{x}(t_2) - \mathbf{x}(t_1)\| &= \left\| \int_{t_1}^{t_2} \mathbf{f}(\tau, \mathbf{x}(\tau))\mathrm{d}\tau \right\| \\ &\leq \int_{t_1}^{t_2} \|\mathbf{f}(\tau, \mathbf{x}(\tau))\|\mathrm{d}\tau \\ &\leq M(t_2 - t_1) \end{aligned} \tag{4.2}$$

which shows that $\mathbf{x}$ is Lipschitz, hence the existence of the limit $L = \lim_{t \nearrow T} \mathbf{x}(t)$.

Suppose that T is finite. Let $\overline{I} = [0, T]$ and define an extension $\mathbf{y} : \overline{I} \to \mathbb{R}^n$ of $\mathbf{x}$ with L appended, i.e., $\mathbf{y}(t) = \mathbf{x}(t)$ for all $t \in I$, $\mathbf{y}(T) = L$; thus, $\mathbf{y}$ is uniformly continuous. Since $\mathbf{f}(t, \mathbf{x})$ is locally Lipschitz in $\mathbf{x}$ and $\mathbf{y}$ is continuous, $f(t, \mathbf{y}(t))$ is integrable on $\overline{I}$ and satisfies

$$\lim_{t \nearrow T} \int_0^t \mathbf{f}(\tau, \mathbf{x}(\tau))\mathrm{d}\tau = \int_0^T \mathbf{f}(\tau, \mathbf{y}(\tau))\mathrm{d}\tau \tag{4.3}$$

The integral equation results in

$$\begin{aligned} \mathbf{y}(T) &= \lim_{t \nearrow T} \mathbf{x}(t) \\ &= \mathbf{x}(0) + \lim_{t \nearrow T} \int_0^t \mathbf{f}(\tau, \mathbf{x}(\tau))\mathrm{d}\tau \\ &= \mathbf{y}(0) + \int_0^T \mathbf{f}(\tau, \mathbf{y}(\tau))\mathrm{d}\tau \end{aligned} \tag{4.4}$$

which shows that $\mathbf{y}$ is also a solution extended from $\mathbf{x}$. Because A is closed in $\mathbb{R}^n$, and $\mathbf{y}(t) \in A$ for all $t \in I$, $\mathbf{y}(T)$ is a limit point of A and $\mathbf{y}(T) \in A \subseteq \mathcal{D}$. Therefore, there is a closed ball centered at $\mathbf{y}(T)$ contained in $\mathcal{D}$, and it can be shown that the solution $\mathbf{y}$ can be further extended from Picard's theorem, which is a contradiction to the claim that I is maximal. Therefore, the maximal interval cannot be bounded, i.e., $I = \mathbb{R}_+$.

The uniqueness of the solution follows from the fact that the solutions traverse the domain on which $\mathbf{f}(t, \mathbf{x})$ is locally Lipschitz in $\mathbf{x}$. Consider two solutions $\mathbf{x}_1, \mathbf{x}_2 : \mathbb{R}_+ \to \mathbb{R}^n$ with $\mathbf{x}_1(0) = \mathbf{x}_2(0)$. Since they share the same initial point, there exists $t_0 \in (0, \infty)$ such that the solutions agree on the interval $[0, t_0]$ by Picard's theorem. Let $I \subseteq \mathbb{R}_+$ be the union of all such intervals. Then, by the continuity of the solutions, I is closed and has a right-hand endpoint $T_0 > 0$ such that $I = [0, T_0]$. Suppose that T_0 is finite, i.e., there exists a nonempty open interval $J \subseteq \mathbb{R}_+$ such that I and J are disjoint, $I \cup J$ is an interval, and $\mathbf{x}_1(t) \neq \mathbf{x}_2(t)$ for all $t \in J$. Because $\mathbf{x}_1(T_0)$ is in $\mathcal{D}$, there is a closed ball centered at $\mathbf{x}_1(T_0)$ contained in $\mathcal{D}$, which means that the two solutions must agree on the interval $[T_0, T_0 + \delta]$ for some $\delta > 0$ by Picard's theorem, which is a contradiction. □

Lemma 4.2.2 Let $I = [0, T)$ for some $T > 0$ and A be a nonempty closed subset of I. Then, for every $t \in I$, there is $s \in I$ such that $[s, t] \subseteq A$ as well as either $s = 0$ or $s \in \partial(I \setminus A)$, where singleton intervals are allowed. ◇

Proof: Let $R = \{[u, t] \mid u \leq t,\ [u, t] \subseteq A\}$ and $B = \bigcup R$. First, suppose that B is not closed, and let $a = \inf B$ which exists since A is bounded from below. Then, a belongs to A from the fact that A is closed and $B \subseteq A$, and B has the

form $B = (a, t]$ because B is an interval. However, they immediately yield a contradiction because $\{a\} \cup (a, t] \in R$; hence, B is closed. Now, let $s = \min B$. If $[0, t] \in R$, $s = 0$. If $[0, t] \notin R$, suppose $s \notin \partial(I \setminus A)$. Then, since $s \in A$, there is $\epsilon > 0$ such that $B_\epsilon(s) \subseteq A$. Therefore, s cannot be the minimum of B, which is a contradiction. □

Lemma 4.2.3 Consider the differentiable function $h : \mathbb{R}_+ \times \mathcal{D} \to \mathbb{R}$. Suppose that there are $h_1, h_2 > 0$ with $h_1 < h_2$ such that $\dot{h}(t, \mathbf{x}) = \frac{\partial h}{\partial t} + \frac{\partial h}{\partial \mathbf{x}} \mathbf{f}(t, \mathbf{x}) \geq 0$ whenever $h(t, \mathbf{x}) \in (h_1, h_2)$. Then, the solutions of Eq. (4.1) satisfy $h|_t \geq \min\{h|_0, h_2\}$ if $h|_0 > h_1$. ◇

Proof: First, assume $h|_0 \leq h_2$. Suppose there is $t_1 \in I$ such that $h|_{t_1} \in (h_1, h|_0)$ aiming for contradiction. Let $t_2 = \min\{t \in [0, t_1] \mid h|_t \leq h|_{t_1}\}$ and $t_3 = \max\{t \in [0, t_2] \mid h|_t \geq h|_0\}$. Then, for all $t \in (t_3, t_2)$, $h|_t \in (h|_{t_1}, h|_0)$; thus, $h|_t \in (h_1, h_2)$, from which it follows that $h|_{t_2} - h|_{t_3} = \int_{t_3}^{t_2} \dot{h}|_\tau \mathrm{d}\tau \geq 0$. However, $h|_{t_2} - h|_{t_3} \leq h|_{t_1} - h|_0 < 0$, which is a contradiction. Therefore, $h|_t \geq h|_0$ for all $t \in I$ because $h|_t \leq h_1$ cannot not happen due to continuity. Now, a similar argument can be developed for the case $h|_0 > h_2$. Suppose that there is $s_1 \in I$ such that $h|_{s_1} \in (h_1, h_2)$. Let $s_2 = \min\{t \in [0, s_1] \mid h|_t \leq h|_{s_1}\}$ and $s_3 = \max\{t \in [0, s_2] \mid h|_t \geq h_2\}$. Then, for all $t \in (s_3, s_2)$, $h|_t \in (h|_{s_1}, h_2)$; thus, $h|_t \in (h_1, h_2)$. From the fact that $h|_{s_2} - h|_{s_3} \leq h|_{s_1} - h_2 < 0$, $h|_t \geq h_2$ is obtained. □

Corollary 4.2.1 Suppose the differentiable function $h : \mathbb{R}_+ \times \mathcal{D} \to \mathbb{R}$ satisfies $\dot{h} \geq g(h)$ for some continuous function $g : \mathbb{R} \to \mathbb{R}$ with $g(h_c) > 0$ where $h_c \in \mathbb{R}$. Then, the solutions of Eq. (4.1) satisfy $h|_t \geq h_c$ whenever $h|_0 \geq h_c$. ◇

Proof: Since $g(h_c) > 0$, there is $\delta > 0$ such that $g(x) > 0$ for all $x \in (h_c - \delta, h_c + \delta)$; hence, $\dot{h} \geq 0$ whenever $h \in (h_c - \delta, h_c)$. Now, it directly follows from Lemma 4.2.3 that if $h|_0 \geq h_c$, $h|_t \geq \min\{h|_0, h_c\} = h_c$. □

Definition 4.2.1 (positive invariance) A set S is said to be positively invariant with respect to Eq. (4.1) if for any initial time $t_0 \geq 0$ and state $\mathbf{x}_0 \in S$, a unique solution, defined for all $t \geq t_0$, exists and stays inside S for all future time.

It will be shortly shown in the following chapter that PFC requires the notion of the set stability. It can be thought of as an extension of the original Lyapunov stability theory.

Definition 4.2.2 (set stability) Let $C \subseteq \mathbb{R}^n$.

1) The set

$$N_\epsilon(C) = \{\mathbf{x} \in \mathbb{R}^n \mid d(\mathbf{x}, C) < \epsilon\} \tag{4.5}$$

is called an ϵ-*neighborhood* of C, where

$$d(\mathbf{x}, C) = \inf_{\mathbf{y} \in C} \|\mathbf{y} - \mathbf{x}\| \tag{4.6}$$

is the distance from $\mathbf{x}$ to the set C.

2) C is said to be *uniformly asymptotically stable (UAS)* with respect to the system Eq. (4.1) if C is closed, and there are $\delta > 0$ and a class $\mathcal{KL}$ function $\beta : [0, \delta] \times \mathbb{R}_+ \to \mathbb{R}$ such that

$$d(\mathbf{x}(t), C) \leq \beta(d(\mathbf{x}_0, C), t - t_0) \tag{4.7}$$

for all $t \geq t_0$ and all $\mathbf{x}_0 \in N_\delta(C)$;

3) The region of attraction of C is a set of all initial states, of which the corresponding solution $\mathbf{x}(t)$ is defined for all $t \geq 0$, and

$$\lim_{t \to \infty} d(\mathbf{x}(t), C) = 0 \tag{4.8}$$

Note that 2) in Definition 4.2.2 is a sufficient condition for the stability of a closed invariant set introduced in [61, 64] and the partial stability in [65] when the system is autonomous.

4.3 Barrier Method

In this section, the barrier method integrated with a semidefinite Lyapunov function is proposed. Theorem 4.4.1 provides a sufficient condition for a dynamical system to stay in a subset of the domain that is closed in the Euclidean space. Then, by progressively adding assumptions, the ultimate property of a solution and uniformly asymptotic stability of a closed invariant subset is presented in Corollary 4.3.1 and Theorem 4.4.2, respectively.

Consider the system

$$\begin{aligned} \dot{\mathbf{x}}_s &= \mathbf{f}_s(t, \boldsymbol{\eta}) \\ \dot{\mathbf{x}}_1 &= \mathbf{f}_1(t, \boldsymbol{\eta}) \end{aligned} \tag{4.9}$$

where $\mathbf{x}_s \in \mathbb{R}^{n_s}$ and $\mathbf{x}_1 \in \mathbb{R}^{n_1}$ are the states, and $\boldsymbol{\eta} = (\mathbf{x}_s, \mathbf{x}_1)$. $\mathbf{f}_s : \mathbb{R}_+ \times \mathcal{D} \to \mathbb{R}^{n_s}$ and $\mathbf{f}_1 : \mathbb{R}_+ \times \mathcal{D} \to \mathbb{R}^{n_1}$ are the state functions on the open set $\mathcal{D}_\eta \subseteq \mathbb{R}^n$ where $n = n_s + n_1$. The overall equations are represented by $\dot{\boldsymbol{\eta}} = \mathbf{f}_\eta(t, \boldsymbol{\eta})$. The state $\mathbf{x}_1$ is the part to be stabilized.

Let $V_1 : \mathbb{R}^{n_1} \to \mathbb{R}$ be a continuously differentiable positive definite function and $P_1 = \{\mathbf{x}_1 \in \mathbb{R}^{n_1} \mid (\mathbf{x}_s, \mathbf{x}_1) \in \mathcal{D}_\eta\}$.

Assumption 4.3.1: There are a set $A_1 \subseteq P_1$ and a continuous positive definite function W_{13} on P_1 such that the time-derivative of V_1 satisfies

$$\dot{V}_1 = \frac{\partial V_1}{\partial \boldsymbol{\eta}} \mathbf{f}_\eta(t, \boldsymbol{\eta}) \leq -W_{13}(\mathbf{x}_1) \text{ whenever } \mathbf{x}_1 \in A_1 \tag{4.10}$$

Theorem 4.3.1 Under Assumption 4.3.1, suppose that

1) There exist $\epsilon_{V_1}, c_{V_1}, k > 0$ such that $\epsilon_{V_1} < c_{V_1}$, and

$$[\mathbf{x}_1 \in A_1 \text{ and } W_{13}(\mathbf{x}_1) \geq k] \text{ whenever } V_1(\mathbf{x}_1) \in [\epsilon_{V_1}, c_{V_1}] \tag{4.11}$$

2) There are $h_c \in \mathbb{R}$, $c \in [0, c_{V_1}]$, a continuously differentiable function $h : \mathcal{D}_\eta \to \mathbb{R}$, and a continuous function $g_1 : \mathbb{R} \to \mathbb{R}$ such that

$$[\dot{h} \geq g_1(h) \text{ and } g_1(h_c) > 0] \text{ whenever } V_1(\mathbf{x}) \leq b \tag{4.12}$$

where $b = \max\{c, \epsilon_{V_1}\}$.

Then, every solution starting in

$$S = \{\boldsymbol{\eta} \in \mathcal{D}_\eta \mid V_1(\mathbf{x}_1) \leq c,\ h(\boldsymbol{\eta}) \geq h_c\} \tag{4.13}$$

remains in $\{\boldsymbol{\eta} \in \mathcal{D}_\eta \mid V_1(\mathbf{x}_1) \leq b,\ h(\boldsymbol{\eta}) \geq h_c\}$. ◇

Proof: Let I be the maximal interval of existence of the solution starting in S. Without loss of generality, let the solution start at $t = 0$ and thus satisfy $V_1|_0 \leq c$ and $h|_0 \geq h_c$. Since

$$V_1 \in [\epsilon_{V_1}, c] \subseteq [\epsilon_{V_1}, c_{V_1}] \ \Rightarrow\ \mathbf{x}_1 \in A_1 \tag{4.14}$$

it follows that $\dot{V}_1 \leq -W_{13} \leq -k$ whenever $V_1 \in [\epsilon_{V_1}, c]$. Therefore, $V_1|_t \leq \max\{V_1|_0, \epsilon_{V_1}\} \leq \max\{c, \epsilon_{V_1}\} = b$ for all $t \in I$. Consider the differential equation $\dot{y} = g_1(y)$ with $y(0) = h_c$, whose solution satisfies $y(t) \geq h_c$ from Corollary 4.2.1. Hence, from Lemma 3.4 (comparison lemma) in [61], $h|_t \geq y(t) \geq h_c$ for all $t \in I$. □

Corollary 4.3.1 In addition to the hypothesis of Theorem 4.3.1, suppose that $c \geq \epsilon_{V_1}$, and the set $\Omega = \{\boldsymbol{\eta} \in \mathcal{D}_\eta \mid V_1(\mathbf{x}_1),\ h(\boldsymbol{\eta}) \geq h_c\}$ is closed in $\mathbb{R}^n$, and $\mathbf{f}_\eta$ is bounded on $\mathbb{R}_+ \times \Omega$. Then, Ω is positively invariant, and for every solution

$\boldsymbol{\eta}(t)$ starting in Ω uniformly ultimately stays in the ϵ_{V_1}-sublevel set of W_1. $\diamond$

Proof: $b = c$ because $c \geq \epsilon_{V_1}$. Due to Theorem 4.3.1, every solution starting in Ω remains inside thereafter. Since $\mathbf{f}_\eta$ is bounded on $\mathbb{R}_+ \times \Omega$, Ω is positively invariant by Lemma 4.2.1. On the other hand, from the result $\dot{V}_1 \leq -k$ whenever $V_1 \geq \epsilon_{V_1}$, $V_1|_t \leq V_1|_0 - kt$ for all $t \in [0, T_c]$ where $T_c = (V_1|_0 - \epsilon_{V_1})/k$. Moreover, from Lemma 4.2.3, it follows that $V_1|_t \leq \epsilon_{V_1}$ for all $t > T_c$. Finally, the solution enters $\{\mathbf{x} \in \mathcal{D} \mid V_1(\mathbf{x}_1) \leq \epsilon_{V_1}\}$ in $[0, T_c]$ and stays there for all future time. $\square$

Assumption 4.3.2: There are $r > 0$ and class $\mathcal{K}$ functions $\alpha_{1i} : [0, r] \to \mathbb{R}$, $i = 1, 2, 3$, such that $P_1 \subseteq \overline{B}_r(\mathbf{0})$, and

$$\alpha_{11}(\|\mathbf{x}_1\|) \leq V_1(\mathbf{x}_1) \leq \alpha_{12}(\|\mathbf{x}_1\|), \; W_{13}(\mathbf{x}_1) \geq \alpha_{13}(\|\mathbf{x}_1\|) \tag{4.15}$$

for all $\mathbf{x}_1 \in P_1$.

Corollary 4.3.2 In addition to Assumption 4.3.1 and 4.3.2, suppose that there are $h_c \in \mathbb{R}$, $c > 0$, a continuously differentiable function $h : \mathcal{D}_\eta \to \mathbb{R}$, and a continuous function $g_1 : \mathbb{R} \to \mathbb{R}$ such that

$$[\dot{h} \geq g_1(h) \text{ and } g_1(h_c) > 0] \text{ whenever } V(\mathbf{x}) \leq c \tag{4.16}$$

and $\{\mathbf{x}_1 \in P_1 \mid V_1(\mathbf{x}_1) \leq c\} \subseteq A_1$. Then, there is a class $\mathcal{KL}$ function $\beta : [0, r] \times \mathbb{R}_+ \to \mathbb{R}$ such that

$$\|\mathbf{x}_1(t)\| \leq \beta(\|\mathbf{x}_1(t_0)\|, t - t_0) \tag{4.17}$$

for all $\mathbf{x}(t_0) \in \Omega$ and all $t \geq t_0 \geq 0$. $\diamond$

Proof: Unlike Corollary 4.3.1, this proposition guarantees that the inequality

in Eq. (4.10) applies on the entire region that the solution can reach. It was shown previously that for any initial state in Ω, a unique solution exists for all $t \geq t_0$. The comparison functions in Assumption 4.3.2 give

$$\dot{V} \leq -W_{13}(\mathbf{x}_1) \leq -\alpha_{13}(\|\mathbf{x}_1\|) \leq -\alpha_{13}(\alpha_{12}^{-1}(V)) \tag{4.18}$$

To see the behavior of $V_1|_t$, consider the differential equation $\dot{y} = -(\alpha_{13} \circ \alpha_{12}^{-1})(y)$ with $y(t_0) = V_1|_{t_0}$. For the solution $y(t)$, there is a class $\mathcal{KL}$ function β_0, whose domain contains $[0, \alpha_{12}(r)] \times \mathbb{R}_+$, such that $y(t) \leq \beta_0(y(0), t - t_0)$ by Lemma 4.4 in [61]. The comparison lemma then yields $V_1|_t \leq \beta_0(V_1|_{t_0}, t - t_0)$ for all $t \geq t_0$. Hence, the following is obtained by using the comparison functions

$$\|\mathbf{x}_1(t)\| \leq \alpha_{11}^{-1}(\beta_0(\alpha_{12}(\|\mathbf{x}_1(t_0)\|), t - t_0)) \tag{4.19}$$

where the right-hand side of Eq. (4.19) defines the desired β. □

The consequent of Corollary 4.3.2 does not yet satisfy the requirements of uniform asymptotic stability despite the existence of $\mathcal{KL}$ function β because it does not guarantee an ϵ-neighborhood of the surface $\{\boldsymbol{\eta} \in \mathcal{D}_\eta \mid \mathbf{x}_1 = \mathbf{0}\}$ on which β is active. In this aspect, when classical stability is in demand, the following theorem provides a useful sufficient condition for the surface to be UAS.

Theorem 4.3.2 Let $C = \{\boldsymbol{\eta} \in \mathcal{D}_\eta \mid \mathbf{x}_1 = \mathbf{0}\}$. Under the hypothesis of Corollary 4.3.2, suppose that

1) $\mathcal{D}_\eta$ contains an ϵ-neighborhood of C;

2) $h((\mathbf{x}_s, \mathbf{x}_1))$ is Lipschitz in $\mathbf{x}_1$;

3) There is $l > 0$ such that $h((\mathbf{x}_s, \mathbf{0})) \geq h_c + l$ for all $(\mathbf{x}_s, \mathbf{x}_1) \in \mathcal{D}_\eta$.

Then, C is UAS, and Ω is a subset of the region of attraction. $\diamondsuit$

Proof: Because C is relatively closed in Ω, C is closed. First, for each $\boldsymbol{\eta} = (\mathbf{x}_s, \mathbf{x}_1) \in N_\epsilon(C)$, it follows that $d(\boldsymbol{\eta}, C) = \|\mathbf{x}_1\|$ from

$$\|\boldsymbol{\eta} - \boldsymbol{\eta}_1\| = \|\boldsymbol{\eta} - (\mathbf{x}_{s1}, \mathbf{0})\| = \|(\mathbf{x}_s - \mathbf{x}_{s1}), \mathbf{x}_1\| \geq \|\mathbf{x}_1\|$$

for all $\boldsymbol{\eta}_1 = (\mathbf{x}_{s1}, \mathbf{x}_{11}) \in C$. Therefore, the proof is done if $\delta \in (0, \epsilon]$ is found such that $N_\delta(C) \subseteq \Omega$ because β in Corollary 4.3.2 can be chosen as the desired class $\mathcal{KL}$ function to show UAS. To this end, let

$$\delta = \min\left\{l/L,\ \alpha_{12}^{-1}(c),\ \epsilon\right\}$$

where L is the Lipschitz constant in 2). Let $\boldsymbol{\eta} = (\mathbf{x}_s, \mathbf{x}_1) \in N_\delta(C)$ be arbitrary. From $\|\mathbf{x}_1\| < \delta \leq l/L$, the following is obtained:

$$|h(\mathbf{x}_s, \mathbf{x}_1) - h(\mathbf{x}_s, \mathbf{0})| \leq L\|\mathbf{x}_1\| < Ll/L = l$$

Therefore, $h((\mathbf{x}_s, \mathbf{x}_1)) \geq h(\mathbf{x}_s, \mathbf{0}) - l > h_c$. On the other hand, $V_1(\mathbf{x}_1) \leq \alpha_{12}(\|\mathbf{x}_1\|) < \alpha_{12}(\delta) \leq c$. Hence, $N_\delta(C) \cap \mathcal{D}_\eta \subseteq \Omega$. As $N_\delta(C) \subseteq N_\epsilon(C) \subseteq \mathcal{D}_\eta$, $N_\delta(C)$ is contained in Ω, which completes the proof. $\square$

Remark 4.3.1: Corollary 4.3.2 and Theorem 4.3.2 are interesting in their own sakes. Though the former is not qualified for the classical definition of asymptotic stability, as long as the convergence of the states is the only concern, it provides useful conclusion under relatively weaker requirements. On the other hand, generally, the latter achieves asymptotic stability under a less restrictive constraint, represented by the indicator h.

4.4 Lyapunov Barrier Weighting Method

This section provides sufficient conditions for an augmented system of the previous system in Section 4.3 to have a desired ultimate property and uniform asymptotic stability. The propositions in this section are specifically dedicated for the backstepping control as it will be demonstrated in the development of WPTPFC.

Consider the system

$$\begin{aligned} \dot{\mathbf{x}}_s &= \mathbf{f}_s(t, \mathbf{x}) \\ \dot{\mathbf{x}}_1 &= \mathbf{f}_1(t, \mathbf{x}) \\ \dot{\mathbf{x}}_2 &= \mathbf{f}_2(t, \mathbf{x}) \end{aligned} \tag{4.20}$$

where $\mathbf{x}_s \in \mathbb{R}^{n_s}$, $\mathbf{x}_i \in \mathbb{R}^{n_i}$, $i = 1, 2$, are the states, and $\mathbf{x} = (\mathbf{x}_s, \mathbf{x}_1, \mathbf{x}_2)$. $\mathbf{f}_s : \mathbb{R}_+ \times \mathcal{D} \to \mathbb{R}^{n_s}$ and $\mathbf{f}_i : \mathbb{R}_+ \times \mathcal{D} \to \mathbb{R}^{n_i}$, $i = 1, 2$, are the state functions on the domain $\mathcal{D} = \mathcal{D}_\eta \times \mathcal{D}_2 \subseteq \mathbb{R}^n$, $n = n_s + n_1 + n_2$, for some open sets $\mathcal{D}_\eta \subseteq \mathbb{R}^{n_s+n_1}$ and $\mathcal{D}_2 \subseteq \mathbb{R}^{n_2}$. Two partially coupled states are further introduced: $\boldsymbol{\eta} = (\mathbf{x}_s, \mathbf{x}_1)$ and $\boldsymbol{\zeta} = (\mathbf{x}_1, \mathbf{x}_2)$ with $n_\eta = n_s + n_1$ and $n_\zeta = n_1 + n_2$, where $\boldsymbol{\eta}$ accounts for the constraints of the system, and $\boldsymbol{\zeta}$ is the part to be stabilized to its origin. The overall equations are represented by $\dot{\mathbf{x}} = \mathbf{f}(t, \mathbf{x})$, where $\mathbf{f} : \mathbb{R}_+ \times \mathcal{D} \to \mathbb{R}^n$.

Let $h, w : \mathcal{D}_\eta \to \mathbb{R}$ be continuously differentiable functions. w is constrained by the continuous functions $\underline{w}, \bar{w} : \mathbb{R}^{n_1} \to \mathbb{R}$ as follows:

$$w_0 \leq \underline{w}(\mathbf{x}_1) \leq w(\boldsymbol{\eta}) \leq \bar{w}(\mathbf{x}_1) \tag{4.21}$$

for all $\boldsymbol{\eta} \in \mathcal{D}_\eta$, where $w_0 > 0$. For the continuously differentiable positive definite functions $V_i : \mathbb{R}^{n_i} \to \mathbb{R}$, $i = 1, 2$, let $V : \mathcal{D} \to \mathbb{R}$ be defined by

$$V(\mathbf{x}) = V_1(\mathbf{x}_1) + w(\boldsymbol{\eta}) V_2(\mathbf{x}_2) \tag{4.22}$$

for all $\mathbf{x} \in \mathcal{D}$. Then, from the properties of w, it follows that

$$W_1(\boldsymbol{\zeta}) \leq V(\mathbf{x}) \leq W_2(\boldsymbol{\zeta}) \tag{4.23}$$

where W_1 and W_2 are continuous positive definite functions on $\mathcal{D}_\zeta = P_1 \times \mathcal{D}_2$ defined by $W_1(\boldsymbol{\zeta}) = V_1(\mathbf{x}_1) + \underline{w}(\mathbf{x}_1)V_2(\mathbf{x}_2)$ and $W_2(\boldsymbol{\zeta}) = V_1(\mathbf{x}_1) + \bar{w}(\mathbf{x}_1)V_2(\mathbf{x}_2)$ for all $\boldsymbol{\zeta} \in \mathcal{D}_\zeta$, where P_1 is the projection $\{\mathbf{x}_1 \in \mathbb{R}^{n_1} \mid (\mathbf{x}_s, \mathbf{x}_1) \in \mathcal{D}_\eta\}$, whereby $\mathcal{D}_\zeta$ is an open subset of $\mathbb{R}^{n_\zeta}$. The property that $V(\mathbf{x})$ is bounded by function values that depend only on $\boldsymbol{\zeta}$ will be used to make sure that the stability of the system is independent of $\mathbf{x}_s$.

Definition 4.4.1 Suppose that there is a function $\xi : (0, \infty) \to \mathbb{R}$ that has the following properties:

1) $\xi(h(\boldsymbol{\eta})) \leq w(\boldsymbol{\eta})$ whenever $h(\boldsymbol{\eta}) > 0$;

2) $\xi(\sigma) \to \infty$ as $\sigma \searrow 0$;

3) There is unique $\sigma_c > 0$ such that $\xi(\sigma_c) = w_0$ and the restriction $\xi_r := \xi\restriction_{(0,\sigma_c]}$ is strictly decreasing; hence ξ_r is invertible.

Then, w is a *barrier weighting* for V over h. ξ and h are the *(singular) barrier base* and *constraint indicator* for w, respectively.

Assumption 4.4.1: w is a barrier weighting for V over h, and ξ is a barrier base for w. There are a set $A_\zeta \subseteq \mathcal{D}_\zeta$ and a continuous positive definite function W_3 on $\mathcal{D}_\zeta$ such that the time-derivative of V satisfies

$$\dot{V} = \frac{\partial V}{\partial \mathbf{x}}\mathbf{f}(t, \mathbf{x}) \leq -W_3(\boldsymbol{\zeta}) \text{ whenever } \boldsymbol{\zeta} \in A_\zeta \tag{4.24}$$

Theorem 4.4.1 Under Assumption 4.4.1, suppose that

1) There are $\epsilon_V, c_V, k > 0$ such that $\epsilon_V < c_V$, and

$$[\boldsymbol{\zeta} \in A_\zeta \text{ and } W_3(\boldsymbol{\zeta}) \geq k] \text{ whenever } [W_1(\boldsymbol{\zeta}) \leq c_V \text{ and } W_2(\boldsymbol{\zeta}) \geq \epsilon_V] \tag{4.25}$$

2) There are $a, h_c > 0$, $c \in (0, c_V]$, and a continuous function $g_\zeta : \mathbb{R} \to \mathbb{R}$ such that

$$[\dot{h} \geq g_\zeta(h) \text{ and } g_\zeta(h_c) > 0] \text{ whenever } [V(\mathbf{x}) \leq b \text{ and } V_2(\mathbf{x}_2) \leq a] \tag{4.26}$$

$$h_c \leq \begin{cases} \xi_r^{-1}(b/a), & b \geq w_0 a \\ \sigma_c, & \text{otherwise} \end{cases} \tag{4.27}$$

where $b = \max\{c, \epsilon_V\}$.

Then, every solution starting in $S = \{\mathbf{x} \in \mathcal{D} \mid V(\mathbf{x}) \leq c,\ h(\boldsymbol{\eta}) \geq h_c\}$ remains in $\{\mathbf{x} \in \mathcal{D} \mid V(\mathbf{x}) \leq b,\ h(\boldsymbol{\eta}) \geq h_c\}$. $\diamond$

Proof: Let I be the maximal interval of existence of the solution starting in S. Without loss of generality, let the solution start at $t = 0$ and thus satisfy $V|_0 \leq c$ and $h|_0 \geq h_c$. Since

$$V \in [\epsilon_V, c] \ \Rightarrow\ [W_1 \leq c \leq c_V \text{ and } W_2 \geq \epsilon_V] \ \Rightarrow\ \boldsymbol{\zeta} \in A_\zeta \tag{4.28}$$

$\dot{V} \leq -W_3 \leq -k$ whenever $V \in [\epsilon_V, c]$. Therefore, $V|_t \leq \max\{V|_0, \epsilon_V\} \leq \max\{c, \epsilon_V\} = b$ is obtained for all $t \in I$ by applying Corollary 4.2.1. On the other hand, from the inequalities

$$V(\mathbf{x}) \geq V_1(\mathbf{x}_1) + \max\{\xi(h), w_0\}\, V_2(\mathbf{x}_2) \tag{4.29}$$

and $V|_t \leq b$, it follows that $b \geq \max\{\xi(h|_t), w_0\} V_2|_t$ for all $t \in I$. The behavior of $h|_t$ is inspected by partitioning I into two subsets along the cases $V_2|_t > a$ and the other:

1) Let $V_2|_t > a$. Note first that $h_c \leq \sigma_c$ in any case from (4.27). Therefore, if $\xi(h|_t) < w_0$, $h|_t > \sigma_c \geq h_c$ due to 3) in Definition 4.4.1. On the other hand, when $\xi(h|_t) \geq w_0$, it follows that $\xi(h|_t) = \xi_r(h|_t)$ and $b \geq \max\{\xi(h|_t), w_0\} V_2|_t = \xi(h|_t)V_2|_t > \xi(h|_t)a$, where the resulting inequality $w_0 \leq \xi(h|_t) < b/a$ shows that b must have been chosen so that $b > w_0 a$ for this case to be feasible; hence, $h|_t > \xi_r^{-1}(b/a) \geq h_c$. Consequently, regardless of the value of $\xi(h|_t)$, $h|_t > h_c$. Note that h_c is positive due to the domain of ξ_r.

2) Now, let $V_2|_t \leq a$. Lemma 4.2.2 ensures the existence of the closed time interval $[s, t]$ in I such that $s = 0$ or $\partial\{t \in I \mid V_2|_t > a\}$. First, let us examine the case when $s = 0$. Consider the differential equation $\dot{y} = g_\zeta(y)$ with $y(s) = h_c$, whose solution satisfies $y(\tau) \geq h_c$ for all $\tau \in [s, t]$ by Corollary 4.2.1. $\dot{h}|_t \geq g_\zeta(h|_t)$ follows from (4.26) and $h|_0 \geq h_c$ from $\mathbf{x}(0) \in S$. Hence, from the comparison lemma, $h|_\tau \geq y(\tau) \geq h_c$ for all $\tau \in [s, t] = [0, t]$. If $s \in \partial\{t \in I \mid V_2|_t > a\}$, from the fact that $h|_t > h_c$ whenever $V_2|_t > a$, it follows that $\lim_{\tau \nearrow s} h|_\tau \geq h_c$; thus, $h|_s \geq h_c$ by continuity. Therefore, similar to the previous case, $h|_\tau \geq y(\tau) \geq h_c$ for all $\tau \in [s, t]$, which leads to $h|_t \geq h_c$.

Finally, combining the preceding results yields $h|_t \geq h_c$ for all $t \in I$. □

In Theorem 4.4.1, if there is a class $\mathcal{K}$ function $\alpha : [0, g_1(h_c)] \to \mathbb{R}$ such that $g_\zeta(h) \geq g_1(h) - \alpha(V_2)$ whenever $V \leq b$ for the same b, the existence of a is

guaranteed. Choose $a < \alpha^{-1}(g_1(h_c))$. Then, it follows that $g_\zeta(h_c) \geq g_1(h_c) - \alpha(V_2) \geq g_1(h_c) - \alpha(a) > 0$ whenever $V \leq b$ and $V_2 \leq a$. This property motivated the development of the barrier weighting method in that the bounding function g_1 can be reused for the augmented system in this case.

Now, several useful propositions that apply to more specialized systems are derived.

Corollary 4.4.1 In addition to the hypothesis of Theorem 4.4.1, suppose that

1) $c \geq \epsilon_V$;

2) There are $c_2 > 0$ and a continuous function $g_2 : \mathbb{R} \to \mathbb{R}$ such that $\dot{V}_2 \leq g_2(V_2)$ with $g_2(c_2) < 0$;

3) The set $\Omega = \{\mathbf{x} \in \mathcal{D} \mid V(\mathbf{x}) \leq c,\ h(\boldsymbol{\eta}) \geq h_c,\ V_2(\mathbf{x}_2) \leq c_2\}$ is closed in $\mathbb{R}^n$, and $\mathbf{f}$ is bounded on $\mathbb{R}_+ \times \Omega$.

Then, Ω is positively invariant, and for every solution $\mathbf{x}(t) = (\mathbf{x}_s(t), \boldsymbol{\zeta}(t))$ starting in Ω, $\boldsymbol{\zeta}(t)$ uniformly ultimately stays in the ϵ_V-sublevel set of W_1. $\diamond$

Proof: The proof is similar to Corollary 4.3.1. $b = c$ because $c \geq \epsilon_V$. Due to Theorem 4.4.1 and the existence of the function g_2, every solution starting in Ω remains inside thereafter. Since $\mathbf{f}$ is bounded on $\mathbb{R}_+ \times \Omega$, Ω is positively invariant by Lemma 4.2.1. On the other hand, from the result $\dot{V} \leq -k$ whenever $V \geq \epsilon_V$, $V|_t \leq V|_0 - kt$ for all $t \in [0, T_c]$ where $T_c = (V|_0 - \epsilon_V)/k$. Moreover, from Lemma 4.2.3, $V|_t \leq \epsilon_V$ for all $t > T_c$. Because $V(\mathbf{x}) \leq \epsilon_V$ implies $W_1(\boldsymbol{\zeta}) \leq \epsilon_V$, it is concluded that the solution enters $\{\mathbf{x} \in \mathcal{D} \mid W_1(\boldsymbol{\zeta}) \leq \epsilon_V\}$ in $[0, T_c]$ and stays there for all future time. $\square$

Remark 4.4.1: In 2) of Corollary 4.4.1, if $c_2 \leq a$ is further assumed, the condition $h_c \leq \xi_r^{-1}(b/a)$ in Theorem 4.4.1 becomes obsolete because $V_2|_t \leq c_2 \leq a$ for all $t \in I$, and (4.26) will ensure $h|_t \geq h_c$ for any h_c. Therefore, h_c can be any positive number in this case. Moreover, 2) can be omitted if $c_2 \geq c/w_0$ because $V(\mathbf{x}) \leq c$ implies $V_2(\mathbf{x}_2) \leq c_2$ from $w_0 V_2 \leq V \leq c \leq w_0 c_2$.

Assumption 4.4.2: There are $r > 0$ and class $\mathcal{K}$ functions $\alpha_i : [0, r] \to \mathbb{R}$, $i = 1, 2, 3$, such that $\mathcal{D}_\zeta \subseteq \overline{B}_r(\mathbf{0})$, and

$$\alpha_1(\|\boldsymbol{\zeta}\|) \leq W_1(\boldsymbol{\zeta}),\ W_2(\boldsymbol{\zeta}) \leq \alpha_2(\|\boldsymbol{\zeta}\|),\ W_3(\boldsymbol{\zeta}) \geq \alpha_3(\|\boldsymbol{\zeta}\|) \tag{4.30}$$

for all $\boldsymbol{\zeta} \in \mathcal{D}_\zeta$.

Corollary 4.4.2 In addition to Assumptions 4.4.1 and 4.4.2, suppose that

1) There exist $a, c, h_c > 0$ and a continuous function $g_\zeta : \mathbb{R} \to \mathbb{R}$ such that

$$[\dot{h} \geq g_\zeta(h) \text{ and } g_\zeta(h_c) > 0] \text{ whenever } [V(\mathbf{x}) \leq c \text{ and } V_2(\mathbf{x}_2) \leq a] \tag{4.31}$$

$$h_c \leq \begin{cases} \xi_r^{-1}(c/a), & c \geq w_0 a \\ \sigma_c, & \text{otherwise} \end{cases} \tag{4.32}$$

as well as 2) and 3) of Corollary 4.4.1.

2) A_ζ in Assumption 4.4.1 contains the set $\{\boldsymbol{\zeta} \in \mathcal{D}_\zeta \mid W_1(\boldsymbol{\zeta}) \leq c,\ V_2(\mathbf{x}_2) \leq c_2\}$.

Then, there is a class $\mathcal{KL}$ function $\beta : [0, r] \times \mathbb{R}_+ \to \mathbb{R}$ such that

$$\|\boldsymbol{\zeta}(t)\| \leq \beta(\|\boldsymbol{\zeta}(t_0)\|, t - t_0) \tag{4.33}$$

for all $\mathbf{x}(t_0) \in \Omega$ and all $t \geq t_0 \geq 0$. $\diamondsuit$

Corollary 4.4.2 can be shown by following the proof of Corollary 4.3.2.

Theorem 4.4.2 Let $C = \{\mathbf{x} \in \mathcal{D} \mid \boldsymbol{\zeta} = \mathbf{0}\}$. Under the hypothesis of Corollary 4.4.2, suppose that

1) $\mathcal{D}$ contains an ϵ-neighborhood of C;

2) $h((\mathbf{x}_s, \mathbf{x}_1))$ is Lipschitz in $\mathbf{x}_1$;

3) There is $l > 0$ such that $h((\mathbf{x}_s, \mathbf{0})) \geq h_c + l$ for all $(\mathbf{x}_s, \mathbf{x}_1) \in \mathcal{D}_\eta$.

Then, C is UAS, and Ω is a subset of the region of attraction. $\diamondsuit$

Proof: For each $\mathbf{x} \in N_\epsilon(C)$, $d(\mathbf{x}, C) = \|\mathbf{x}_1, \mathbf{x}_2\|$ from

$$\|\mathbf{x} - \mathbf{y}\| = \|\mathbf{x} - (\mathbf{y}_s, \mathbf{0}, \mathbf{0})\| = \|(\mathbf{x}_s - \mathbf{y}_s), \mathbf{x}_1, \mathbf{x}_2\| \geq \|\mathbf{x}_1, \mathbf{x}_2\|$$

for all $\mathbf{y} = (\mathbf{y}_s, \mathbf{y}_1, \mathbf{y}_2) \in C$. Let

$$\delta = \min\left\{l/L,\ \alpha_2^{-1}(c),\ \alpha_{22}^{-1}(c_2),\ \epsilon\right\}$$

where L is the Lipschitz constant in 2), and $\alpha_{22} : [0, r] \to \mathbb{R}$ is a class $\mathcal{K}$ function such that $V_2(\mathbf{x}_2) \leq \alpha_{22}(\|\mathbf{x}_2\|)$. Now, follow the proof of Theorem 4.3.2. $\square$

Chapter 5

Weighted-Perpendicular-Tangent-based Path-Following Control

In this chapter, the weighted-perpendicular-tangent-based PFC is designed. The reference point for PFC called the perpendicular is defined and its properties are investigated in depth. It is a locally closest point to a desired path but has more advantageous properties than the closest point that is commonly used in the literature. The target plant is a point mass vehicle that has two input configuration: velocity direction input (VDI) and steering input (SI). The VDI control is designed first and the SI control law is design by using the VDI control law through an integrator backstepping-like control method. The Lyapunov barrier weighting method (BWM) is then applied to inherit the singularity avoidance capability the VDI control law has. Simple design examples are presented for each input system, and their numerical simulations are shown, which demonstrates the effectiveness of the proposed method.

5.1 Notation

- $\|\cdot\|$ denotes the Euclidean norm.
- A C^r function is said to be of class M^r if its derivatives are all bounded and the r-th order derivative is locally Lipschitz.
- A C^1 parametric curve $\boldsymbol{\gamma} : \mathbb{R} \to \mathbb{R}^3$ satisfying $\|\boldsymbol{\gamma}'(s)\| = 1$ for all $s \in \mathbb{R}$ is said to be naturally parametrized.
- For the derivatives of the curve denoted by $\mathbf{T}(s) = \boldsymbol{\gamma}'(s)$, $\boldsymbol{\kappa}(s) = \mathbf{T}'(s)$, and $\boldsymbol{\kappa}_2(s) = \mathbf{T}''(s)$, the first and second ones are called the tangent and curvature vectors, respectively, and $\kappa(s) = \|\boldsymbol{\kappa}(s)\|$ is the curvature.
- The world frame defined in Euclidean space is the only frame of reference that is used; therefore, both vector and matrix notations will be used interchangeably to represent three-dimensional vectors.

5.2 Path-Following Problem

In this section, the reference point is defined, and the baseline equations of motion for the path-following problem are derived.

5.2.1 Perpendicular Foot

Let $\boldsymbol{\gamma} : \mathbb{R} \to \mathbb{R}^3$ be a naturally parametrized path (curve), and $\mathbf{p} \in \mathbb{R}^3$.

Definition 5.2.1 The path parameter α is called the *foot parameter* of $\mathbf{p}$ onto $\boldsymbol{\gamma}$ if it satisfies the following equation for a fixed $\mathbf{p}$:

$$(\boldsymbol{\gamma}(\alpha) - \mathbf{p})^\top \boldsymbol{\gamma}'(\alpha) = \mathbf{e}(\alpha, \mathbf{p})^\top \mathbf{T}(\alpha) = 0 \tag{5.1}$$

where $\mathbf{e}(\alpha, \mathbf{p}) = \boldsymbol{\gamma}(\alpha) - \mathbf{p}$. $\boldsymbol{\gamma}(\alpha)$ and $\mathbf{e}(\alpha, \mathbf{p})$ are called the *(perpendicular) foot* and the *perpendicular* at α, respectively.

From this point on, any path and path derivatives at a foot will be occasionally written without arguments for brevity. That is, $\boldsymbol{\gamma} = \boldsymbol{\gamma}(\alpha)$, $\mathbf{T} = \mathbf{T}(\alpha)$, $\boldsymbol{\kappa} = \boldsymbol{\kappa}(\alpha)$, and $\boldsymbol{\kappa}_2 = \boldsymbol{\kappa}_2(\alpha)$, respectively.

To investigate the behavior of α over $\mathbf{p}$, let us derive the Jacobian of $\mathbf{T}(s)^\top \mathbf{e}(s, \mathbf{p})$ with respect to $(s, \mathbf{p})$:

$$\frac{\partial \mathbf{T}(s)^\top \mathbf{e}(s, \mathbf{p})}{\partial (s, \mathbf{p})} = \begin{bmatrix} \Delta(s, \mathbf{e}(s, \mathbf{p})) & -\mathbf{T}(s)^\top \end{bmatrix} \tag{5.2}$$

where $\Delta : \mathbb{R} \times \mathbb{R}^3 \to \mathbb{R}$ is defined by

$$\Delta(s, \mathbf{e}) = \mathbf{e}^\top \mathbf{T}'(s) + \mathbf{T}(s)^\top \mathbf{T}(s) = \mathbf{e}^\top \boldsymbol{\kappa}(s) + 1 \tag{5.3}$$

From this result, though Eq. (5.1) can have multiple solutions over a single $\mathbf{p}$ for general paths, the sensitivity of one of the foot parameters α with respect

to $\mathbf{p}$ is available by the implicit function theorem if $\Delta(\alpha, \mathbf{e}(\alpha, \mathbf{p})) \neq 0$. The derivative of Eq. (5.1) with respect to $\mathbf{p}$ taking α as a function of $\mathbf{p}$ on some neighborhood of $\mathbf{p}$ yields

$$\mathbf{e}^\top \mathbf{T}' \frac{\partial \alpha}{\partial \mathbf{p}} + \mathbf{T}^\top \left(\mathbf{T} \frac{\partial \alpha}{\partial \mathbf{p}} - \mathbf{I} \right) = 0$$

Therefore, the sensitivity is obtained as

$$\frac{\partial \alpha}{\partial \mathbf{p}} = \frac{1}{\Delta} \mathbf{T}^\top \tag{5.4}$$

where $\Delta = \Delta(\alpha, \mathbf{e}(\alpha, \mathbf{p}))$. The sensitivity has a singularity at $\Delta = 0$.

The sensitivity takes an important role in this study. Therefore, to gain some intuition about Δ, the geometric properties of the condition $\Delta = 0$ is investigated by the following theorem:

Theorem 5.2.1 $\Delta = 0$ if and only if $\kappa > 0$ and $\mathbf{p}$ is on the straight line λ passing through the center of curvature, $\boldsymbol{\gamma} + \boldsymbol{\kappa}/\kappa^2$, and parallel to $\mathbf{T} \times \boldsymbol{\kappa}$. $\diamondsuit$

Proof: (Sufficiency) For each $c \in \mathbb{R}$, let $\mathbf{p} = \boldsymbol{\gamma} + \boldsymbol{\kappa}/\kappa^2 + c\mathbf{T} \times \boldsymbol{\kappa}$ be the parametrization of λ. Then, $\mathbf{e} = \boldsymbol{\gamma} - \mathbf{p} = -\boldsymbol{\kappa}/\kappa^2 - c\mathbf{T} \times \boldsymbol{\kappa}$, which leads to $\Delta = \mathbf{e}^\top \boldsymbol{\kappa} + 1 = -\|\boldsymbol{\kappa}\|^2/\kappa^2 + 1 = 0$.
(Necessity) Let $\Delta = 0$. κ cannot be zero because $\boldsymbol{\kappa} = \mathbf{0}$ leads to $\mathbf{e}^\top \boldsymbol{\kappa} + 1 = 1 \neq 0$. In the case of $\kappa > 0$, $\boldsymbol{\kappa}$ and $\mathbf{T} \times \boldsymbol{\kappa}$ form orthogonal bases of $\mathbf{e}$ from the fact that $\mathbf{T}^\top \mathbf{T}' = \mathbf{T}^\top \boldsymbol{\kappa} = 0$ due to $\|\mathbf{T}\| = 1$; therefore, $\mathbf{e} = c_1 \boldsymbol{\kappa} + c_2 \mathbf{T} \times \boldsymbol{\kappa}$. From $\Delta = \mathbf{e}^\top \boldsymbol{\kappa} + 1 = c_1 \kappa^2 + 1 = 0$, it follows that $c_1 = -1/\kappa^2$. Now, the claim follows because for each $c_2 \in \mathbb{R}$, the point $\mathbf{p} = \boldsymbol{\gamma} + \boldsymbol{\kappa}/\kappa^2 - c_2 \mathbf{T} \times \boldsymbol{\kappa}$ is on the line λ. $\square$

Let $\mathbf{p} : \mathbb{R}_+ \to \mathbb{R}^3$ be a differentiable function that represents the position of the vehicle P. Now, the motion of the corresponding foot parameter of P is

studied. Consider the following dynamics of the path parameter s:

$$\dot{s} = \frac{1}{\Delta(s, \mathbf{e}(s, \mathbf{p}(t)))} \mathbf{T}(s)^\top \dot{\mathbf{p}}(t) \tag{5.5}$$

Let $E(t) = \mathbf{e}(s(t), \mathbf{p}(t))^\top \mathbf{T}(s(t))$ for the solution $s(t)$ of the differential equation. Then, we have

$$\begin{aligned} \dot{E} &= \dot{\mathbf{e}}^\top \mathbf{T} + \mathbf{e}^\top \dot{\mathbf{T}} \\ &= (\dot{\boldsymbol{\gamma}} - \dot{\mathbf{p}})^\top \mathbf{T} + \mathbf{e}^\top \dot{\mathbf{T}} \\ &= (\mathbf{T}\dot{s} - \dot{\mathbf{p}})^\top \mathbf{T} + \mathbf{e}^\top \mathbf{T}' \dot{s} \\ &= (\mathbf{T}^\top \mathbf{T} + \mathbf{e}^\top \mathbf{T}')\dot{s} - \dot{\mathbf{p}}^\top \mathbf{T} \\ &= \frac{1 + \mathbf{e}^\top \boldsymbol{\kappa}}{\Delta} \mathbf{T}^\top \dot{\mathbf{p}} - \dot{\mathbf{p}}^\top \mathbf{T} \\ &= 0 \end{aligned} \tag{5.6}$$

Therefore, $E(t)$ will stay zero whenever $E(0) = 0$, or equivalently, whenever $s(0)$ is the foot parameter of $\mathbf{p}(0)$, $s(t)$ will also be the foot parameter of $\mathbf{p}(t)$ on the interval of existence of the solution. Due to the singularity of the dynamics on $\Delta = 0$, it is demanded that Δ should be bounded away from zero to continue the solution indefinitely, which motivated this study on singularity avoidance techniques.

5.2.2 Vehicle Dynamics

In this study, two types of input that determines the motion of P are considered: the velocity direction input and the steering input, and each system has its own state equation. The former can be applied to kinematics-level systems whose input is velocity and the latter can be applied to dynamics-level systems driven by normal acceleration. In either cases, the speed of P is given as a function $U = U(t)$, that is,

$$\|\dot{\mathbf{p}}(t)\| = U(t) \tag{5.7}$$

where $U : \mathbb{R}_+ \to \mathbb{R}$ is an exogenously determined bounded C^1 signal; there exist $U_\mathrm{m}, U_\mathrm{M} > 0$ such that $U_\mathrm{m} \le U(t) \le U_\mathrm{M}$ for all $t \ge 0$.

Let $\overline{\mathbf{v}}$ be the velocity direction vector of P, that is,

$$\overline{\mathbf{v}}(t, \dot{\mathbf{p}}) := \frac{\dot{\mathbf{p}}}{\|\dot{\mathbf{p}}\|} = \frac{\dot{\mathbf{p}}}{U(t)} \tag{5.8}$$

In the velocity direction system, $\mathbf{p}$ is the state, and the input $\overline{\mathbf{u}}_v$, called the *velocity direction input*, is a unit vector that determines the direction of the velocity vector:

$$\overline{\mathbf{v}} = \overline{\mathbf{u}}_v \tag{5.9}$$

or

$$\dot{\mathbf{p}} = U\overline{\mathbf{u}}_v \tag{5.10}$$

On the other hand, the steering input system has $\mathbf{p}$ and $\dot{\mathbf{p}}$ as the states, and the *steering input* (SI) $\mathbf{u}_s$ changes the velocity vector:

$$\dot{\overline{\mathbf{v}}} = \frac{\mathrm{d}}{\mathrm{d}t}\left(\frac{\dot{\mathbf{p}}}{U}\right) = \frac{\ddot{\mathbf{p}}}{U} - \frac{\dot{\mathbf{p}}}{U^2}\dot{U} = \frac{\ddot{\mathbf{p}}}{U} - \frac{\dot{U}}{U}\overline{\mathbf{v}} = \mathbf{u}_s \tag{5.11}$$

or

$$\ddot{\mathbf{p}} = \dot{U}\overline{\mathbf{v}} + U\mathbf{u}_s \tag{5.12}$$

Because $\|\overline{\mathbf{v}}\| = 1$, the input $\mathbf{u}_s$ must be perpendicular to $\overline{\mathbf{v}}$ from

$$\overline{\mathbf{v}} \cdot \dot{\overline{\mathbf{v}}} = \overline{\mathbf{v}} \cdot \mathbf{u}_s = 0 \tag{5.13}$$

By using this property, $\ddot{\mathbf{p}}$, the acceleration of P, can be decomposed into the two orthogonal components as shown in Eq. (5.11): $\ddot{\mathbf{p}} = \mathbf{a}_T + \mathbf{a}_N$ with the tangential acceleration $\mathbf{a}_T = \dot{U}\overline{\mathbf{v}}$ and the normal acceleration $\mathbf{a}_N = U\mathbf{u}_s$. $\mathbf{a}_T$ is parallel to the velocity direction, and $\mathbf{a}_N$ is always perpendicular to $\mathbf{a}_T$. $\mathbf{u}_s$ can be seen as a scaled version of $\mathbf{a}_N$.

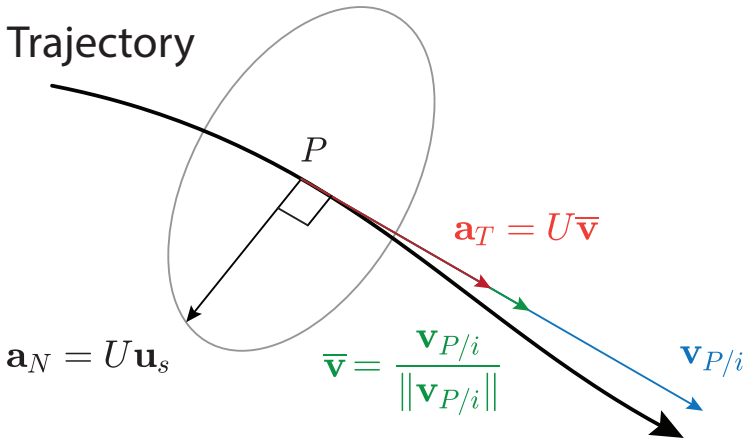

Figure 5.1: Acceleration geometry

5.2.3 Problem Statement

To define the PFC problem, the perpendicular foot dynamics Eq. (5.5) is combined with the vehicle dynamics Eqs. (5.10) and (5.11) taking the foot as the reference point for the PFC problem. No matter what input type the combined system has, the domain $\mathcal{D}$ of the system should exclude the surface $\Delta(\alpha, \mathbf{e}(\alpha, \mathbf{p})) = 0$. Therefore, an arbitrary number $\Delta_0 \in (0, 1)$ is chosen as a bound for Δ to define the domains for each system. The set $\mathcal{F} \subseteq \mathcal{D}$ of all initial conditions for $(s, \mathbf{p})$ that form a perpendicular foot is called the *consistent set* for the system [44]; the path parameter trajectory $s(t)$ that starts from this set will be always denoted by $\alpha(t)$ to avoid confusion with general parameters. Every solution starting in $\mathcal{F}$ must remain inside on the interval of existence due to the foot dynamics Eq. (5.6). In particular, in SI system, once $\dot{\mathbf{p}}(0) = U(0)$, $\dot{\mathbf{p}}(t) = U(t)$ thereafter because $\|\overline{\mathbf{v}}(t)\|$ will not change from its initial value due to the input orthogonality condition Eq. (5.13). This setup is summarized in Tables 5.1 and 5.2. The subscripts v and s on the set symbols stand for VDI and SI, respectively.

Table 5.1: VDI system representation

VDI	
States	$s, \mathbf{p}$
Input	$\overline{\mathbf{u}}_v$
Foot dynamics	$\dot{s} = \dfrac{U(t)}{\Delta(s, \mathbf{e}(s, \mathbf{p}))} \mathbf{T}(s)^\top \overline{\mathbf{u}}_v$
Position dynamics	$\dot{\mathbf{p}} = U(t) \overline{\mathbf{u}}_v$
Input constraint	$\lVert \overline{\mathbf{u}}_v \rVert = 1$
Domain	$\mathcal{D}_{\mathrm{v}} = \left\{ (s, \mathbf{p}) \in \mathbb{R}^4 \;\middle\vert\; \Delta(s, \mathbf{e}(s, \mathbf{p})) > \Delta_0 \right\}$
Consistent set	$\mathcal{F}_{\mathrm{v}} = \left\{ (s, \mathbf{p}) \in \mathcal{D}_{\mathrm{v}} \;\middle\vert\; \mathbf{e}(s, \mathbf{p})^\top \mathbf{T}(s) = 0 \right\}$

Table 5.2: SI system representation

SI	
States	$s, \mathbf{p}, \dot{\mathbf{p}}$
Input	$\mathbf{u}_s$
Foot dynamics	$\dot{s} = \dfrac{U(t)}{\Delta(s, \mathbf{e}(s, \mathbf{p}))} \mathbf{T}(s)^\top \overline{\mathbf{v}}$
Position dynamics	$\ddot{\mathbf{p}} = \dot{U}(t) \overline{\mathbf{v}} + U(t) \mathbf{u}_s$
Input constraint	$\overline{\mathbf{v}}^\top \mathbf{u}_s = 0$
Domain	$\mathcal{D}_{\mathrm{s}} = \left\{ (s, \mathbf{p}, \dot{\mathbf{p}}) \in \mathbb{R}^7 \;\middle\vert\; \Delta(s, \mathbf{e}(s, \mathbf{p})) > \Delta_0 \right\}$
Consistent set	$\mathcal{F}_{\mathrm{s}} = \left\{ (s, \mathbf{p}, \dot{\mathbf{p}}) \in \mathcal{D}_{\mathrm{s}} \;\middle\vert\; \mathbf{e}(s, \mathbf{p})^\top \mathbf{T}(s) = 0,\ \dot{\mathbf{p}} = U(0) \right\}$

Definition 5.2.2 (path-following problem) A control law for the systems in Tables 5.1 and 5.2 is called a PF *controller* if it drives the closed-loop system to have a nonempty set $R \subseteq \mathcal{F}$ of initial states such that for the solution starting in R,

1. The solution is unique and defined for all $t \geq 0$;

2. The perpendicular is regulated:

$$\|\mathbf{e}(\alpha(t), \mathbf{p}(t))\| \to 0 \text{ as } t \to \infty \tag{5.14}$$

3. The velocity direction $\dot{\mathbf{p}}(t)/U(t)$ converge to the path tangent $\mathbf{T}(\alpha(t))$ at the foot:

$$\left\| \frac{\dot{\mathbf{p}}(t)}{U(t)} - s_{\mathrm{d}} \mathbf{T}(\alpha(t)) \right\| \to 0 \text{ as } t \to \infty, \tag{5.15}$$

where $s_{\mathrm{d}} \in \{-1, 1\}$ is a predetermined constant called the path direction, which is used to choose the direction in which the point P traverses the path.

From the Definition 5.2.2, PFC can be classified as a constrained output regulation problem in that the regulation of the output $\mathbf{e}(\alpha, \mathbf{p})$ is required and that Δ should be bounded from below by some positive constant $\Delta_{\mathrm{c}} \in (\Delta_0, 1)$. On the other hand, from Eqs. (5.5) and (5.15), it can be seen that the foot parameter $|\alpha(t)|$ eventually grows unbounded because there are $\epsilon, T > 0$ such that $\left|\mathbf{T}(\alpha(t))^\top \dot{\mathbf{p}}(t)\right| > \epsilon$ for all $t > T$. In the PFC problem, the initial time is fixed to 0 for simplicity.

5.2.4 Path and Initial Position

As stated earlier, a single position $\mathbf{p}$ can have multiple distinct foots on a path. It will be shortly shown that only the initial foots with positive distance convexity ($\Delta > 0$) are eligible for the path-following problem. Because $\Delta = 1$ whenever $\rho = 0$ and the solution $\Delta|_t$ is a continuous function of t, a solution trajectory with the initial foot that satisfies $\Delta < 0$ must pass through the surface $\Delta = 0$ as $\rho(t)$ approaches zero, which cannot happen. Fortunately, foots with $\Delta < 0$ are naturally out of our interest because of its geometric inadequacy. To verify this, let $f(s) = \|\boldsymbol{\gamma}(s) - \mathbf{p}\|^2/2$ for some fixed $\mathbf{p} \in \mathbb{R}^3$. Then, $f(\alpha) = \|\boldsymbol{\gamma}(\alpha) - \mathbf{p}\|^2/2 = \rho^2/2$, $f'(\alpha) = 0$, and $f''(\alpha) = 1 + (\boldsymbol{\gamma} - \mathbf{p})^\top \mathbf{T}' = \Delta$. Therefore, $f(s)$ has its local minimum, local maximum, and inflection point at $s = \alpha$ if $\Delta > 0$, $\Delta < 0$, and $\Delta = 0$, respectively. Because $f(\alpha)$ is proportional to the square of the local distance ρ, the foots with $\Delta < 0$ have a local maximum local distance. There is no reason a local maximum should be chosen as a reference point when a local minimum can be always found. The foregoing discussion is summarized in Fig. 5.2.

5.2.5 Closest Point and Perpendicular Foot

The perpendicular foot (PF) shares several properties with the closest point (CP). The line that connects the reference point and the point $\mathbf{p}$, which represents the perpendicular in the PF geometry, is orthogonal to the tangent $\mathbf{T}$. Since CP requires the distance to be minimum, the derivative of the distance $\|\mathbf{e}(s)\|^2$ must be zero, where $\mathbf{e}(s) = \boldsymbol{\gamma}(s) - \mathbf{p}$. That is,

$$\begin{aligned} \frac{\mathrm{d}}{\mathrm{d}s}\|\mathbf{e}(s)\|^2 &= 2\boldsymbol{\gamma}'(s) \cdot (\boldsymbol{\gamma}(s) - \mathbf{p}) \\ &= 0 \end{aligned} \tag{5.16}$$

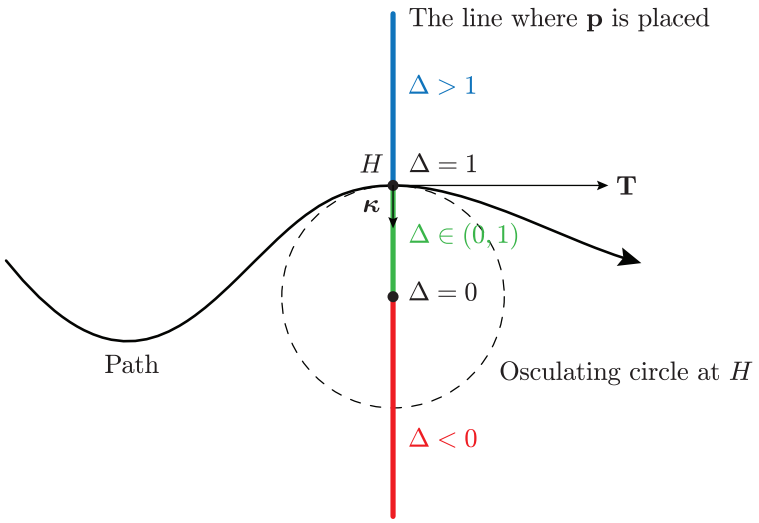

Figure 5.2: Geometry of Δ. The sign of the distance convexity Δ is geometrically determined by the position of $\mathbf{p}$ relative to the osculating circle at the foot H.

Equation 5.16 is a necessary condition for the point $\boldsymbol{\gamma}(s)$ to be the closest point on the path for $\mathbf{p}$. This is identical to the PF condition in (5.1); thus, every CP is PF. CP has several advantages: 1) CP represents the shortest route for the vehicle to the desired path; 2) If CP is uniquely determined by each $\mathbf{p}$, CP is a function of the vehicle position $\mathbf{p}$ only. The second property is a key feature that most CP-based research resort to because it greatly simplifies the controller design.

However, it entails a critical problem that the assumption is valid for only straight lines. For general paths, it is not guaranteed that CP is unique for all $\mathbf{p}$, and CP is not even continuous with respect to the motion of $\mathbf{p}$. Some paths have a region where CP does not exist at all for $\mathbf{p}$ in the region. In practice, CP can only be found by using a numerical method for general paths. Moreover, general approaches do not guarantee a global solution. Therefore, even if a unique CP exists for $\mathbf{p}$, finding one is another challenge.

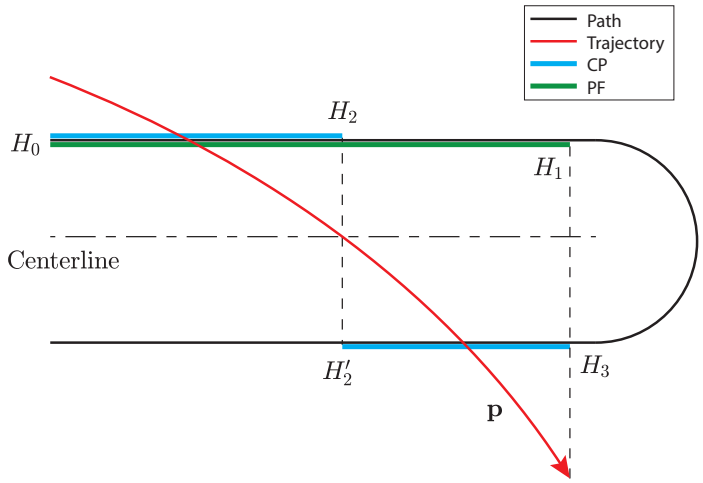

Figure 5.3: Comparison between CP and PF: CF is discontinuous, while PF is continuous for the trajectory of $\mathbf{p}$ on the U-shaped path. CP undergoes a jump discontinuity from H_2 to H_2' during the movement from H_0 to H_3. PF starts from H_0 and arrives at H_1 in a continuous motion.

In contrast, PF consists of an augmented state, path parameter s, which is controlled by the associated state equation (5.5). Therefore, PF is always continuous with respect to $\mathbf{p}$, and PF needs not be unique for each $\mathbf{p}$ since s keeps track of a continuous trajectory of PF. Fig. 5.3 illustrates a situation where a jump discontinuity occurs in CP for a moving $\mathbf{p}$, while PF is continuous.

To see another advantage of PF over CP, consider a planar path

$$\boldsymbol{\gamma}(\sigma) = \begin{bmatrix} \cos(2\pi\sigma) + 2\exp(-\sigma) \\ \sin(2\pi\sigma) \end{bmatrix} \tag{5.17}$$

The image $\Gamma = \{\boldsymbol{\gamma}(\sigma) \mid \sigma \in \mathbb{R}\}$ of the path resembles a sagging spring, and it can be seen by inspection that the left-most side of the path in x-y plane approaches the line $x = -1$ as $\sigma \to \infty$ as shown in Fig. 5.4. Let $\mathbf{p} = [-1\ 0]^\top$ be the position of a vehicle. Then, it is easy to see that $d(\mathbf{p}, \Gamma) = \inf_{\mathbf{y}\in\Gamma} \|\mathbf{p} - \mathbf{y}\| = 0$ but $\mathbf{p} \notin \Gamma$. Therefore, the CP for $\mathbf{p}$ on the path $\boldsymbol{\gamma}$ does not exist. In contrast, there are

infinite number of PFs with $\Delta > 0$ exist, which can be verified from Figs. 5.4 and 5.5, where the red x-shaped markers represent the feet with positive distance convexity $\Delta(\sigma) = \mathbf{e}(\sigma) \cdot \boldsymbol{\kappa}(\sigma) + 1$, and $E(\sigma) = \mathbf{e}(\sigma) \cdot \mathbf{T}(\sigma)$ is the orthogonality. This example shows that PF can be used for a much larger class of desired paths. Furthermore, from the practical point of view, an estimate of PF can be found easily by general unconstrained optimization algorithms since every local minimum solution yields one of the PFs for each $\mathbf{p}$.

Aside from the desirable properties of PF, the singularity that occurs when the zero distance convexity $\Delta = 0$ is a disadvantage that both reference points have, which can be seen from the fact that CP has the same sensitivity (5.4) as PF; the speed of the reference point becomes indefinite as Δ approaches zero. The discussions are summarized in Table 5.3.

Table 5.3: Comparison: the closest point and perpendicular foot

	Closest point	Perpendicular foot
Numerical approach	ineffective for general paths	easily found by numerical approaches
Number of states	0	1
Continuity w.r.t. $\mathbf{p}$	generally discontinuous	continuous
Singularity (indefinite reference speed)	occurs when $\Delta = 0$	

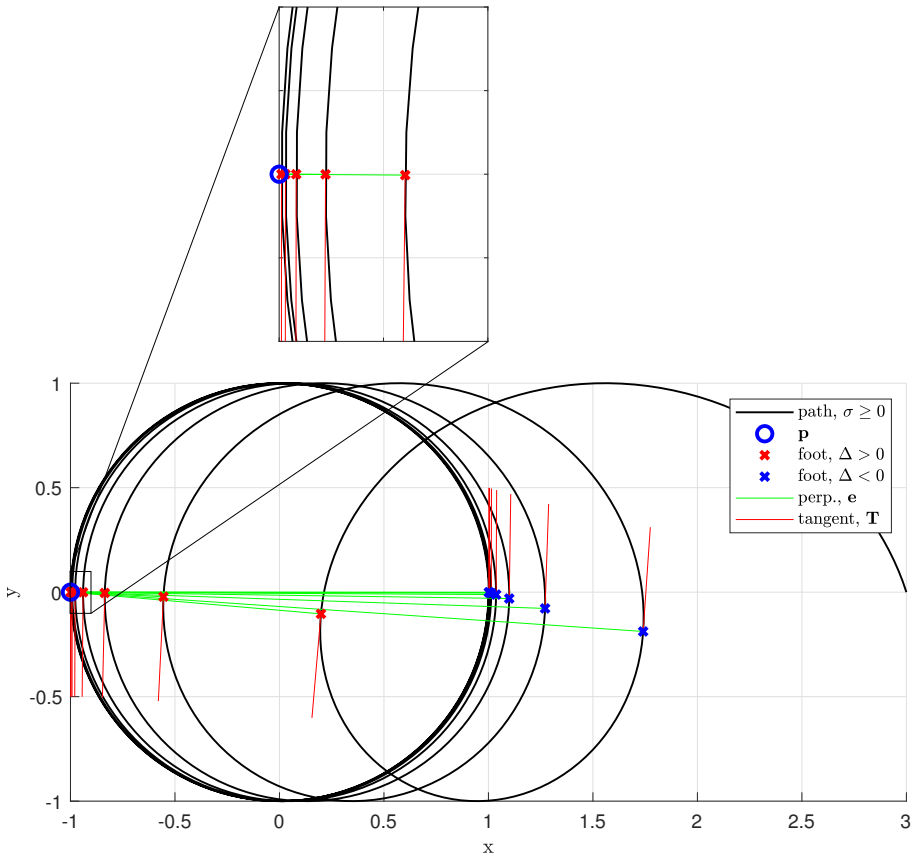

Figure 5.4: Perpendicular feet on a spring-like path

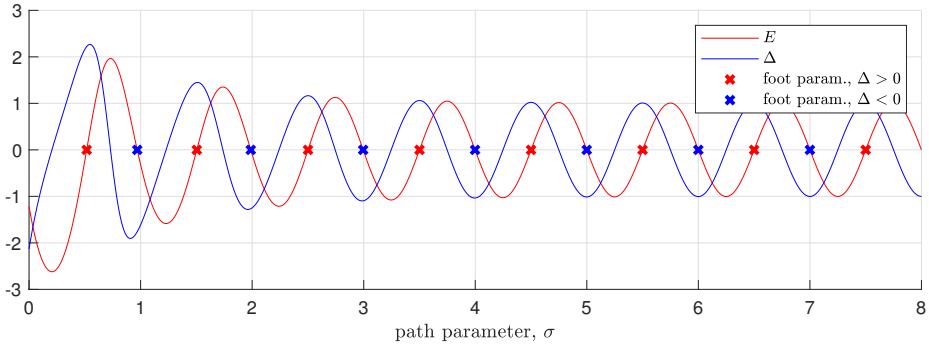

Figure 5.5: The orthogonality E and the distance convexity Δ

5.3 Velocity Direction Control

5.3.1 Dynamics

First, a change of variables is introduced to efficiently formulate PFC problem: $(\alpha, \mathbf{p}) \mapsto (\alpha, \mathbf{e})$ from the domain $\mathcal{D}_{\mathrm{v}}$ of the VDI system into the error space $\overline{\mathcal{D}}_{\mathrm{v}}$, defined by $\mathbf{e} = \mathbf{e}(\alpha, \mathbf{p}) = \boldsymbol{\gamma}(\alpha) - \mathbf{p}$. This is a natural choice for PFC because the perpendicular $\mathbf{e}(\alpha, \mathbf{p})$ serves as a tracking error in the problem. The state in the error space is denoted by $\mathbf{x}_{\mathrm{v}} = (\alpha, \mathbf{e})$. The state function $\mathbf{f}_{\mathrm{v}} : \mathbb{R}_+ \times \overline{\mathcal{D}}_{\mathrm{v}} \times \mathbb{R}^3 \to \mathbb{R}^4$ is then obtained by

$$\dot{\alpha} = \frac{U(t)}{\Delta(\alpha, \mathbf{e})} \mathbf{T}(\alpha)^\top \overline{\mathbf{u}}_v \tag{5.18a}$$

$$\begin{aligned} \dot{\mathbf{e}} &= \mathbf{T}(\alpha)\dot{\alpha} - \dot{\mathbf{p}} = \frac{U(t)}{\Delta(\alpha, \mathbf{e})} \mathbf{T}(\alpha)\mathbf{T}(\alpha)^\top \overline{\mathbf{u}}_v - U(t)\overline{\mathbf{u}}_v \\ &= U(t)\mathbf{A}(\alpha, \mathbf{e})\overline{\mathbf{u}}_v \end{aligned} \tag{5.18b}$$

where $\mathbf{A}(\alpha, \mathbf{e}) = \mathbf{T}(\alpha)\mathbf{T}(\alpha)^\top / \Delta(\alpha, \mathbf{e}) - \mathbf{I}_3$, and $\dot{\mathbf{x}}_{\mathrm{v}} = \mathbf{f}_{\mathrm{v}}(t, \mathbf{x}_{\mathrm{v}}, \overline{\mathbf{u}}_v)$. The domain and consistent set of the transformed system are

$$\begin{aligned} \overline{\mathcal{D}}_{\mathrm{v}} &= \left\{ \mathbf{x}_{\mathrm{v}} \in \mathbb{R}^4 \;\middle|\; \Delta(\alpha, \mathbf{e}) > \Delta_0 \right\} \\ \overline{\mathcal{F}}_{\mathrm{v}} &= \left\{ \mathbf{x}_{\mathrm{v}} \in \overline{\mathcal{D}}_{\mathrm{v}} \;\middle|\; \mathbf{e}^\top \mathbf{T}(\alpha) = 0 \right\} \end{aligned} \tag{5.19}$$

In particular, the magnitude of the perpendicular is called the *local distance* and denoted by $\rho := \|\mathbf{e}\|$.

Remark 5.3.1: $\overline{\mathcal{D}}_{\mathrm{v}}$ is nonempty, open, and connected. To see it is connected, let us first show that $(s, k\mathbf{e}) \in \overline{\mathcal{D}}_{\mathrm{v}}$ for all $(s, \mathbf{e}) \in \overline{\mathcal{D}}_{\mathrm{v}}$ and all $k \in [0, 1]$. Suppose

$\mathbf{e}^\top \boldsymbol{\kappa}(s) + 1 > \Delta_0$. Then, because $\Delta_0 \in (0, 1)$,

$$\begin{aligned}(k\mathbf{e})^\top \boldsymbol{\kappa}(s) + 1 &\geq k(\mathbf{e}^\top \boldsymbol{\kappa}(s) + 1) - k + 1 \\ &> k\Delta_0 + 1 - k \geq \min\{1, \Delta_0\} \\ &= \Delta_0\end{aligned}$$

On the other hand, it is easy to see that $(s, \mathbf{0}) \in \overline{\mathcal{D}}_{\mathrm{v}}$ for all $s \in \mathbb{R}$. Therefore, for each $(s_1, \mathbf{e}_1)$ and $(s_2, \mathbf{e}_2)$ in $\overline{\mathcal{D}}_{\mathrm{v}}$, the union

$$\{(s_1, k\mathbf{e}_1) \mid k \in [0, 1]\} \cup \{(s, \mathbf{0}) \mid s \in [s_1, s_2]\} \cup \{(s_2, k\mathbf{e}_2) \mid k \in [0, 1]\}$$

is a polygonal path contained in $\overline{\mathcal{D}}_{\mathrm{v}}$, which means $\overline{\mathcal{D}}_{\mathrm{v}}$ is path-connected, hence connected.

Define a positive semidefinite control Lyapunov function (CLF) $V : \mathbb{R}^3 \to \mathbb{R}_+$ by

$$V(\mathbf{x}_{\mathrm{v}}) = \frac{1}{2}\mathbf{e}^\top \mathbf{e} = \frac{1}{2}\rho^2 \tag{5.20}$$

whose derivative is

$$\dot{V}(t, \mathbf{x}_{\mathrm{v}}, \overline{\mathbf{u}}_v) = \mathbf{e}^\top \dot{\mathbf{e}} = U\mathbf{e}^\top \mathbf{A}\overline{\mathbf{u}}_v = -U\mathbf{e}^\top \overline{\mathbf{u}}_v \tag{5.21}$$

on $\overline{\mathcal{F}}_{\mathrm{v}}$, where $\mathbf{e}^\top \mathbf{T} = 0$ and

$$\mathbf{e}^\top \mathbf{A} = \mathbf{e}^\top \left(\frac{1}{\Delta}\mathbf{T}\mathbf{T}^\top - \mathbf{I}\right) = -\mathbf{e} \tag{5.22}$$

5.3.2 Controller Design

Definition 5.3.1 The functions $w_{\mathrm{T}} = w_{\mathrm{T}}(t, \mathbf{x}_{\mathrm{v}})$, $w_{\mathrm{e}} = w_{\mathrm{e}}(t, \mathbf{x}_{\mathrm{v}})$, and $w_\mu = w_\mu(t, \mathbf{x}_{\mathrm{v}})$ are *tangent, approach, and rotation weighting functions*, respectively,

if

1. they are all bounded, Lipschitz in $\mathbf{x}_{\mathrm{v}}$, and C^1 functions from $\mathbb{R}_+ \times \overline{\mathcal{D}}_{\mathrm{v}}$ into $\mathbb{R}$, whose derivatives are continuous in t and locally Lipschitz in $\mathbf{x}_{\mathrm{v}}$ on their domain;

2. they satisfy

$$\begin{aligned} |w_{\mathrm{T}}(t, \mathbf{x}_{\mathrm{v}})| &\leq u_{\mathrm{T}} \\ w_{\mathrm{T}}(t, (\alpha, \mathbf{0})) &= \epsilon_{\mathrm{T}} s_{\mathrm{d}} \\ l_{\mathrm{e}} \leq w_{\mathrm{e}}(t, \mathbf{x}_{\mathrm{v}}) &\leq u_{\mathrm{e}} \\ |w_{\mu}(t, \mathbf{x}_{\mathrm{v}})| &\leq u_{\mu} \end{aligned} \tag{5.23}$$

   for all $(t, \mathbf{x}_{\mathrm{v}}) \in \mathbb{R}_+ \times \overline{\mathcal{D}}_{\mathrm{v}}$, where u_{T}, ϵ_{T}, l_{e}, u_{e}, and u_{μ} are positive constants.

Using the weighting functions, define a function

$$\boldsymbol{\nu} = \boldsymbol{\nu}(t, \alpha, \mathbf{e}) = w_{\mathrm{T}}\mathbf{T} + w_{\mathrm{e}}\mathbf{e} + w_{\mu}\mathbf{e} \times \mathbf{T}. \tag{5.24}$$

In Fig. 5.6, $\mathbf{e}$ and $\mathbf{T}'$ lie on the plane Σ_T that is perpendicular to $\mathbf{T}$. On the other hand, $\mathbf{T}$ and $\mathbf{e} \times \mathbf{T}$ lie on the plane Σ_e that is perpendicular to $\mathbf{e}$. Since all three terms on the right-hand side of Eq. (5.24) are orthogonal to each other, it follows that

$$\|\boldsymbol{\nu}\|^2 = {w_{\mathrm{T}}}^2 + {w_{\mathrm{e}}}^2\|\mathbf{e}\|^2 + {w_{\mu}}^2\|\mathbf{e} \times \mathbf{T}\|^2 = {w_{\mathrm{T}}}^2 + \left({w_{\mathrm{e}}}^2 + {w_{\mu}}^2\right)\rho^2, \tag{5.25}$$

where $\|\mathbf{e} \times \mathbf{T}\|^2 = \|\mathbf{e}\|^2 - (\mathbf{e} \cdot \mathbf{T})^2 = \rho^2$.

Lemma 5.3.1 $\|\boldsymbol{\nu}\|$ is bounded away from zero on $\overline{\mathcal{D}}_{\mathrm{v}}$. $\diamond$

Proof: Let $L > 0$ be the Lipschitz constant of w_{T}. Then, for all $(t, (\alpha, \mathbf{e})) \in$

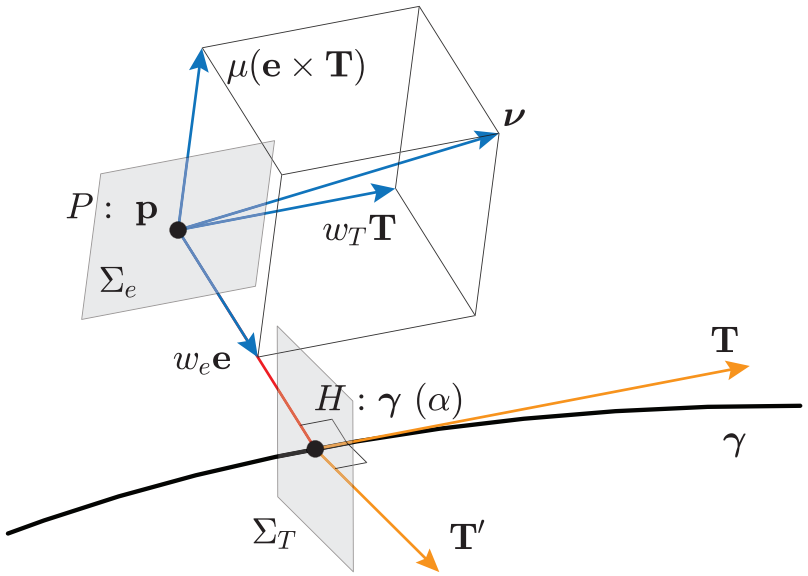

Figure 5.6: Geometry of $\boldsymbol{\nu}$

$\mathbb{R}_+ \times \overline{\mathcal{D}}_{\mathrm{v}}$ and all $(t_0, \alpha_0) \in \mathbb{R}_+ \times \mathbb{R}$, it follows that

$$\begin{aligned}
&|w_{\mathrm{T}}(t, (\alpha, \mathbf{e})) - w_{\mathrm{T}}(t_0, (\alpha_0, \mathbf{0}))| \\
&\qquad = |w_{\mathrm{T}}(t, (\alpha, \mathbf{e})) - w_{\mathrm{T}}(t_0, (\alpha, \mathbf{0}))| \\
&\qquad = |w_{\mathrm{T}} - \epsilon_{\mathrm{T}} s_{\mathrm{d}}| \\
&\qquad \leq L\|(\alpha, \mathbf{e}) - (\alpha, \mathbf{0})\| = L\rho
\end{aligned}$$

noting that $w_T(t, (\alpha, \mathbf{0})) = \epsilon_{\mathrm{T}} s_{\mathrm{d}}$ for any t and α by definition. Therefore, $\epsilon_{\mathrm{T}} s_{\mathrm{d}} - L\rho \leq w_{\mathrm{T}} \leq \epsilon_{\mathrm{T}} s_{\mathrm{d}} + L\rho$. When $\rho \leq \epsilon_{\mathrm{T}}/L$, it follows that ${w_{\mathrm{T}}}^2 \geq (\epsilon_{\mathrm{T}} - L\rho)^2$ for each $s_{\mathrm{d}} \in \{-1, 1\}$ and

$$\begin{aligned}
\|\boldsymbol{\nu}\|^2 &\geq {w_{\mathrm{T}}}^2 + {w_{\mathrm{e}}}^2\rho^2 \geq \epsilon_{\mathrm{T}}^2 - 2L\epsilon_{\mathrm{T}}\rho + L^2\rho^2 + l_{\mathrm{e}}^2\rho^2 \\
&= \left(L^2 + l_{\mathrm{e}}^2\right)\left(\rho - \frac{L\epsilon_{\mathrm{T}}}{L^2 + l_{\mathrm{e}}^2}\right)^2 + \frac{l_{\mathrm{e}}^2\epsilon_{\mathrm{T}}^2}{L^2 + l_{\mathrm{e}}^2} \\
&\geq \frac{l_{\mathrm{e}}^2\epsilon_{\mathrm{T}}^2}{L^2 + l_{\mathrm{e}}^2}.
\end{aligned}$$

In the case $\rho > \epsilon_{\mathrm{T}}/L$, $\|\boldsymbol{\nu}\| \geq l_{\mathrm{e}}\rho > l_{\mathrm{e}}\epsilon_{\mathrm{T}}/L$. Let $\epsilon = l_{\mathrm{e}}\epsilon_{\mathrm{T}}/\sqrt{L^2 + l_{\mathrm{e}}^2}$. Then, the choice of ϵ is independent of t and $(\alpha, \mathbf{e})$; thus, $\|\boldsymbol{\nu}\| \geq \epsilon > 0$ on $\overline{\mathcal{D}}_{\mathrm{v}}$. □

From Lemma 5.3.1, the control law $\overline{\mathbf{u}}_v = \boldsymbol{\phi}(t, \mathbf{x}_{\mathrm{v}})$ can be designed as follows:

$$\boldsymbol{\phi}(t, \mathbf{x}_{\mathrm{v}}) = \frac{\boldsymbol{\nu}}{\|\boldsymbol{\nu}\|}. \tag{5.26}$$

The closed-loop system is then

$$\begin{aligned} \dot{\mathbf{x}}_{\mathrm{v}} &= (\dot{\alpha}, \dot{\mathbf{e}}) = \mathbf{g}_{\mathrm{v}}(t, \mathbf{x}_{\mathrm{v}}) \\ &= \left(\frac{U}{\Delta} \mathbf{T}^{\top} \boldsymbol{\phi}, U \mathbf{A} \boldsymbol{\phi} \right) \end{aligned} \tag{5.27}$$

where $\mathbf{g}_{\mathrm{v}}(t, \mathbf{x}_{\mathrm{v}}) = \mathbf{f}_{\mathrm{v}}(t, \mathbf{x}_{\mathrm{v}}, \boldsymbol{\phi}(t, \mathbf{x}_{\mathrm{v}}))$. It can be seen by inspection that $\mathbf{g}_{\mathrm{v}}$ is bounded and locally Lipschitz in $\mathbf{x}_{\mathrm{v}}$ on $\mathbb{R}_+ \times \overline{\mathcal{D}}_{\mathrm{v}}$. The derivative of V along the solution of Eq. (5.27) is

$$\begin{aligned} \dot{V}(t, \mathbf{x}_{\mathrm{v}}, \boldsymbol{\phi}(t, \mathbf{x}_{\mathrm{v}})) &= \mathbf{e}^{\top} \dot{\mathbf{e}} = -U \mathbf{e}^{\top} \boldsymbol{\phi} \\ &= -U \frac{1}{\|\boldsymbol{\nu}\|} \mathbf{e}^{\top} (w_{\mathrm{T}} \mathbf{T} + w_{\mathrm{e}} \mathbf{e} + w_{\mu} \mathbf{e} \times \mathbf{T}) \\ &= -U \frac{w_{\mathrm{e}}}{\|\boldsymbol{\nu}\|} \mathbf{e}^{\top} \mathbf{e} \\ &= -U \mathcal{X}, \end{aligned} \tag{5.28}$$

where

$$\mathcal{X} = \mathcal{X}(t, \mathbf{x}_{\mathrm{v}}) = \frac{w_{\mathrm{e}} \rho^2}{\sqrt{{w_{\mathrm{T}}}^2 + ({w_{\mathrm{e}}}^2 + {w_{\mu}}^2)\, \rho^2}}. \tag{5.29}$$

Let $\beta : \mathbb{R}_+ \to \mathbb{R}$ be a class $\mathcal{K}$ function defined by

$$\beta(\rho) = \frac{l_{\mathrm{e}} \rho^2}{\sqrt{u_{\mathrm{T}}^2 + \left(u_{\mathrm{e}}^2 + u_{\mu}^2\right) \rho^2}}$$

Then, $\mathcal{X}(t, \mathbf{x}_{\mathrm{v}}) \geq \beta(\rho)$ for all $(t, \mathbf{x}_{\mathrm{v}}) \in \mathbb{R}_+ \times \overline{\mathcal{F}}_{\mathrm{s}}$; thus,

$$\dot{V} \leq -U_{\mathrm{m}} \beta(\rho) \tag{5.30}$$

On the other hand, it can be seen that the regulation of the local distance, $\rho \to 0$, implies Eq. (5.15) from

$$\begin{aligned} \rho \to 0 \quad &\Rightarrow \quad \boldsymbol{\nu} \to w_{\mathrm{T}}|_{\rho=0}\mathbf{T} = \epsilon_{\mathrm{T}} s_{\mathrm{d}}\mathbf{T} \\ &\Rightarrow \quad \boldsymbol{\phi} \to s_{\mathrm{d}}\mathbf{T} \;\Rightarrow\; \dot{\mathbf{p}} = U\boldsymbol{\phi} \to U s_{\mathrm{d}}\mathbf{T}. \end{aligned} \tag{5.31}$$

Therefore, only the regulation of ρ is needed to ensure that $\boldsymbol{\phi}$ is a PF controller.

Definition 5.3.2 A set $R \subseteq \overline{\mathcal{F}}_{\mathrm{v}}$ in Definition 5.2.2 is called a region of operation for VDI PF controller if the following set is UAS:

$$C_{\mathrm{v}}(R) = \{\mathbf{x}_{\mathrm{v}} \in R \mid \rho = 0\} \tag{5.32}$$

Now, let us find a region of operation. Let $\boldsymbol{\gamma}$ be of a class M^2. Then, curvature κ of the path is bounded from above. Let $\bar{\kappa}$ be the least upper bound of κ and suppose $\bar{\kappa} > 0$. Let $r_{\mathrm{q}} = (1 - \Delta_{\mathrm{c}})/\bar{\kappa}$ for some $\Delta_{\mathrm{c}} \in (0, 1)$, and let Q be a tube of a constant cross-section radius r_{q} centered at the path:

$$Q = \left\{\mathbf{x}_{\mathrm{v}} \in \overline{\mathcal{F}}_{\mathrm{v}} \;\middle|\; \rho \leq r_{\mathrm{q}}\right\} \tag{5.33}$$

For all $\mathbf{x}_{\mathrm{v}} \in Q$, $V \leq r_{\mathrm{q}}^2/2$, and

$$\Delta = \mathbf{e}^{\top}\boldsymbol{\kappa} + 1 \geq 1 - \|\mathbf{e}\|\|\boldsymbol{\kappa}\| \geq 1 - r_{\mathrm{q}}\kappa = 1 - (1 - \Delta_{\mathrm{c}})\frac{\kappa}{\bar{\kappa}} \geq \Delta_{\mathrm{c}}.$$

Proposition 5.3.1 Q is a region of operation. ◇

Proof: Because

$$\dot{V} \leq -U_{\mathrm{m}}\beta(\rho) = -U_{\mathrm{m}}\beta(\sqrt{2V}) \tag{5.34}$$

on Q, $\rho(t)$ monotonically decreases. Therefore, the solution $\mathbf{x}_{\mathrm{v}}(t)$ will stay in the closed set Q. Since $\mathbf{f}_{\mathrm{v}}(t, \mathbf{x}_{\mathrm{v}}, \boldsymbol{\phi}(t, \mathbf{x}_{\mathrm{v}}))$ is bounded and locally Lipschitz in

$\mathbf{x}_\mathrm{v}$ on $\overline{\mathcal{D}}_\mathrm{v}$, a unique solution exists over $\mathbb{R}_+$ by Lemma 4.2.1. Moreover, from Lemma 4.4 in [61] and from the fact that V is a class $\mathcal{K}_\infty$ function of ρ and $\beta(\sqrt{\cdot})$ is a locally Lipschitz class $\mathcal{K}$ function, it follows that there is a class $\mathcal{KL}$ function $\zeta : [0, r_\mathrm{q}] \times \mathbb{R}_+ \to \mathbb{R}$ such that $V|_t \leq \zeta(V|_0, t)$. Because $d(\mathbf{x}_\mathrm{v}, C_\mathrm{v}(Q)) = \|\mathbf{e}\| = \sqrt{2V}$, the set $C_\mathrm{v}(Q)$ is UAS. □

Remark 5.3.2 (rate of convergence): From $\dot{V} = \rho\dot{\rho}$ and Eq. (5.30), the differential inequality $\dot{\rho}(t) \leq g(\rho(t))$, $\rho(0) = \rho_0 \in [0, r_\mathrm{q}]$, is obtained, where

$$g(y) = -U_\mathrm{m} \frac{l_\mathrm{e} y}{\sqrt{u_\mathrm{T}^2 + c_1^2 y^2}}$$

and $c_1 = \sqrt{u_\mathrm{e}^2 + u_\mu^2}$. The differential equation $\dot{y} = g(y)$, $y(0) = \rho_0$ can be solved by separation of variables to obtain $y(t; \rho_0) = G^{-1}(G(\rho_0) - U_\mathrm{m} l_\mathrm{e} t)$ for all $\rho_0 \in (0, r_\mathrm{q}]$, and $y(t; 0) = 0$, where $G : (0, \infty) \to \mathbb{R}$ is a strictly increasing bijection defined by

$$G(y) = \sqrt{u_\mathrm{T}^2 + c_1^2 y^2} + \frac{u_\mathrm{T}}{2} \log \left(\frac{\sqrt{u_\mathrm{T}^2 + c_1^2 y^2} - u_\mathrm{T}}{\sqrt{u_\mathrm{T}^2 + c_1^2 y^2} + u_\mathrm{T}} \right).$$

Then, by the comparison lemma, $\rho(t) \leq y(t; \rho_0)$ for all $t \geq 0$ and $y(t; \rho_0)$ can be chosen as the class $\mathcal{KL}$ function ζ in Proposition 5.3.1, i.e., $\zeta(\rho_0, t) = y(t; \rho_0)$. The bound function $y(\cdot; \rho_0)$ can be used to estimate the time required for the local distance to be less than a given value; for any $y_1 \in (0, \rho_0]$, $\rho(t) \leq y_1$ for all $t \geq t_1 = \frac{1}{U_\mathrm{m} l_\mathrm{e}} (G(\rho_0) - G(y_1))$. The schematic of the bound $y(t; \rho_0)$ is shown in Fig. 5.7. On the other hand, there is a more conservative bound:

$$g(y) \leq -\frac{U_\mathrm{m} l_\mathrm{e}}{\sqrt{u_\mathrm{T}^2 + c_1^2 r_\mathrm{q}^2}} y \tag{5.35}$$

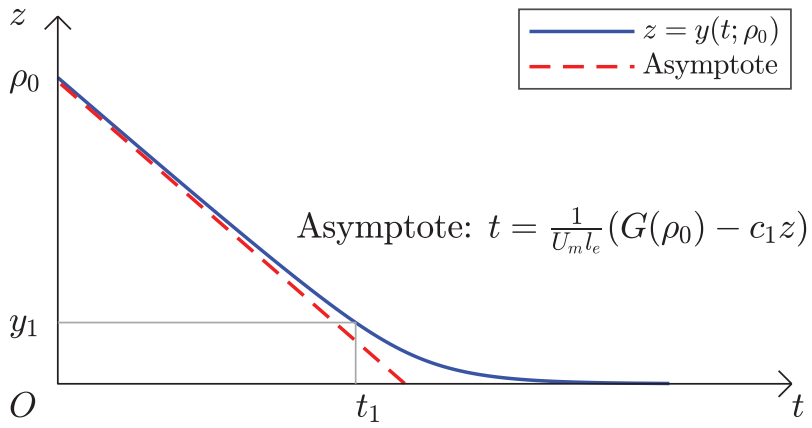

Figure 5.7: Rate of convergence

for all $y \in [0, r_q]$, which implies that any $\rho(t)$ with $\rho_0 \in [0, r_q]$ decays exponentially at the same rate since $\rho(t)$ monotonically decreases and the coefficient of y is constant.

Remark 5.3.3 (trajectory shaping): The velocity direction control, represented by Eq. (5.24), is composed of the three mutually orthogonal vectors $\mathbf{T}$, $\mathbf{e}$, and $\mathbf{e} \times \mathbf{T}$. In particular, if $w_\mu > 0$, the trajectory of P draws a spiral curve around the path in accordance with the right-hand rule about the tangent vector at the foot while approaching the path asymptotically as exemplified in Fig. 5.8. Since $\boldsymbol{\nu}$ is eventually normalized to form $\boldsymbol{\phi}$ and $w_e \geq l_e$ on its domain, the control design is equivalently considered as the design of the two weighting-ratio functions $\hat{w}_T := w_T/w_e$ and $\hat{w}_\mu := w_\mu/w_e$. $\hat{w}_T$ and $\hat{w}_\mu$ determine how faster the maneuverable point P advances forward along the path and rotates around the path, respectively, than it approaches the path. By appropriately shaping the weighting functions, the trends of the transient trajectory can be easily and intuitively designed. Furthermore, by allowing the approach weight-

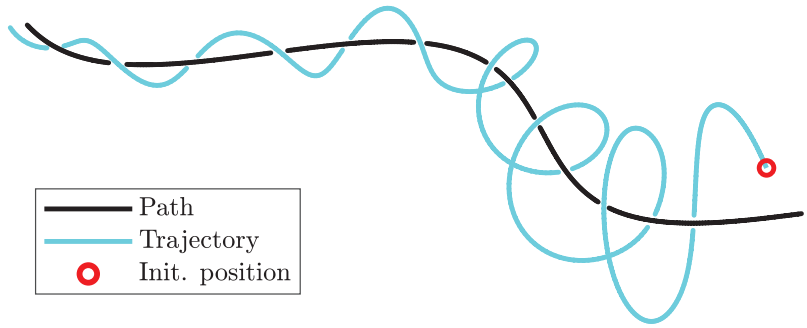

Figure 5.8: Solution trajectory by constant weighting functions with $\hat{w}_T > 0$ and $\hat{w}_\mu > 0$ for a sinusoidal path.

ing to have a negative value, e.g., the constraint on w_e is replaced by $|w_\mathrm{e}| \leq c_e$ for some $c_e > 0$, the control law can be easily modified such that the maneuverable point P keeps a specified standoff distance from the path, whose trajectory is adjusted by w_μ.

Remark 5.3.4 (invariance of image): If any of the weighting functions are not an explicit function of time t, that is, $\boldsymbol{\phi} = \boldsymbol{\phi}(\mathbf{x}_\mathrm{v})$, the image of the position

$$\{\boldsymbol{\gamma}(\alpha(t)) - \mathbf{e}(t) \mid t \in \mathbb{R}_+\}$$

of a solution trajectory is invariant with respect to the speed profile $U(t)$. To this end, consider two speed profiles $U_1(t)$ and $U_2(t)$ and corresponding equations of motion $\dot{\mathbf{x}}_\mathrm{v} = (U_i(t)\mathbf{T}^\top\boldsymbol{\phi}/\Delta, U_i(t)\mathbf{A}\boldsymbol{\phi})$, $i = 1, 2$, whose solutions for the same initial state $\mathbf{x}_{\mathrm{v}0} \in \overline{\mathcal{F}}_\mathrm{v}$ are denoted by $\mathbf{x}_{\mathrm{v}i}(t) = (\alpha_i(t), \mathbf{e}_i(t))$. Consider the transformation $f : \mathbb{R}_+ \to \mathbb{R}_+$ defined by $f(\tau) = \int_0^\tau U_1(\xi)\mathrm{d}\xi$, which is bijective because $U_1(t) \geq U_\mathrm{m} > 0$ by assumption. Let $\tau = \tau(t) = f^{-1}\left(\int_0^t U_2(\xi)\mathrm{d}\xi\right)$ be the new time variable for the system with U_2, where $\tau : \mathbb{R}_+ \to \mathbb{R}_+$ is also a

bijection because $U_2(t) \geq U_\mathrm{m}$. Since $\frac{\mathrm{d}\tau}{\mathrm{d}t} = U_2(t)/U_1(\tau)$, the foot dynamics with U_2 can be parametrized with τ as follows:

$$\dot{\alpha} = U_2(t)\frac{\mathbf{T}^\top \boldsymbol{\phi}}{\Delta} = \frac{\mathrm{d}\alpha}{\mathrm{d}\tau}\frac{\mathrm{d}\tau}{\mathrm{d}t} = \frac{\mathrm{d}\alpha}{\mathrm{d}\tau}\frac{U_2(t)}{U_1(\tau)}.$$

Because $U_2(t)$ is nonzero, $\frac{\mathrm{d}\alpha}{\mathrm{d}\tau} = U_1(\tau)\mathbf{T}^\top\boldsymbol{\phi}/\Delta$. $\frac{\mathrm{d}\mathbf{e}}{\mathrm{d}\tau} = U_1(\tau)\mathbf{A}\boldsymbol{\phi}$ is obtained through a similar process. The result shows that the solution $\mathbf{x}_{\mathrm{v}1}(t)$ is a reparametrization of $\mathbf{x}_{\mathrm{v}2}(t)$. Hence, the claim follows from the fact that the image of a curve is invariant under reparametrization.

5.3.3 Direct Approaching

It is guaranteed that if the trajectory starts inside the tube Q, there is no possibility that the trajectory would make the term $\Delta = \mathbf{e}^\top\mathbf{T}' + 1$ excessively close to zero for all future time while the perpendicular $\mathbf{e}$ is regulated. However, the problem is that Q is significantly smaller than $\overline{\mathcal{F}}_\mathrm{v}$. To expand the region, let us inspect the dynamics of the closed-loop system expanded further from Eq. (5.27) on $\overline{\mathcal{F}}_\mathrm{v}$ as follows:

$$\begin{aligned}\dot{\alpha} &= \frac{U}{\Delta}\mathbf{T}^\top\boldsymbol{\phi} = \frac{U}{\Delta\|\boldsymbol{\nu}\|}\mathbf{T}^\top\boldsymbol{\nu} \\ &= \frac{U}{\Delta\|\boldsymbol{\nu}\|}\mathbf{T}^\top\left(w_\mathrm{T}\mathbf{T} + w_\mathrm{e}\mathbf{e} + w_\mu\mathbf{e}\times\mathbf{T}\right) = U\frac{w_\mathrm{T}}{\Delta\|\boldsymbol{\nu}\|}\end{aligned} \tag{5.36a}$$

$$\begin{aligned}\dot{\mathbf{e}} &= U\mathbf{A}\boldsymbol{\phi} = \frac{U}{\|\boldsymbol{\nu}\|}\mathbf{A}\boldsymbol{\nu} = \frac{U}{\|\boldsymbol{\nu}\|}\left(\frac{w_\mathrm{T}}{\Delta}\mathbf{T} - \boldsymbol{\nu}\right) \\ &= \frac{U}{\|\boldsymbol{\nu}\|}\left\{w_\mathrm{T}\left(\frac{1}{\Delta} - 1\right)\mathbf{T} - w_\mathrm{e}\mathbf{e} - w_\mu\mathbf{e}\times\mathbf{T}\right\}.\end{aligned} \tag{5.36b}$$

Consider the weighting function design satisfying

$$\forall\rho > r_\mathrm{q} : [w_\mathrm{T} = 0 \text{ and } w_\mu = 0] \tag{5.37}$$

in addition to Eq. (5.23). Then, whenever $\rho > r_{\mathrm{q}}$, the dynamics reduces to $\dot{\mathbf{x}}_{\mathrm{v}} = (\dot{\alpha}, \dot{\mathbf{e}}) = (0, -U\mathbf{e}/\rho)$ whose general solution, for the initial condition $\mathbf{x}_{\mathrm{v}0} = (\alpha_0, \mathbf{e}_0)$ with $\rho(0) > r_{\mathrm{q}}$, is $\alpha(t) = \alpha_0$ and $\mathbf{e}(t) = \left(1 - \frac{1}{\rho(0)} \int_0^t U(\tau)\mathrm{d}\tau\right) \mathbf{e}_0$ defined on $I = \left\{ t \in \mathbb{R}_+ \;\middle|\; \int_0^t U(\tau)\mathrm{d}\tau < \rho(0) - r_{\mathrm{q}} \right\}$. Note that $\rho(t) = \|\mathbf{e}(t)\| = \rho(0) - \int_0^t U(\tau)\mathrm{d}\tau \leq \rho(0)$, which leads to the result that if $\Delta|_0 > 0$,

$$\begin{aligned}
\Delta|_t &= \mathbf{e}(t)^\top \mathbf{T}'(\alpha(t)) + 1 \\
&= \left(1 - \frac{1}{\rho(0)} \int_0^t U(\tau)\mathrm{d}\tau\right) \mathbf{e}_0^\top \mathbf{T}'(\alpha_0) + 1 \\
&= \frac{\rho(t)}{\rho(0)} \left(\Delta|_0 - 1\right) + 1 \geq \min\left\{\Delta|_0,\ 1\right\}
\end{aligned}$$

Thus, $\Delta|_t \geq \Delta_{\mathrm{c}}$ whenever $\Delta|_0 \geq \Delta_{\mathrm{c}}$ for all $t \in I$. This weight design temporarily makes the foot stop (curvature of the path at the foot remains constant) until P enters the tube Q, where the entrance to the tube in finite time is guaranteed. In other words, the velocity $\dot{\mathbf{p}}$ is directly headed towards its foot until it enters the tube. The method is called the direct approaching. The resultant property of Eq. (5.37) greatly expands the region of operation compared to Q. Let

$$Q_{\mathrm{c}} = \left\{ \mathbf{x}_{\mathrm{v}} \in \overline{\mathcal{F}}_{\mathrm{v}} \;\middle|\; \Delta \geq \Delta_{\mathrm{c}} \right\}. \tag{5.38}$$

It is easy to see that Q_{c} is a region of operation because $Q \subseteq Q_{\mathrm{c}}$, and $\rho(t)$ monotonically decreases on $Q_{\mathrm{c}} \setminus Q$.

5.3.4 Singularity Avoidance

As shown previously, the region of operation is excessively confined when dealing with M^2 paths. Though the direct approaching expands the region to a satisfactory extent, it is a conservative singularity avoidance that the maneuverability should be significantly restricted to the simplest motion. If $\bar{\kappa}$ is large, the tube Q becomes too thin and the control law may require an impractically high acceleration at the boundary of the tube. To prevent undesired actuator

saturation, the speed U must be decreased before entering the tube.

In this section, it will be shown that, for M^3 paths, the region of operation can be expanded while retaining its maneuverability compared to the techniques for M^2 paths represented in the foregoing discussion. Therefore, it will be assumed from this point on that the path $\boldsymbol{\gamma}$ is a class M^3 function, that is, $\boldsymbol{\gamma}''' = \mathbf{T}''$ is bounded and locally Lipschitz.

Theorem 5.3.1 Let

$$K_{\mathrm{v}} = K_{\mathrm{v}}(t, \mathbf{x}_{\mathrm{v}}) = w_{\mathrm{T}} \frac{\mathbf{e}^{\top} \boldsymbol{\kappa}_2}{\Delta} + w_{\mathrm{e}} (1 - \Delta) - w_{\mu} \mathbf{e}^{\top} (\mathbf{T} \times \boldsymbol{\kappa}) . \tag{5.39}$$

Suppose that the weighting functions w_{T}, w_{e}, and w_{μ} are designed so that there are $c_1 > 0$ and a continuous function $g_{\mathrm{v}} : [\Delta_{\mathrm{c}}, \infty) \to \mathbb{R}$ such that $K_{\mathrm{v}} \geq g_{\mathrm{v}}(\Delta)$ and $g_{\mathrm{v}}(\Delta_{\mathrm{c}}) > 0$ on $\Omega = \left\{ \mathbf{x}_{\mathrm{v}} \in \overline{\mathcal{F}}_{\mathrm{v}} \;\middle|\; V \leq c_1,\ \Delta \geq \Delta_{\mathrm{c}} \right\}$. Then, Ω is a region of operation. $\diamond$

Proof: The derivative of Δ on $\overline{\mathcal{F}}_{\mathrm{v}}$ is

$$\begin{aligned} \dot{\Delta} &= \frac{\partial \Delta}{\partial \alpha} \dot{\alpha} + \frac{\partial \Delta}{\partial \mathbf{e}} \dot{\mathbf{e}} = U \left\{ \frac{\mathbf{e}^{\top} \mathbf{T}''}{\Delta} \mathbf{T}^{\top} + (\mathbf{T}')^{\top} \mathbf{A} \right\} \boldsymbol{\phi} \\ &= U \mathbf{K}_{\mathrm{s}}^{\top} \boldsymbol{\phi} = \frac{U}{\|\boldsymbol{\nu}\|} \mathbf{K}_{\mathrm{s}}^{\top} (w_{\mathrm{T}} \mathbf{T} + w_{\mathrm{e}} \mathbf{e} + w_{\mu} \mathbf{e} \times \mathbf{T}) \\ &= \frac{U}{\|\boldsymbol{\nu}\|} K_{\mathrm{v}}, \end{aligned} \tag{5.40}$$

where

$$\begin{aligned} \mathbf{K}_{\mathrm{s}} &= \frac{\mathbf{e}^{\top} \mathbf{T}''}{\Delta} \mathbf{T} + \mathbf{A}^{\top} \mathbf{T}' = \frac{\mathbf{e}^{\top} \boldsymbol{\kappa}_2}{\Delta} \mathbf{T} + \frac{1}{\Delta} \mathbf{T} \mathbf{T}^{\top} \boldsymbol{\kappa} - \boldsymbol{\kappa} \\ &= \frac{\mathbf{e}^{\top} \boldsymbol{\kappa}_2}{\Delta} \mathbf{T} - \boldsymbol{\kappa} \end{aligned}$$

from $\mathbf{T}^\top \boldsymbol{\kappa} = 0$. Therefore,

$$\dot{\Delta} \geq \frac{U_\mathrm{m}}{b_\nu} K_\mathrm{v} \geq \frac{U_\mathrm{m}}{b_\nu} g_\mathrm{v}(\Delta) \tag{5.41}$$

on Ω, where $b_\nu = \sqrt{u_\mathrm{T}^2 + 2(u_\mathrm{e}^2 + u_\mu^2)c_1}$ from $\rho^2 = 2V \leq 2c_1$. On the other hand, $\Delta(\alpha, \mathbf{0}) = 1 > 0$, and $\Delta(\alpha, \mathbf{e})$ is Lipschitz in $\mathbf{e}$ because $\Delta(\alpha, \mathbf{e}_2) - \Delta(\alpha, \mathbf{e}_1) = (\mathbf{e}_2 - \mathbf{e}_1)^\top \boldsymbol{\kappa}(\alpha)$ for all $\mathbf{e}_1, \mathbf{e}_2 \in \mathbb{R}^3$ and $\boldsymbol{\kappa}$ is bounded. Therefore, from Corollary 4.3.2, $C_\mathrm{v}(\Omega)$ is UAS, and Ω is a subset of region of attraction. □

The bound estimation $y(t; \rho_0)$ in Remark 5.3.2 now holds for any initial state in Ω for a control system that satisfies the conditions of Theorem 5.3.1. Therefore, any trajectory $\rho(t)$ starting in Ω decays at an exponential rate, i.e., the closed invariant set $C_\mathrm{v}(\Omega)$ is exponentially stable. Note that when the desired path is a straight line, that is, $\kappa(s) = \|\mathbf{T}'(s)\| = 0$ for all $s \in \mathbb{R}$ ($\Leftrightarrow \bar{\kappa} = 0$), the singularity avoidance is not required and the set $\overline{\mathcal{F}}_\mathrm{v}$ is the largest region of operation because $\Delta = \mathbf{e}^\top \mathbf{T}' + 1 = 1 > \Delta_\mathrm{c}$ for all $\mathbf{x}_\mathrm{v} \in \overline{\mathcal{F}}_\mathrm{v}$.

5.3.5 Design Example

The conditions required for the design of a velocity direction control law are Eq. (5.23) and the assumptions in Theorem 5.3.1. First, two shaping functions are defined: A *sinusoidal cutoff function* is a strictly increasing class M^1 function $q(\cdot; x_1, x_2) : \mathbb{R} \to \mathbb{R}$ defined for each $x_1, x_2 \in \mathbb{R}$ by

$$q(x; x_1, x_2) = \begin{cases} 0, & x < x_1 \\ \dfrac{x - x_1}{x_2 - x_1} + \dfrac{1}{2\pi} \sin \dfrac{2\pi (x - x_c)}{x_2 - x_1}, & x_1 \leq x < x_2 \\ 1, & x \geq x_2, \end{cases}$$

where $x_c = (x_1 + x_2)/2$. It can be thought of as a smooth blending of 0 and 1. An *algebraic sigmoid function* is a strictly increasing class M^1 odd function $r(\cdot; k) : \mathbb{R} \to \mathbb{R}$ defined for each $k > 0$ by $r(x; k) = kx/\sqrt{x^2 + k^2}$. $|r(x; k)| < k$ for all $x \in \mathbb{R}$. $|r(x; k)| \to k$ as $x \to \infty$ and the derivative $r'(x; k) = k^3/\left(x^2 + k^2\right)^{3/2}$ approaches 1 as x vanishes.

The following weighting function design is proposed in this dissertation:

$$\begin{aligned} w_{\mathrm{T}} &= u_{\mathrm{T}} q(\Delta; \Delta_T, 1) \\ w_{\mathrm{e}} &= 1 \\ w_\mu &= -r\left(\frac{k_{\mu 0}}{1 + k_{\mu 1}\rho^2}\mathbf{e}^\top(\mathbf{T} \times \mathbf{T}'); u_\mu\right), \end{aligned} \tag{5.42}$$

where $\Delta_T \in (\Delta_{\mathrm{c}}, 1)$ is the cutoff point, $k_{\mu 0} > 0$ is the rotation intensity, and $k_{\mu 1} > 0$ is the fade-out factor. All the weighting functions are bounded and Lipschitz in $\mathbf{x}$ on $\mathbb{R}_+ \times \mathcal{D}$. Moreover, $K_{\mathrm{v}} \geq 1 - \Delta_T > 0$ whenever $\Delta_{\mathrm{c}} < \Delta \leq \Delta_T$ because 1) w_{T} becomes zero; and 2) w_μ guarantees the third term in the right-hand side of Eq. (5.39) to be always nonnegative. The term ρ^2 in the denominator inside w_μ is used to fade out the effect of w_μ as P gets far from the foot.

Remark 5.3.5: It is recommended to raise Δ as much as possible before P gets sufficiently close to the desired path because small Δ generally results in a large normal acceleration. By inspecting the structure of K_{v}, it can be seen that positive w_{e} will increase $\Delta|_t$ whenever it is close to Δ_{c}. On the other hand, w_μ in Eq. (5.42) is used to always increase $\Delta|_t$ unless either $\mathbf{e}(t)$ or $\mathbf{T}'(\alpha(t))$ is zero. A solution trajectory with such w_μ will draw a spiral curve around the path traversing from the region of low Δ to higher one, that is, the point P will try to move opposite to the direction toward which the path bends.

5.4 Steering Control

5.4.1 Dynamics

Similar to the VDI case, let us introduce the time-dependent change of variable $(\alpha, \mathbf{p}, \dot{\mathbf{p}}) \mapsto (\alpha, \mathbf{e}, \mathbf{z})$ from the domain $\mathcal{D}_\mathrm{s}$ of the SI system into the error space $\overline{\mathcal{D}}_\mathrm{s}$, defined by $\mathbf{e} = \boldsymbol{\gamma}(\alpha) - \mathbf{p}$ and

$$\mathbf{z} = \overline{\mathbf{v}}(t, \dot{\mathbf{p}}) - \boldsymbol{\phi}(t, \mathbf{x}_\mathrm{v}) \tag{5.43}$$

$\mathbf{z}$ represents the difference between the velocity direction $\overline{\mathbf{v}}$ and the VDI PF controller $\boldsymbol{\phi}$; it can be expected that if $\mathbf{z}(t) \equiv \mathbf{0}$, P would behave as if it were driven by the VDI PF controller $\overline{\mathbf{v}} = \boldsymbol{\phi}$. The state in the error space is denoted by $\mathbf{x}_\mathrm{s} = (\alpha, \mathbf{e}, \mathbf{z})$, and the state function $\mathbf{f}_\mathrm{s} : \mathbb{R}_+ \times \overline{\mathcal{D}}_\mathrm{s}$ is obtained from $\overline{\mathbf{v}} = \mathbf{z} + \boldsymbol{\phi}$ as

$$\begin{aligned}
\dot{\alpha} &= \frac{U(t)}{\Delta(\alpha, \mathbf{e})} \mathbf{T}(\alpha)^\top \overline{\mathbf{v}}(t, \dot{\mathbf{p}}) && (5.44a)\\
&= \frac{U(t)}{\Delta(\alpha, \mathbf{e})} \mathbf{T}(\alpha)^\top (\mathbf{z} + \boldsymbol{\phi}(t, \mathbf{x}_\mathrm{v})) \\
\dot{\mathbf{e}} &= U(t) \mathbf{A}(\alpha, \mathbf{e}) \overline{\mathbf{v}} && (5.44b)\\
&= U(t) \mathbf{A}(\alpha, \mathbf{e}) (\mathbf{z} + \boldsymbol{\phi}(t, \mathbf{x}_\mathrm{v})) \\
\dot{\mathbf{z}} &= \dot{\overline{\mathbf{v}}} - \dot{\boldsymbol{\phi}} && (5.44c)\\
&= \mathbf{u}_s - \boldsymbol{\Phi}(t, \mathbf{x}_\mathrm{s})
\end{aligned}$$

where

$$\boldsymbol{\Phi}(t, \mathbf{x}_\mathrm{s}) = \frac{\partial \boldsymbol{\phi}}{\partial t} + \frac{\partial \boldsymbol{\phi}}{\partial \mathbf{x}_\mathrm{v}} \dot{\mathbf{x}}_\mathrm{v} = \frac{\partial \boldsymbol{\phi}}{\partial t} + U \frac{\partial \boldsymbol{\phi}}{\partial \mathbf{x}_\mathrm{v}} \begin{bmatrix} \mathbf{T}^\top / \Delta \\ \mathbf{A} \end{bmatrix} \overline{\mathbf{v}} \tag{5.45}$$

and $\dot{\mathbf{x}}_{\mathrm{s}} = \mathbf{f}_{\mathrm{s}}(t, \mathbf{x}_{\mathrm{s}}, \mathbf{u}_s)$. The domain and consistent set of the transformed system are

$$\begin{aligned} \overline{\mathcal{D}}_{\mathrm{s}} &= \left\{ \mathbf{x}_{\mathrm{s}} \in \mathbb{R}^7 \;\middle|\; \Delta(\alpha, \mathbf{e}) > \Delta_0 \right\} \\ \overline{\mathcal{F}}_{\mathrm{s}} &= \left\{ \mathbf{x}_{\mathrm{s}} \in \overline{\mathcal{D}}_{\mathrm{s}} \;\middle|\; \mathbf{e}^\top \mathbf{T}(\alpha) = 0,\ \|\overline{\mathbf{v}}\| = 1 \right\} \end{aligned} \tag{5.46}$$

$\mathbf{z}$ can be seen as a state augmented to the VDI system, while the *steering input* is taken as a new input.

$\mathbf{z}$ has the important properties:

$$\begin{aligned} \mathbf{z}^\top (\overline{\mathbf{v}} + \boldsymbol{\phi}) &= (\overline{\mathbf{v}} - \boldsymbol{\phi})^\top (\overline{\mathbf{v}} + \boldsymbol{\phi}) \\ &= 1^2 - \boldsymbol{\phi}^\top \overline{\mathbf{v}} + \overline{\mathbf{v}}^\top \boldsymbol{\phi} - 1^2 \\ &= 0 \end{aligned} \tag{5.47}$$

and $\|\mathbf{z}\| \leq \|\overline{\mathbf{v}}\| + \|\boldsymbol{\phi}\| = 2$ on $\overline{\mathcal{F}}_{\mathrm{s}}$. On the other hand, the derivatives of V and Δ now contain a $\mathbf{z}$ term:

$$\begin{aligned} \dot{V} &= \mathbf{e}^\top \dot{\mathbf{e}} = U \mathbf{e}^\top \mathbf{A} (\boldsymbol{\phi} + \mathbf{z}) \\ &= -U\mathcal{X} - U\mathbf{z}^\top \mathbf{e} \end{aligned} \tag{5.48}$$

$$\begin{aligned} \dot{\Delta} &= U \mathbf{K}_{\mathrm{s}}^\top \overline{\mathbf{v}} = U \mathbf{K}_{\mathrm{s}}^\top (\boldsymbol{\phi} + \mathbf{z}) \\ &= U \frac{K_{\mathrm{v}}}{\|\boldsymbol{\nu}\|} + U \mathbf{K}_{\mathrm{s}}^\top \mathbf{z} \end{aligned} \tag{5.49}$$

which follows from Eq. (5.40).

Consider the functions

$$V_{\mathrm{z}}(\mathbf{z}) = \frac{1}{2} \mathbf{z}^\top \mathbf{z} \tag{5.50}$$

and the C^1 function $w_{\mathrm{z}} : \overline{\mathcal{D}}_{\mathrm{v}} \to \mathbb{R}$ bounded from below by $w_0 > 0$. Form a positive semidefinite composite CLF $V_{\mathrm{c}} : \overline{\mathcal{D}}_{\mathrm{s}} \to \mathbb{R}_+$ defined by

$$V_{\mathrm{c}}(\mathbf{x}_{\mathrm{s}}) = V(\mathbf{x}_{\mathrm{v}}) + w_{\mathrm{z}}(\mathbf{x}_{\mathrm{v}}) V_{\mathrm{z}}(\mathbf{z}) \tag{5.51}$$

whose derivative is

$$\begin{aligned}\dot{V}_{\mathrm{c}}(t, \mathbf{x}_{\mathrm{s}}, \mathbf{u}_s) &= \dot{V} + \frac{\dot{w}_{\mathrm{z}}}{2}\mathbf{z}^\top\mathbf{z} + w_{\mathrm{z}}\mathbf{z}^\top\dot{\mathbf{z}} \\ &= -U\mathcal{X} - U\mathbf{z}^\top\mathbf{e} + \frac{f_{\mathrm{w}}}{2}\mathbf{z}^\top\mathbf{z} + w_{\mathrm{z}}\mathbf{z}^\top(\mathbf{u}_s - \boldsymbol{\Phi}),\end{aligned} \tag{5.52}$$

where $\dot{w}_{\mathrm{z}} = f_{\mathrm{w}}(t, \mathbf{x}_{\mathrm{s}})$. Note that $V_{\mathrm{c}}(\mathbf{x}_{\mathrm{s}})$ is positive definite with respect to $(\mathbf{e}, \mathbf{z})$.

5.4.2 Controller Design

To design SI PF controller, first, the domain is restricted to

$$\overline{\mathcal{D}}_{\mathrm{s}}^{\mathrm{c}} = \left\{\mathbf{x}_{\mathrm{s}} \in \overline{\mathcal{D}}_{\mathrm{s}} \;\middle|\; \|\mathbf{z}\| < 2\right\} \tag{5.53}$$

Since $\|\mathbf{z}\| < 2$ if and only if $1 + \overline{\mathbf{v}}^\top\boldsymbol{\phi} > 0$ from $\|\mathbf{z}\|^2 = (\overline{\mathbf{v}} - \boldsymbol{\phi})^\top(\overline{\mathbf{v}} - \boldsymbol{\phi}) = 2 - 2\overline{\mathbf{v}}^\top\boldsymbol{\phi}$, the domain can be equivalently written as $\overline{\mathcal{D}}_{\mathrm{s}}^{\mathrm{c}} = \left\{\mathbf{x}_{\mathrm{s}} \in \overline{\mathcal{D}}_{\mathrm{s}} \;\middle|\; 1 + \overline{\mathbf{v}}^\top\boldsymbol{\phi} > 0\right\}$. The corresponding consistent set is $\overline{\mathcal{F}}_{\mathrm{s}}^{\mathrm{c}} = \overline{\mathcal{F}}_{\mathrm{s}} \cap \overline{\mathcal{D}}_{\mathrm{s}}^{\mathrm{c}}$.

Definition 5.4.1 A function $\boldsymbol{\eta} : \mathbb{R}_+ \times \overline{\mathcal{D}}_{\mathrm{s}}^{\mathrm{c}} \to \mathbb{R}^3$ is a *direction error regulator* if

1. $\boldsymbol{\eta}(t, \mathbf{x}_{\mathrm{s}})$ is piecewise continuous in t and locally Lipschitz in $\mathbf{x}_{\mathrm{s}}$;
2. There is a positive definite function $W_{\mathrm{z}} : B_2(\mathbf{0}) \to \mathbb{R}$ such that $\boldsymbol{\eta}$ satisfies the inequality

$$\mathbf{z}^\top\boldsymbol{\eta}(t, \mathbf{x}_{\mathrm{s}}) \geq W_{\mathrm{z}}(\mathbf{z}) \tag{5.54}$$

   for all $(t, \mathbf{x}_{\mathrm{s}}) \in \mathbb{R}_+ \times \overline{\mathcal{F}}_{\mathrm{s}}^{\mathrm{c}}$;
3. For every $\rho_{\mathrm{c}} > 0$ and $z_{\mathrm{c}} \in (0, 2)$, $\boldsymbol{\eta}$ is bounded on

$$\mathbb{R}_+ \times \left\{\mathbf{x}_{\mathrm{s}} \in \overline{\mathcal{F}}_{\mathrm{s}}^{\mathrm{c}} \;\middle|\; \rho \leq \rho_{\mathrm{c}},\ \Delta \geq \Delta_{\mathrm{c}},\ \|\mathbf{z}\| \leq z_{\mathrm{c}}\right\}$$

For a direction error regulator $\boldsymbol{\eta}$, define the function (base controller) $\boldsymbol{\psi}_{\mathrm{b}}$:

$\mathbb{R}_+ \times \overline{\mathcal{D}}_{\mathrm{s}}^{\mathrm{c}} \to \mathbb{R}^3$ by

$$\boldsymbol{\psi}_{\mathrm{b}}(t, \mathbf{x}_{\mathrm{s}}) = \boldsymbol{\Phi}(t, \mathbf{x}_{\mathrm{s}}) + \frac{1}{w_{\mathrm{z}}(\mathbf{x}_{\mathrm{v}})} \left(U\mathbf{e} - \frac{f_{\mathrm{w}}(t, \mathbf{x}_{\mathrm{s}})}{2}\mathbf{z} - U\boldsymbol{\eta}(t, \mathbf{x}_{\mathrm{s}}) \right), \tag{5.55}$$

Then, the control law $\mathbf{u}_s = \boldsymbol{\psi}(t, \mathbf{x}_{\mathrm{s}})$, where $\boldsymbol{\psi} : \mathbb{R}_+ \times \overline{\mathcal{D}}_{\mathrm{s}}^{\mathrm{c}} \to \mathbb{R}^3$, can be designed as follows:

$$\boldsymbol{\psi} = \frac{1}{1 + \overline{\mathbf{v}}^\top \boldsymbol{\phi}} \overline{\mathbf{v}} \times \{ \boldsymbol{\psi}_{\mathrm{b}} \times (\overline{\mathbf{v}} + \boldsymbol{\phi}) \} \tag{5.56}$$

which can be rearranged on $\overline{\mathcal{F}}_{\mathrm{s}}^{\mathrm{c}}$ as

$$\boldsymbol{\psi} = \boldsymbol{\psi}_{\mathrm{b}} - \frac{\overline{\mathbf{v}}^\top \boldsymbol{\psi}_{\mathrm{b}}}{1 + \overline{\mathbf{v}}^\top \boldsymbol{\phi}} (\overline{\mathbf{v}} + \boldsymbol{\phi}) . \tag{5.57}$$

$\boldsymbol{\psi}$ is designed so that $\overline{\mathbf{v}}^\top \mathbf{u}_s = \overline{\mathbf{v}}^\top \boldsymbol{\psi} = 0$. Applying the control law yields the closed-loop system

$$\begin{aligned} \dot{\mathbf{x}}_{\mathrm{s}} &= (\dot{\alpha}, \dot{\mathbf{e}}, \dot{\mathbf{z}}) = \mathbf{f}_{\mathrm{s}}(t, \mathbf{x}_{\mathrm{s}}, \boldsymbol{\psi}(t, \mathbf{x}_{\mathrm{s}})) \\ &= \left(\frac{U}{\Delta} \mathbf{T}^\top \overline{\mathbf{v}}, U\mathbf{A}\overline{\mathbf{v}}, \boldsymbol{\psi} \right) \end{aligned} \tag{5.58}$$

together with the derivative of the CLF

$$\begin{aligned} \dot{V}_{\mathrm{c}} &= -U\mathcal{X} - U\mathbf{z}^\top \mathbf{e} + \frac{f_{\mathrm{w}}}{2} \mathbf{z}^\top \mathbf{z} + w_{\mathrm{z}} \mathbf{z}^\top (\boldsymbol{\psi} - \boldsymbol{\Phi}) \\ &= -U\mathcal{X} - U\mathbf{z}^\top \boldsymbol{\eta} - w_{\mathrm{z}} \frac{\overline{\mathbf{v}}^\top \boldsymbol{\psi}_{\mathrm{b}}}{1 + \overline{\mathbf{v}}^\top \boldsymbol{\phi}} \mathbf{z}^\top (\overline{\mathbf{v}} + \boldsymbol{\phi}) \\ &\overset{(5.47)}{=} -U\mathcal{X} - U\mathbf{z}^\top \boldsymbol{\eta} \\ &\leq -U_{\mathrm{m}} (\beta(\rho) + W_{\mathrm{z}}(\mathbf{z})) \end{aligned} \tag{5.59}$$

obtained by applying Eq. (5.57) to Eq. (5.52), and

$$\begin{aligned} \dot{V}_{\mathrm{z}} &= \mathbf{z}^\top \dot{\mathbf{z}} = \mathbf{z}^\top (\boldsymbol{\psi} - \boldsymbol{\Phi}) = \mathbf{z}^\top (\boldsymbol{\psi}_{\mathrm{b}} - \boldsymbol{\Phi}) \\ &= \frac{1}{w_{\mathrm{z}}} \mathbf{z}^\top \left(U\mathbf{e} - \frac{f_{\mathrm{w}}}{2}\mathbf{z} - U\boldsymbol{\eta} \right) \end{aligned} \tag{5.60}$$

on $\overline{\mathcal{F}}_{\mathrm{s}}^{\mathrm{c}}$.

Remark 5.4.1: The discussion in Remark 5.3.4 about invariance of the image of a position trajectory is still valid in the steering input case. Suppose that the weighting functions and the direction error regulator are all time-invariant, that is, $\boldsymbol{\phi} = \boldsymbol{\phi}(\mathbf{x})$ and $\boldsymbol{\eta} = \boldsymbol{\eta}(\mathbf{x}_\mathrm{s})$. Then, $\frac{\partial \boldsymbol{\Phi}}{\partial t}$ in Eq. (5.45) is canceled out and $\boldsymbol{\Phi}$ has $U(t)$ as a factor, hence $\boldsymbol{\psi}_\mathrm{b}$ and $\boldsymbol{\psi}$. Consequently, by the same rationale in Remark 5.3.4, the image of the position $\mathbf{p}$ is invariant with respect to the speed profile $U(t)$.

Now, the region of operation is defined for steering input system analogous to Definition 5.3.2.

Definition 5.4.2 A set $R \subseteq \overline{\mathcal{F}}_\mathrm{s}^\mathrm{c}$ in Definition 5.2.2 is called a region of operation for SI PF controller if the following set is UAS:

$$C_\mathrm{s}(R) = \{\mathbf{x}_\mathrm{s} \in R \mid \rho = 0,\ \|\mathbf{z}\| = 0\} \tag{5.61}$$

5.4.3 Singularity Avoidance

In this section, the barrier weighting method developed in the previous chapter, characterized by Definition 4.4.1 and Theorem 4.4.2, is used to achieve singularity avoidance of the SI system.

Proposition 5.4.1 In the hypothesis of Theorem 5.3.1, let g_v be decreasing on $[0, \Delta_\mathrm{c}]$. Let w_z be a barrier weighting with a barrier base ξ such that $\xi(\sigma_c) = w_0$ and Δ be the constraint indicator. Suppose further that there are $z_\mathrm{c} \in (0, 2)$ and a continuous function $g_\mathrm{z} : \mathbb{R} \to \mathbb{R}$ such that $\dot{V}_\mathrm{z} \leq g_\mathrm{z}(V_\mathrm{z})$ with $g_\mathrm{z}(z_\mathrm{c}^2/2) < 0$. Then, for each $c_1 > 0$, there is $\Delta_{\mathrm{c}1} \in (0, \Delta_\mathrm{c}]$ such that the following set is a

region of operation:

$$\Omega = \left\{ \mathbf{x}_\mathrm{s} \in \overline{\mathcal{F}}_\mathrm{s}^\mathrm{c} \;\middle|\; V_\mathrm{c}(\mathbf{x}_\mathrm{s}) \leq c_1,\ \Delta \geq \Delta_{\mathrm{c}1}, V_\mathrm{z}(\mathbf{z}) \leq z_\mathrm{c}^2/2 \right\} \tag{5.62}$$

$\diamond$

Proof: Let $\mathbf{x}_\mathrm{s} \in \Omega$. Then, recalling from Eq. (5.25), we have

$$\|\boldsymbol{\nu}\| \leq b_\nu = \sqrt{u_\mathrm{T}^2 + 2(u_\mathrm{e}^2 + u_\mu^2)c_1} \tag{5.63}$$

and $\rho = \sqrt{2V} \leq \sqrt{2V_\mathrm{c}} \leq \sqrt{2c_1}$.

$$\|\mathbf{K}_\mathrm{s}\| = \left\| \frac{\mathbf{e}^\top \boldsymbol{\kappa}_2}{\Delta} \mathbf{T} - \boldsymbol{\kappa} \right\| \leq \frac{\rho \|\boldsymbol{\kappa}_2\|}{\Delta} + \kappa < \frac{\sqrt{2c_1}\|\boldsymbol{\kappa}_2\|}{\Delta_0} + \kappa \tag{5.64}$$

Since κ and $\boldsymbol{\kappa}_2$ are all bounded, there is $b_s > 0$ such that $\|\mathbf{K}_\mathrm{s}\| \leq b_s$ on Ω. Therefore, the following inequality holds:

$$\dot{\Delta} = U \frac{K_\mathrm{v}}{\|\boldsymbol{\nu}\|} + U \mathbf{K}_\mathrm{s}^\top \mathbf{z} \geq \frac{U_\mathrm{m}}{b_\nu} g_\mathrm{v}(\Delta) - U_\mathrm{M} b_s \|\mathbf{z}\| \tag{5.65}$$

Choose $a > 0$ such that

$$a < \frac{1}{2} \left(\frac{U_\mathrm{m} g_\mathrm{v}(\Delta_\mathrm{c})}{U_\mathrm{M} b_s b_\nu} \right)^2 \tag{5.66}$$

and define $g : \mathbb{R} \to \mathbb{R}$ by

$$g(x) = \frac{U_\mathrm{m}}{b_\nu} g_\mathrm{v}(x) - U_\mathrm{M} b_s \sqrt{2a} \tag{5.67}$$

Then, whenever $V_\mathrm{z}(\mathbf{z}) \leq a$, or equivalently, $\|\mathbf{z}\| \leq \sqrt{2a}$, it follows that $\dot{\Delta} \geq$

$g(\Delta)$, and

$$\begin{aligned} g(\Delta_{\mathrm{c}1}) &= \frac{U_{\mathrm{m}}}{b_\nu} g_{\mathrm{v}}(\Delta_{\mathrm{c}1}) - U_{\mathrm{M}} b_s \sqrt{2a} \\ &\geq \frac{U_{\mathrm{m}}}{b_\nu} g_{\mathrm{v}}(\Delta_{\mathrm{c}}) - U_{\mathrm{M}} b_s \sqrt{2a} \\ &> 0 \end{aligned} \tag{5.68}$$

If $c_1 \geq w_0 a$, choose $\Delta_{\mathrm{c}1} \leq \xi_r^{-1}(c_1/a)$. Otherwise, let $\Delta_{\mathrm{c}1} \leq \sigma_c$. Then, from Corollary 4.4.2, Ω is UAS. □

What makes this singularity avoidance method unique is that it is designed simply by multiplying the barrier weighting w_{z} to V_{z} of the composite CLF V_{c}, which utilizes the specific characteristics of the velocity direction control system and backstepping control structure: As stated previously, $\Delta|_t$ cannot approach Δ_{c} by Theorem 5.3.1 if $\mathbf{z}(t) \equiv \mathbf{0}$. Using this property, the method manages to enforce $\mathbf{z}(t) \approx \mathbf{0}$ whenever it has to: Suppose that $\mathbf{z}(t)$ is nonzero as it may usually be. Then, whenever $\Delta|_t$ approaches Δ_{c}, the barrier weighting w_{z} must increase indefinitely; thus, $\mathbf{z}(t)$ will squeeze its magnitude in order to make $V_{\mathrm{c}}(\mathbf{x}_{\mathrm{s}}(t))$ monotonically decrease.

Remark 5.4.2: The open-loop system has the inherent singular surface $\Delta = 0$, and the closed-loop system has the additional singular surface $\|\mathbf{z}\| = 2$ as shown in Eq. (5.56) recalling that $1 + \overline{\mathbf{v}}^\top \boldsymbol{\phi} = 2 - \|\mathbf{z}\|^2/2$. The proposed control law is designed to keep Δ away from below by a positive constant Δ_{c} through the barrier weighting method to prevent any malfunction that can occur when Δ approaches 0. Likewise, $\mathbf{z}$ is also protected by the function g_{z}.

5.4.4 Design Example

Consider the assumptions in Section 5.4.3 to design a steering control law. One of the useful functions for barrier weighting design is a strictly decreasing

function

$$\xi(\Delta) = \frac{b_0^2}{\Delta^2}$$

where $b_0 > 0$ is the barrier intensity. A barrier weighting function and a direction error regulator are designed as

$$w_{\mathrm{z}} = \mathrm{logsumexp}\left(\sqrt{w_0^2 + {w_1}^2\rho^2},\ \xi(\Delta);\ k_l\right) \tag{5.69}$$

and

$$\boldsymbol{\eta} = \frac{1}{2} w_{\mathrm{z}} k_{\mathrm{s}} \left(2 - \|\mathbf{z}\|\right) \mathbf{z} - \frac{f_{\mathrm{w}}}{2U}\mathbf{z}, \tag{5.70}$$

respectively, where $w_1 > 0$ is the asymptotic weight slope,

$$k_{\mathrm{s}} = k_{\mathrm{s}}(\mathbf{x}_{\mathrm{s}}) = \max\left\{\frac{f_{\mathrm{w}}}{U w_{\mathrm{z}} \left(2 - \|\mathbf{z}\|\right)},\ \frac{1}{w_1}\right\} + \epsilon_{\mathrm{s}}, \tag{5.71}$$

and $\epsilon_{\mathrm{s}} > 0$. For $k_l > 0$, $\mathrm{logsumexp}(\cdot,\ \cdot;\ k_l) : \mathbb{R} \times \mathbb{R} \to \mathbb{R}$ is a smooth approximation of the maximum function defined by

$$\begin{aligned} \mathrm{logsumexp}(x_1, x_2; k_l) &= \frac{1}{k_l}\log(\exp(k_l x_1) + \exp(k_l x_2)) \\ &\geq \max\{x_1, x_2\} \end{aligned} \tag{5.72}$$

The design represented by Eqs. (5.69) and (5.70) yields

$$\begin{aligned} \mathbf{z}^\top \boldsymbol{\eta} &= \frac{1}{2} w_{\mathrm{z}} k_{\mathrm{s}} \|\mathbf{z}\|^2 \left(2 - \|\mathbf{z}\|\right) - \frac{f_{\mathrm{w}}}{2U}\|\mathbf{z}\|^2 \\ &= \left\{\frac{1}{2} w_{\mathrm{z}} k_{\mathrm{s}} \left(2 - \|\mathbf{z}\|\right) - \frac{f_{\mathrm{w}}}{2U}\right\}\|\mathbf{z}\|^2 \\ &\geq \frac{\epsilon_{\mathrm{s}}}{2} w_{\mathrm{z}} \left(2 - \|\mathbf{z}\|\right)\|\mathbf{z}\|^2 \\ &\geq \frac{\epsilon_{\mathrm{s}}}{2} w_0 \left(2 - \|\mathbf{z}\|\right)\|\mathbf{z}\|^2 \end{aligned} \tag{5.73}$$

that is positive whenever $\|\mathbf{z}\| \in (0, 2)$, i.e., the most right-hand side of Eq. (5.73) can be chosen as $W_{\mathrm{z}}(\mathbf{z})$ in Eq. (5.54). Furthermore, to satisfy the assumption

in Theorem 5.4.1, the derivative of V_{z} is inspected:

$$\begin{aligned}
\dot{V}_{\mathrm{z}} &= \frac{1}{w_{\mathrm{z}}}\left(U\mathbf{z}^{\top}\mathbf{e} - \frac{f_{\mathrm{w}}}{2}\|\mathbf{z}\|^2 - U\mathbf{z}^{\top}\boldsymbol{\eta}\right) \\
&= \frac{1}{w_{\mathrm{z}}}\left[U\mathbf{z}^{\top}\mathbf{e} - \frac{U}{2}w_{\mathrm{z}}k_{\mathrm{s}}(2-\|\mathbf{z}\|)\|\mathbf{z}\|^2\right] \\
&= U\left[\frac{\|\mathbf{z}\|\rho}{\sqrt{w_0^2 + {w_1}^2\rho^2}} - \frac{k_{\mathrm{s}}}{2}(2-\|\mathbf{z}\|)\|\mathbf{z}\|^2\right] \\
&\leq U\left[\frac{\|\mathbf{z}\|}{w_1} - \frac{k_{\mathrm{s}}}{2}(2-\|\mathbf{z}\|)\|\mathbf{z}\|^2\right] \\
&\leq U\left[\frac{\|\mathbf{z}\|}{w_1} - \frac{1}{2}\left(\frac{1}{w_1} + \epsilon_{\mathrm{s}}\right)(2-\|\mathbf{z}\|)\|\mathbf{z}\|^2\right] \\
&= \frac{U_{\mathrm{m}}}{2w_1}\|\mathbf{z}\|\left[2 - (1+w_1\epsilon_{\mathrm{s}})(2-\|\mathbf{z}\|)\|\mathbf{z}\|\right] \\
&= \frac{U_{\mathrm{m}}}{2w_1}\sqrt{2V_{\mathrm{z}}}\left[2 - (1+w_1\epsilon_{\mathrm{s}})(2-\sqrt{2V_{\mathrm{z}}})\sqrt{2V_{\mathrm{z}}}\right] \\
&= g_{\mathrm{z}}(V_{\mathrm{z}})
\end{aligned} \tag{5.74}$$

Therefore, noting that $V_{\mathrm{z}} \leq z_{\mathrm{c}}^2/2 < 2$ on Ω, $g_{\mathrm{z}}(V_{\mathrm{z}}) < 0$ can be obtained by increasing $w_1\epsilon_{\mathrm{s}}$.

Remark 5.4.3: k_{s} is a function that serves as a scaling factor of the decreasing rate of V_{z} as shown in the third line of Eq. (5.74). Recalling that $\dot{w}_{\mathrm{z}} = f_{\mathrm{w}}$, if $\Delta|_t$ approaches 0, $\xi(\Delta|_t)$ will increase rapidly, which renders the first element in Eq. (5.71) active, and V_{z} will be decreased accordingly to prevent w_{z} from rising indefinitely. Then, P is forced to follow the velocity direction control law that is guaranteed to avoid $\Delta = 0$.

5.5 Numerical Simulations

Three numerical simulations of the path-following problem are given in this section. The first one is the result of the velocity input case, and the others are of the steering input case. The parameters used for the control law are summarized in Table 5.4. ($s_{\mathrm{d}} = 1$ in all simulations.)

Table 5.4: Control parameters

Categories	Parameters
Δ	$\Delta_{\mathrm{c}} = 0.2$
w_{T}	$u_{\mathrm{T}} = 1,\ \Delta_T = 0.5$
w_μ	$u_\mu = 4,\ k_{\mu 0} = 2,\ k_{\mu 1} = 0.25$
ξ	$b_0 = 16$
w_{z}	$w_0 = 1,\ w_1 = 16$
k_{s}	$\epsilon_{\mathrm{s}} = 0.9375 = 1 - 1/w_1$

Factors that should be noted before conducting numerical simulations are twofold: 1) Even if a given parametric path is not naturally parametrized, the PFC law can be directly applied with only minor modifications; 2) The integration error on the foot α, possibly caused by numerical roundoff errors or by an error due to inconsistent initial conditions, can be effectively rejected by designing a simple foot stabilizing controller. These techniques are summarized in Appendix B.1.

5.5.1 Rotation weighting function

A simple circular path, represented by

$$\boldsymbol{\gamma}(\sigma) = [\cos\sigma \quad \sin\sigma \quad 0]^\top$$

is chosen to illustrate the role of the rotation weighting function. The maneuverable point P starts from the point $\sigma(0) = 0,\ \mathbf{p}(0) = [0.5\ 0\ 2]^\top$ and moves at a

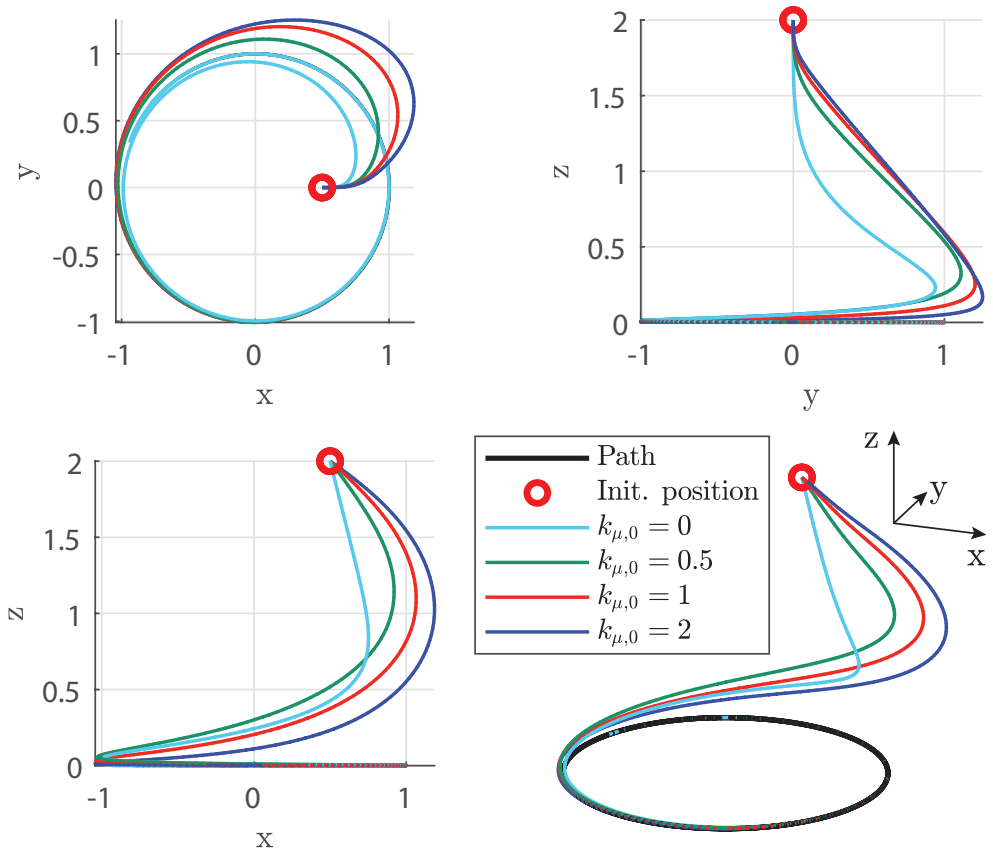

Figure 5.9: Solution trajectory of the circular path scenario in Section 5.5.1 for different rotation intensity $k_{\mu 0}$.

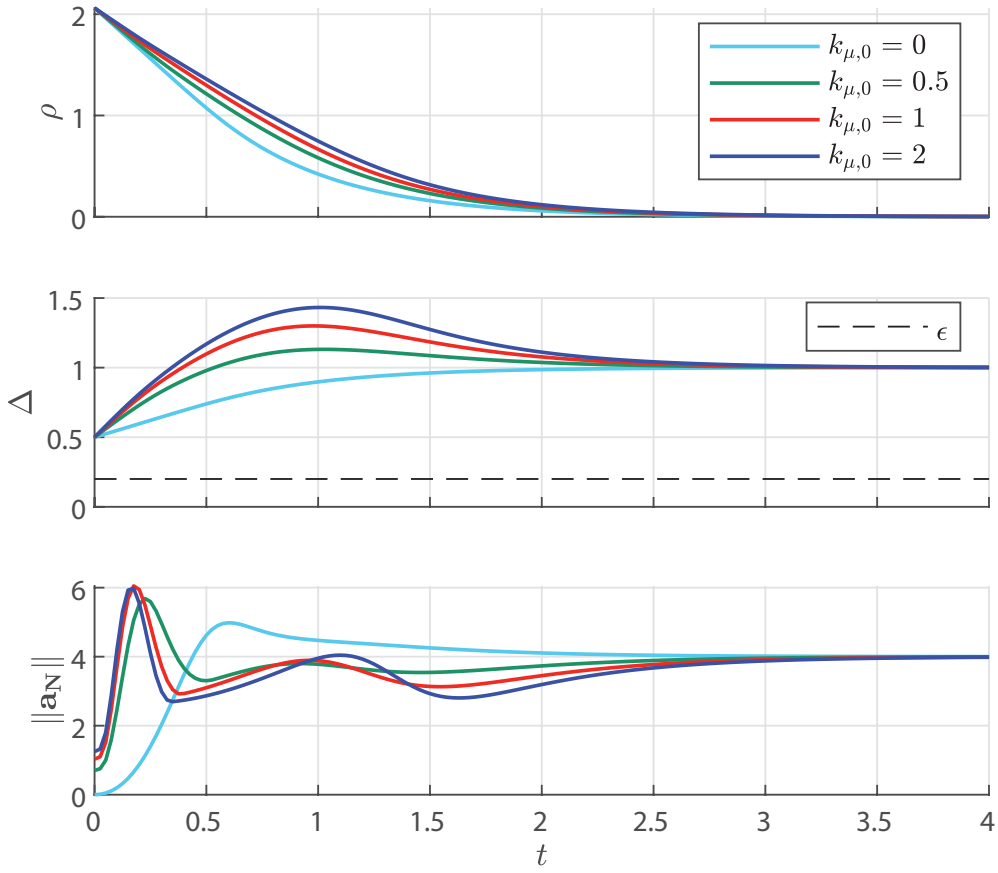

Figure 5.10: History of the circular path scenario in Section 5.5.1 for different rotation intensity $k_{\mu 0}$.

constant speed: $U(t) = 2$. The rotation intensity $k_{\mu 0}$ is selected among 0, 0.5, 1, and 2, where $k_{\mu 0} = 0$ implies that the rotation weighting is not applied because the condition leads to $w_\mu|_t \equiv 0$. As shown in Figs. 5.9 and 5.10, nonzero $k_{\mu 0}$ raises the distance convexity Δ immediately after the simulation starts. (init. in the figure stands for initial.) Noting that $\Delta = 0$ at the center of the circle, it can be seen that the result is consistent with the tendency of the solution trajectory projected to $x - y$ plane in Fig. 5.10 in that the trajectory moves from the interior of the circle (low-Δ area) to the outer region (high-Δ area). Though the convergence rate of ρ slightly decreases as $k_{\mu 0}$ increases, it follows that the system safety is improved by the sufficiently raised Δ. The surge in the normal acceleration $\mathbf{a}_N$ history at the beginning of the simulation is attributed to the design of w_T; because w_T is designed to be 0 whenever $\Delta = \Delta_T = 0.5$ and nonzero otherwise, the magnitude of the velocity components tangent to the path, $w_\mathrm{T}\mathbf{T}/\|\boldsymbol{\nu}\|$, rises from 0 as P approaches the circle, which is a major cause of the change in heading.

5.5.2 Singularity Avoidance

The planar desired path, represented by

$$\boldsymbol{\gamma}(\sigma) = [2\sigma + 1 - \exp(-\sigma) \quad 8\exp(-\sigma/16)\sin(\sigma) \quad 0]^\top$$

and the initial condition $\sigma(0) = 3.742$, $\mathbf{p}(0) = [10.5 \ \ -2.75 \ 0]^\top$, and $\overline{\mathbf{v}}(0) = [0.848 \ 0.530 \ 0]^\top$ are selected to show the performance of the singularity avoidance. The speed is constant: $U(t) = 2$. The barrier intensity b_0 is chosen among 0, 16, and 256. The simulation results are shown in Figs. 5.11 and 5.11, where perp., vel., dir., and cont. are the abbreviations for perpendicular, velocity, direction, and control, respectively, and the tinted region represents the area swept out by the perpendicular. The motion of P is vulnerable to the singular-

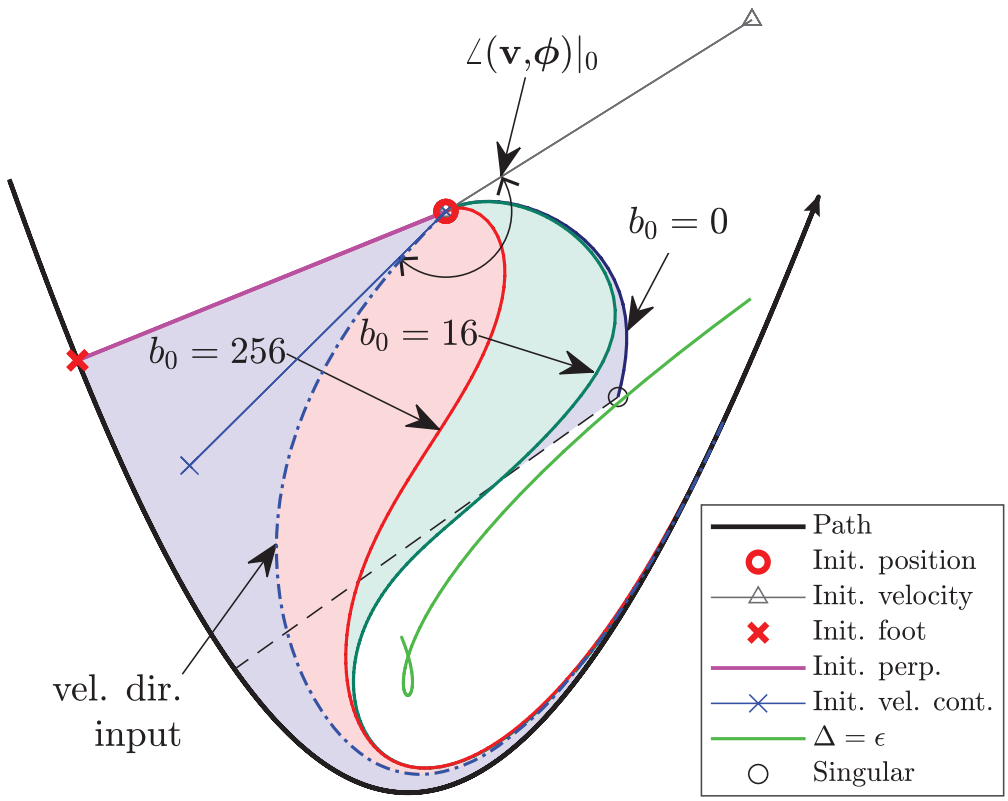

Figure 5.11: Solution trajectory of the singularity avoidance scenario in Section 5.5.2 for different barrier intensities b_0.

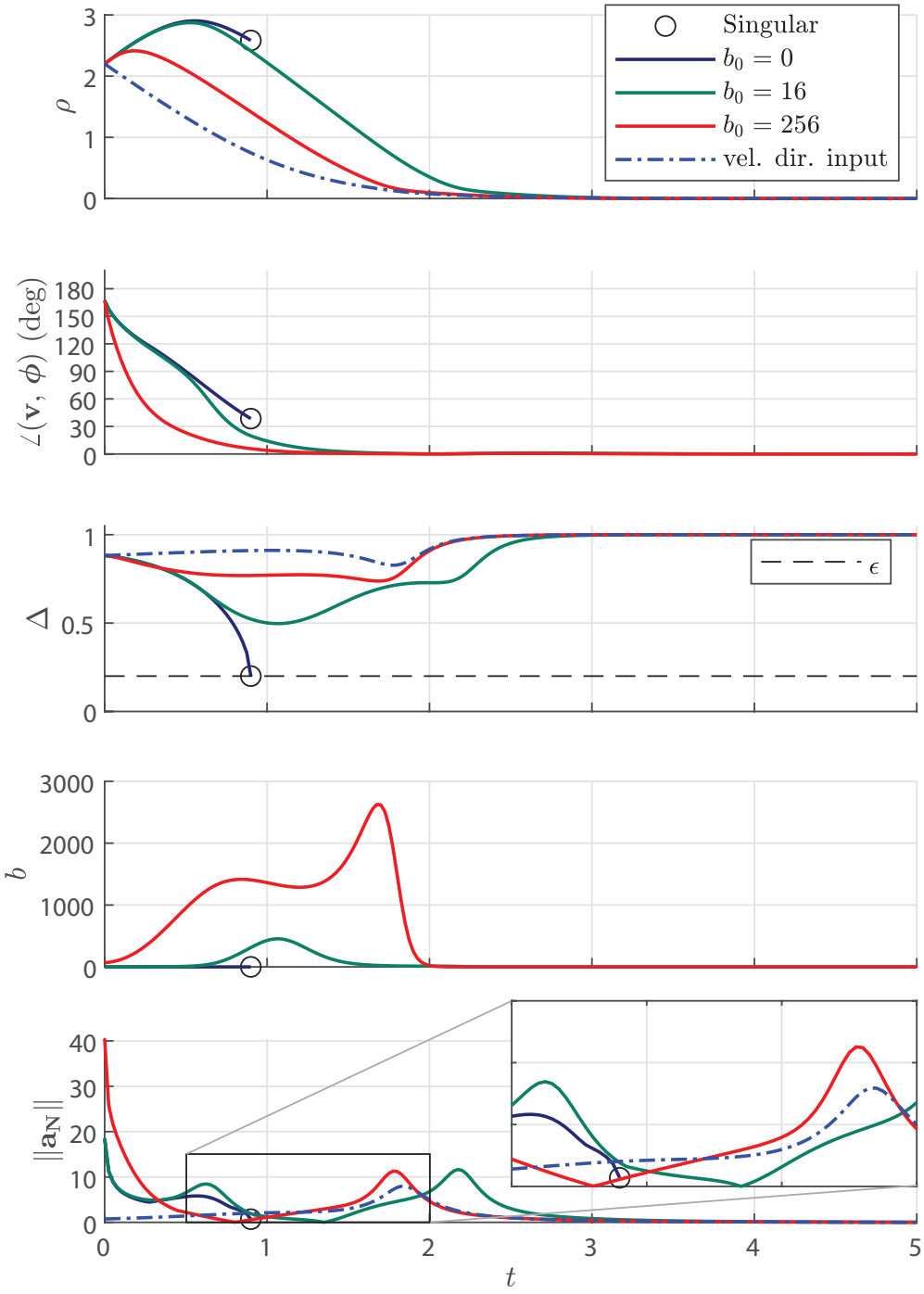

Figure 5.11: History of the singularity avoidance scenario in Section 5.5.2 for different barrier intensities b_0.

ity $\Delta = \Delta_c$ when $b_0 = 0$, i.e., the barrier is inactive. In contrast, when $b_0 > 0$, the trajectory smoothly avoids the singularity because the angle between the velocity direction $\overline{\mathbf{v}}$ and the velocity direction control $\boldsymbol{\phi}$, denoted by $\angle(\overline{\mathbf{v}}, \boldsymbol{\phi})$, is made rapidly decreased as Δ approaches Δ_c as discussed in Remark 5.4.3. It is natural to expect that large b_0 will make Δ stay larger than lower b_0 as exemplified by the cases of $b_0 = 16$ and $b_0 = 256$. However, b_0 should be carefully chosen because large b_0 can incur an undesirably high normal acceleration for large $\angle(\overline{\mathbf{v}}, \boldsymbol{\phi})|_0$.

5.5.3 Various Initial Position and Velocity

The desired path is represented by

$$\boldsymbol{\gamma}(\sigma) = [\cos(\sigma) \quad \sin(\sigma) + \sigma/2 \quad \cos(\sigma/2)]^\top$$

and the numerical solutions for the several initial conditions are shown in Figs. 5.12 and 5.12. The initial foot parameters, positions, and corresponding Δ are summarized in Table 5.5. The initial velocities have the same magnitude but distinct directions to consider various $\angle(\overline{\mathbf{v}}, \boldsymbol{\phi})$. To also consider time-varying speed of P, U is commanded to make a sinusoidal wave of large magnitude. It is observed that all the solution histories of the local distance ρ and the angle difference $\angle(\overline{\mathbf{v}}, \boldsymbol{\phi})$ tend to zero as time passes. The trends of $\angle(\overline{\mathbf{v}}, \boldsymbol{\phi})$ shows that as the initial angle gets bigger than 90 deg, the decreasing rate of the angle becomes smaller. Noticing that $\angle(\overline{\mathbf{v}}, \boldsymbol{\phi}) = \arccos(\overline{\mathbf{v}} \cdot \boldsymbol{\phi}) = \arccos(1 - V_z)$, it can be seen that it is the direct consequence of the design in Eq. (5.70) since the decreasing rate of $\|\mathbf{z}\|$ reduces whenever $\|\mathbf{z}\|$ approaches 0 or 2. It effectively prevents the resultant normal acceleration from diverging as the initial angle approaches 180 deg.

The two solutions that have the largest initial normal acceleration among

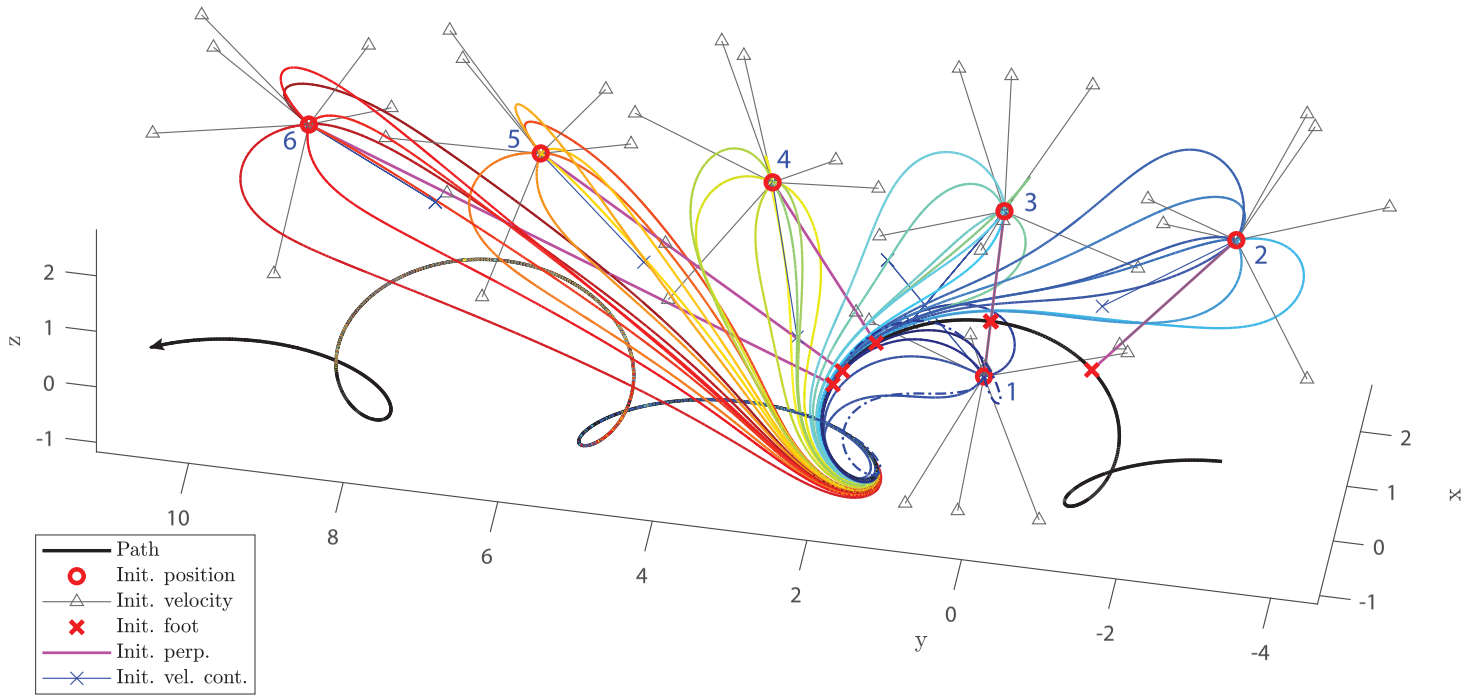

Figure 5.12: Solution trajectories of the various initial-value problems in Section 5.5.3.

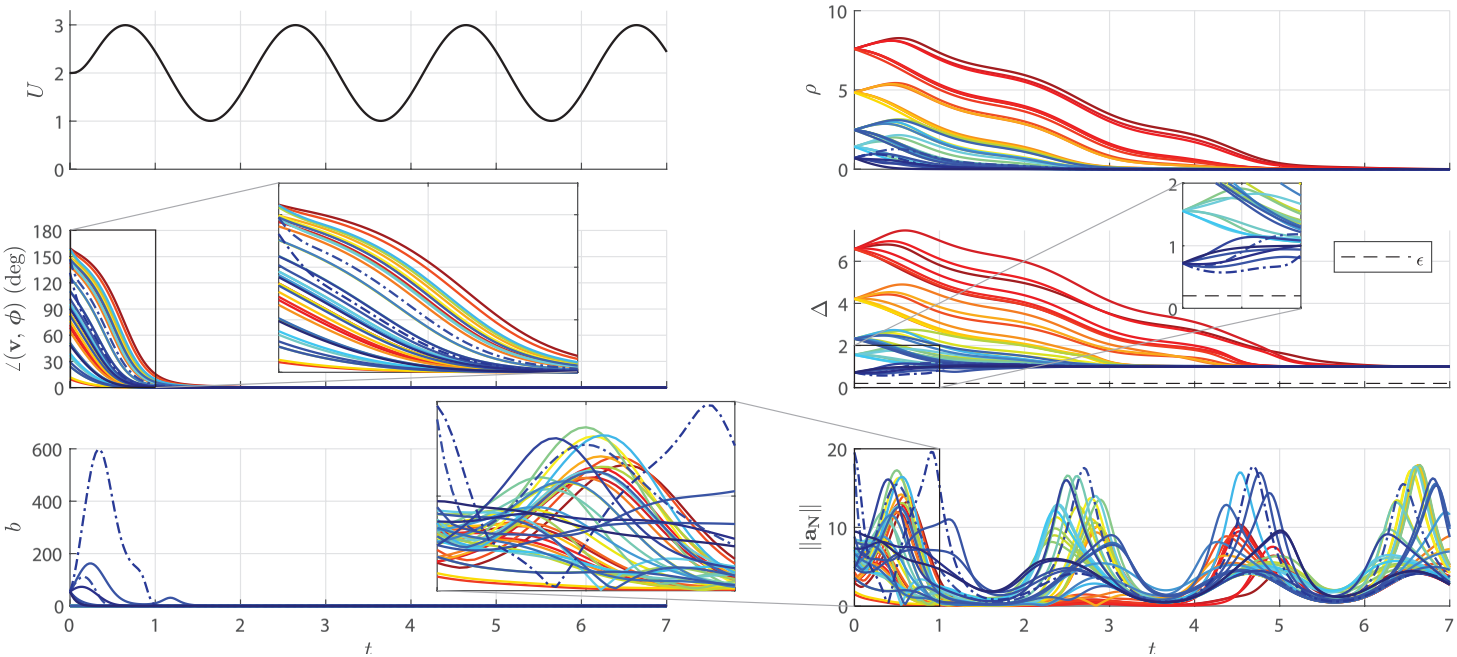

Figure 5.12: History of the various initial-value problems in Section 5.5.3.

Table 5.5: Initial conditions (ICs)

IC index	$\sigma(0)$	$\mathbf{p}(0)^\top$	$\Delta\|_0$
1	0	[0.5 0 0.5]	0.722
2	-1.054	[2 $-$ 3 2]	2.319
3	0	[2 0 2]	1.556
4	1.054	[2 3 2]	2.319
5	1.512	[2 6 2]	4.214
6	1.705	[2 9 2]	6.587

the simulation results are denoted by dashed lines, which all belong to IC 1. These outliers are an exception to the foregoing trends. IC 1 particularly has $\Delta|_0$ smaller than 1; therefore, it renders the barrier active. In general, low initial Δ together with the initial velocity heading opposite to its foot exhibits a large normal acceleration because P has to turn its velocity direction swiftly to avoid the singularity. This characteristic can be seen from the history of $\angle(\overline{\mathbf{v}}, \boldsymbol{\phi})$ in these two cases that the angle decreases faster than the other results at the beginning of the simulation. Though it is not guaranteed, Δ has a tendency that once $\Delta|_0 > 1$, $\Delta|_t$ keeps larger than 1 for all future time giving no chance for the barrier to be active.

Chapter 6

Unification of Flight Control System and WPTPFC

The flight control system and WPTPFC developed in Chapter 3 and 5 are unified in this chapter. The flight control system is composed of the tracking controllers of the angular velocity, aerodynamic roll angle, aerodynamic angles, and flight-path angle (FPA), while WPTPFC generates a velocity direction input and a steering input. In order to unify the methods, the compatibility of between the subsystems should be inspected carefully for efficient integration. The dissertation gives a close look at factors to be noted for practical uses of the methods. The numerical simulations verify the effectiveness of the proposed approaches.

6.1 Parameter Normalization

To use the WPTPFC control gains chosen in Chapter 2.3 for a physical system involving aerial vehicles, the vehicle states need to be normalized with reference values. In this dissertation, the vehicle state variables that have the length dimension including the desired path are normalized with the reference L_{ref}. That is, the perpendicular $\mathbf{e}$ in Section 5.2.1 and the speed of the vehicle U in Section 5.2.2 are normalized as

$$\begin{aligned} \mathbf{e} &= \frac{1}{L_{\text{ref}}}(\boldsymbol{\gamma}(\alpha) - \mathbf{p}) \\ U &= \frac{\overline{V}_T}{L_{\text{ref}}} \end{aligned} \tag{6.1}$$

where $\mathbf{p}$ and $\overline{V}_T$ are the vehicle's position and ground speed, respectively. The reference is chosen as $L_{\text{ref}} = 2,000$ m for the F/A-18 HARV aircraft model.

6.2 WPTPFC: Velocity Direction Control

VDI WPTPFC designed in Section 5.3 generates a unit vector $\boldsymbol{\phi}$ that represents the velocity direction command for the vehicle, whereby it inherently requires an velocity direction tracking controller in the inner loop as shown in Fig. 6.1. The angles in the vehicle dynamics relevant to the flight direction are the course angle χ and the longitudinal flight-path angle γ. Therefore, it is natural to pair the FPA tracking controller developed in Chapter 3 with the VDI control system.

In order to integrate the FPA tracking control and VDI control, the VDI control law $\boldsymbol{\phi}$ should be converted to a flight-path angle coordinates. One of the ways is to find a solution of the following system of trigonometric equations

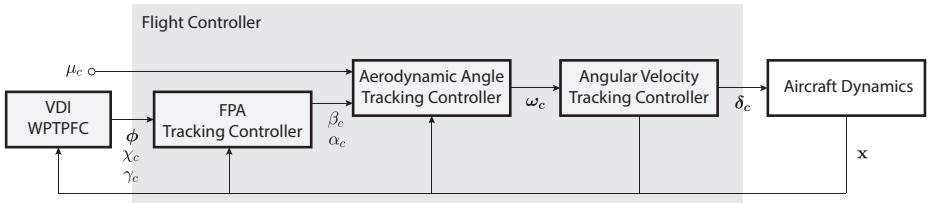

Figure 6.1: Block diagram of the unified system: VDI WPTPFC and the flight control system

for the unknown $\boldsymbol{\xi}_f = [\chi\ \gamma]^\top$ and given $\boldsymbol{\phi}$:

$$\boldsymbol{\phi}^i = \mathbf{C}_{i/\sigma}\mathbf{i} = \begin{bmatrix} \cos\chi\cos\gamma \\ \sin\chi\cos\gamma \\ -\sin\gamma \end{bmatrix} \tag{6.2}$$

where $\boldsymbol{\phi}^i$ is the VDI control represented in the NED coordinate system i. Let $\boldsymbol{\phi}^i = [\phi_1\ \phi_2\ \phi_3]^\top$. Then, an analytic principal solution can be obtained as

$$\begin{aligned} \gamma_\mathrm{c} &= -\arcsin(\phi_3) \\ \chi_\mathrm{c} &= \mathrm{atan2}(\phi_2, \phi_1) \end{aligned} \tag{6.3}$$

However, in spite of its simplicity, the solution is not a good choice for the FPA command. Because they can only have values in the principal region of the domain, $(-\pi, \pi]$ for atan2, a discontinuous jump will occur when χ_c crosses $\pm\pi$. This dissertation proposes an efficient remedy to this issue in the following section.

6.2.1 FPA Command Filter

First, augment $\boldsymbol{\xi}_{f_c} = [\chi_c \ \gamma_c]^\top$ to the state variables, and consider the change of variable

$$\overline{\mathbf{v}}_c = \begin{bmatrix} \cos\chi_c \cos\gamma_c \\ \sin\chi_c \cos\gamma_c \\ -\sin\gamma_c \end{bmatrix} \tag{6.4}$$

Then, $\overline{\mathbf{v}}_c$ is a unit vector, and χ_c and γ_c represent the azimuth and elevation angle of $\overline{\mathbf{v}}_c$, respectively, as shown in Fig. 6.2. Now, design the dynamics of $\overline{\mathbf{v}}_c$ by

$$\dot{\overline{\mathbf{v}}}_c = k_f \left[\boldsymbol{\phi} - (\boldsymbol{\phi} \cdot \overline{\mathbf{v}}_c)\overline{\mathbf{v}}_c\right] \tag{6.5}$$

for some $k_f > 0$. The dynamics has the following properties:

1. $\dot{\overline{\mathbf{v}}}_c$ is orthogonal to $\overline{\mathbf{v}}_c$:

$$\begin{aligned} \overline{\mathbf{v}}_c \cdot \dot{\overline{\mathbf{v}}}_c &= k_f \left[\overline{\mathbf{v}}_c \cdot \boldsymbol{\phi} - (\boldsymbol{\phi} \cdot \overline{\mathbf{v}}_c)\|\overline{\mathbf{v}}_c\|^2\right] \\ &= 0 \end{aligned} \tag{6.6}$$

   This property ensures the dynamics is well-defined for the unit vector $\overline{\mathbf{v}}_c$.

2. $\overline{\mathbf{v}}_c$ tracks $\boldsymbol{\phi}$. To see this, let $V = \|\boldsymbol{\phi} - \overline{\mathbf{v}}_c\|^2/2 = 1 - \boldsymbol{\phi} \cdot \overline{\mathbf{v}}_c$. Then, V is the direction difference between $\boldsymbol{\phi}$ and $\overline{\mathbf{v}}_c$, and its derivative satisfies the following inequality:

$$\begin{aligned} \dot{V} &= -\boldsymbol{\phi} \cdot \dot{\overline{\mathbf{v}}}_c - \dot{\boldsymbol{\phi}} \cdot \overline{\mathbf{v}}_c \\ &= -k_f \left[1 - (\boldsymbol{\phi} \cdot \overline{\mathbf{v}}_c)^2\right] - \dot{\boldsymbol{\phi}} \cdot \overline{\mathbf{v}}_c \\ &= -k_f (1 + \boldsymbol{\phi} \cdot \overline{\mathbf{v}}_c)(1 - \boldsymbol{\phi} \cdot \overline{\mathbf{v}}_c) - \dot{\boldsymbol{\phi}} \cdot \overline{\mathbf{v}}_c \\ &\leq -k_f (1 + \boldsymbol{\phi} \cdot \overline{\mathbf{v}}_c) V + \|\dot{\boldsymbol{\phi}}\| \end{aligned} \tag{6.7}$$

   Let $c_1, c_2 \in (0, 2)$ and $c_1 < c_2$. Suppose that the derivative of the VDI

control $\boldsymbol{\phi}$ is bounded: $\|\dot{\boldsymbol{\phi}}\| \leq b$ for some $b > 0$. Then, it follows that

$$\begin{aligned} V \in [c_1, c_2] &\Rightarrow 1 - \boldsymbol{\phi} \cdot \overline{\mathbf{v}}_c \in [c_1, c_2] \\ &\Rightarrow 1 + \boldsymbol{\phi} \cdot \overline{\mathbf{v}}_c \geq 2 - c_2 > 0 \\ &\Rightarrow \dot{V} \leq -k_f(2 - c_2)V + b \\ &\Rightarrow \dot{V} \leq -k_f c_1(2 - c_2) + b \end{aligned} \tag{6.8}$$

Therefore, a choice of gain $k_f > \frac{b}{c_1(2-c_2)}$ ensures the derivative of V to be always negative whenever $V \in [c_1, c_2]$. That is, V along the solution for every initial condition that satisfies $V \leq c_2$ is uniformly ultimately bounded:

$$\limsup_{t \to \infty} V|_t \leq c_1 \tag{6.9}$$

Consequently, no matter how fast $\boldsymbol{\phi}$ excurses, an ultimate bound of $V|_t$ can be arbitrarily reduced by decreasing c_1, which implies an increased gain k_f. The dynamics can be thought of as a constrained first-order low pass filter for $\boldsymbol{\phi}$.

Now, the dynamics of $\overline{\mathbf{v}}_c$ is transformed to χ_c and γ_c-dynamics. Let the right-hand side of Eq. (6.5) be denoted by $[f_1 \ f_2 \ f_3]^\top$. Taking derivative of the right-hand side of Eq. (6.4) with Eq. (6.5) applied yields

$$\begin{bmatrix} -\dot{\chi}_c \sin\chi_c \cos\gamma_c - \dot{\gamma}_c \cos\chi_c \sin\gamma_c \\ \dot{\chi}_c \cos\chi_c \cos\gamma_c - \dot{\gamma}_c \sin\chi_c \sin\gamma_c \\ -\dot{\gamma}_c \cos\gamma_c \end{bmatrix} = \begin{bmatrix} f_1 \\ f_2 \\ f_3 \end{bmatrix} \tag{6.10}$$

Then, given that $\cos\gamma_c \neq 0$, $\cos\chi_c \neq 0$, and $\sin\chi_c \neq 0$, the state equation for

$\dot{\chi}_c$ and $\dot{\gamma}_c$ are obtained by

$$\dot{\chi}_c = \frac{1}{\cos\chi_c \cos\gamma_c}\left(f_2 - \frac{\sin\chi_c \sin\chi_c}{\cos\gamma_c} f_3\right) \tag{6.11a}$$

$$\dot{\chi}_c = \frac{1}{\sin\chi_c \cos\gamma_c}\left(\frac{\cos\chi_c \sin\chi_c}{\cos\gamma_c} f_3 - f_1\right) \tag{6.11b}$$

and

$$\dot{\gamma}_c = -\frac{f_3}{\cos\gamma_c} \tag{6.12}$$

The resulting state equations are equivalent to the $\overline{\mathbf{v}}_c$-dynamics. In particular, Eqs. (6.11a) and (6.11b) represent the same dynamics, but a significant difference comes from the fractions outside the parenthesis. Equation (6.11a) is singular at $\cos\chi_c = 0$, while Eq. (6.11b) is singular at $\sin\chi_c = 0$. Therefore, a state function that is free from the singularity caused by χ_c can be designed by switching; Eq. (6.11a) is used when $|\cos\chi_c| \geq 1/\sqrt{2}$, and Eq. (6.11b) is used otherwise, where this switching criterion does not incur a chattering phenomenon because the state equation is always locally Lipschitz whenever $\gamma_c \neq 0$. Since the solution of the state equation does not suffer from discontinuities, it can be used as a filtered FPA command for the given VDI control.

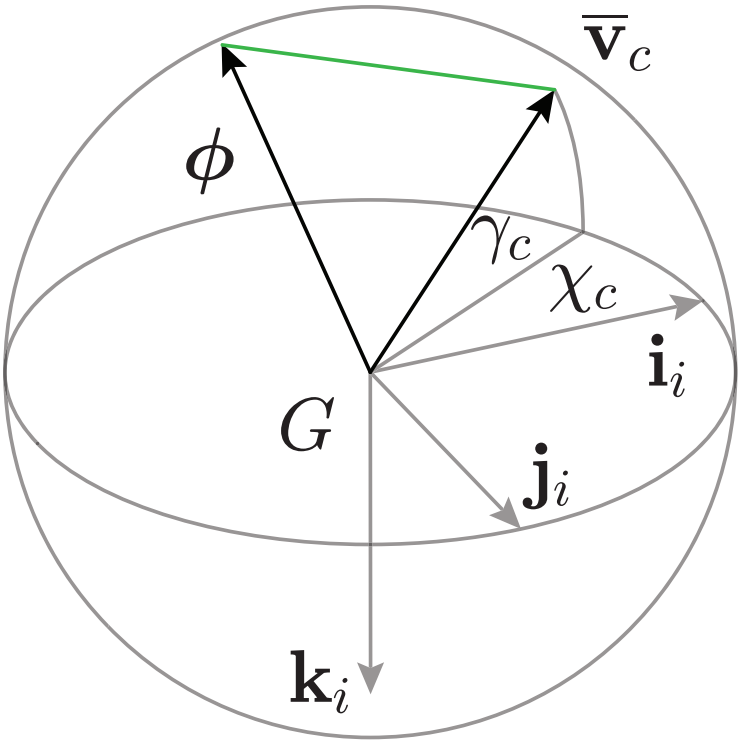

Figure 6.2: FPA command filter geometry. The green line segment is the part to be regulated.

6.3 WPTPFC: Steering Control

SI WPTPFC gives the steering command $\boldsymbol{\psi}$. As discussed in Section 5.2.2 and 5.4.2, the steering input $\mathbf{u}_s$ is a scaled version of the normal acceleration $\mathbf{a}_N$; $\mathbf{a}_N = \overline{V}_T \mathbf{u}_s$. Therefore, the normal acceleration command $\mathbf{a}_{Nc}$ is obtained by

$$\mathbf{a}_{Nc} = \overline{V}_T \boldsymbol{\psi} \tag{6.13}$$

and an inner-loop subsystem for SI control should be chosen accordingly in order to track the commanded normal acceleration. To this end, the normal component of the total force exerted on a vehicle is investigated. The component can be found by projecting $\mathbf{F} = \mathbf{F}_A + \mathbf{T} + m\mathbf{g}$ onto the plane perpendicular to the inertial velocity $\mathbf{v} = \mathbf{v}^i_{G/i}$. Let the vector projection of $\mathbf{a}$ onto the plane orthogonal to the unit vector $\mathbf{u}$ be denoted by

$$\text{oproj}(\mathbf{u}, \mathbf{a}) = \mathbf{a} - (\mathbf{a} \cdot \mathbf{u})\mathbf{u}$$

Applying the Newton's second law of motion $\frac{1}{m}\mathbf{F} = \ddot{\mathbf{p}}$ to Eq. (5.11) yields

$$\frac{1}{m}\text{oproj}(\overline{\mathbf{v}}, \mathbf{F}) = \text{oproj}(\overline{\mathbf{v}}, \ddot{\mathbf{p}}) = \mathbf{a}_N = \overline{V}_T \boldsymbol{\psi} \tag{6.14}$$

where $\overline{\mathbf{v}} = \mathbf{v}/\|\mathbf{v}\| = \mathbf{v}/\overline{V}_T$.

The normal acceleration of an aerial vehicle is effectively manipulated by controlling the aerodynamics angles $\boldsymbol{\xi}_a = [\beta \ \alpha]^\top$ because $\text{oproj}(\overline{\mathbf{v}}, \mathbf{F}_A)$ is susceptible to β and α in an ordinary flight condition. Therefore, it is reasonable to take $\boldsymbol{\xi}_a$ as input to yield to normal acceleration command $\mathbf{a}_{Nc}$; the aerodynamic angle tracking control law developed in Section 3.4 is paired with the SI control as shown in Fig. 6.3.

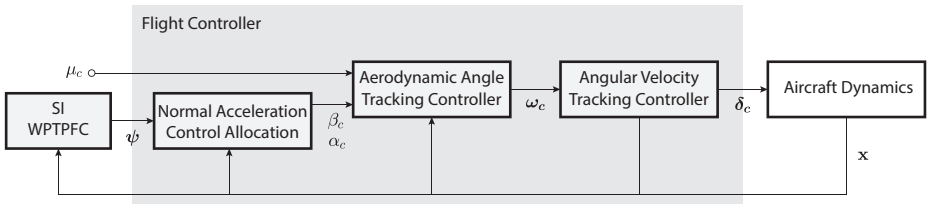

Figure 6.3: Block diagram of the unified system: SI WPTPFC and the flight control system

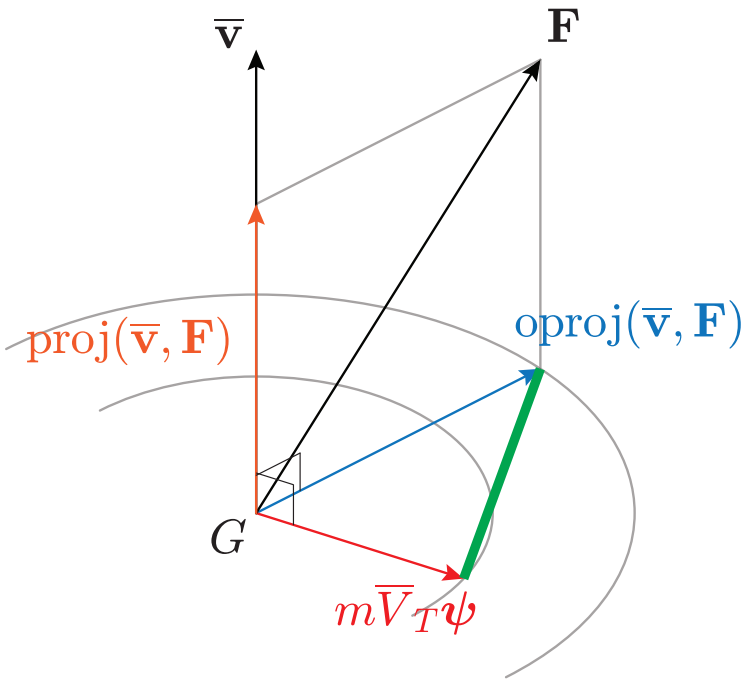

Figure 6.4: Force projection and orthogonal projection. The green line segment is the part to be minimized by the control allocation.

6.3.1 Normal Acceleration Control Allocation

Now, the unification of the two control laws boils down to finding an aerodynamic angle command $\boldsymbol{\xi}_{ac} = [\beta_c \ \alpha_c]^\top$ that makes the error between $\mathrm{oproj}(\overline{\mathbf{v}}, \mathbf{F})$ and $m\overline{V}_T\boldsymbol{\psi}$ minimized while fixing all the variables other than $\boldsymbol{\xi}_a$ as illustrated in Fig. 6.4. This is a control allocation problem that can be formalized as an optimization problem:

$$\begin{aligned} &\text{minimize} && \left\|\mathrm{oproj}(\overline{\mathbf{v}}, \mathbf{F}) - m\overline{V}_T\boldsymbol{\psi}\right\|^2 + w_s\|\boldsymbol{\xi}_a\|^2 \\ &\text{subject to} && c_a(\boldsymbol{\xi}_a) \leq 0 \end{aligned} \tag{6.15}$$

where t and $\mathbf{x}_v^{(a)}$ are fixed, $w_s > 0$ is the regularization weighting, $\mathbf{x}_v^{(a)}$ denotes the state vector with $\boldsymbol{\xi}_a$ removed, and c_a is a function that represents the flight envelope of β and α. A minimizer of Eq. (6.15) is chosen as $\boldsymbol{\xi}_{ac}$. Similar to Section 3.5, it is assumed that a unique solution exists for the optimization problem Eq. (6.15), and the solution is continuous in t and $\mathbf{x}_v^{(a)}$.

6.3.2 Low-pass Filter for VDI Control

SI WPTPFC requires the derivative of the VDI control $\boldsymbol{\phi}$ to get the steering control $\boldsymbol{\psi}$ as shown in Eqs. (5.44c) and (5.55). However, depending on the VDI design, the derivative of $\boldsymbol{\phi}$ can be undesirably complex due to the "explosion of terms" [66]. For this reason, a first-order Loss-pass Filter (LPF) is used.

6.4 Numerical Simulation

The unified control systems are applied to two scenarios through numerical simulations in this section. The goal of the control system is to make an aerial vehicle follow general three-dimensional paths with bounded curvature under time-varying ambient wind condition.

In all scenarios, the engines of the F/A-18 HARV model are not actively controlled, which implies that the ground speed is solely determined by the ambient wind and the aircraft's maneuvers. This is a deliberate setup made in order to differentiate PFC from trajectory tracking. Unlike trajectory tracking control, PFC does not need any timing law for path parameters. Therefore, the performance requirements imposed on the target plants are relatively mitigated. For example, PFC is a better choice for unpowered vehicles such as gliders or powered vehicles being impaired in flight.

6.4.1 Scenario 1: straight line tracking

The VDI control is applied in this scenario, and the scenario is chosen to demonstrate the base performance of the control system. The desired path is given by

$$\gamma(\sigma)^i = L_{\text{ref}} \begin{bmatrix} \sigma & 5 & -2 - 0.4\sigma \end{bmatrix}^\top \tag{6.16}$$

where $L_{\text{ref}} = 2000$ m is the reference length for normalization defined in Section 6.1. The path increases its altitude as the path parameter σ grows. The ambient wind is time-varying and its average speed is 21.2 m/s. The aircraft starts at $L_{\text{ref}}[0\ 0\ -3]^\top$, and the thrust is fixed to 50 % of its maximum.

As shown in Fig. 6.5, the ground speed of the aircraft increases before it converges to the path as the perpendicular foot is located below the initial position of the aircraft. Then, due to the relatively steep slope of the path, the

airspeed gradually decreases after the aircraft touches the path in spite of the thrust. As a result, the speed of the aircraft varies widely in the scenario. The state profile reveals that the tracking performance of the flight control system is not deteriorated by such a condition.

An important result to be noted in this scenario is the response of the local distance ρ, which indicates the path-following performance of the unified system. In Fig. 6.7, the distance asymptotically regulated and the estimated ultimate bound is 34 m. The ultimate bound is practically acceptable in this windy condition, and it can be further reduced through gain tuning or an augmentation of a simple adaptive law will effectively reduce the bound.

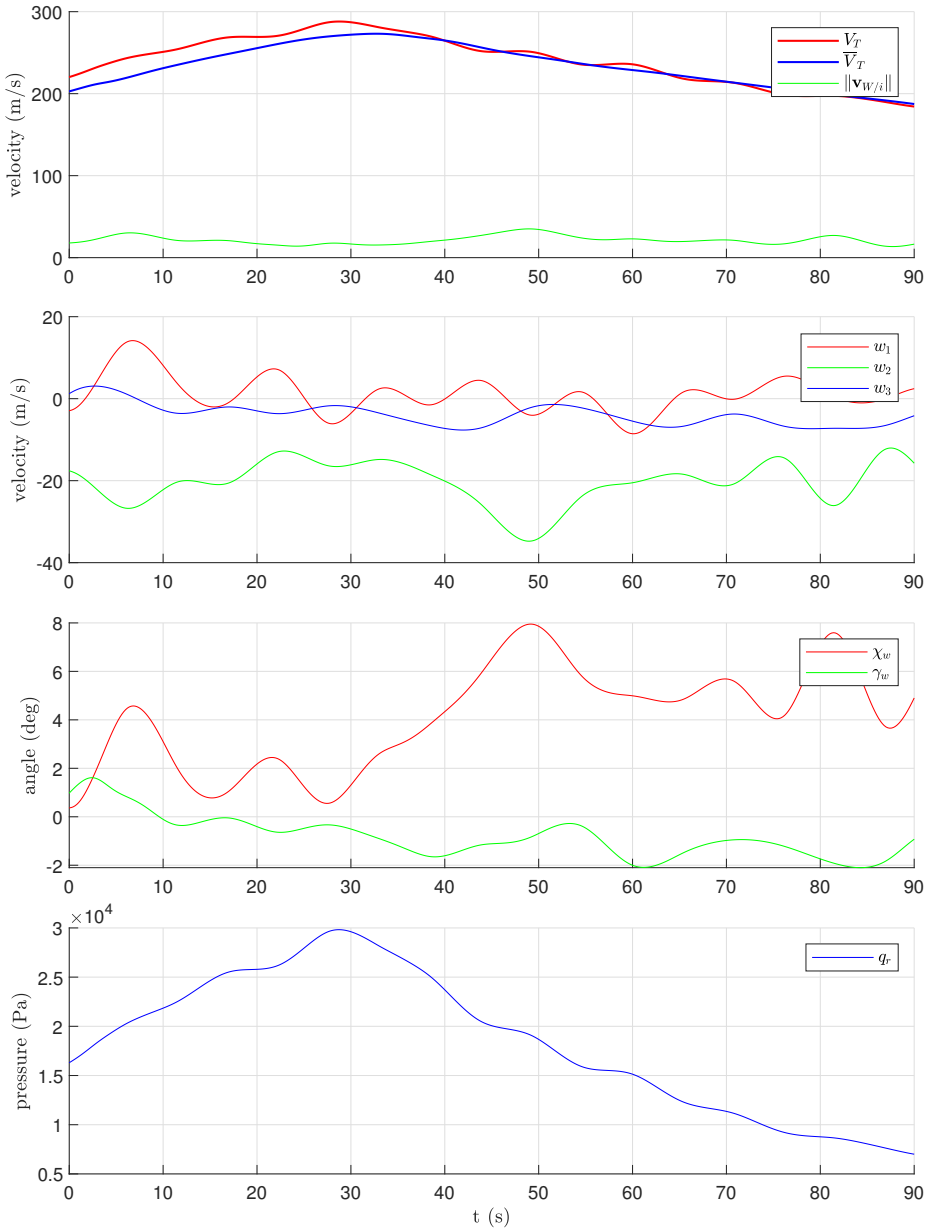

Figure 6.5: Scenario 1: straight line tracking. (top) Vehicle speed and ambient wind speed profile. (second) wind velocity profile. (third) path-relative wind angles (bottom) dynamic pressure

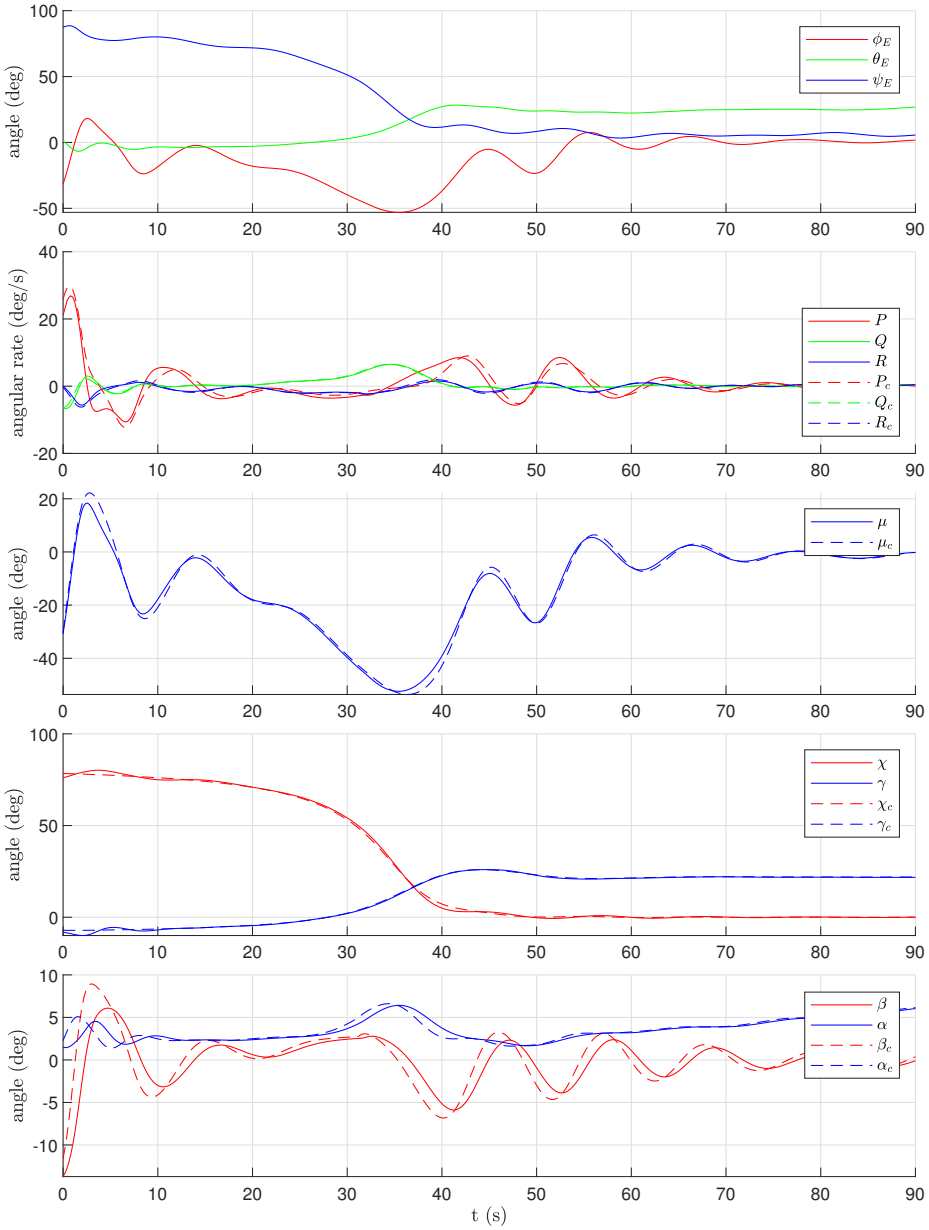

Figure 6.6: Scenario 1: straight line tracking. (top) Euler angles. (second) angular velocity and command. (third) aerodynamic roll angle. (fourth) FPA. (bottom) sideslip and angle of attack.

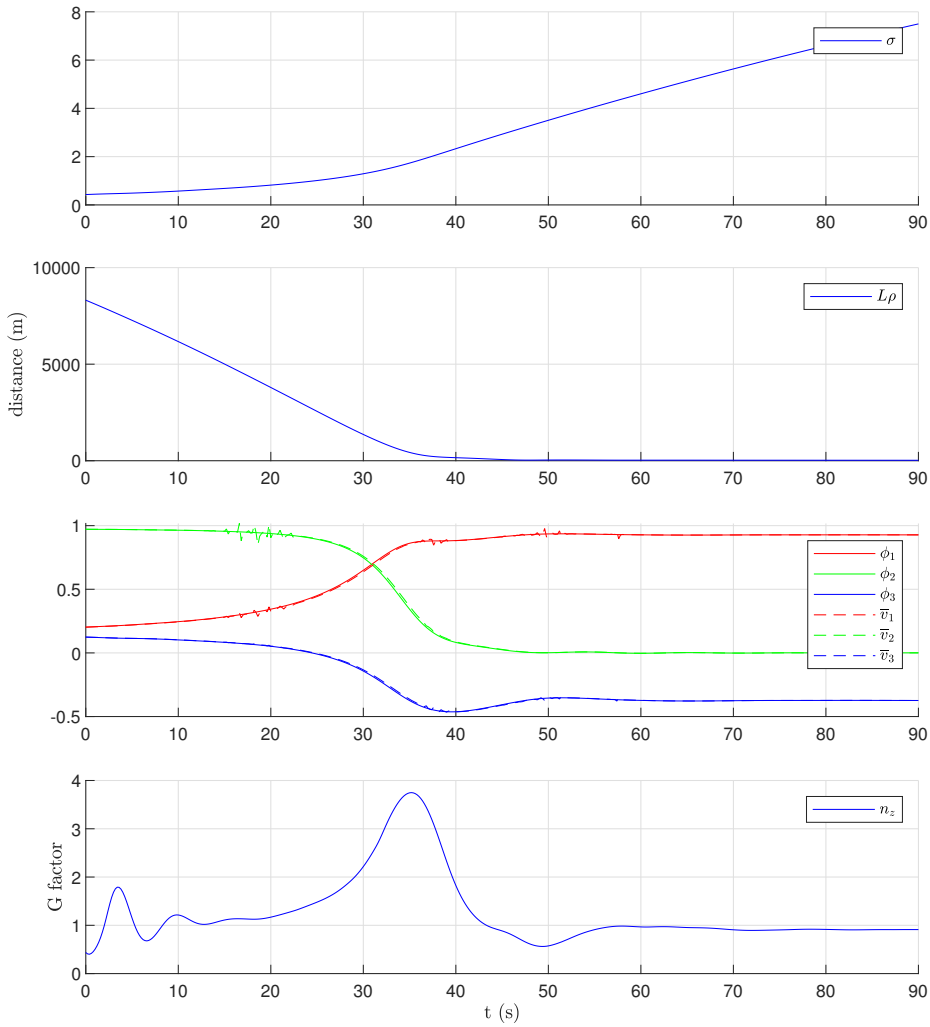

Figure 6.7: Scenario 1: straight line tracking. (top) path parameter. (second) local distance to the path. (third) VDI control and FPA command filter. (fourth) G factor.

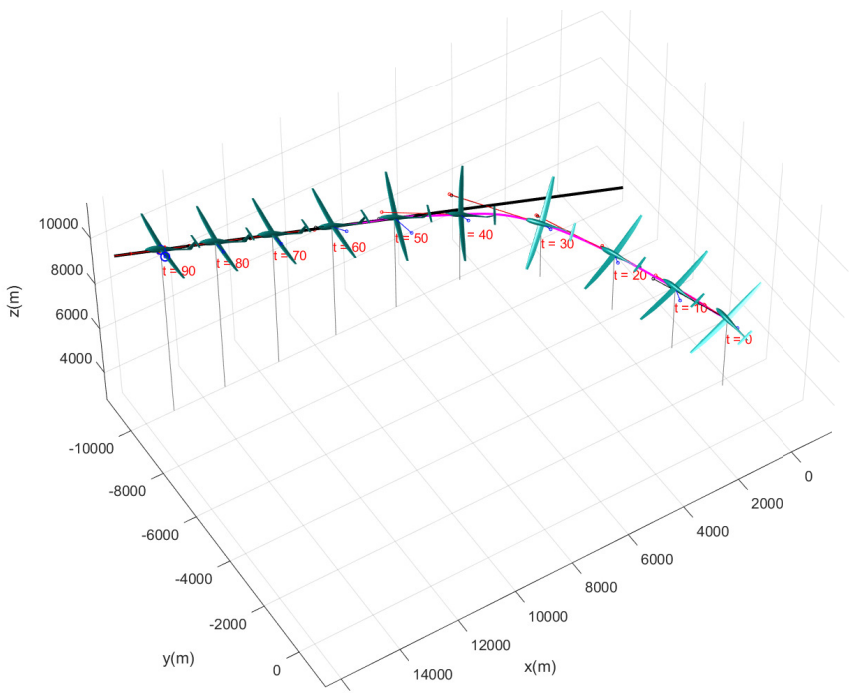

Figure 6.8: Scenario 1: straight line tracking. Trajectory of the vehicle converging to the straight line (black).

6.4.2 Scenario 2: descending vertical helix tracking

The SI control is applied in this scenario. The environment of Scenario 2 is much harsher than that of Scenario 1, and it is chosen to demonstrate the robust performance of the control system. The desired path is given by

$$\gamma(\sigma)^i = L_{\text{ref}} \begin{bmatrix} \cos\sigma & \sin\sigma + 3 & -2 + 0.1\sigma \end{bmatrix}^\top \tag{6.17}$$

and the aircraft starts at $L_{\text{ref}}[0\ 0\ -3]^\top$. The path descends as the path parameter σ grows.

The ambient wind is time-varying and its average speed is 60.3 m/s. The condition is particularly unrealistic in general sense since most airports do not allow aircraft to takeoff and land in 20 m/s or more ambient wind speeds (especially for crosswinds). However, the simulation result will verify the proposed approach more effectively with this condition. Moreover, the two engines of the aircraft are assumed to be completely failed during airborne maneuver. Therefore, the dynamic pressure of the aircraft can be maintained only by the initial kinetic energy and an adequate gliding path. The descending rate of the helical path is determined by considering the dynamics of the F/A-18 HARV model. Hence, the dynamic pressure will stay in the safe envelope if the aircraft successfully follows the desired path.

As shown in Fig. 6.9, the ambient wind speed intermittently reaches about 70 % of the aircraft's airspeed, which could be disastrous if it were a tailwind because the aircraft could lose its dynamic pressure and fall into loss of control. The severity of the ambient wind can also be seen from the profile of the path-relative wind angles, where lateral path-relative wind angle χ_w exceeds 20 deg at $t = 65$ s. In moderate flight conditions, χ_w stays less than 10 deg in general.

In Fig. 6.10, the SI WPTPFC successfully drives the aircraft to follow the

helical path as shown by the local distance profile. The estimated ultimate bound is 34 m, which is the same as the VDI control case in Scenario 1. The airspeed of the aircraft stops decreasing after $t = 70$ s keeping at least 150 m/s, which is safe for F/A-18 HARV at this altitude.

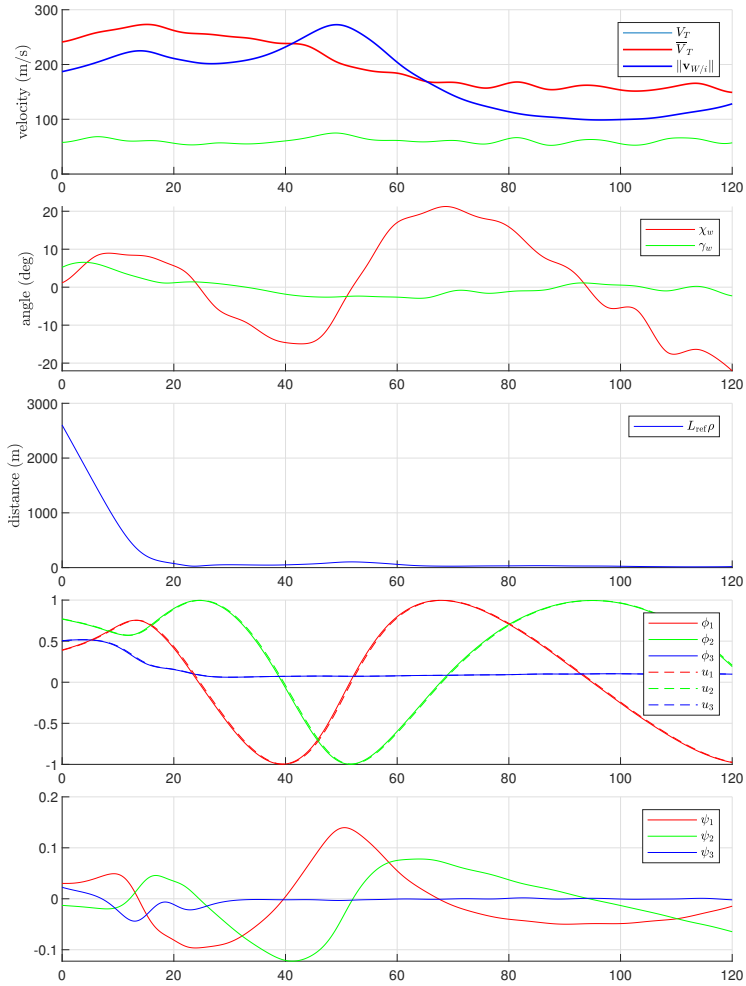

Figure 6.9: Scenario 2: descending helix tracking. (top) vehicle speeds and ambient wind speed. (second) path-relative wind angles. (third) local distance. (fourth) VDI control. (bottom) SI control.

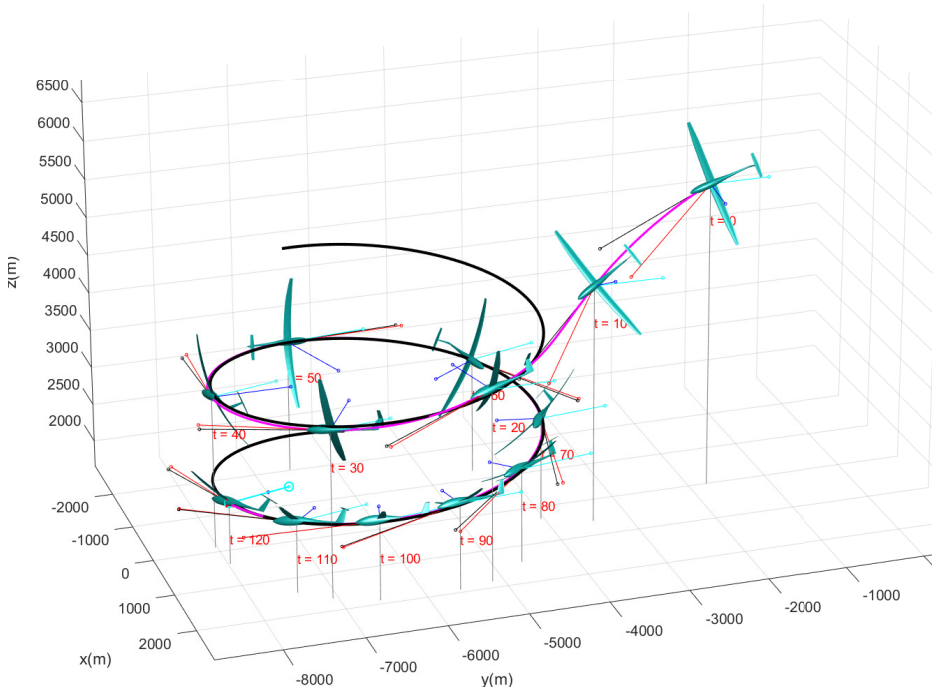

Figure 6.10: Scenario 2: descending helix tracking. Trajectory of the vehicle converging to the descending helix (black).

6.4.3 Various simulation results

In this section, a total of four curves are selected as a desired path to show the performance of the unified control system, and they are specified in Table 6.1. The aircraft starts at $L_{\text{ref}}[0\ 0\ -2]^\top$, and the ambient wind is given by

$$\mathbf{v}^i_{W/i}(t) = \begin{bmatrix} -60 & 0 & -15 \end{bmatrix}^\top + d(t)\ (\text{m/s})$$

for some continuous function $d : \mathbb{R}_+ \to \mathbb{R}^{3\times 1}$ such that $\|d(t)\| \leq 10$ (m/s). The SI control is used for these simulations.

Table 6.1: Various paths

Path name	Components
Ascending helix	$L_{\text{ref}}[\cos\sigma + 3 \quad \sin\sigma \quad 2 - 0.2\sigma]^\top$
Ascending wave	$L_{\text{ref}}[\frac{3}{4}\cos\sigma + 4 \quad \frac{3}{4}\sin\sigma \quad -0.2\sigma - 2]^\top$
Canted circle	$L_{\text{ref}}[\cos\sigma + 4 \quad \frac{\sqrt{2}}{2}\sin\sigma \quad \frac{\sqrt{2}}{2}\sin\sigma - 2]^\top$
Barrel roll	$L_{\text{ref}}[0.5\cos\sigma + 3 \quad 0.4\sigma \quad 0.5\sin\sigma + 0.05\sigma - 2]^\top$

Figures 6.11 and 6.12 show the result for the ascending helix, Figs. 6.13 and 6.14 show the result for the ascending wave, Figs. 6.15 and 6.16 show the result for the canted circle, and Figs. 6.17 and 6.18 show the aircraft performing barrel roll. The simulations demonstrate that the aircraft can follow various paths well as intended.

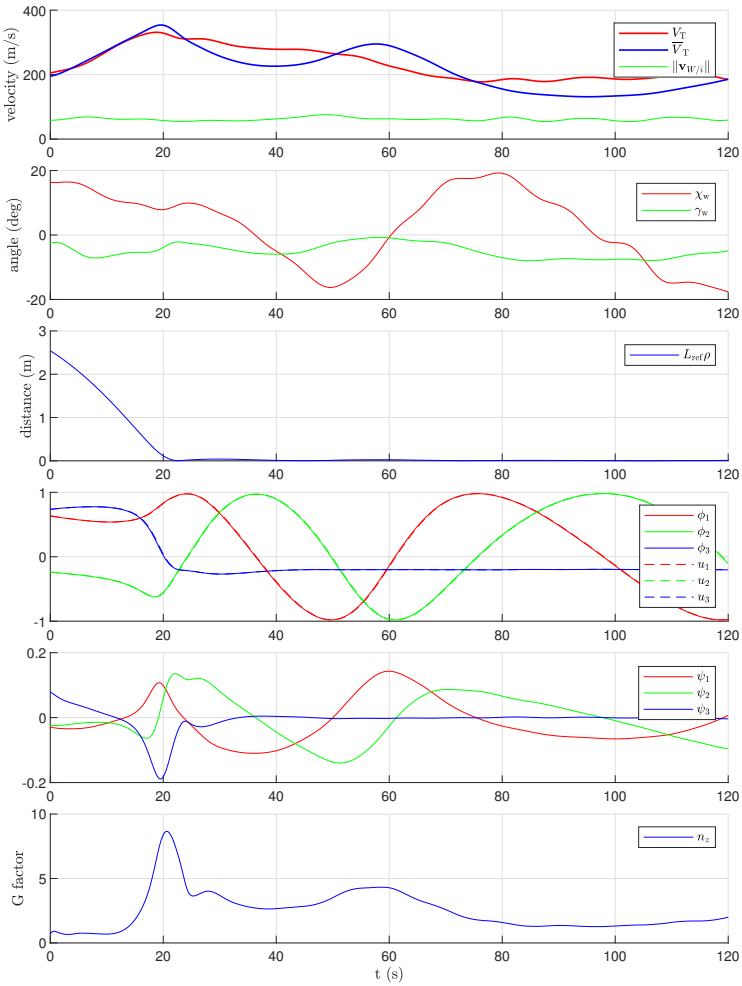

Figure 6.11: Simulation result for the ascending helix. (top) vehicle speeds and ambient wind speed. (second) path-relative wind angles. (third) local distance. (fourth) VDI control. (fifth) SI control. (bottom) G factor.

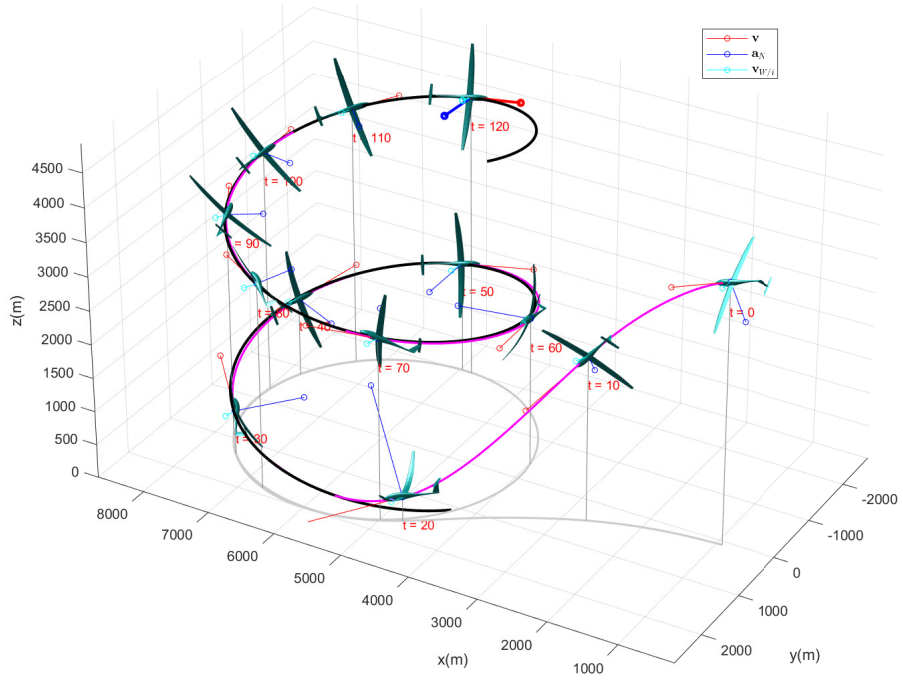

Figure 6.12: Trajectory of the vehicle for the ascending helix.

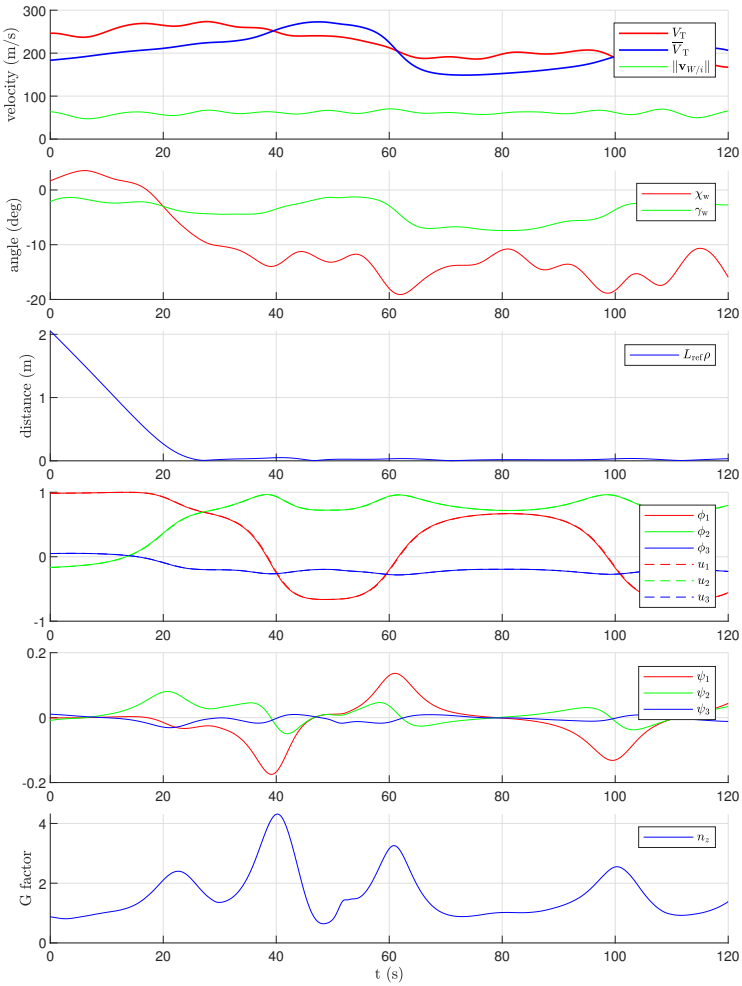

Figure 6.13: Simulation result for the ascending wave. (top) vehicle speeds and ambient wind speed. (second) path-relative wind angles. (third) local distance. (fourth) VDI control. (fifth) SI control. (bottom) G factor.

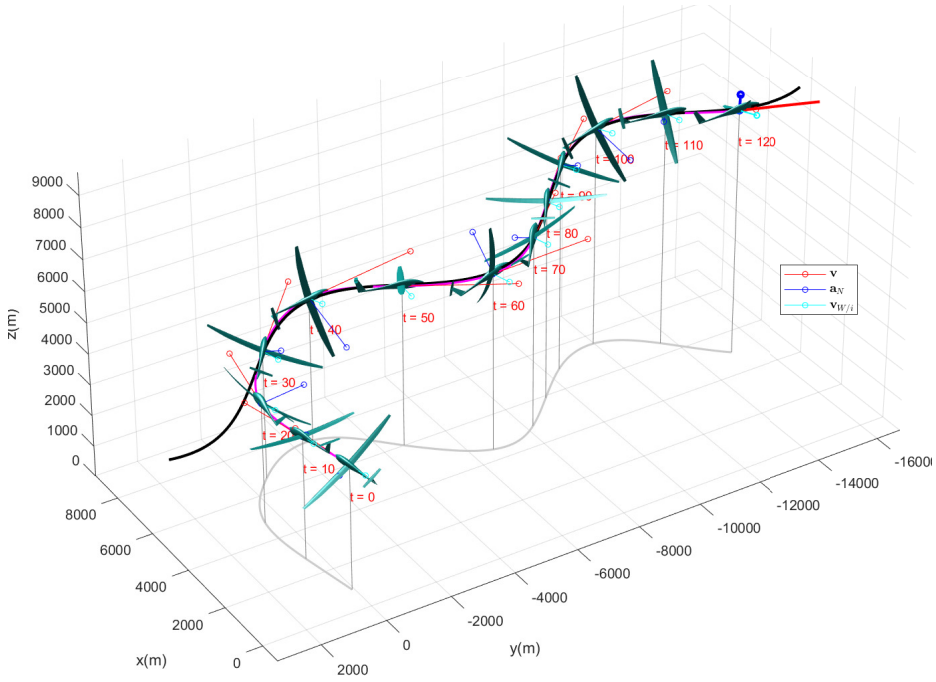

Figure 6.14: Trajectory of the vehicle for the ascending wave.

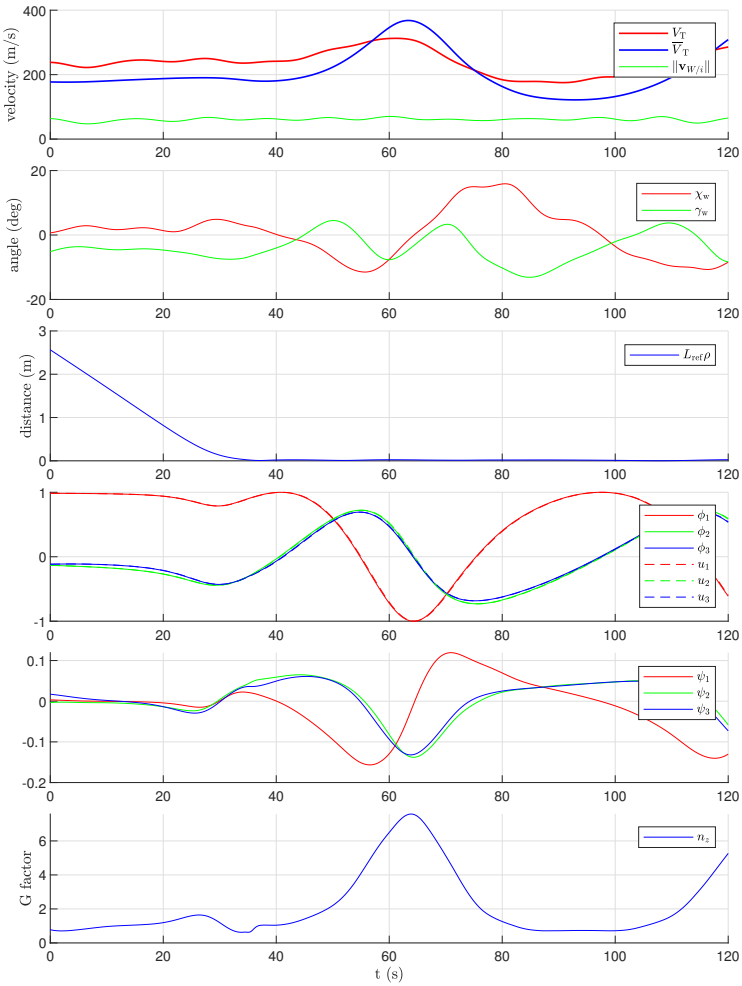

Figure 6.15: Simulation result for the canted circle. (top) vehicle speeds and ambient wind speed. (second) path-relative wind angles. (third) local distance. (fourth) VDI control. (fifth) SI control. (bottom) G factor.

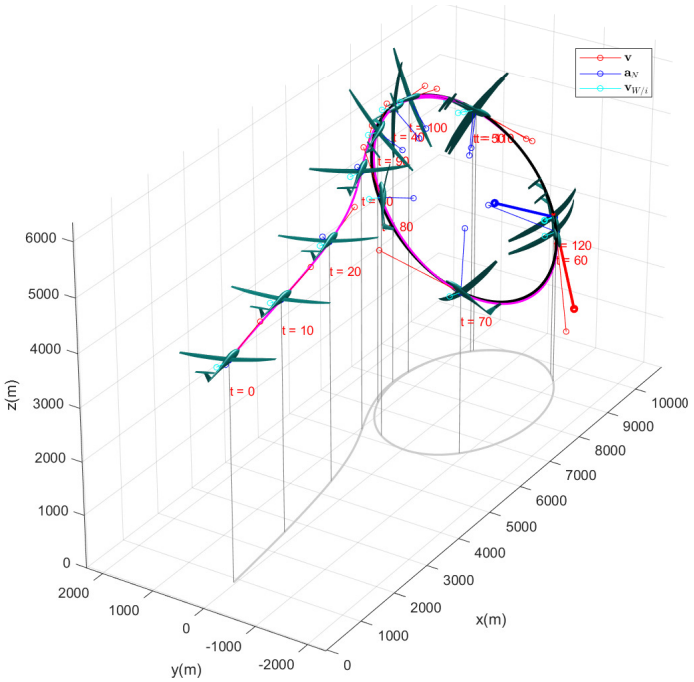

Figure 6.16: Trajectory of the vehicle for the canted circle.

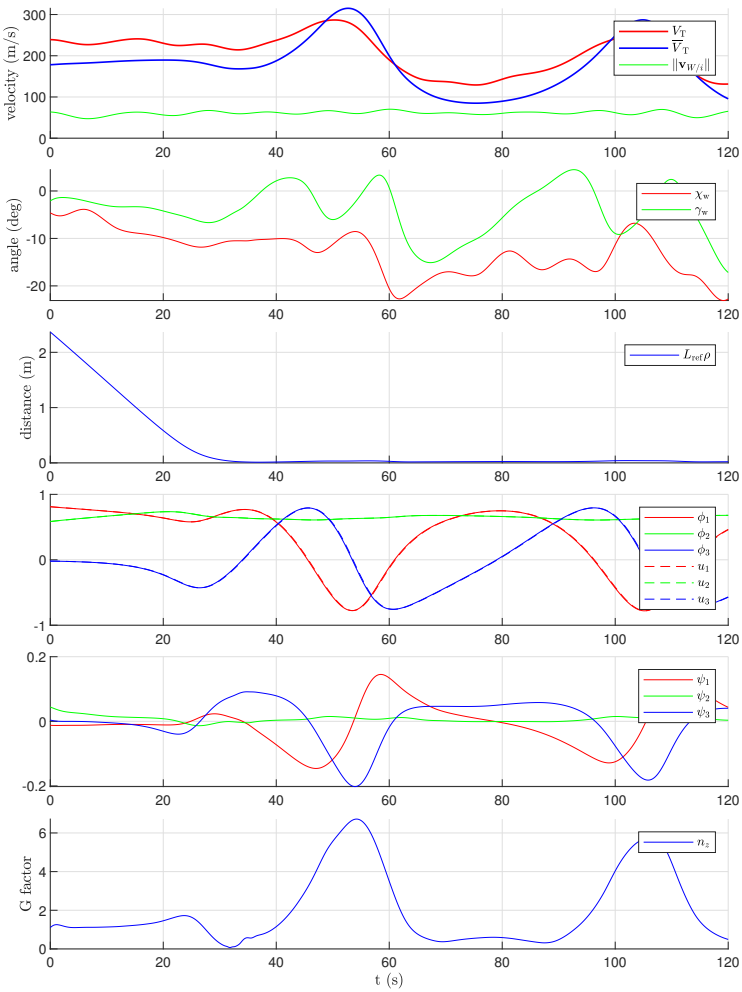

Figure 6.17: Simulation result for the barrel roll. (top) vehicle speeds and ambient wind speed. (second) path-relative wind angles. (third) local distance. (fourth) VDI control. (fifth) SI control. (bottom) G factor.

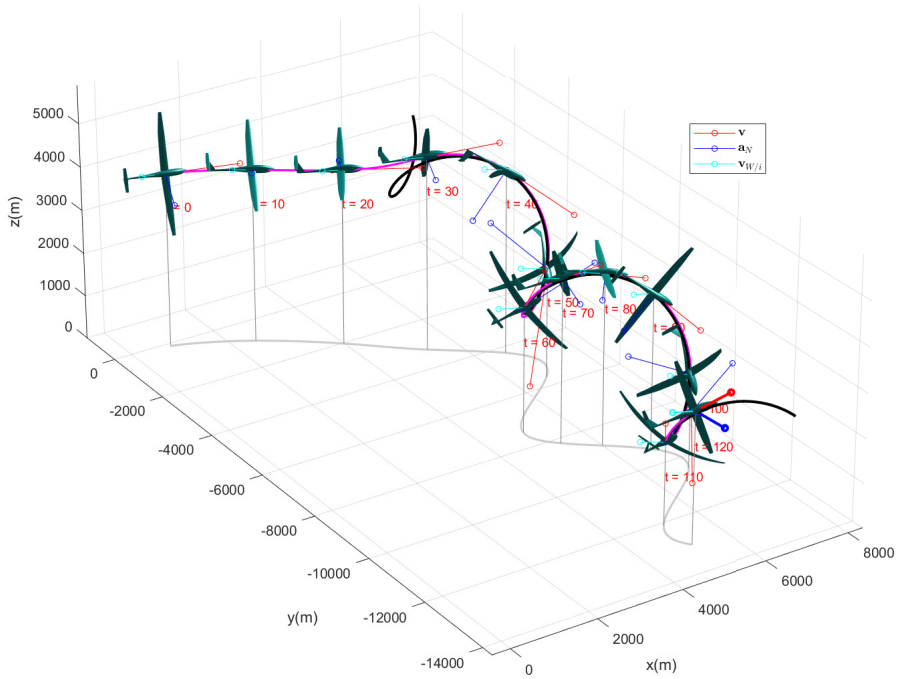

Figure 6.18: Trajectory of the vehicle for the barrel roll.

Chapter 7

Conclusion

7.1 Concluding Remarks

In this dissertation, the equation of motion of the three-dimensional flight dynamics considering continuously differentiable time-varying ambient winds was derived. One of the worthwhile results is the definition of the path-relative wind angles and the aerodynamic roll angle, which can be effectively utilized for the design of trajectory tracking or a coordinated flight control law in the presence of time-varying ambient winds. Each state function was formulated to help design a cascade controller.

The dissertation also presented a novel Path-Following Control (PFC) method for vehicles applicable to general sufficiently smooth three-dimensional regular parametric paths. The target plants include vehicles equipped with steering actuators and moving with a specified nonzero time-varying traversing speed. The perpendicular foot was proposed to inherit the advantage of the closest point reference but reject the discontinuity issue and the need for numerical

optimization. Two controllers were designed sequentially: kinematics-level velocity direction input control followed by dynamics-level steering input control. The weighted combination of the perpendicular, tangent, and the cross product of the two forms a velocity direction control law. In the steering control design, the velocity direction controller was reused through the backstepping control scheme. Each control design consists of singularity avoidance methods to effectively expand the region of operation. In particular, the Lyapunov barrier weighting method for backstepping was proposed, whose notion is not restricted to the design of PFC.

The two control methods were unified by designing a control allocation to make them compatible. The jump discontinuity issue due to the use of an inverse trigonometric function was effectively addressed by developing a a continuous conversion method. A constrained first-order low-pass filter was designed for Steering Input (SI) Weighted-Perpendicular-Tangent-based PFC (WPTPFC) unification to avoid a tedious work to obtain the derivative of the velocity direction input (VDI) control.

7.2 Future Research

Future work includes the development of PFC for deforming paths, i.e., the paths are dependent on the time as well as the path parameter. A dynamic reference point that is free of inherent singularity has to be designed to consider general smoothly deforming paths though the reference is less efficient than the foot in transient performance.

Appendix A

Flight Dynamics

A.1 Components of the Equations of Motion

The components of the several selected terms that appear in the derivation are summarized in the following with appropriate simplification, where c and s stand for cos and sin, respectively:

1. Ground speed

$$\begin{aligned}\overline{V}_T\left(t, V_T, \boldsymbol{\xi}_f\right) = V_T \mathrm{c}\chi_w \mathrm{c}\gamma_w + w_N(t)\mathrm{c}\gamma\mathrm{c}\chi \\ + w_E(t)\mathrm{c}\gamma\mathrm{s}\chi - w_D(t)\mathrm{s}\gamma\end{aligned} \tag{A.1}$$

   where $\mathbf{v}^i_{W/i}(t) = [w_N(t)\ w_E(t)\ w_D(t)]^\top$.

2. Path-relative wind angles

$$\chi_w\left(t, V_T, \chi\right) = \arcsin\left(\frac{w_N(t)\mathrm{s}\chi - w_E(t)\mathrm{c}\chi}{V_T}\right) \tag{A.2a}$$

$$\gamma_w\left(t, V_T, \boldsymbol{\xi}_f\right) = \arcsin\left(\frac{w_N(t)\mathrm{s}\gamma\mathrm{c}\chi + w_E(t)\mathrm{s}\gamma\mathrm{s}\chi + w_D(t)\mathrm{c}\gamma}{V_T \mathrm{c}\chi_w}\right) \tag{A.2b}$$

3. Force

$$\mathbf{F}^{w}\left(t,\mathbf{x},\boldsymbol{\delta},T\right)=\begin{bmatrix}-qSC_{D}+T\mathrm{c}\bar{\alpha}\mathrm{c}\beta-mg\mathrm{c}\chi_{w}\mathrm{s}\bar{\gamma}\\ qSC_{Y}-T\mathrm{c}\bar{\alpha}\mathrm{s}\beta+mg\left(\mathrm{s}\mu\mathrm{c}\bar{\gamma}+\mathrm{c}\mu\mathrm{s}\chi_{w}\mathrm{s}\bar{\gamma}\right)\\ -qSC_{L}-T\mathrm{s}\bar{\alpha}+mg\left(\mathrm{c}\mu\mathrm{c}\bar{\gamma}-\mathrm{s}\mu\mathrm{s}\chi_{w}\mathrm{s}\bar{\gamma}\right)\end{bmatrix} \tag{A.3}$$

where $\bar{\gamma}=\gamma_{w}+\gamma$.

4. State functions

$$\boldsymbol{\eta}_{f}\left(t,\mathbf{x},\boldsymbol{\delta},T\right)=\begin{bmatrix}\left(\begin{array}{l}qS\left(-C_{D}\mathrm{s}\chi_{w}+C_{Y}\mathrm{c}\mu\mathrm{c}\chi_{w}+C_{L}\mathrm{s}\mu\mathrm{c}\chi_{w}\right)\\ \quad+T\left(\mathrm{s}\bar{\alpha}\mathrm{s}\mu\mathrm{c}\chi_{w}+\mathrm{c}\bar{\alpha}\mathrm{c}\beta\mathrm{s}\chi_{w}-\mathrm{c}\bar{\alpha}\mathrm{s}\beta\mathrm{c}\mu\mathrm{c}\chi_{w}\right)\end{array}\right)\\ \left(\begin{array}{l}qS\{C_{D}\mathrm{c}\chi_{w}\mathrm{s}\gamma_{w}+C_{Y}\left(\mathrm{s}\mu\mathrm{c}\gamma_{w}+\mathrm{c}\mu\mathrm{s}\chi_{w}\mathrm{s}\gamma_{w}\right)\\ \quad+C_{L}\left(\mathrm{s}\mu\mathrm{s}\chi_{w}\mathrm{s}\gamma_{w}-\mathrm{c}\mu\mathrm{c}\gamma_{w}\right)\}\\ \quad+T\{\mathrm{s}\bar{\alpha}\left(\mathrm{s}\mu\mathrm{s}\chi_{w}\mathrm{s}\gamma_{w}-\mathrm{c}\mu\mathrm{c}\gamma_{w}\right)\\ \quad-\mathrm{c}\bar{\alpha}\mathrm{s}\beta\left(\mathrm{s}\mu\mathrm{c}\gamma_{w}+\mathrm{c}\mu\mathrm{s}\chi_{w}\mathrm{s}\gamma_{w}\right)-\mathrm{c}\bar{\alpha}\mathrm{c}\beta\mathrm{c}\chi_{w}\mathrm{s}\gamma_{w}\}\end{array}\right)\end{bmatrix} \tag{A.4}$$

$$\begin{aligned}f_{V}\left(t,\mathbf{x},\boldsymbol{\delta}\right)=&-\frac{qS}{m}C_{D}+\dot{w}_{N}(t)\left(\mathrm{s}\chi_{w}\mathrm{s}\chi-\mathrm{c}\chi_{w}\mathrm{c}\bar{\gamma}\mathrm{c}\chi\right)\\&-\dot{w}_{E}(t)\left(\mathrm{s}\chi_{w}\mathrm{c}\chi+\mathrm{c}\chi_{w}\mathrm{c}\bar{\gamma}\mathrm{s}\chi\right)\\&+\dot{w}_{D}(t)\mathrm{c}\chi_{w}\mathrm{s}\bar{\gamma}-g\mathrm{c}\chi_{w}\mathrm{s}\bar{\gamma}\end{aligned} \tag{A.5}$$

$$\begin{aligned}f_{\overline{V}}(t,\mathbf{x},\boldsymbol{\delta})=\frac{qS}{m}\{&-C_{D}\mathrm{c}\chi_{w}\mathrm{c}\gamma_{w}+C_{Y}(\mathrm{s}\mu\mathrm{s}\gamma_{w}-\mathrm{c}\mu\mathrm{s}\chi_{w}\mathrm{c}\gamma_{w})\\&-C_{L}(\mathrm{c}\mu\mathrm{s}\gamma_{w}+\mathrm{s}\mu\mathrm{s}\chi_{w}\mathrm{c}\gamma_{w})\}-g\mathrm{s}\gamma\end{aligned} \tag{A.6}$$

$$\begin{aligned}g_{\overline{V}}(t,\mu,\boldsymbol{\xi}_{a})=\frac{1}{m}\{&\mathrm{c}\bar{\alpha}\mathrm{s}\beta\left(\mathrm{c}\mu\mathrm{s}\chi_{w}\mathrm{c}\gamma_{w}-\mathrm{s}\mu\mathrm{s}\gamma_{w}\right)\\&-\mathrm{s}\bar{\alpha}\left(\mathrm{c}\mu\mathrm{s}\gamma_{w}+\mathrm{s}\mu\mathrm{s}\chi_{w}\mathrm{c}\gamma_{w}\right)\\&+\mathrm{c}\bar{\alpha}\mathrm{c}\beta\mathrm{c}\chi_{w}\mathrm{c}\gamma_{w}\}\end{aligned} \tag{A.7}$$

$$\mathbf{g}_{\mu}\left(\boldsymbol{\xi}_{a}\right)=\begin{bmatrix}\dfrac{\mathrm{c}\alpha}{\mathrm{c}\beta} & 0 & \dfrac{\mathrm{s}\alpha}{\mathrm{c}\beta}\end{bmatrix} \tag{A.8}$$

A.2 Angle Conversion

In this section, the conversion between the proposed angles and the conventional air-relative (or air-mass-relative) angles is derived. The air-relative angles are composed of three angles: the air-relative roll angle μ_a, the air-relative course angle χ_a, and the air-relative flight path angle γ_a [29]. The air-relative flight path angles are defined when $|V_D - w_D| < V_T$ as follows:

$$\begin{aligned} \chi_a &= \operatorname{atan2}(V_E - w_E, V_N - w_N) \\ \gamma_a &= \arcsin\left(\frac{w_D - V_D}{V_T}\right). \end{aligned} \tag{A.9}$$

The air-relative roll angle is defined such that the following is satisfied:

$$\mathbf{C}_x(\mu_a)\,\mathbf{C}_y(\gamma_a)\,\mathbf{C}_z(\chi_a) = \mathbf{C}_{w/i}. \tag{A.10}$$

Then, the conversion is represented by a mapping between the following coordinates:

$$\left(\overline{V}_T, \chi, \gamma, \mu\right) \leftrightarrow \left(V_T, \chi_a, \gamma_a, \mu_a\right). \tag{A.11}$$

Let $\mathcal{F}_{a_1}$ and $\mathcal{F}_{a_2}$ be the intermediate frames formed by the sequential rotations by χ_a and γ_a, respectively, i.e., the corresponding coordinate systems satisfy

$$\begin{aligned} \mathbf{C}_{a_1/i} &= \mathbf{C}_z(\chi_a) \\ \mathbf{C}_{a_2/a_1} &= \mathbf{C}_y(\gamma_a). \end{aligned} \tag{A.12}$$

Using the frames, the geometrical relations between the two coordinates in Eq. (A.11) are shown in Fig. A.1.

Equation (2.14) in the inertial coordinate system is $V_T\mathbf{C}_{i/w}\mathbf{i} = \overline{V}_T\mathbf{C}_{i/\sigma}\mathbf{i} -$

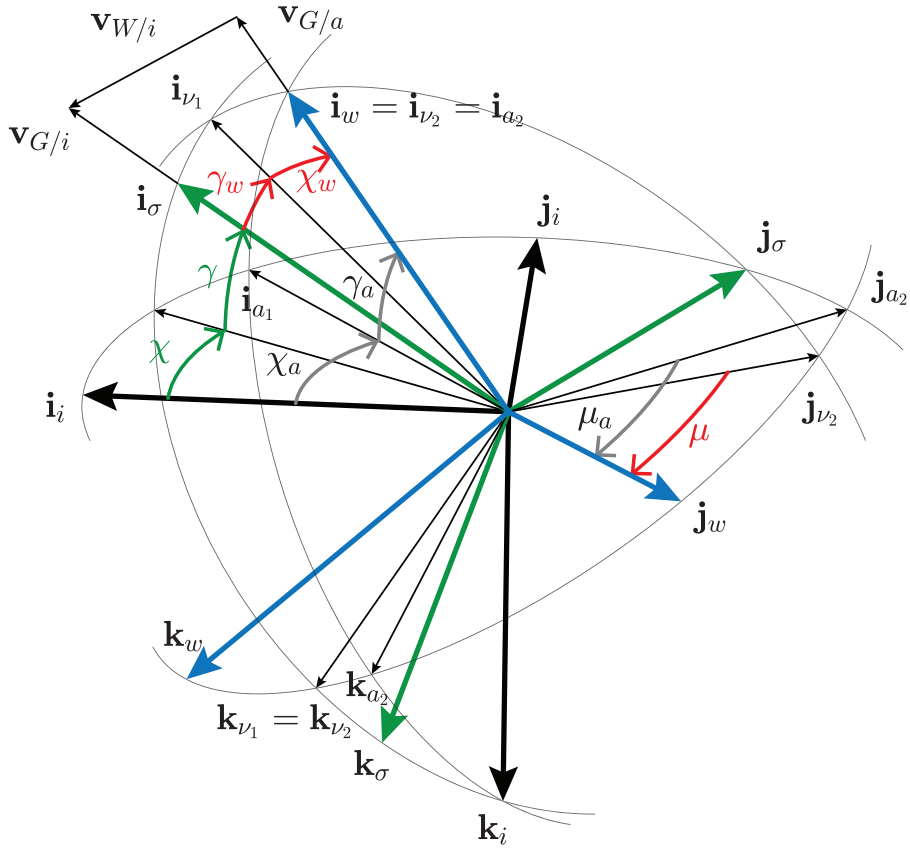

Figure A.1: Relation between the proposed angles and the air-relative angles

$\mathbf{v}^i_{W/i}$ or

$$V_T \begin{bmatrix} \mathrm{c}\gamma_a \mathrm{c}\chi_a \\ \mathrm{c}\gamma_a \mathrm{s}\chi_a \\ -\mathrm{s}\gamma_a \end{bmatrix} = \overline{V}_T \begin{bmatrix} \mathrm{c}\gamma \mathrm{c}\chi \\ \mathrm{c}\gamma \mathrm{s}\chi \\ -\mathrm{s}\gamma \end{bmatrix} - \begin{bmatrix} w_N \\ w_E \\ w_D \end{bmatrix}, \tag{A.13}$$

which gives

$$\begin{aligned} \chi_a &= \operatorname{atan2}\left(\overline{V}_T \mathrm{s}\chi \mathrm{c}\gamma - w_E, \overline{V}_T \mathrm{c}\chi \mathrm{c}\gamma - w_N\right) \\ \gamma_a &= \arcsin\left(\frac{\overline{V}_T \mathrm{s}\gamma + w_D}{V_T}\right) \end{aligned} \tag{A.14}$$

and

$$\begin{aligned} \chi &= \operatorname{atan2}\left(V_T \mathrm{s}\chi_a \mathrm{c}\gamma_a + w_E, V_T \mathrm{c}\chi_a \mathrm{c}\gamma_a + w_N\right) \\ \gamma &= \arcsin\left(\frac{V_T \mathrm{s}\gamma_a - w_D}{\overline{V}_T}\right) \\ \overline{V}_T &= \sqrt{\left(V_T \mathrm{c}\gamma_a \mathrm{c}\chi_a + w_N\right)^2 + \left(V_T \mathrm{c}\gamma_a \mathrm{s}\chi_a + w_E\right)^2 + \left(V_T \mathrm{s}\gamma_a - w_D\right)^2}\,. \end{aligned} \tag{A.15}$$

On the other hand, from $\mathbf{C}_{w/i} = \mathbf{C}_\mu \mathbf{C}_{\chi_w} \mathbf{C}_{\gamma_w} \mathbf{C}_{\sigma/i}$, Eq. (A.10) yields

$$\begin{aligned} \mathrm{s}\mu_a &= \mathrm{s}\chi_a \left\{\mathrm{c}\chi \left(\mathrm{c}\mu \mathrm{s}\bar{\gamma} + \mathrm{s}\mu \mathrm{s}\chi_w \mathrm{c}\bar{\gamma}\right) + \mathrm{s}\mu \mathrm{c}\chi_w \mathrm{s}\chi\right\} \\ &\quad -\mathrm{c}\chi_a \left\{\mathrm{s}\chi \left(\mathrm{c}\mu \mathrm{s}\bar{\gamma} + \mathrm{s}\mu \mathrm{s}\chi_w \mathrm{c}\bar{\gamma}\right) - \mathrm{s}\mu \mathrm{c}\chi_w \mathrm{c}\chi\right\} \\ \mathrm{c}\mu_a &= \mathrm{c}\chi_a \left\{\mathrm{s}\chi \left(\mathrm{s}\mu \mathrm{s}\bar{\gamma} - \mathrm{c}\mu \mathrm{s}\chi_w \mathrm{c}\bar{\gamma}\right) + \mathrm{c}\mu \mathrm{c}\chi_w \mathrm{c}\chi\right\} \\ &\quad -\mathrm{s}\chi_a \left\{\mathrm{c}\chi \left(\mathrm{s}\mu \mathrm{s}\bar{\gamma} - \mathrm{c}\mu \mathrm{s}\chi_w \mathrm{c}\bar{\gamma}\right) - \mathrm{c}\mu \mathrm{c}\chi_w \mathrm{s}\chi\right\} \end{aligned} \tag{A.16}$$

and

$$\begin{aligned} \mathrm{s}\mu &= \mathrm{s}\bar{\gamma}\mathrm{s}\chi \left(\mathrm{c}\mu_a \mathrm{c}\chi_a + \mathrm{s}\mu_a \mathrm{s}\gamma_a \mathrm{s}\chi_a\right) \\ &\quad -\mathrm{s}\bar{\gamma}\mathrm{c}\chi \left(\mathrm{c}\mu_a \mathrm{s}\chi_a - \mathrm{s}\mu_a \mathrm{s}\gamma_a \mathrm{c}\chi_a\right) + \mathrm{s}\mu_a \mathrm{c}\gamma_a \mathrm{c}\bar{\gamma} \\ \mathrm{c}\mu &= \mathrm{s}\bar{\gamma}\mathrm{c}\chi \left(\mathrm{s}\mu_a \mathrm{s}\chi_a + \mathrm{c}\mu_a \mathrm{s}\gamma_a \mathrm{c}\chi_a\right) \\ &\quad -\mathrm{s}\bar{\gamma}\mathrm{s}\chi \left(\mathrm{s}\mu_a \mathrm{c}\chi_a - \mathrm{c}\mu_a \mathrm{s}\gamma_a \mathrm{s}\chi_a\right) + \mathrm{c}\mu_a \mathrm{c}\gamma_a \mathrm{c}\bar{\gamma}, \end{aligned} \tag{A.17}$$

which are directly used to obtain the value of roll angles using atan2 function.

Appendix B

WPTPFC

B.1 Foot Dynamics

B.1.1 Curve Parametrization

Consider a class C^1 curve $\boldsymbol{\gamma} : \mathbb{R} \to \mathbb{R}^3$ and assume that there is $\epsilon > 0$ such that $\|\boldsymbol{\gamma}'(\sigma)\| \geq \epsilon$ for all $\sigma \in \mathbb{R}$. Then, the function $l : \mathbb{R} \to \mathbb{R}$ defined by $l(\sigma) = \int_a^\sigma \|\boldsymbol{\gamma}'(\xi)\| \mathrm{d}\xi$ for some $a \in \mathbb{R}$ is a global diffeomorphism. Consider now the reparametrization, $s = l(\sigma)$, the derivative of whose inverse is

$$\frac{\mathrm{d}\sigma}{\mathrm{d}s} = \frac{\mathrm{d}l^{-1}(s)}{\mathrm{d}s} = \frac{1}{\frac{\mathrm{d}l(\sigma)}{\mathrm{d}\sigma}} = \frac{1}{\|\boldsymbol{\gamma}'(\sigma)\|}. \tag{B.1}$$

Define $\bar{\boldsymbol{\gamma}} = \boldsymbol{\gamma} \circ l^{-1}$. Then, $\bar{\boldsymbol{\gamma}}'(s) = \frac{\mathrm{d}\boldsymbol{\gamma}}{\mathrm{d}\sigma}\frac{\mathrm{d}\sigma}{\mathrm{d}s} = \frac{\boldsymbol{\gamma}'(\sigma)}{\|\boldsymbol{\gamma}'(\sigma)\|}$. Since $\|\bar{\boldsymbol{\gamma}}'(s)\| = 1$ for all $s \in \mathbb{R}$, $\bar{\boldsymbol{\gamma}}$ is the natural parametrization of $\boldsymbol{\gamma}$, and $\mathbf{T} = \bar{\boldsymbol{\gamma}}'(s)$. The curvature vector can be obtained from

$$\mathbf{T}' = \frac{\mathrm{d}}{\mathrm{d}\sigma}\left(\frac{\boldsymbol{\gamma}'}{\|\boldsymbol{\gamma}'\|}\right)\frac{\mathrm{d}\sigma}{\mathrm{d}s} = \frac{\boldsymbol{\gamma}''}{\|\boldsymbol{\gamma}'\|^2} - \frac{\boldsymbol{\gamma}' \cdot \boldsymbol{\gamma}''}{\|\boldsymbol{\gamma}'\|^4}\boldsymbol{\gamma}' = \frac{\boldsymbol{\gamma}' \times (\boldsymbol{\gamma}'' \times \boldsymbol{\gamma}')}{\|\boldsymbol{\gamma}'\|^4}. \tag{B.2}$$

In the path-following problem, the actual reparametrization l that involves an integral need not be found because the foot parameter α is not explicitly used. Instead, only the position, tangent, and curvature vectors at each foot are needed.

The dynamics of a general foot parameter σ that satisfies $\alpha = l(\sigma)$ is then,

$$\dot{\sigma} = \frac{\partial \sigma}{\partial \alpha}\dot{\alpha} = \frac{\dot{\alpha}}{\|\boldsymbol{\gamma}'(\sigma)\|} = \frac{U}{\Delta\|\boldsymbol{\gamma}'\|}\mathbf{T}^\top \overline{\mathbf{v}}. \tag{B.3}$$

By using these relations, all the equations can be adapted to any parametric paths that satisfy the required assumptions. For example, $\dot{\mathbf{e}} = \mathbf{T}\dot{\alpha} - \dot{\mathbf{p}} = \mathbf{T}\|\boldsymbol{\gamma}'\|\dot{\sigma} - U\overline{\mathbf{v}}$ and $\dot{\mathbf{T}} = \mathbf{T}'\dot{\alpha} = \mathbf{T}'\|\boldsymbol{\gamma}'\|\dot{\sigma}$.

B.1.2 Robust Foot Control

Suppose that the dynamics of σ and $\mathbf{e}$ are corrupted by bounded uncertainties u_σ and $\mathbf{u}_e$, respectively. Noticing that the dynamics of the foot parameter can be modified by a designer, this dissertation proposes to apply an additive control term f to the foot dynamics:

$$\dot{\sigma} = \frac{1}{\Delta\|\boldsymbol{\gamma}'\|}\left(U\mathbf{T}^\top\overline{\mathbf{v}} + f + u_\sigma\right) \tag{B.4a}$$

$$\dot{\mathbf{e}} = \mathbf{T}\left\|\boldsymbol{\gamma}'\right\|\dot{\sigma} - U\overline{\mathbf{v}} + \mathbf{u}_e. \tag{B.4b}$$

Let $E = \mathbf{e}^\top\mathbf{T}$; then, E represents the degree of orthogonality of the vectors $\mathbf{e}$ and $\mathbf{T}$, which should be always zero to ensure that σ is one of the foots of P. Its derivative is

$$\begin{aligned}
\dot{E} &= \mathbf{T}^\top\dot{\mathbf{e}} + \mathbf{e}^\top\dot{\mathbf{T}} \\
&= \mathbf{T}^\top\left(\mathbf{T}\|\boldsymbol{\gamma}'\|\dot{\sigma} - U\overline{\mathbf{v}} + \mathbf{u}_e\right) + \mathbf{e}^\top\mathbf{T}'\|\boldsymbol{\gamma}'\|\dot{\sigma} \\
&= \left(1 + \mathbf{e}^\top\mathbf{T}'\right)\|\boldsymbol{\gamma}'\|\dot{\sigma} - U\mathbf{T}^\top\overline{\mathbf{v}} + \mathbf{T}^\top\mathbf{u}_e \\
&= u_\sigma + \mathbf{T}^\top\mathbf{u}_e + f
\end{aligned} \tag{B.5}$$

recalling that $\Delta = \mathbf{e}^\top \mathbf{T}' + 1$. For some $k_\sigma > 0$, if the stabilizing controller is chosen as $f = -k_\sigma E$, it follows that

$$\frac{\mathrm{d}}{\mathrm{d}t}\left(\frac{1}{2}E^2\right) \leq |E|\left(|u_\sigma| + \|\mathbf{u}_e\|\right) - k_\sigma E^2. \tag{B.6}$$

Let b_u be an upper bound of $|u_\sigma| + \|\mathbf{u}_e\|$. Then, $E|_t$ is uniformly ultimately bounded by $b_u/k_\sigma + \epsilon$ for some $\epsilon > 0$. By choosing k_σ sufficiently large, the integration error on $\sigma(t)$ can be effectively suppressed. It can be intuitively interpreted that if the estimated foot parameter is behind the true value, that is, the perpendicular and tangent vector of the path at the foot form an obtuse angle (indicated by E), the rate of change of the foot parameter is increased, and vice versa. This approach is much more accurate and reliable than finding the closest point with numerical optimization [21] because in general, optimization does not guarantee the required continuity and smoothness of the estimated closest point with respect to time.

Bibliography

[1] F. H. Proctor, D. A. Hinton, and R. L. Bowles, "A windshear hazard index," in *Conference on Aviation, Range and Aerospace Meteorology*, (Orlando, FL), September 2000.

[2] K.-U. Hahn, "Takeoff and landing in a downburst," *Journal of Aircraft*, vol. 24, no. 8, pp. 552–558, 1987.

[3] R. W. Beard and T. W. McLain, *Small Unmanned Aircraft: Theory and Practice*. Princeton, NJ: Princeton University Press, 2012.

[4] N. R. Lawrance and S. Sukkarieh, "Autonomous exploration of a wind field with a gliding aircraft," *Journal of Guidance Control and Dynamics*, vol. 34, no. 3, pp. 719–733, 2011.

[5] J. Farrell, M. Sharma, and M. Polycarpou, "Backstepping-based flight control with adaptive function approximation," *Journal of Guidance, Control, and Dynamics*, vol. 28, no. 6, pp. 1089–1102, 2005.

[6] L. Sonneveldt, E. Van Oort, Q. Chu, and J. Mulder, "Nonlinear adaptive trajectory control applied to an F-16 model," *Journal of Guidance, Control, and Dynamics*, vol. 32, no. 1, pp. 25–39, 2009.

[7] G. Xia, R. Dong, J. Xu, and Q. Zhu, "Linearized model of carrier-based aircraft dynamics in final-approach air condition," *Journal of Aircraft*, vol. 53, no. 1, pp. 33–47, 2015.

[8] A. Altan and R. Hacıoğlu, "Model predictive control of three-axis gimbal system mounted on uav for real-time target tracking under external disturbances," *Mechanical Systems and Signal Processing*, vol. 138, p. 106548, 2020.

[9] S. J. Lee, S. H. Kim, and H. J. Kim, "Robust translational force control of multi-rotor uav for precise acceleration tracking," *IEEE Transactions on Automation Science and Engineering*, vol. 17, no. 2, pp. 562–573, 2019.

[10] J. Dodenhöft, F. Holzapfel, R. Choe, K. Ackerman, and N. Hovakimyan, "Design and evaluation of an l1 adaptive controller for nasa's transport class model," in *AIAA Guidance, Navigation, and Control Conference*, (Grapevine, TX), January 2016.

[11] J. Yang, S. Li, C. Sun, and L. Guo, "Nonlinear-disturbance-observer-based robust flight control for airbreathing hypersonic vehicles," *IEEE Transactions on Aerospace and Electronic Systems*, vol. 49, no. 2, pp. 1263–1275, 2013.

[12] K. K. Hassan, *Nonlinear Systems*. Upper Saddle River, NJ: Prentice Hall, 2002.

[13] A. P. Aguiar and J. P. Hespanha, "Trajectory-tracking and path-following of underactuated autonomous vehicles with parametric modeling uncertainty," *IEEE Transactions on Automatic Control*, vol. 52, no. 8, pp. 1362–1379, 2007.

[14] E. Lefeber, K. Y. Pettersen, and H. Nijmeijer, "Tracking control of an underactuated ship," *IEEE Transactions on Control Systems Technology*, vol. 11, no. 1, pp. 52–61, 2003.

[15] K. D. Do, Z.-P. Jiang, and J. Pan, "Robust adaptive path following of underactuated ships," *Automatica*, vol. 40, no. 6, pp. 929–944, 2004.

[16] Y. A. Kapitanyuk, A. V. Proskurnikov, and M. Cao, "A guiding vector-field algorithm for path-following control of nonholonomic mobile robots," *IEEE Transactions on Control Systems Technology*, vol. 26, no. 4, pp. 1372–1385, 2018.

[17] A. P. Aguiar, J. P. Hespanha, and P. V. Kokotović, "Performance limitations in reference tracking and path following for nonlinear systems," *Automatica*, vol. 44, no. 3, pp. 598–610, 2008.

[18] R. Skjetne and T. I. Fossen, "Nonlinear maneuvering and control of ships," in *Proc. MTS/IEEE Oceans 2001. An Ocean Odyssey*, (Honolulu, HI), Nov. 2001.

[19] C. Altafini, "Path following with reduced off-tracking for multibody wheeled vehicles," *IEEE Transactions on Control Systems Technology*, vol. 11, no. 4, pp. 598–605, 2003.

[20] M. Breivik and T. I. Fossen, "Principles of guidance-based path following in 2D and 3D," in *Proc. 44th IEEE Conference on Decision and Control*, (Seville, Spain), Dec. 2005.

[21] R. J. Gill, D. Kulić, and C. Nielsen, "Spline path following for redundant mechanical systems," *IEEE Transactions on Robotics*, vol. 31, no. 6, pp. 1378–1392, 2015.

[22] D. Belleter, M. A. Maghenem, C. Paliotta, and K. Y. Pettersen, "Observer based path following for underactuated marine vessels in the presence of ocean currents: A global approach," *Automatica*, vol. 100, pp. 123–134, 2019.

[23] G. Ambrosino, M. Ariola, U. Ciniglio, F. Corraro, E. De Lellis, and A. Pironti, "Path generation and tracking in 3-D for UAVs," *IEEE Transactions on Control Systems Technology*, vol. 17, no. 4, pp. 980–988, 2009.

[24] K. Y. Pettersen and E. Lefeber, "Way-point tracking control of ships," in *Proc. 40th IEEE Conference on Decision and Control*, (Orlando, FL), Dec. 2001.

[25] A. M. Lekkas and T. I. Fossen, "Integral LOS path following for curved paths based on a monotone cubic Hermite spline parametrization," *IEEE Transactions on Control Systems Technology*, vol. 22, no. 6, pp. 2287–2301, 2014.

[26] J.-M. Kai, T. Hamel, and C. Samson, "A unified approach to fixed-wing aircraft path following guidance and control," *Automatica*, vol. 108-108491, 2019.

[27] N. A. Shneydor, *Missile Guidance and Pursuit: Kinematics, Dynamics, and Control*. Walnut Street, PH: Woodhead Publishing, 1998.

[28] D. R. Nelson, D. B. Barber, T. W. McLain, and R. W. Beard, "Vector field path following for miniature air vehicles," *IEEE Transactions on Robotics*, vol. 23, no. 3, pp. 519–529, 2007.

[29] W. Frost and R. L. Bowles, "Wind shear terms in the equations of aircraft motion," *Journal of Aircraft*, vol. 21, no. 11, pp. 866–872, 1984.

[30] T. Çimen, "A generic approach to missile autopilot design using state-dependent nonlinear control," in *18th IFAC World Congress*, (Milano, Italy), August 2011.

[31] V. M. Goncalves, L. C. Pimenta, C. A. Maia, B. C. Dutra, and G. A. Pereira, "Vector fields for robot navigation along time-varying curves in n-dimensions," *IEEE Transactions on Robotics*, vol. 26, no. 4, pp. 647–659, 2010.

[32] W. Yao and M. Cao, "Path following control in 3D using a vector field," *Automatica*, vol. 117, article 108957, 2020.

[33] C. Nielsen, C. Fulford, and M. Maggiore, "Path following using transverse feedback linearization: application to a maglev positioning system," *Automatica*, vol. 46, no. 3, pp. 585–590, 2010.

[34] S. Park, J. Deyst, and J. P. How, "Performance and Lyapunov stability of a nonlinear path following guidance method," *Journal of Guidance, Control, and Dynamics*, vol. 30, no. 6, pp. 1718–1728, 2007.

[35] L. Lapierre, D. Soetanto, and A. Pascoal, "Nonlinear path following with applications to the control of autonomous underwater vehicles," in *Proc. 42nd IEEE Conference on Decision and Control*, (Maui, HI), Dec. 2003.

[36] D. J. Gates, "Nonlinear path following method," *Journal of Guidance, Control, and Dynamics*, vol. 33, no. 2, pp. 321–332, 2010.

[37] G. M. Siouris, *Missile Guidance and Control Systems*. New York, NY: Springer, 2004.

[38] R. Skjetne, T. I. Fossen, and P. V. Kokotović, "Robust output maneuvering for a class of nonlinear systems," *Automatica*, vol. 40, no. 3, pp. 373–383, 2004.

[39] T. Faulwasser and R. Findeisen, "Nonlinear model predictive control for constrained output path following," *IEEE Transactions on Automatic Control*, vol. 61, no. 4, pp. 1026–1039, 2016.

[40] A. Pavlov, H. Nordahl, and M. Breivik, "MPC-based optimal path following for underactuated vessels," in *Proc. 8th IFAC International Conference on Manoeuvring and Control of Marine Craft*, (Guarujá, Brazil), Sep. 2009.

[41] P. Lu, E.-J. van Kampen, C. de Visser, and Q. Chu, "Aircraft fault-tolerant trajectory control using incremental nonlinear dynamic inversion," *Control Engineering Practice*, vol. 57, pp. 126–141, 2016.

[42] S. N. Singh, M. L. Steinberg, and A. B. Page, "Nonlinear adaptive and sliding mode flight path control of F/A-18 model," *IEEE Transactions on Aerospace and Electronic Systems*, vol. 39, no. 4, pp. 1250–1262, 2003.

[43] Y. Seo and Y. Kim, "Design of fault tolerant control system for engine failure of single-engined aircraft," in *AIAA Guidance, Naviation, and Control Conference*, (San Diego, CA), January 2019.

[44] J. Sjöberg, *Optimal control and model reduction of nonlinear DAE models*. PhD thesis, Institutionen för Systemteknik, Linköping, Sweden, 2008.

[45] F. Blanchini and S. Miani, *Set-Theoretic Methods in Control*. Basel, Switzerland: Birkhäuser, 2 ed., 2015.

[46] A. D. Ames, X. Xu, J. W. Grizzle, and P. Tabuada, "Control barrier function based quadratic programs for safety critical systems," *IEEE Transactions on Automatic Control*, vol. 62, no. 8, pp. 3861–3876, 2017.

[47] B. L. Stevens, F. L. Lewis, and E. N. Johnson, *Aircraft Control and Simulation: Dynamics, Controls Design, and Autonomous Systems*. Hoboken, NJ: John Wiley & Sons, 2015.

[48] O. Härkegård, *Backstepping and control allocation with applications to flight control*. PhD thesis, Linköpings universitet, Linköping, Sweden, 2003.

[49] M. Bodson, "Evaluation of optimization methods for control allocation," *Journal of Guidance, Control, and Dynamics*, vol. 25, no. 4, pp. 703–711, 2002.

[50] M. R. Hjelmfelt, "Structure and life cycle of microburst outflows observed in colorado," *Journal of Applied Meteorology*, vol. 27, no. 8, pp. 900–927, 1988.

[51] R. Bulirsch, F. Montrone, and H. J. Pesch, "Abort landing in the presence of windshear as a minimax optimal control problem, part 1: Necessary conditions," *Journal of Optimization Theory and Applications*, vol. 70, no. 1, pp. 1–23, 1991.

[52] R. B. Bobbitt and R. M. Howard, "Escape strategies for turboprop aircraft in microburst windshear," *Journal of Aircraft*, vol. 29, no. 5, pp. 745–752, 1992.

[53] J. W. Langelaan, N. Alley, and J. Neidhoefer, "Wind field estimation for small unmanned aerial vehicles," *Journal of Guidance, Control, and Dynamics*, vol. 34, no. 4, pp. 1016–1030, 2011.

[54] C.-T. Chen, *Linear System Theory and Design.* New York, NY: Oxford University Press, 1999.

[55] P. R. Belanger, "Estimation of angular velocity and acceleration from shaft-encoder measurements," in *International Conference on Robotics and Automation*, (Nice, France), May 1992.

[56] R. G. Brown, P. Y. Hwang, *et al.*, *Introduction to Random Signals and Applied Kalman Filtering.* Hoboken, NJ: John Wiley & Sons, 1992.

[57] A. H. Bowers, J. W. Pahle, R. J. Wilson, B. C. Flick, and R. L. Rood, "An overview of the nasa f-18 high alpha research vehicle," NASA Technical Memorandum 4772, 1996.

[58] K. B. Ngo, R. Mahony, and Z.-P. Jiang, "Integrator backstepping using barrier functions for systems with multiple state constraints," in *Proc. 44th IEEE Conference on Decision and Control*, (Seville, Spain), pp. 8306–8312, Dec. 2005.

[59] K. P. Tee, S. S. Ge, and E. H. Tay, "Barrier Lyapunov functions for the control of output-constrained nonlinear systems," *Automatica*, vol. 45, no. 4, pp. 918–927, 2009.

[60] Y.-J. Liu, J. Li, S. Tong, and C. P. Chen, "Neural network control-based adaptive learning design for nonlinear systems with full-state constraints," *IEEE Transactions on Neural Networks and Learning Systems*, vol. 27, no. 7, pp. 1562–1571, 2016.

[61] H. K. Khalil, *Nonlinear Systems.* Upper Saddle River, NJ: Prentice Hall, 3rd ed., 2002.

[62] N. A. Shneydor, *Differential Equations, Dynamical Systems, and Linear Algebra*. London, UK: Academic Press, 1974.

[63] R. K. Miller and A. N. Michel, *Ordinary Differential Equations*. New York, NY: Academic Press, 1982.

[64] M. I. El-Hawwary and M. Maggiore, "Reduction principles and the stabilization of closed sets for passive systems," *IEEE Transactions on Automatic Control*, vol. 55, no. 4, pp. 982–987, 2010.

[65] V. I. Vorotnikov, *Partial Stability and Control*. Cambridge, MA: Birkhäuser, 1998.

[66] D. Swaroop, J. K. Hedrick, P. P. Yip, and J. C. Gerdes, "Dynamic surface control for a class of nonlinear systems," *IEEE Transactions on Automatic Control*, vol. 45, no. 10, pp. 1893–1899, 2000.

초록

본 논문에서는 대기바람이 존재하는 환경에서 운용되는 비행체에 적용할 수 있는 경로추종 기법을 제안하였다. 연속 미분가능한 대기바람 속도를 고려하는 비행체 운동방정식을 유도하고, 이를 기반으로 한 비행제어 법칙을 설계하였다. 또한, 비행체가 충분히 매끈한 경로를 추종하도록 하는 수직-접선벡터 가중치 기반 경로추종 제어를 개발하고 비행제어 법칙과 통합하였다.

본 논문에서 제안한 운동방정식은 공력각과 관성 경로각을 상태변수로 가진다. 두 개의 경로대비 바람각(path-relative wind angle)을 정의하여 대기바람에 의해 발생하는 대기속도와 대지속도 벡터 성분의 차이를 매개화 하였다. 대기바람이 존재하는 상황에서 공력롤각을 정의하여 대기바람이 존재하는 환경에서도 균형선회가 수월하게 하였다. 제안한 운동방정식은 계단식 구조를 가지도록 정식화하여 제어법칙을 설계하는 데 도움이 되도록 하였다. 또한, 제안한 모델은 바람이 존재하는 상황에서도 관성 경로각의 거동을 효율적으로 표현하므로 경로추종 제어법칙을 설계하기에 유리하다.

한편, 수직-접선벡터 가중치 기반 경로추종 제어는 경로에 대한 수선의 발(perpendicular foot)을 기준점으로 채택하여, 기존 기법에서 널리 쓰이는 최단점이 가지는 특이점, 불연속성 등의 문제들을 보완하였다. 시스템 입력으로는 속도방향 벡터(velocity direction)와 조향 벡터(steering)을 고려하였다. 특히, 장벽가중치 기법(barrier weighting method)을 적용하여 조향벡터 입력 시스템에 백스텝핑 기법을 도입할 때 기준점 운동방정식이 가지는 특이점을 효과적으로 회피하도록 하였다.

위의 연구내용은 시간비례 분해기법(time-scale decomposition)을 적용하여 비행제어 법칙과 경로추종 제어기법을 통합하였다. 개별적으로 설계된 비행제어법칙 간의 호환성을 검토하고, 적절한 변환 및 조종할당 기법을 개발하였다. 본 논문에서 제안한 기법의 성능을 평가하기 위해 수치 시뮬레이션을 수행하였다.

주요어: 비행동역학, 대기바람, 경로추종, 백스텝핑, 장벽가중치기법

학번: 2013-23070